Master's thesis

NTNU
Norwegian University of Science and Technology
Faculty of Engineering
Department of Geoscience and Petroleum

Erlend Andreassen

Assessment of minimum principal stress and potential hydraulic jacking at Løkjelsvatn Hydropower Project

Master's thesis in Geotechnology
Supervisor: Krishna Kanta Panthi
June 2021

NTNU
Norwegian University of
Science and Technology

Erlend Andreassen

Assessment of minimum principal stress and potential hydraulic jacking at Løkjelsvatn Hydropower Project

Master's thesis in Geotechnology
Supervisor: Krishna Kanta Panthi
June 2021

Norwegian University of Science and Technology
Faculty of Engineering
Department of Geoscience and Petroleum

NTNU
Norwegian University of
Science and Technology

NTNU
Norwegian University of Science and Technology

Department of Geoscience and Petroleum

Your ref.: MS/N38T58/IGP/EAKP Date: 14.01.2021

TGB4945 Engineering Geology - MSc thesis
for
Eng. geo. student Erlend Andreassen

Assessment of minimum principal stress and potential hydraulic jacking at Løkjellsvatn Hydropower Project

Background

In Norwegian hydropower projects, hydraulic fracturing test is being carried out to define approximate minimum principal stress in the rock mass so that the start point for unlined pressure shaft / tunnel is fixed. The hydraulic fracturing test is expensive which limits maximum possible test locations for reliable in-situ stress level in the vicinity of interest. The test provides not always reliable information about minimum principal stress due to the presence of pre-existing joints, schistosity in the rock mass and human errors. There is a strong need to develop a robust, an easy to test and economically cheaper methodology. Hydraulic splitting might be among the alternatives that may full-fill the need. This MSc thesis will present analysis results of the stress measurement carried out using, hydraulic fracturing, hydraulic splitting and numerical modeling at Løkjelsvatn hydropower project located at Etne of west Norway oriented in this direction and will focus on the following issues:

MSc thesis task

This MSc thesis is the continuation of the project work during autumn 2020 where candidate reviewed different stress measurement methods and briefly presented about Løkjelsvatn hydropower project. The MSc thesis will cover the test results and analysis and will have following main tasks:

- Theory review on different stress measurement methods practiced in hydropower sector, review geo-tectonic environment prevailing in Norway and in-situ rock stress situation with the highlight on horizontal stress variation within the country.
- Theory review on the Norwegian design principle for unlined pressure tunnels used as waterways for hydropower projects. Review rock engineering principle in the assessment of stability and leakage potential from hydropower tunnels.
- Carry out laboratory assessment, describe methodology for hydraulic fracturing, jacking, and splitting test.

- Carry out comprehensive assessment and evaluation on the in-situ stress state at the case project area using test results, analytical and numerical solutions.
- Assess potential hydraulic jacking and leakage potential from the pressure tunnel of the case project.
- Discuss uncertainties associated to the estimation of minimum principal stress using in-situ test and other theoretical methods.
- Conclude the work with recommendations.

Relevant computer software packages

Candidate shall use *roc-science package* and other relevant computer software for the master study.

Background information for the study

- Relevant information about the project such as reports, maps, information and data received from the supervisors and collected by the candidate.
- The information provided by the professor about rock engineering and hydropower.
- Scientific papers and books related to international tunnelling cases.
- Literatures in rock engineering, rock support principles, rock mechanics and tunnelling.

Cooperating partner

YIT Infra Norge is the cooperating partner for this project work.

The thesis work is to start on January 15, 2021 and to be completed by June 11, 2021.

The Norwegian University of Science and Technology (NTNU)
Department of Geoscience and Petroleum

January 14, 2021

Dr. Krishna K. Panthi
Professor of geological engineering, main supervisor

Abstract

The Løkjelsvatn hydropower plant is a new and modern plant under construction in Litledalen in Etne municipality, Vestland. By completion, the power plant increases the annual power production in the valley without extensive encroachment on nature. Results from rock stress measurements show lower values than expected based on overburden criteria. In combination with challenges related to significant water leakage and the need for grouting in some areas, it has delayed the completion and given challenging circumstances for the involved.

The limitations of overburden criteria, such as The Norwegian Criteria for Confinement as a tool for predicting the minor principal stress, are well known. It is, therefore, crucial to verify the stress level before determining the final placement of the transition zone. Otherwise, hydraulic jacking of the rock mass, leading to excessive leakages from the tunnel system, can cause economic and material consequences. Today, the number of rock stress measurements are limited to a minimum due to practical and economic reasons. Therefore, it is necessary with a fast and cost-efficient measurement method that gives a reliable result without impeding the tunnel construction notable by increasing the number of test sites. Thus identify any anomalies in the stress state without increasing cost to traditional tests.

This study has considered stress and leakage potential at Løkjelsvatn to assess the appropriateness for unlined pressure tunnels through a combined case and literature study. The study includes mapping engineering-geological parameters at the transition zone, laboratory examination, numerical modeling in RS2, and a semi-analytical approach to estimate water leakage from the pressurized parts of the tunnel system. In addition, in collaboration with PhD candidate Henki Ødegaard, rock stress measurements have been carried out with a newly developed test, called Rapid Step-Rate Test (RSRT), to assess the validity and compare data with results from more established measurement methods, such as hydraulic fracturing.

Results from hydraulic fracturing provide a 1.33 factor of safety. Compared with experiences in similar Norwegian projects, there are reasons to believe that hydraulic failure will not occur. Numerical modeling shows that the confinement pressure is greater than the water pressure for the entire pressurized part of the tunnel system, which is assumed to avoid leakage. The correlation with the RSRT seems to be equal to 1.22. The experience with the RSRT test is satisfying and shows that it is possible to carry out rock stress measurements fast (typically 10-20 min pr. test) and cost-efficiently to increase the number of test locations compared to traditional tests.

Sammendrag

Løkjelsvatn kraftverk er et nytt og moderne kraftverk som bygges ut i Litledalen i Etne kommune, Vestland. Med sin ferdigstillelse vil kraftverket sammen med eksisterende anlegg i dalen øke den totale kraftproduksjonen i vassdraget uten større inngrep eller endring i reguleringen av Løkjelsvatnet. Resultater fra bergspenningsmålinger viser lavere verdier enn forventet ut fra overdekningskriterier. Dette i kombinasjon med tidvis store utfordringer knyttet til betydelig innlekkasje av vann og behov for berginjeksjon har forskjøvet ferdigstillelsen og skapt hodebry for de involverte.

Svakhetene med overdekningskriterier for bestemmelse av endelig utforming er godt kjent i bransjen. Det er derfor avgjørende at spenningsnivået verifiseres før endelig plassering av konus, ellers kan utlekkasje fra tunnelsystemet medføre store økonomiske og materielle konsekvenser. I dag begrenses antall bergspenningsmålinger til et minimum som følge av praktiske og økonomiske årsaker. En rask og effektiv målemetode som gir et godt nok resultat kan være løsningen for å øke antall testlokaliteter og på den måten identifisere eventuelle anomalier i spenningsnivået.

Denne masteroppgaven har gjennom et kombinert case- og litteraturstudie sett nærmere på spennings- og lekkasjeforhold ved Løkjelsvatn for å vurdere egnetheten til bergmassen som utgangspunkt for uforede trykktunneler. Arbeidet omfatter både kartlegging av ingeniørgeologske parametere ved konus, laboratorieforsøk, numerisk modellering i RS2 og en semi-analytisk tilnærming for å estimere vannlekkasje fra de trykksatte deler av tunnelsystemet. I tillegg er det i samarbeid med PhD kandidat Henki Ødegaard planlagt og gjennomført bergspenningsmålinger med en nyutviklet test for å vurdere egnetheten og sammenlikne data med resultater fra mer etablerte målemetoder.

Resultater fra hydraulisk splitting gir en sikkerhetsfaktor på 1.33. Sammenliknet med tilsvarende sikkerhetsfaktorer og ingeniørgeologiske parametere ved norske prosjekter er det lite som tyder på at hydraulisk failure vil oppstå. Modellering av dette resultatet viser at spenningsnivået er større enn vanntrykket for hele den trykksatte delen av tunnelsystemet hvilket forutsettes for å unngå utlekkasje. Sammenhengen med Rapid Step Rate Test (RSRT) synes å være lik 1.22. Det konkluderes med at erfaringene er lovende og antyder at det er mulig å gjennomføre bergspenningsmålinger raskt, billig og med et godt nok resultat.

Preface

This master thesis is written in spring 2021 at the Department of Geoscience and Petroleum at the Norwegian University of Science and Technology (NTNU) in Trondheim. The thesis is a continuation of a project thesis written fall 2020 on the same subject and wraps up a five-year master's program in Geotechnology – Engineering Geology and Rock Mechanics.

The thesis focuses on understanding unlined pressure tunnels and shafts built for hydropower projects and other underground structures in various rock stress levels. In the years ahead it will be an increased focus on upgrading existing hydropower plants. A substantial part of the green shift is to replace fossil energy sources with non-emissions alternatives. Today, many Norwegian plants have a significant upgrade potential, and in many cases, the upgrade involves constructing new tunnels, such as at Løkjelsvatn in Etne.

I think the master's thesis theme can contribute to future hydropower development due to an increasing focus on safety, not only financially but also for third parties, such as the environment.

Professor Dr. Krishna Kanta Panthi has been the main supervisor.

Erlend Andreassen

Trondheim, June 10, 2021

Acknowledgments

I wish to express my gratitude to my supervisor, Professor Krishna Kanta Panthi, for generously sharing his experiences, guidance, and enthusiasm for my work.

I am also thankful to PhD candidate Henki Ødegaard for valuable conversations, discussions, and the opportunity to verify the applicability of a completely new test procedure for rock stress measurements.

Further, I would like to extend my special thanks to Bodil Øyre in YIT Infra Norge, the project team, and other staff at Løkjelsvatn hydropower project for their support before and during the field test, providing data and reports from the project.

I will give a big round of applause to my fellow students at NTNU for an excellent company during five years in Trondheim. Thank you for all the efforts you have put into baking cakes every Friday.

Finally, I wish to thank my dear Marthe for her moral motivation and encouragement and for help in reviewing this thesis. Your efforts have been invaluable!

Contents

Abstract i

Sammendrag ii

Preface iii

Acknowledgements iv

1 Introduction 1

1.1 Background . . . 1

1.2 Objectives and scope . . . 4

1.3 Methodology . . . 5

1.4 Limitations . . . 6

2 Rock stresses 7

2.1 Basic theory . . . 7

2.2 In-situ rock stresses . . . 8

2.2.1 Gravitational stresses . . . 9

2.2.2 Tectonic stresses . . . 10

2.2.3 Residual stresses . . . 10

2.2.4 Terrestrial stresses . . . 11

2.3 Factors affecting in-situ rock stress . . . 12

2.3.1 Anisotropy and schistosity . . . 12

2.3.2 Inhomogenities and geological structures . . . 13

2.3.3 Discontinuities . . . 15

2.3.4 Geological structures . . . 16

2.3.5 Topographic stresses . . . 16

2.4 Induced stresses . . . 17

2.4.1 Rock stress redistribution around a tunnel . . . 18

2.4.2 Stress induced instability in strong and isotropic rock masses . 19

2.4.3 Stress induced instability in weak and anisotropic rock masses 20
2.4.4 Stresses around circular openings related to hydropower projects 21
2.5 Stresses in Norway . . . 22

3 Stress measurement methods 25
3.1 Flat jack . . . 26
3.2 2D overcoring . . . 26
3.2.1 Strength and weaknesses . . . 28
3.3 3D overcoring . . . 29
3.3.1 Methodology . . . 29
3.3.2 Practical example . . . 30
3.3.3 Strength and weaknesses . . . 31
3.4 Hydraulic fracturing . . . 32
3.4.1 Methodology . . . 32
3.4.2 Practical example . . . 33
3.4.3 Strength and weaknesses . . . 34
3.5 Hydraulic jacking . . . 34
3.5.1 Methodology . . . 35
3.5.2 Interpretation of data from hydraulic jacking tests . . . 35
3.5.3 Strengths and weaknesses . . . 37

4 Water in the rock mass 38
4.1 Introduction . . . 38
4.2 Consequences of water leakage . . . 38
4.2.1 Environmental . . . 38
4.2.2 Effects of water leakage into a tunnel . . . 38
4.3 Theoretical background . . . 39
4.3.1 Hydraulic conductivity of rock mass . . . 39
4.3.2 Factors controlling hydraulic conductivity . . . 40
4.4 Approaches for assessing ground water inflow . . . 40
4.4.1 Semi-analytical methods . . . 41

5 Norwegian design principles 42
5.1 General . . . 42
5.2 Design features for unlined pressure tunnels . . . 43

5.3 The Norwegian Criterion for Confinement . . . 44
5.4 Limitations with analytical methods for final determination of hydropower schemes . . . 45
5.5 Further development of design principle . . . 47
5.5.1 Use of safety factor . . . 48
5.5.2 State-of-art criteria . . . 48
5.5.3 Development of a standardized, simplified hydraulic jacking test 49

6 Løkjelsvatn hydropower project 50
6.1 General . . . 50
6.2 Geology . . . 51
6.2.1 Regional geology . . . 51
6.2.2 Project geology . . . 52
6.2.3 Topography and weakness zones . . . 54
6.3 Rock stress measurements during construction by SINTEF . . . 56
6.4 Leakage during construction . . . 57
6.5 Description of test area . . . 57
6.5.1 Geology . . . 57
6.5.2 Rock mass classification based on the Q-system . . . 60
6.5.3 Rock mass classification based on GSI . . . 61

7 Laboratory examination 63
7.1 X-ray Powder Diffraction (XRD) . . . 63
7.1.1 Procedure . . . 64
7.1.2 Results . . . 64
7.2 Sonic velocity . . . 65
7.2.1 Procedure . . . 65
7.2.2 Results . . . 66
7.3 Uniaxial compressive strength test . . . 67
7.3.1 Procedure . . . 67
7.3.2 Results . . . 68
7.4 Acoustic emission . . . 69
7.4.1 Procedure . . . 69
7.4.2 Results . . . 69
7.5 Brazilian test . . . 71
7.5.1 Procedure . . . 71

7.5.2 Results . . . 72
7.6 Point load test . . . 73
7.6.1 Procedure . . . 73
7.6.2 Results . . . 73

8 Field measurements at Løkjelsvatn 75
8.1 3D Overcoring . . . 75
8.1.1 Setup and procedure . . . 75
8.1.2 Results . . . 75
8.2 Hydraulic fracturing . . . 76
8.2.1 Setup and procedure . . . 76
8.2.2 Results . . . 76
8.3 Hydraulic jacking . . . 77
8.3.1 Setup and test procedure . . . 77
8.3.2 Results . . . 78
8.3.3 Interpretation of results from RSRT . . . 79

9 Numerical modeling 83
9.1 Establishing input parameters for numerical modeling . . . 85
9.1.1 Stress conditions . . . 85
9.1.2 Hoek-Brown parameters . . . 86
9.1.3 Compressive strength . . . 86
9.1.4 Elastic parameters . . . 87
9.2 Step 1: In-situ stress model . . . 88
9.2.1 Results . . . 89
9.3 Step 2: Stress analysis on the pressurized tunnel/shaft . . . 90
9.3.1 Model geometry . . . 91
9.3.2 Results . . . 93

10 Assessment of hydraulic failure and leakage potential at Løkjelsvatn hydropower plant 96
10.1 Comparison with Norwegian criterion for confinement . . . 96
10.2 Comparison with suggested developments of the Norwegian confinement criteria . . . 98
10.3 Semi-analytical solution to estimate leakage potential . . . 99

11 Discussions 101

11.1 Assessment of common and future practice for the final design of hydropower plants . . . 101
11.1.1 Evaluation of past and present practice for design of Norwegian hydropower power plants . . . 101
11.1.2 Evaluation of Norwegian confinement criteria from Løkjelsvatn 102
11.1.3 Evaluation of results and experiences from RSRT as a tool for measuring rock stresses . . . 103
11.2 Assessment on hydraulic failure and leakage potential at Løkjelsvatn hydropower plant . . . 105
11.2.1 Evaluation of results from rock stress measurements . . . 105
11.2.2 Evaluation of calculated in-situ stresses from numerical modeling 106
11.2.3 Evaluation of leakage potential . . . 107
11.2.4 Evaluation of the leak potential from semi-analytical estimation 107
11.2.5 Uncertainties in leakage assessments . . . 108
11.2.6 Evaluation of topography and geological parameters . . . 109
11.3 Comparison with Norwegian failure and successful cases . . . 109

12 Conclusions and recommendations **111**
12.1 Conclusion . . . 111
12.2 Recommandations . . . 112

Bibliography **114**

Appendix **120**

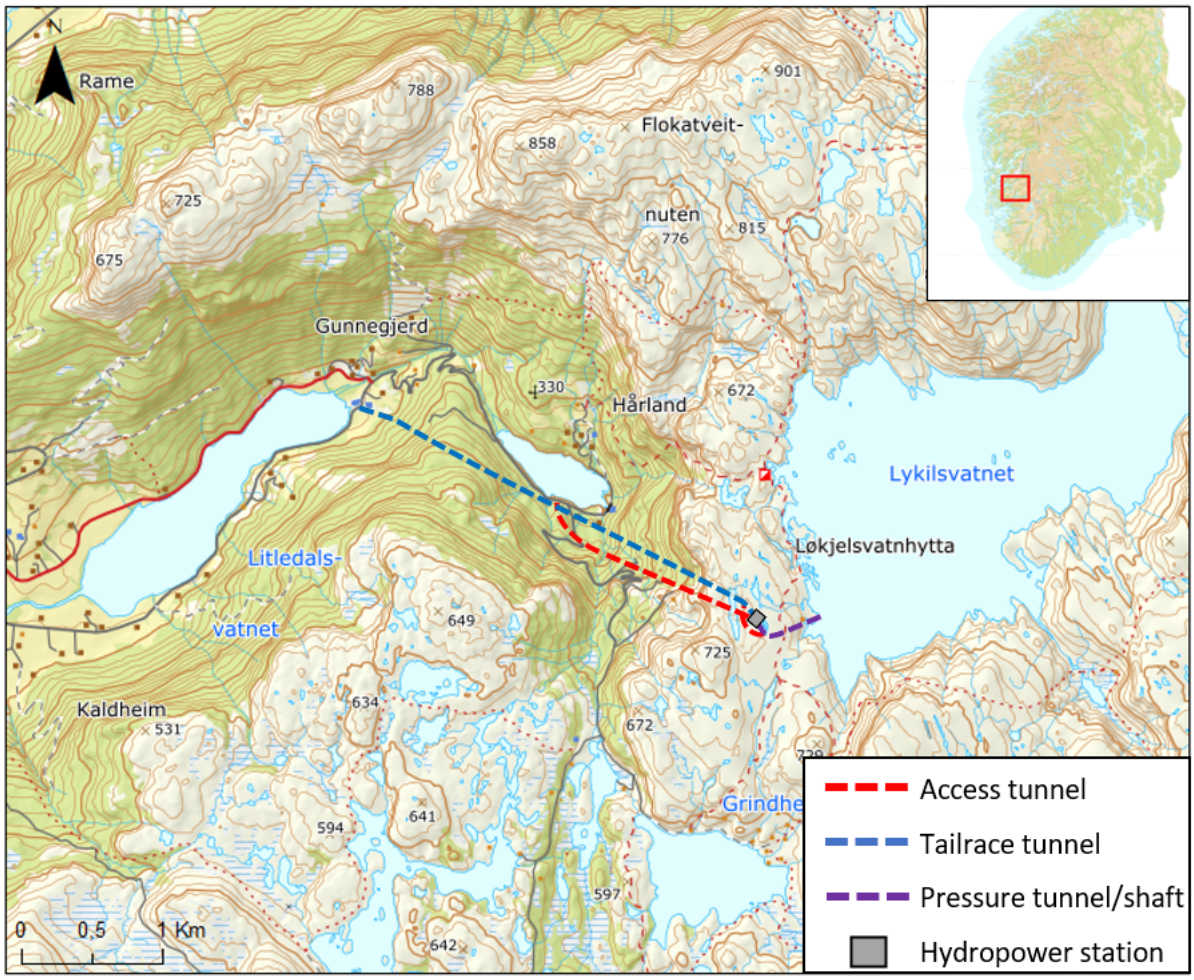
N
Rame
788
901
Flokatveit-
858
nuten
776
815
725
675
Gunnegjerd
330
Hårland
672
Lykilsvatnet
Løkjelsvatnhytta
Litledals-
vatnet
649
725
634
Kaldheim
531
672
641
594
597
642
0
0,5
1 Km
Access tunnel
Tailrace tunnel
Pressure tunnel/shaft
Hydropower station

Chapter 1

Introduction

1.1 Background

To meet climate changes, the world must reduce its dependency on fossil fuels. Emission from fossil energy sources is the dominant contributor to climate changes, accounting for around 60% of total global greenhouse gas emissions, while renewable energy only accounts for 17% of energy sources, (UN, 2021). In order to achieve the sustainable development goals, reduce climate changes and secure access to sustainable energy by 2030, a significantly larger share of energy must come from renewable energy sources such as hydropower, wind power, wave power, or solar power, (UN, 2021). In order to achieve this, hydropower will play a vital part.

In Norway, hydropower is the foundation of the power system and accounts for almost 90% of the total electricity production, (Ministry of Petroleum and Energy, 2021). In the early 1950s the large-scale development of hydropower begun. According to NVE (2021), there were at the beginning of 2021, 1 681 hydropower plants in Norway. In a typical year, Norwegian hydropower plants produce 136.4 TWh, which corresponds to 8 525 000 households, (Ministry of Petroleum and Energy, 2021; SSB, 2018). As can be seen in Figure 1.1, the total installed capacity at the end of 2020 was 33 055 MW. Today, most of the Norwegian hydropower plants have been complete. Still, smaller plants and upgrade of existing plants will enable additional capacity also in the future. The total amount of electricity produced by hydropower makes Norway one of the world's largest producers and an important contributor to ensure renewable energy for the world's population in the future.

There are several reasons why Norway has become a major player when it comes to hydropower development. Panthi (2014) highlights topographical and geographical advantages as decisive for this development. In some coastal areas, the amount of precipitation is between 1 000 to 3 000 mm pr. year. Besides, approximately 40% of Norway's total area is located above 600 MASL, (Panthi, 2014). Another advantage is that the Norwegian rock mass is considered *good*. From an international perspective, the Norwegian rock mass is described as a typical *hard-rock*-province with generally strong rock mass, (Broch, 2013).

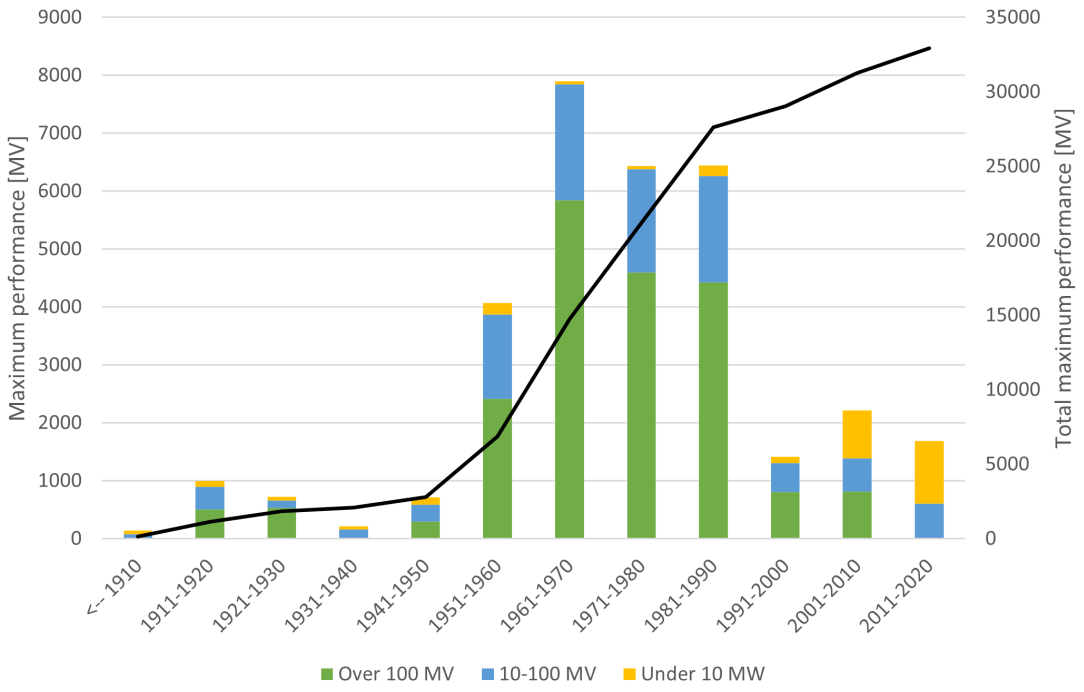

Figure 1.1: Hydropower development in Norway according to year of commissioning. Solid line represents total maximum performance, (NVE, 2021).

A strong rock mass helps to reduce the need for rock support when building waterways and tunnels. The generally good quality has led to the main design principle in the Norwegian hydropower projects, which is to treat the rock mass as a natural concrete mass that is able to absorb hydrostatic forces. Consequentially, unlined pressure shafts and tunnels have been the most common design principle since the 1960s, (Broch, 2013; Panthi, 2014). Palmström and Broch (2017) define the term *unlined tunnel* as "... a tunnel where the water is in direct contact with the rock or only limited parts of the tunnel are lined with concrete or shotcrete to protect against local tunnel collapses or major rock falls." The extensive use of this principle means that a significant proportion of the more than 4 000 km of waterway tunnels in Norway are built with minimal use of rock support, (Broch, 2013).

Although it is prevailing with unlined tunnels in Norway, it is common practice to encapsulate a few meters on the hydropower station's upstream side to lead the water into the hydropower station safely. As can be seen in the illustration of a typical hydropower scheme, which is presented in Figure 1.2, this area is called *transition zone*. However, it is desirable to reduce the length with steel or concrete lining for both cost and time-saving reasons, (Ødegaard and Nilsen, 2018). The transition between unlined and lined tunnel is considered the most critical area in the tunnel system. This is because the water reaches its maximum in this area, (Panthi and Basnet, 2018). Therefore, controlling the rock stresses in this area of the plant is considered a key factor. If the rock stresses are not sufficient, it can cause large costs and delays in the construction, (Ødegaard et al., 2020).

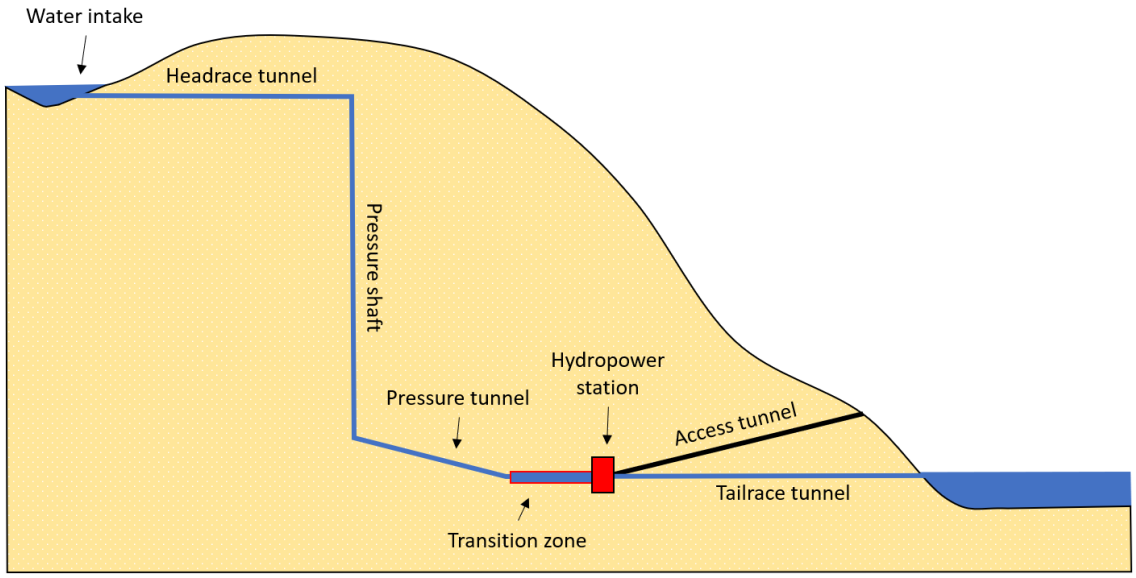

Figure 1.2: Illustration of a typical hydropower scheme with different parts in the plant.

Even though large-scale development of new Norwegian hydropower is completed, we will sill see smaller developments of hydropower in the years ahead. Besides, new knowledge and technological development contribute to a significant potential for upgrading and upscalling of excisting hydropower plants. A study of upgraded facilities after the year 2000 shows that the improvement in installed capacity is between 6% and 60%, with an average of 26%, (Lia et al., 2017). Upgrading of existing plants will be important to ensure security of supply from renewable energy in the future.

Løkjelsvatn hydropower plant is an example of a new power plant that increases the energy production. The plant is located in Etne municipality in Vestland county and is operated by Sunnhordaland Kraftlag (SKL). When the upgrade is completed, the Løkjelsvatn hydropower plant will produce 163 GWh by utilizing a 550 meter high waterfall (5.5 MPa). All together, the plants in the valley will provide 238 GWh, which the construction of Løkjelsvatn hydropower plant contributes to increase the total production by 20 GWh, (SKL, 2018).

Originally, the hydropower plant scheme was designed with longer unlined shaft and tunnels. However, during the construction period, rock stress measurements have shown that the magnitude of minimum principal stress is less than expected from a theoretical perspective. The lack of confinement pressure in the rock mass has forced the location of the hydropower station deeper into the rock mass to increase overall confinement pressure. The project must control the rock stresses. If not, unwanted hydraulic failure can lead to adverse events and even major disasters. The only way to verify rock stresses is by using stress measurements.

This thesis will study the project at Løkjelsvatn in more detail to assess whether there is a potential of hydraulic failure and extensive leakage based on empirical and semi-analytical approaches. As part of this work, the applicability of a newly developed rock stress measurement procedure will be tested.

1.2 Objectives and scope

This thesis is an extension of the Project work in the subject *TGB4570 - Engineering Geology, Specialization Project*, which was completed in the autumn semester of 2020. Through a literature study, the thesis focused on rock stresses and rock stress measurements. This master's thesis continues in the same direction but will look deeper into stress and leakage assessments for Løkjelsvatn hydropower plant to evaluate the potential for hydraulic failure and leakages from the unlined tunnel and shaft. The following summarizes the objectives and scopes:

- Theory review on the Norwegian design principle for unlined pressure tunnels used as waterways for hydropower projects. Review of rock engineering principles in the assessment of stress induced instabilities and leakage potential from hydropower tunnels.
- Theory review on different stress measurement methods practiced in hydropower sector, review geo-tectonic environment prevailing in Norway and in-situ rock stress situation with the highlight on horizontal stress variation within the country.
- Carry out laboratory assessment, describe the methodology for hydraulic fracturing, jacking, and fracturing test.
- Carry out comprehensive assessment and evaluation of the in-situ stress state at the case project area using test results, analytical and numerical solutions.
- Assess potential hydraulic jacking and leakage potential from the pressure tunnel of the case project.
- Discuss uncertainties associated with the estimation of minimum principal stress using in-situ tests and other theoretical methods.
- Conclude the work with recommendations.

1.3 Methodology

The methodology and structure of the thesis can be summarized as follows:

1. **Literature study**

   The literature is found from different sources. Oria, the search engine of the NTNU University Library, has been a helpful starting point for finding relevant sources. Furthermore, proceedings and publications from The Norwegian Tunneling Society (NFF) and the International Society for Rock Mechanics (ISRM) have been useful in the process. In addition, the author has received relevant articles from the supervisor, Professor Dr. Krishna Kanta Panthi, and PhD candidate Henki Ødegaard. The main topics of the literature study are:

   (a) Rock stresses and factors affecting the orientations and magnitudes.

   (b) Different stress measurement methods

   (c) Water in the rock mass

   (d) Design of Norwegian hydropower projects

2. **Study of Løkjelsvatn hydropower project**

   Information about the project has been collected through studies of available maps, illustrations, drawings, and reports. The results from the field mapping before the construction are collected in the detailed investigation report and carried out by SWECO (2017). This report has been the primary source when describing the project. In addition, engineering geological notes and field mapping from the tunnel contribute to the study.

3. **Field measurement at Løkjelsvatn**

   One of the main objectives of this thesis is to carry out field measurements at Løkjelsvatn, analyze and interpret the results. A Rapid Step-Rate Test (RSRT) proposed and described by PhD candidate Henki Ødegaard was tested in January 2021. The tests were carried out at the same time as engineering geological parameters were mapped. Besides, reports with data from previous rock stress measurements at Løkjelsvatn have been collected for comparison. Results from 3D overcoring and hydraulic fracturing at the planned transition zones have also been collected.

4. **Estimation of rock mass properties**

   Several samples were collected during field work in order to test the properties at the Rock Mechanics Laboratory in Trondheim. Further, the results were used in numerical assessments. The following tests were carried out:

   (a) UCS with Acoustic Emission sensors (AE)

   (b) Point load test

   (c) Brazil test

(d) XRD

(e) Sonic velocity test

5. Stress and leakage assessment

In order to assess the stress instability and leakage potential, different approaches and techniques have been performed. The different approaches have been listed below:

(a) Numerical: Finite element analysis with RS2. The principal stresses are calculated along the tunnel. Then, the results are compared and evaluated with measured stress values.

(b) Numerical: Finite element analysis with RS2. Study of the zone of interest around the pressurized tunnel

(c) Leakage assessment: A further developed semi-analytical equation proposed by Panthi (2006). The equation gives an estimation of leakage from unlined pressure tunnels and shafts.

(d) Analytical comparison with the Norwegian confinement criteria. Overburden criteria are evaluated.

6. Evaluating and assessing the results

1.4 Limitations

The main limitations to the analysis are related to assigning one Q-value for results of water inflow. In the assessment, it is assumed that the Q-values remain constant along the pressurized tunnel and shaft. The plant was inspected only once, which made it difficult to monitor the rock mass quality. In addition, the walls of the tunnel are almost completely covered with shotcrete, which makes mapping difficult. Ideally, the Q-values should be mapped continuously to identify variations.

Besides, the Q-system developed by the Norwegian Geotechnical Institute (NGI) is mainly intended for evaluating the rock mass for stability and the need for support and reinforcement. Therefore, other rock mass classification systems might be more suitable for comparing the water inflows.

As the final design of the system has been changed several times, there may be minor deviations. In the calculations, maps and reports were received from the contractor at the beginning of 2021. If changes have occurred after this, this has not been taken into account. Nevertheless, it is assumed that the calculation basis and the results provide a sufficient basis for assessing the general conditions.

Chapter 2

Rock stresses

In the literature, rock stresses can be divided into two main groups: *in-situ* and *induced stresses*, (Amadei and Stephansson, 1997). In-situ stresses are the naturally occurring stresses in the rock mass. In contrast to in-situ stresses, induced stresses or secondary stresses, occurs in the rock mass when changing the natural conditions. In the following, basic theory of stresses in rock will be presented.

2.1 Basic theory

The understanding of stress is fundamental to rock mechanics principles and applications. Stresses, denoted by σ, occur when a material is affected by external forces. As seen in Equation 2.1, the term *stress* is defined as force (F) pr. area (A). In rock mechanics, the basic principle is that a system (e.g. a rock mass or a rock sample) responds to stress by changing in volume or form. The change in volume or form due to applied stress is called *strain*, denoted by ϵ, (Hudson and Harrison, 1997).

$$\Delta\sigma = \lim_{\Delta A \to 0} \frac{\Delta F}{\Delta A} \tag{2.1}$$

Stress is a force characterized with both magnitude and orientation. The stress acting on an arbitrary plane can be decomposed into two components, a vertical and a horizontal component. These components constitute respectively the normal (σ_n) and shear stresses (τ) of the stress acting on the plane. This is exemplified in Figure 2.1.

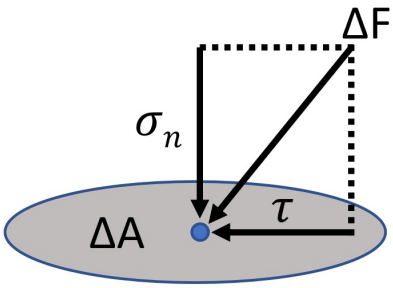

Figure 2.1: Normal and shear stresses as a function of the force, F, acting on a surface with area, A. Modified after Li (2018).

The most common way to describe the stress state for any point in the rock mass is to use an enclosing volume element with reference to a given set of axes, as shown in Figure 2.2. The volume element can be oriented so that the shear stresses on every surface become zero, (Hudson et al., 2003). With this orientation, the normal stresses will constitute the principal stresses acting on the volume element. In 3D, these three components are considered as major (σ_1), intermediate (σ_2) and minor principal stress (σ_3). Therefore, the stress state at any point in the rock mass is determined by the orientation and magnitude of these three principle stresses, (Hudson et al., 2003).

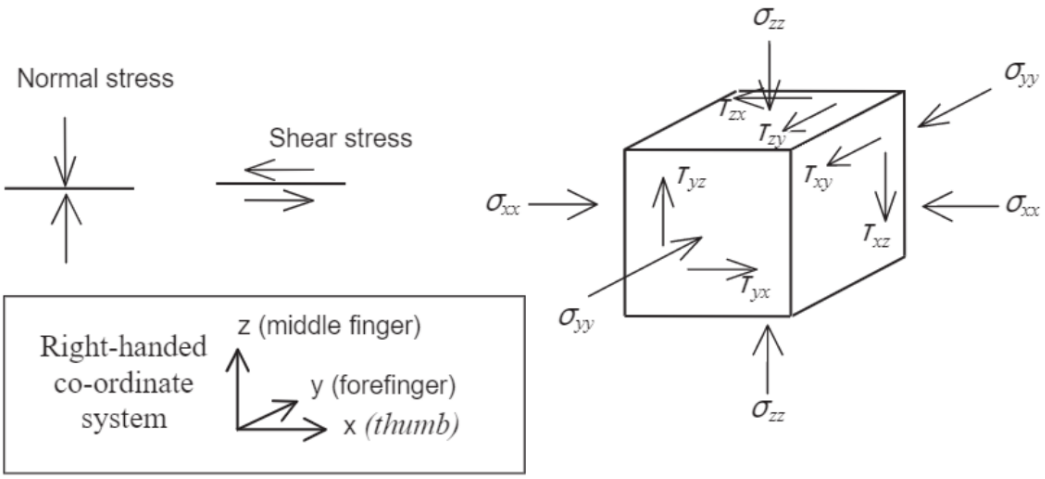

Figure 2.2: The normal and shear stress components on an infinitesimal cube in the rock mass with reference to given set of axes, x-y-z, (Hudson et al., 2003).

2.2 In-situ rock stresses

According to a division provided by Amadei and Stephansson (1997), in-situ stresses in the rock mass, are a sum of four components: *gravitational*, *tectonic*, *residual*, and *terrestrial stresses*. Each of these components contributes to the magnitude of the stresses in a given point. This section will present these types of in-situ rock stresses.

2.2.1 Gravitational stresses

The gravitational stress, denoted by σ_v, is a result of gravity and the weight of the overlying rock mass, (Amadei and Stephansson, 1997). It is common practice when calculating the distribution of stresses to assume that the vertical stress component increases linearly with the depth (z):

$$\sigma_v = \gamma_{rock} \cdot z \tag{2.2}$$

where γ_{rock} represents the specific gravity of the overlying rock mass.

There is some evidence to suggest that the rock mass's unit weight varies between 0.025 and 0.033 MPa/m, (Amadei and Stephansson, 1997). In Figure 2.3a, the vertical stress component is plotted against the depth with data from several measuring points worldwide. The graph shows that a gradient equal to 0.027 MPa/m provides a sufficient adaptation to the measurements, (Brown and Hoek, 1978).

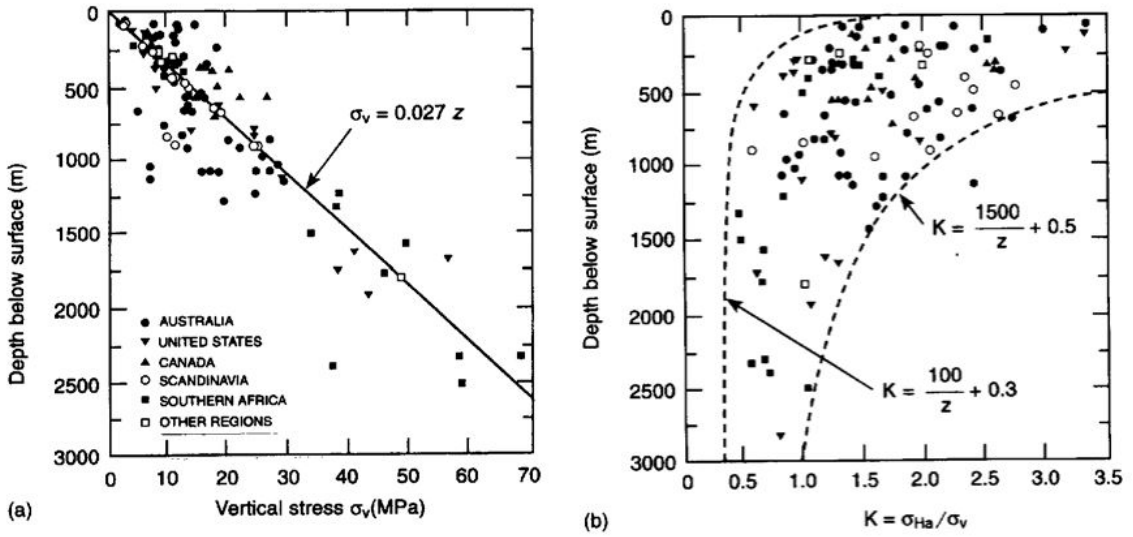

Figure 2.3: (a) Depth plotted against vertical stress for a series of measurements around the world. (b) Variation of average horizontal to vertical stress ratio with depth. Modified after Brown and Hoek (1978).

Experience has provided evidence of how gravity affects the vertical stress component, (Brown and Hoek, 1978). In the same way that weight affects the vertical stress component, gravity affects the horizontal stress conditions. Horizontal stresses occur due to prevented volume expansion. Hooke's law of elasticity for three dimensions describes the relationship between the minor horizontal (σ_h) and vertical stress components as shown in Equation 2.3, (Hudson and Harrison, 1997).

$$\sigma_h = \frac{\nu}{1-\nu} \cdot \sigma_v \tag{2.3}$$

where ν represents Poisson's ratio. According to Li (2018), Poisson's ratio is typically 0.25 or lower for common Norwegian rocks like gneisses and granites. Consequently, the gravitational contribution to the minor horizontal stress is theoretically 1/3 of the vertical stress. On the other hand, in areas with tectonic activities, it is common to include a tectonic component in horizontal stress calculations. The magnitude of the minor horizontal stress is unknown and may be expressed by the following equation, (Panthi, 2012b):

$$\sigma_h = \frac{\nu}{1-\nu} \cdot \sigma_v + \sigma_{tec} \tag{2.4}$$

where σ_{tec} is a tectonic component and represents locked-in stress due to tectonic activities. The magnitude of this component varies and depends on geographical location, geological environment, and distance to fault systems, (Panthi, 2012b).

As shown in Figure 2.3b, the ratio between horizontal and vertical stresses (K-value) is mostly greater than 0 for shallow depths. This ratio is typically in Scandinavia, and in some places, it has been measured very high horizontal stresses close to the surface, (Myrvang, 2002). According to Li (2018), this deviation from elasticity theory is due to geological, topographical, and/or tectonic phenomena.

2.2.2 Tectonic stresses

Tectonic stresses are generally understood to deal with relative displacement between tectonic plates. These stresses occurs when the displacement of the tectonic plates subjects the Earth's crust to tectonic forces. Amadei and Stephansson (1997) consider tectonic stresses to be either *active* or *passive*. The active stresses are due to current tectonic activity. By comparison, the passive tectonic stresses results from tectonic activity in the past. If the stresses applied are high enough, fractures, cracks and faults can develop in the rock mass, (Hudson and Harrison, 1997).

Zoback et al. (1989) state various origin to tectonic mechanisms for high horizontal stresses. Based on the collection of data, different mechanisms were categorized and presented in Figure 2.4. According to Amadei and Stephansson (1997), there are two main groups of active tectonic stresses: local stresses and regional forces. These broad-scale forces occur related to the displacement in and around plate boundaries (points 1-4 in Figure 2.4). On the other hand, the local stresses are related to deflection forces, isostatic compensation, and deflection of the seabed surface (points 5-7 in Figure 2.4).

2.2.3 Residual stresses

Nilsen and Palmstrøm (2000) use the term *residual stresses* about stresses that have been locked into the rock material during earlier geological events. A typical example is stresses caused by contraction during cooling of rock melt. To illustrate

this effect, by cooling quartzitic magma from 300 °C to 0 °C, it has been shown under ideal conditions that it is possible to obtain stresses in the order of 23 MPa, (Savage, 1978).

Cooling in granitic intrusions might be the reason why it is measured high horizontal stresses in the Oslo region, (Nilsen, 2016). The region consists of a host of igneous rocks, like different types of granites. On the other hand, in some areas, deviating values of vertical stresses have been measured. Nilsen (2016) points out deglaciation as a possible explanation to explain this discrepancy. This phenomenon may occur in localities where erosion happens faster than adaptation in rock masses.

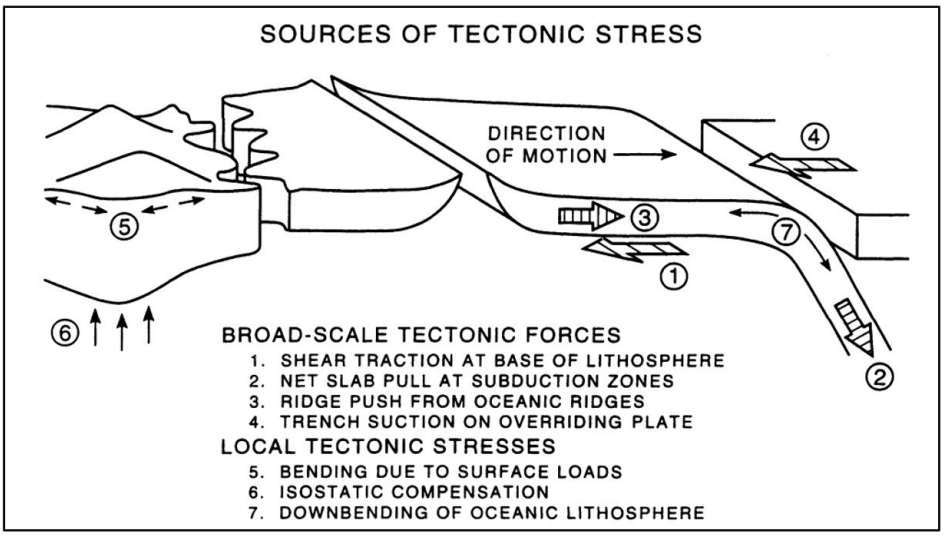

Figure 2.4: The categorized tectonic forces that are responsible for tectonic stresses, (Zoback et al., 1989).

2.2.4 Terrestrial stresses

The final category of in-situ stresses is terrestrial stresses. Terrestrial stresses are induced by diurnal and seasonal variations of temperatures, moon pull, and the Coriolis force, (Hudson and Harrison, 1997). According to Amadei and Stephansson (1997), these effects are often neglected. However, in some cases, terrestrial stresses can affect the measurement results, especially at shallow to very shallow depths. Hooker and Duvall (1971) exemplify this by studies of the San Andreas Fault. The study showed that near-surface stresses are affected by temperature differences. This effect gradually decreases by the depth and can be neglected at depths greater than 10 m.

2.3 Factors affecting in-situ rock stress

In many cases, it is practical when dealing with simple engineering geological problems to assume that the rock mass is continuous, homogeneous, isotropic, and linear-elastic. In reality, the rock mass is rarity ideal. Therefore, it is difficult to calculate the exact stress conditions in the rock mass, (Hudson and Harrison, 1997). Consequentially, it is essential to know which effects can affect the in-situ stress state. This section presents various factors that can affect the in-situ stress state and which, in some cases, can explain the reason for some discrepancies between theoretically and measured stress levels.

2.3.1 Anisotropy and schistosity

A rock mass is anisotropic if the properties varies in different directions, (Amadei and Stephansson, 1997). According to Nilsen and Palmstrøm (2000), anisotropic properties depend on the mineral composition, fracture conditions, schistosity, foliation, and bedding. For instance, mica and chlorite minerals, amphiboles, and some pyroxenes affect the anisotropic properties of the rock mass. Bedded and schistose rocks, such as schist, shale, and phyllite, have anisotropic properties. Amadei et al. (1987) claim that most of the rock mass near the earth's surface has anisotropic properties due to various sedimentation, tectonic activity, weathering, and metamorphism. The effect decreases with depth due to increasing pressure and temperature, (Amadei and Stephansson, 1997).

A model developed by Amadei et al. (1987) shows that anisotropic conditions in the rock mass affect the stress field of the gravitational stresses. Only the strength and orientation of the horizontal stress components are dependent by the anisotropy in the rock mass. On the other hand, the vertical stress component is unaffected by anisotropic conditions.

The degree of anisotropy affects the strength of the rock sample, (Panthi, 2006). As can be seen in Figure 2.5, there is an difference between compressive strength measured on cores drilled parallel and normal to the schistosity plane. The strength of intact rock specimens is minimum when the schistocity plane is inclined approximately 30° from the direction of loading ($\beta = 30°$C), and maximum when the schistocity plane is perpendicular to the direction of loading ($\beta = 0°$), (Panthi, 2006). A ratio of more than 2.5 between maximum and minimum uniaxial compressive strength has been measured in some anisotropic samples. On the other hand, some metamorphic rocks, such as quartzite and gneiss, have almost isotropic properties. Consequentally, the ratio is approximately 1, (Nilsen and Palmstrøm, 2000).

The point load test is an realible test to indicate the degree of anisotropy. The point load test measures induced tensional strength and gives the maximum strength at a loading direction normal to the plane of schistocity and a minimum strength parallel to the schistosity plane. Table 2.1 classifies different rock types based on the strength anisotropy index, I_a.

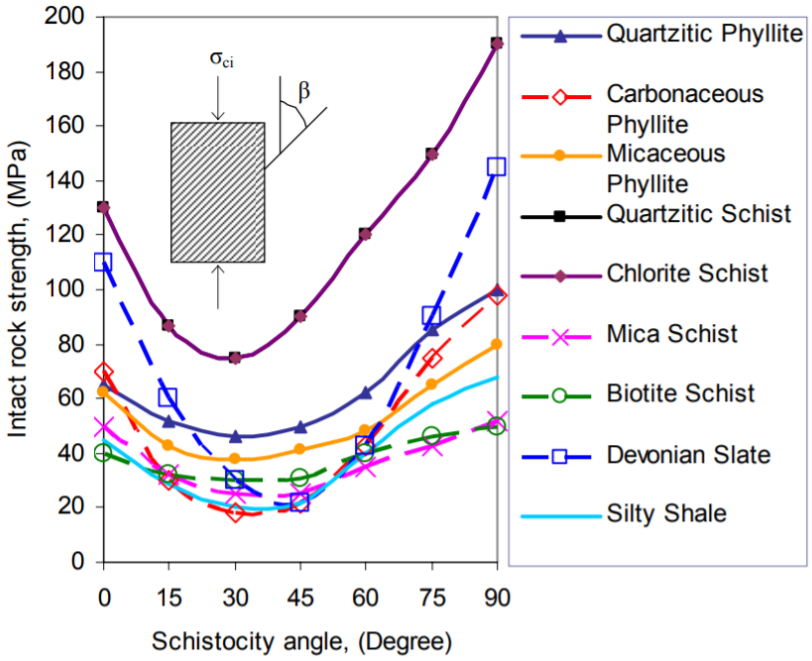

Figure 2.5: Uniaxial compressive strength at different angle of schistocity plane, Panthi (2006).

2.3.2 Inhomogenities and geological structures

Variations in the geology in the rock mass, different types of geological structures and inhomogeneities might affect the distribution and magnitude of in situ stresses, (Hudson and Harrison, 1997). Variations like discontinuities, dikes, layers of sedimentary rocks and ore bodies are typical examples of inhomogeneities, (Li, 2018). As a result of the variation in composition, both the principal stress components' magnitude and orientations may be affected. According to Amadei and Stephansson (1997), the changes is due to changes in stiffness that can be explained by the E-modulus.

In areas where the E-modulus varies, peak values of stresses occur in areas with the largest E-modulus. According to Li (2018), varying stress fields and stress jumps have been observed close to inhomogeneities. An example of the influence of stiffness is given by Martin and Chandler (1993). The experiment was based on a significant number of rock stress measurements in an approximately homogeneous pluton. The results indicate variations in magnitude and direction of the stresses within a relatively small area.

Table 2.1: Classification of rock strength anisotropy, Panthi (2006).

Class	Descriptive class	Strength anisotropy index (I_a)	Typical rock types
I	Isotropic or close to isotropic	1.0 – 1.2	Rocks having platy/prismatic minerals <10% with shape factors 2 and platy minerals in random orientation. *Rock types: Most of the igneous rocks and very high grade metamorphic rocks, i.e. diorite, granite, gabbro, quartzite, granitic gneiss, granulite etc.*
II	Slightly anisotropic	1.2 – 1.5	Rocks having platy/prismatic minerals 10–20% with shape factors 2-4 and platy minerals in compositional layering. *Rock types: High grade metamorphic rocks and some strong sedimentary rock, i.e. quartz-feldspatic gneiss, marble, migmatite, sandstone, limestone, etc.*
III	Moderately anisotropic	1.5 – 2.5	Rocks having platy/prismatic minerals 20–40% with shape factors 4-8 and foliation plane distinctly visible. *Rock Types: Medium-high grade metamorphic rocks, i.e. mica gneiss, quartzitic schist, mica schist, biotite schist, etc.*
IV	Highly anisotropic	2.5 – 4.0	Rocks having platy/prismatic minerals 40–60% with shape factors 8-12 and very closely foliated. *Rock Types: Low - medium grade metamorphic rocks such as phyllite, silty slate, etc.*
V	Extremely anisotropic	>4.0	Rocks having platy/prismatic minerals > 60% with shape factors >12 and fissile rocks. *Rock Types: Low grade metamorphic and argillaceous sedimentary rock, i.e. slate, carbonaceous phyllite, shale, etc.*

2.3.3 Discontinuities

A discontinuity is a structural or geological feature that changes the homogeneity in the rock mass. Nilsen and Palmstrøm (2000) describe discontinuities as "[...] the general term for any mechanical discontinuities in a rock having zero or close to zero tensile strength." The size of discontinuities might vary from structures of up to several kilometers in extend down to a few centimeters. According to Hudson and Harrison (1997), discontinuities is caused by mechanical, termic or chemical processes. These events might have occured at different times in a geological perspective. Panthi (2006) claims that movement in the rock mass caused by geological events is the main source of discontinuities.

According to Hudson and Harrison (1997), the discontinuities are possibly the single most important factor governing the mechanical properties of the rock mass in an engineering perspective. Similar, it will change the orientation of the stress trajectories. The stress field will reflect the geometry of the discontinuity. Amadei and Stephansson (1997) divide stress changes close to discontinuities in three main types based on the relative stiffness of the discontinuity compared to the rock mass:

1. If the discontinuity is open, the major principal stress is diverted parallel to the discontinuity as shown in Figure 2.6.

2. If the discontinuity is made of a material with similar properties as the surrounding rock, the principal stresses are unaffected.

3. If the material in the discontinuity is rigid, the major principal stress is diverted perpendicular to the discontinuity. In general, geological structures and heterogeneities disturb the regional stress field and make the local stress field quite different from the regional stress field.

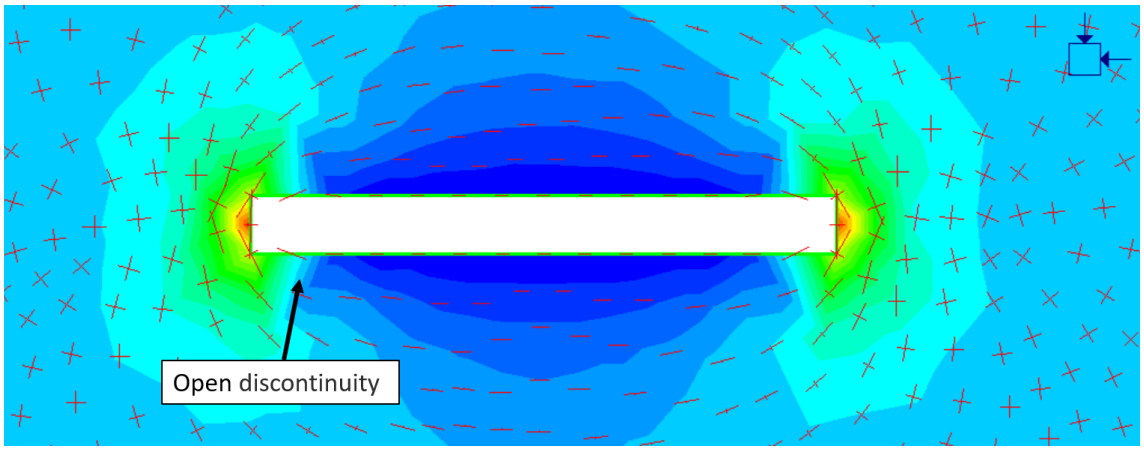

Figure 2.6: Illustration of how an open discontinuity affects the direction of stress trajectories in isotropic stress state.

2.3.4 Geological structures

Like heterogeneities and discontinuities, geological structures affect the stress conditions in the rock mass. Rock stress measurements have shown that geological structures at different scales (from micro to regional) can disturb the in-situ stress state, (Amadei and Stephansson, 1997). The driving forces are tectonic forces as presented in Section 2.2.2. Tectonic forces can contribute to the development of folds at all levels up to the regional level. These fold-induced stresses can develop to a level so high that new joints or faults occur, (Li, 2018).

According to Stephansson et al. (1991), faults will generate stress concentration at the contact point between the blocks in the fault and stress refraction developing adjacent to the fault. In these cases, the principal stresses will be located perpendicular to and parallel with the fault, (Li, 2018). During the development of a fold, the lithosphere will be compressed, (Amadei and Stephansson, 1997). As can be seen in figure Figure 2.7, the compression leads to increased and decreased stress concentration at the same time. Folds create both compressive and tensiles stresses in foldings, (Li, 2018).

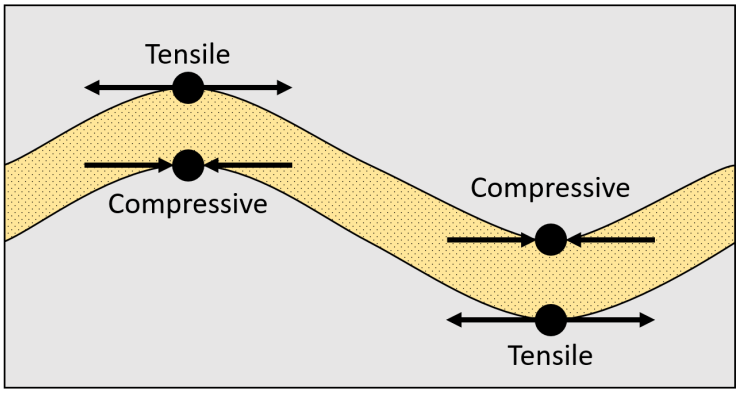

Figure 2.7: Compressive and tensile stresses in folds. Based on Li (2018).

2.3.5 Topographic stresses

As described in Section 2.2.1, the overlying rock's weight affects the magnitude of the horizontal component. Equation 2.3 demands a stress situation where the shear stresses are not present. However, when the surface consists of unevenness like valleys and mountains, an imbalance in the stress situation occurs, (Li, 2018). This effect is illustrated in Figure 2.8. The reason why the effect occurs is the boundary conditions in the layer between the free surface and the rock mass. There are no shear forces at the point of contact between air and rock mass. Consequently, one of the principal stresses directions must be parallel to the valley side, (Li, 2018).

One of the first attempts to describe topography's influence on the stresses is found in Nilsen (1979). The method in the thesis considers a section of the valley side in 2D. The results show that the major principal stress is oriented approximately parallel to the valley, and the minor principal stress is oriented normal to the surface side, (Nilsen, 1979).

The disadvantage of 2D consideration is that it is not possible to include variations along the valley. However, more powerful computers and newly developed software programs enable 3D-analysis. Ziegler et al. (2016) conducted a 3D-analysis of the in-situ stress condition in an area in Switzerland. In many ways, the topography in Switzerland is similar Norway. The model showed some variation in the results compared with observations and measurements in the field. Nevertheless, the computed directions of the major principal stress component follow the spalling direction in the valleys.

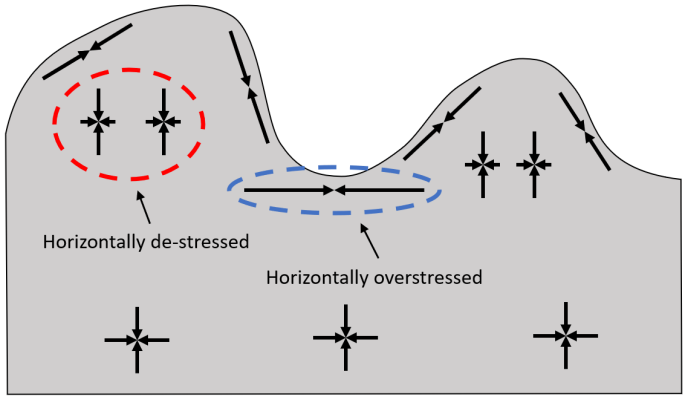

Figure 2.8: Orientation of principal stress indicated by crosses in an area with mountains and valleys. Based on Li (2018)

2.4 Induced stresses

After excavation of an underground opening, the in-situ stresses in the rock mass are disturbed. Heidbach et al. (2016) denote that induced stress "... is disturbed due to man-made changes in the underground or loads on the surface such as impoundment, drilling, tunnelling, mining, fluid stimulation, reservoir depletion, re-injection of waste water." As a result, stresses are redistributed along the periphery of the excavation.

In idealized situations, where a circular opening (with radius r) in an elastic material with isostatic stress conditions ($\sigma_h = \sigma_v = \sigma$) is excavated, the redistribution of stress in a given point at a distance, a, with angle θ from the horizontal, might expressed by Kirsch equations (Equation 2.5, 2.6 and 2.7) and this formed the basis for many early studies of rock behavior around tunnels and shafts, (Hoek, 2007).

$$\sigma_r = \frac{\sigma_1 + \sigma_3}{2} \cdot (1 - \frac{a^2}{r^2}) + \frac{\sigma_1 - \sigma_3}{2} \cdot (1 - \frac{4a^2}{r^2} + \frac{3a^2}{r^4}) \cdot \cos 2\theta \tag{2.5}$$

$$\sigma_\theta = \frac{\sigma_1 + \sigma_3}{2} \cdot (1 + \frac{a^2}{r^2}) - \frac{\sigma_1 - \sigma_3}{2} \cdot (1 + \frac{3a^2}{r^4}) \cdot \cos 2\theta \tag{2.6}$$

$$\tau_{r\theta} = \frac{\sigma_1 - \sigma_3}{2} \cdot (1 + \frac{2a^3}{r^2} - \frac{3a^4}{r^4}) \cdot \sin 2\theta \tag{2.7}$$

where σ_r represents the radial stresses and σ_θ is the tangential stresses, while $\tau_{r\theta}$ represents the shear stresses in the given point. The parameters in Kirsch equations depends on the ratio a/r. The stresses normalize as the ratio between radial distance (a) and opening radius (r) increases significantly. As shown in Figure 2.9, the stress components vary along the periphery in cases where $r = a$.

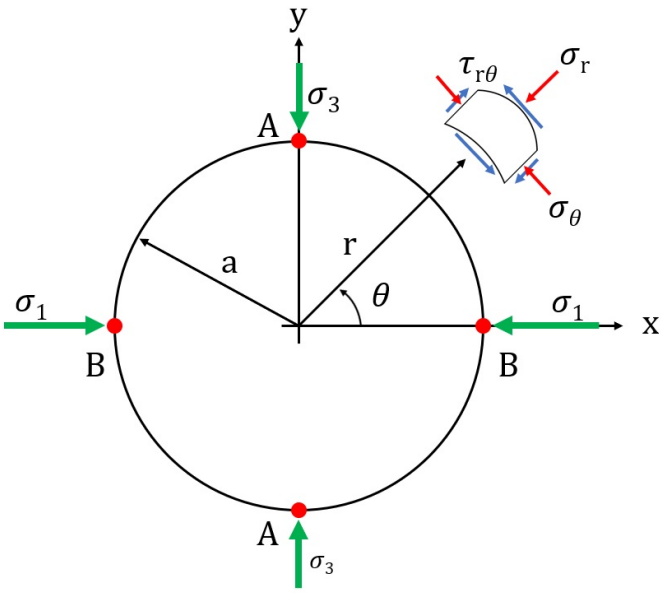

Figure 2.9: Stress components at the periphery of a circular opening with parameters in Kirsch equations. Modified after Li (2018).

2.4.1 Rock stress redistribution around a tunnel

After excavation of an underground opening, the stresses are redistributed along the periphery of the excavation. This zone is referred to as the *stress-distribution zone* (SRZ), (Basnet and Panthi, 2019). The extent of the zone depends on the excavation technique, the quality of the rock mass, and the ratio between the major and minor principal stress, (Li, 2018). According to Nilsen and Palmstrøm (2000), the stresses will stabilize at a constant level at a distance from the tunnel contour corresponding to approximately half the tunnel width. The redistribution of stresses around a circular opening in an elastic material in isostatic stress conditions may be expressed as shown in Figure 2.10, (Panthi, 2006).

The stress conditions are seldom isostatic. Thus, different magnitude of major principal stress and minor principal stress give variation in the magnitude of tangential stresses, (Li, 2018). Based on Figure 2.9, maximum and minimum tangential stresses occur when $\theta = 0°$ or $90°$. The actual values will be as follows:

$$\sigma_{\theta,max} = 3\sigma_1 - \sigma_3 \tag{2.8}$$

$$\sigma_{\theta,min} = 3\sigma_3 - \sigma_1 \tag{2.9}$$

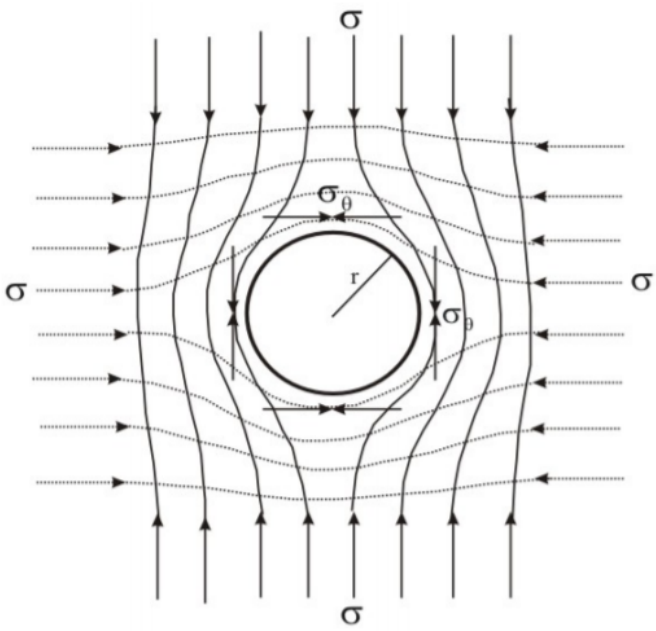

Figure 2.10: Stress trajectories in rock mass surrounding a circular opening, (Panthi, 2006)

Equation 2.8 and 2.9 can be used to indicate the development of the stability of boreholes. If the minimum tangential stress component is less than zero, the tensile fracture will develop parallel with the largest major stress component. On the other hand, breakout failure occurs if the maximum tangential stress component exceeds the uniaxial compressive strength of the rock mass, (Li, 2018).

2.4.2 Stress induced instability in strong and isotropic rock masses

The stability of underground excavations depends both on the strength of the rock mass and the stresses induced in this rock. The induced stresses are a function of the shape of the excavation and the in-situ stresses, (Hoek, 2007). According to Nilsen and Palmstrøm (2000), there are mainly two forms of instability caused by induced stresses: 1) *Rock burst or rock spalling*, and 2) *Tunnel squeezing or deformation*. These form for instabilities are generally caused by induced stresses exceeding the rock mass strength, (Hoek, 2007).

Fracturing occuring parallell to the tunnel periphere is called rock spalling and normally occures in strong and brittle rock masses, (Nilsen and Palmstrøm, 2000). The failure may occur gradually and manifest itself as spalling or slabbing or it may occur explosive in the form of a rock burst. Hoek (2007) defines rock burst as "... explosive failures of rock which occur when very high stress concentrations are induced around underground openings." This fracturing process might be accompanied with vibrations and loud noises, (Hoek, 2007). According to Panthi (2006), rock burst or spalling might occur in cases where the ratio between maximum tangential stress and the rock mass strength exceeds 50%.

2.4.3 Stress induced instability in weak and anisotropic rock masses

Equation 2.5 to 2.9 are simplified and are only describing idealized conditions. In cases where the rock mass is inhomogeneous and anisotropic with plastic behaviour, the equations are not valid anymore, (Panthi, 2006). In weak and anisotropic rock masses such as shales, mudstones, stiltsones, phyllites and tuffs, the maximum tangential stresses are moved further into the rock mass until the elastic zone is reached, (Hoek, 2007). This is due to reduced strength in the rock mass and leads to a fractured zone around the opening. As a result, reduced strength in the rock mass forms a plastic zone where micro-fractured rock mass formed deeply into the walls as an be seen in Figure 2.11, (Panthi, 2006).

Squeezing or deformation might occur in weak rocks like shale, slates and phyllites, and weakness or fracture zones. Common to these rocks is that they either have anisotropic or low strength properties. Squeezing occurs when the strength is less than induced tangential stresses along the periphery. It takes place as a gradual formation of micro-cracks along the schistocity or foliation plane, (Panthi, 2012a). This leads to a visco-plastic zone of micro-fractured around the excavated area and the maximum tangential stresses are moved beyond the plastic zone and into the rock mass, (Panthi, 2006).

Plastic deformation is known to be time depended. This type of deformation starts before and immediately after the excavation, and continues even after the rock support has been applied in some cases, (Hoek and Marinos, 2000). Over time, this will provide build up pressure in the rock support. In some cases, temporary support has failed to avoid deformation and failure in weak rock masses, (Panthi, 2006).

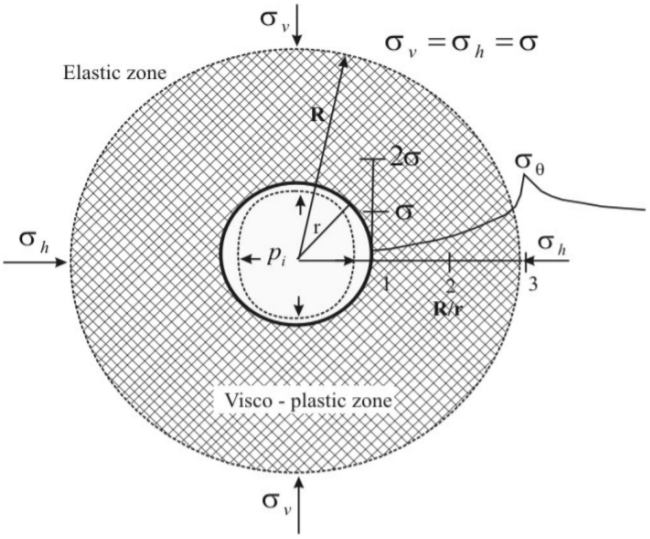

Figure 2.11: An illustration of the visco-plastic zone around a circular tunnel with radius, R, (Panthi, 2006).

2.4.4 Stresses around circular openings related to hydropower projects

To make tunnels water-tight play an important role in improving the stability and safety of underground installations. In unlined tunnels or shafts, the rock mass is exposed to water pressure, P_w, equivalent to the hydrostatic pressure (H). According to Hartmaier et al. (1998), the main phenomena that are likely to happen in the rock mass around an unlined tunnel/shaft due to water pressure is hydraulic failure, such as hydraulic fracturing and/or hydraulic jacking and/or water leakage.

Hydraulic fracturing occurs in intact or rock masses with relatively few existing joints or fractures. This occurs in cases where the water pressure is higher than both minimum tangential stresses and the tensile strength, (σ_t), (Haimson and Cornet, 2003). The fracture will propagate from the tunnel periphery into the rock mass. Once the fracture is propagated beyond SRZ, the water pressure has to exceed minimum principle stress and tensile strength to propagate further, (Basnet and Panthi, 2019).

On the other hand, hydraulic jacking will occur if the rock mass consist of existing fractures or joints. The joint is mechanically jacked if the water pressure exceeds the minimum tangential stress around the tunnel inside the SRZ. Similar to hydraulic fracturing, there is a difference in opening criteria depending on whether the fracture is outside or inside the SRZ. Outside of the SRZ, hydraulic jacking is continued if the water pressure is only the stress acting normal to the joints. Figure 2.12 shows hydraulic fracturing/jacking under idealized conditions.

The main differences between hydraulic fracturing and hydraulic jacking is highlighted in Table 2.2. The table shows that if the water pressure is less than the minimum main stress, the rock mass is safe against hydraulic jacking. Similarly, the tunnel will be safe against hydraulic fracturing if it is safe against hydraulic jacking, (Basnet and Panthi, 2019). Hence, it is of great interest to know magnitude of the minor principle stress.

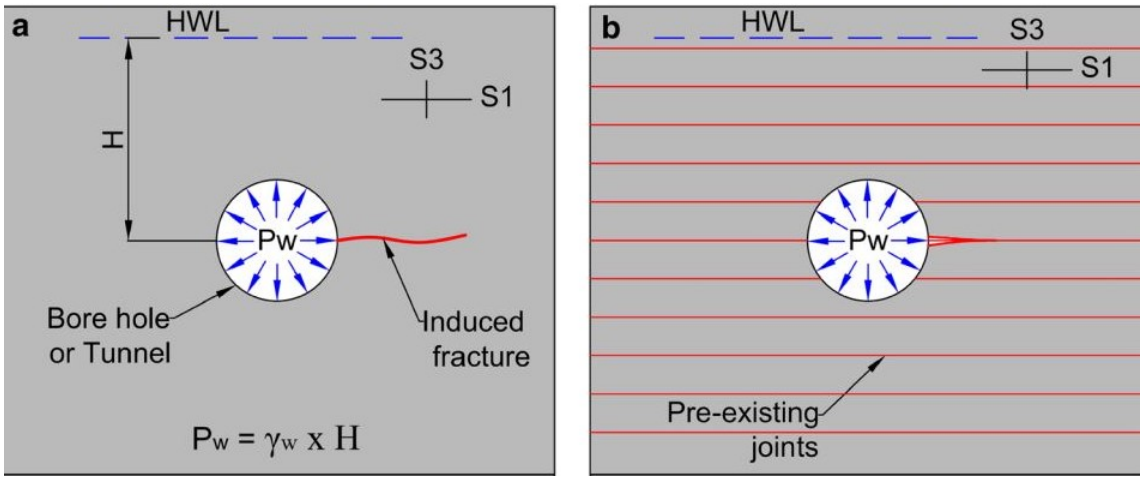

Figure 2.12: Illustration showing how hydraulic fracturing (a) and hydraulic jacking (b) develop with water pressure under idealized conditions. Modified after Basnet and Panthi (2019).

Table 2.2: Required pressure for hydraulic failure, (Basnet and Panthi, 2019).

Location	Pressure at failure	
	Hydraulic fracturing (P_f)	Hydraulic jacking (P_r)
At tunnel periphery	$^*\sigma_{\theta,min} + \sigma_t$	$^*\sigma_{\theta,min}$
Outside SRZ	$\sigma_3 + \sigma_t$	σ_3

$^*\sigma_{\theta,min}$=3σ_3-σ_1

2.5 Stresses in Norway

Over several decades, stress measurements in Norway show that the vertical stresses correspond largely to the theoretically calculated stresses, (Roberts and Myrvang, 2004). On the other hand, the horizontal stresses deviate from the theoretical ones. The deviation in the horizontal stresses is most prominent in Precambrian rocks and Permian intrusives in the Oslo field.

Arne Myrvang, a former professor at NTNU, summed up the in-situ stress trends in Norway at an annual conference organized by The Norwegian Tunneling Society (NFF) in 2002, (Myrvang, 2002):

1. The gravitational stress component matches well with the theoretical ones.
2. The measured horizontal stresses are almost always deviating from the theoretical ones. In Norway and Scandinavia in general, the major principle stress is almost always horizontal. This is exemplified in northwestern parts of Norway and some parts of the Precambrian bedrock in northern parts of Norway, where the major principle is significant.
3. In many cases, high stresses in the horizontal plane can also be found at shallow depths. This results in a high K-value.

Roberts and Myrvang (2004) point out that the vertical stresses match well with the theoretical ones. In combination with challenging topography, especially in western parts of Norway, high horizontal stresses are advantageous for the tunnel's stability. However, in worst case, low horizontal stresses can lead to collapse without extensive use of rock support. In such cases, the costs in the project increase significantly, (Nilsen, 2016).

Myrvang (2002) claims that the "ridge push" from the Mid-Atlantic Ridge as described in Section 2.2.2 is the main mechanism to the high horizontal stresses in some parts of Norway. Simonsen (2018) studied rock stress measurements in Norway from the beginning of the 1990s until 2018. The thesis reaches the conclusion that the average ratio between $\sigma_H/\sigma_v = 1,2$ in Norway. In addition, 64% of all data could either be categorized as reverse or lateral faults based on stress directions, which indicates that the major principal stress is horizontal.

The orientation of the in-situ horizontal stresses on the mainland in Norway is highlighted in Figure 2.13. The material was collected and studied through PhDs from NTNU in the late 1990s. Hanssen (1997) studied the field of tension on land, while Fejerskov (1996) looked more closely at the Norwegian continental shelf. Fejerskov divided the area of interest into four regions: the Barents Sea, the Norwegian Sea, and the northern and southern parts of the North Sea. Several hundred boreholes from Norwegian, British, and Danish petroleum activity were studied. The orientation to the major horizontal stress component, σ_H, was estimated based on observed fractures along the boreholes. When compared with Hanssen's results, there is a clear connection between divided regions and similar areas onshore, (Fejerskov, 1996).

In northern Norway, the major horizontal stress component is oriented towards N to S. In Central Norway, the orientation is proximate more W/NW to E/NE. The orientation is towards NW-SE in western parts of Norway. There is a secondary but less prominent tendency in the same region, where the orientation is N/NE to S/SW. In this context, Roberts and Myrvang (2004) conclude that the Møre-Trøndelag fault separates Central Norway and Western Norway. The reorientation from N to S, to N/NE to S/SW may be due to "ridge push" at the Mid-Atlantic plate, but other factors may also affect development, (Fejerskov and Myrvang, 1995).

Stress measurements in Norway show that there is a correlation between geological areas and in-situ stress state. In general, the magnitude of the principal stresses is higher in the bedrock than in the Caledonian nappes, (Fejerskov and Myrvang, 1995). High horizontal stresses are prominent in Precambrian rocks and Permian intrusives (approximately 250 million years ago), (Myrvang, 1996). Nearly 50% of the Norwegian mainland consists of gneisses and granites of Precambrian age (more than 540 million years ago), while approximately 30% of the Norwegian mainland consists of rocks from Cambrian to Silurian (420-540 million years ago). Rock types formed in Cambrian to Silurian are found in what is known as the Caledonian mountain range. This mountain range extends from the southernmost parts of Vestland county to Troms and Finnmark, (Nilsen, 2016). The Caledonian mountain building event occurred as a result of the collision between Baltika and Laurentia in Cambrium to Silurian and contributed to rock mass fracturing.

On the other hand, approximately 2% of the Norwegian mainland consists of Permian age. These rocks are mainly located around Oslo, (Nilsen, 2016). In this area, there are several examples of rock stress measurements that deviate from the theory. High horizontal stresses have been measured in these rocks, (Nilsen, 2016). Common to these measurements is that they were carried out in igneous rocks in the Oslo field. Nilsen (2016) points out a probable explanation in that residual stresses have arisen in the granites due to volume change in connection with cooling around 300 million years ago.

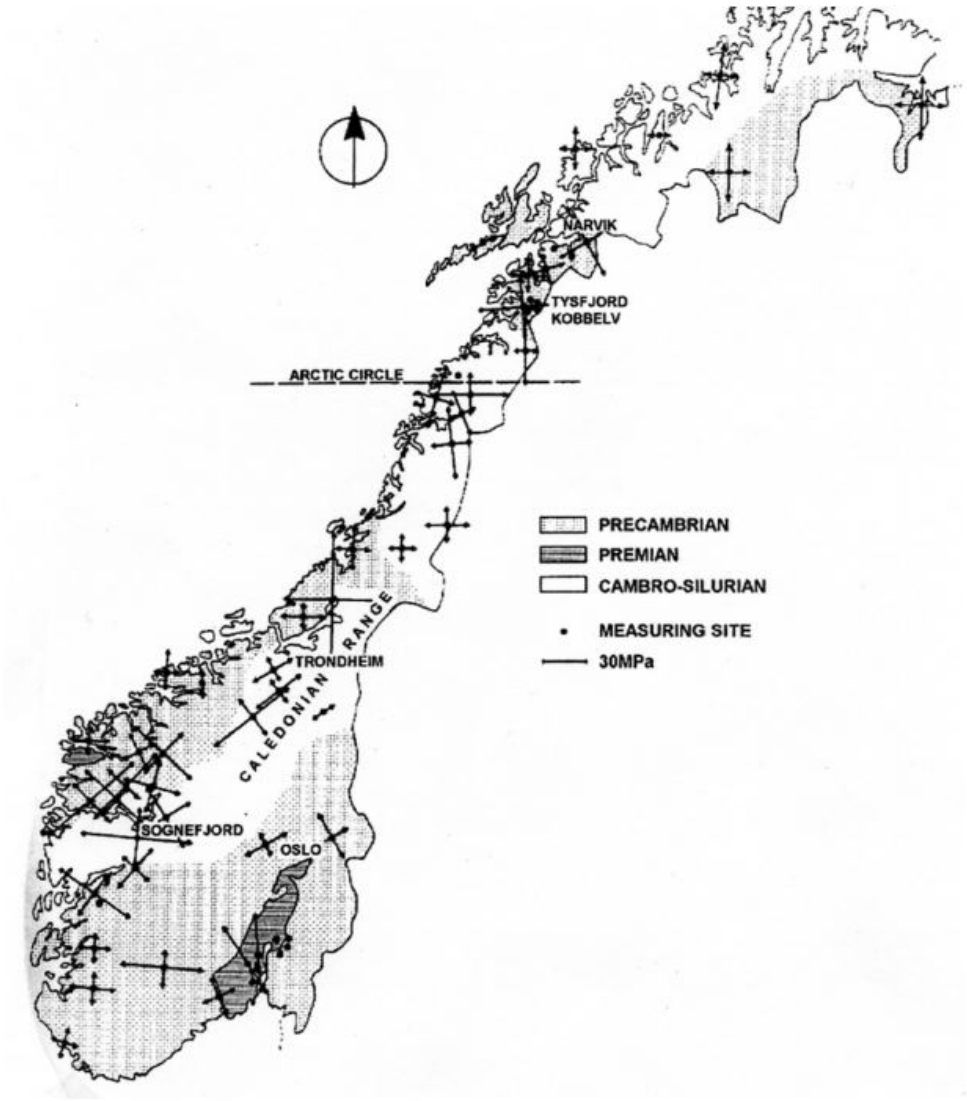

Figure 2.13: Trends in the orientation of the major horizontal stress component in Norway, Myrvang (1996).

Chapter 3

Stress measurement methods

Knowledge about the minimum principal stress is imperative to avoid leakage problems due to hydraulic fracturing or jacking in hydropower projects. Over time, there has been developed several methods to determine the stress situation in the rock mass. There are several methods to evaluate the stress situation. Geological methods (fault slip or volcanic dykes) or geophysical methods (borehole breakouts or focal mechanism solutions) can be useful at a regional level to determine stress directions, (Heidbach et al., 2016). However, in hydropower projects, it is more useful to study the local variations. Nilsen (2016) categorize rock stress measurements into three main categories:

- Direct stress methods
- Stress relief methods.
- Hydraulic methods

Direct stress measurement directly measures the stresses in the rock based on loading compensation. An example is flatjack. Secondly, the category measurement of strains deals with the elastic properties of the rock and the triggered strain. The stress state can be calculated based on strains when the cell is overcored. Finally, the last category deals with water pressure inside a borehole. By studying the relationship between water pressure and flow, the stress state can be described.

The principle of all three methods is that the measuring equipment is placed in pre-drilled holes. The disadvantage of this is that the initial state of tension in the rock mass is disturbed. Thus, this represents a general uncertainty for these measurements, (Nilsen and Palmstrøm, 2000).

3.1 Flat jack

Flatjack represents one of the very first tests for the determination of rock stresses. It was initially developed to study the deformability of the rock mass, (Hudson and Harrison, 1997). Figure 3.1 illustrates the principle of the test. The method of using a flatjack starts with drilling a series of overlapping holes. The flatjack is cast into the continuous cut in the rock mass that develops due to the drilled holes. Furthermore, the rock mass is pushed back to the original distance with the flatjack. The pressure that gives the initial distance is assumed to be equal to the rock stress perpendicular to the slot cut. In advance, several measuring bolts have been drilled in the rock. These are used to measure distances before, during, and after the test.

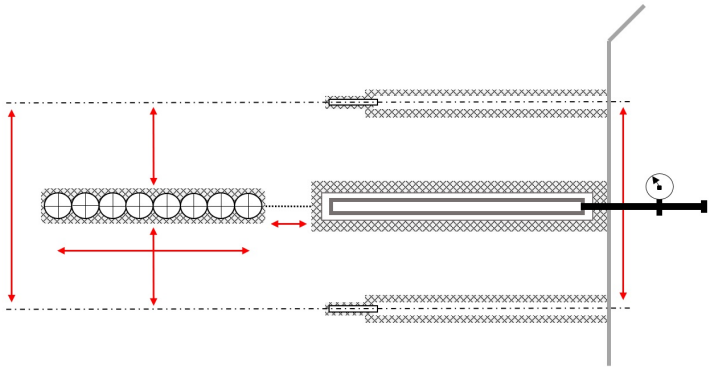

Figure 3.1: Principle of flatjack. Modified after Nilsen (2016).

However, flatjack is not the most common method to determine the minimum principal stress. Amadei and Stephansson (1997) claim that this is due to the limitations in the method. On the other hand, it is only possible to measure near-surface stresses. The test only allows the measurements perpendicular to the cut, (Nilsen, 2016).

3.2 2D overcoring

2D overcoring represents one of the two main types of rock stress measurement in the category of strain measurements described by Nilsen (2016). 2D overcoring is used throughout the world to determine the stress state. Nevertheless, there are several different measuring cells. In Scandanavia, Doorstopper is the most common. On the other, in the USA and Canada, it is more common to use a cell from the US Bureau of Mine (USBM), (Amadei and Stephansson, 1997).

2D overcoring is drilled in the direction of one of the principal stresses. Knowledge of one of these directions will therefore be essential for the accuracy of the results. According to Amadei and Stephansson (1997), there is common to carry out 2D overcoring at locations where it is possible to assume that one of the principal stresses is parallel to the borehole axis. Vertical boreholes and horizontal holes in pillars are typical examples where this technique is suitable, (Li, 2018).

Doorstopper

The Doorstopper method was first used in South Africa in the 1960s. Since the late 1960s, the method has been used by NTNU and SINTEF, (Li, 2018). The cell consists of a cylindrical silicon rubber plug with a strain gauge rosette attached to the bottom of the plug, (Leeman, 1969). Li (2018) describes a strain gauge rosette as a multi-direction strain gauge consisting of either three or four single strain gauges at an angle from one another.

The Doorstopper method utilizes strain relief at the bottom of a borehole to find the in situ stress state. A simplified principle sketch is shown in Figure 3.2. In the following, the procedure is summarized. First, a borehole is bored to a certain depth, and the bottom is flattened. Then, the cell is glued to the end of the borehole, and initial values are read. The cell is then overcored with a special drill. Finally, the core is taken out of the borehole, and the strain is may be read, (Amadei and Stephansson, 1997).

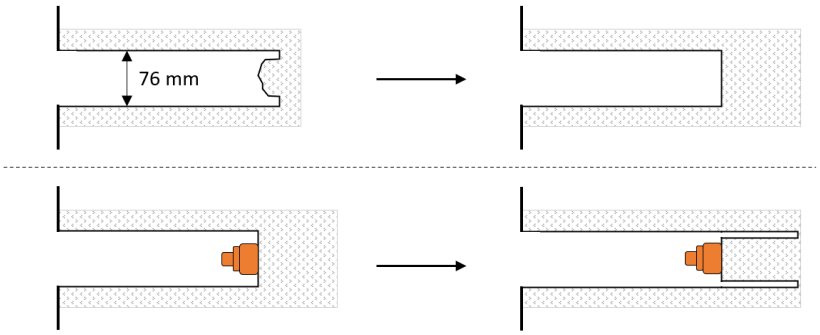

Figure 3.2: 2D Doorstopper overcoring procedure. Modified after Li (2018).

The strain that occurs when the strain gouge is overcored enables calculation of in-situ stress conditions in the rock mass. The calculation requires known values for Poisson's ratio (ν) and the modulus of elasticity (E) using Equation 3.1, (Li, 2018).

$$\sigma_1 = \frac{E}{1-\nu^2} \cdot (\epsilon_1 - \nu\epsilon_2), \quad \sigma_3 = \frac{E}{1-\nu^2} \cdot (\epsilon_2 - \nu\epsilon_1), \tag{3.1}$$

where ϵ_1 and ϵ_2 represents principal strain. These are calculated on the basis of measured strains. Equation 3.1. The equations give the state of stress around the gauge. As a result of increased stress concentration around the borehole due to changes in in-situ conditions, the results will not exactly represent the rock mass conditions. According to Li (2018), a tabulated factor as a function of Poisson's ratio (ν) can correct this uncertainty.

USBM-cell

The US Bureau of Mines developed the USBM-cell in the 60s. Today, the cell is in extensive use in the US and Canada, (Li, 2018). Figure 3.3 illustrates the principle of a USBM-cell. Unlike the Doorstopper-cell, it measures the USBM-cell changes in the boreholes' diameter instead of strain relief.

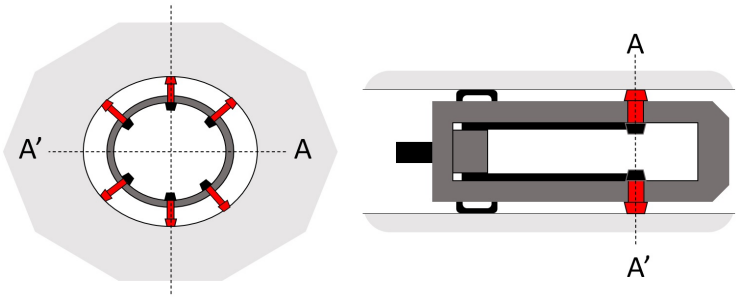

Figure 3.3: Vertically (left) and horizontally (right) section of a USBM-cell. Modified after Myrvang (1996).

The procedure starts with drilling a borehole to a certain depth. Into the borehole, a pilot hole with almost the same diameter as the gauge is drilled further in. Then, the gauge is placed in the pilot hole and the pistons are tensioned to the hole wall to make good contact. The hole is the overbored with a larger diameter at least one overcore diameter past the gauge. The pilot hole diameter changes when the relives an area around the gauge of stress. The radial deformation is measured in three directions, (Jaeger et al., 2009)

3.2.1 Strength and weaknesses

2D overcoring has been developed to determine the major and minor principal stress in a borehole. The simple principle beyond 2D overcoring is the main advantage of this method. The calculations are manageable, and the system is proven. Compared to other stress measurement methods, such as 3D overcoring and hydraulic jacking, 2D overcoring requires only a small piece of the intact rock mass to provide a successful test.

On the other hand, the tests do not provide any information about the direction. The most significant disadvantage is that the procedure decides the borehole's direction. If the borehole is not drilled in one of the principal stresses direction, the deviation will constitute a significant element of uncertainty in the calculations, (Amadei and Stephansson, 1997). Therefore, it is necessary to know the orientation of at least one of the principal stress components.

The different cells (Doorstopper and USBM) have various advantages and disadvantages. For instance, the USBM cell has a proven record and has a high success rate in the field. Besides, no cementing or gluing is required, which is especially suitable in wet conditions. On the other hand, it is necessary to calibrate before and after installation, and three tests are needed to determine the in-situ stress

situation, (Amadei and Stephansson, 1997). Similarly, the Doorstopper cell's advantage is that the cell is suitable in a high-stress situation and the requirement for an intact borehole is less than USBM. However, it can be challenging in wet and cold conditions to achieve good contact when gluing the cell to the borehole wall, (Hudson and Harrison, 1997).

3.3 3D overcoring

3D overcoring allows a spatial determination of the stress state. Six independent components are required to describe a stress field in three dimension, (Li, 2018) In theory, this can be achieved in two ways. Either this can be done through three sets of measurements of the magnitude and orientation of principal stress. Alternatively, the stress situation can be described with the magnitude and orientation of six normal and shear stress components. Although six independent components are required to describe a stress field in three dimensions, the equipment and procedure are designed to measure the spatial situation, (Sjöberg et al., 2003).

3.3.1 Methodology

Similar to 2D overcoring, 3D overcoring measures difference between before and after overcoring. Assuming that the rock mass is continuous, homogeneous, isotropic, and linear-elastic rock behavior, stress state can be determined. The rock's elastic properties (Young's modulus and Poisson's ratio) must be known, (Hudson and Harrison, 1997). Sjöberg et al. (2003) point out that one strives to take measurements only when the rock mass is ideal (homogeneous, isotropic, continuous, and linear-elastic) during field measurements. However, this is seldom wholly the situation in the rock mass. Consequentially, errors are introduced if these conditions not are met.

Over the years, several different triaxial cells have been developed. Amadei and Stephansson (1997) highlight two main types: *CSIR* og *CSIRO HI*. CSIR, also referred to as the Leeman cell, was developed by South African engineers in the late 1960's. Three strain rosettes with known position and orientation is glued inside the cell. The other cell, the CSIRO HI was developed in Australia at the start of the 70s, (Amadei and Stephansson, 1997). The CSIRO HI cell is made up of an epoxy, plastic pipe and a hollow, metallic end piece. The first part consists of two layers. During overcoring the outer layer is pushed away. Inside the outer layer, three or four strain gauges are attached to measure strain, (Hudson and Harrison, 1997).

There are a number of further developments of the triaxial cells. In this thesis the NTNU/SINTEF cell is most relevant. The NTNU/SINTEF cell is a modified version of CSIR with three stress gauge rosettes in different directions, 0°, 90° and 225°. The gauge rosettes is illustrated in Figure 3.4.

3.3.2 Practical example

In Norway, SINTEF is a key player providing services in rock stress measurements, including 3D overcoring. Naturally, SINTEF uses the self-developed cell as described above. To process the large amounts of data, SINTEF has developed a system called DISO (Determination of In-situ Stress Overcoring), (SINTEF, 2003). The system calculates all possible outcomes and calculates the most probable magnitude and direction for the three principal stress components. The procedure is summarized in the following and illustrated in Figure 3.5, (SINTEF, 2003):

1. A diamond drill hole (76 mm) is drilled to wanted depth. The hole bottom is flattened with a special drill bit, and a concentric hole with smaller diameter (36 mm) is drilled approximately 30 cm further.

2. The measuring cell is inserted with a special installing tool containing an orienting device and a cable to read-out unit. The instrument is put in place with detachable aluminum rods. Compressed air is used to expand the cell in the hole, and the strain gauge are cemented to the hole wall.

3. The measuring cell is now fixed to the hole and initial reading (0 recording) is done. The installing tool is removed and the cell is ready for overcoring.

4. The small hole is overcored by the larger diameter bit, thus stress relieving the core. The corresponding strains are recording by the strain gauge rosettes.

5. The core is catched with a special core catcher, and immediately after removal from the hole the second recording is done. From the recorded strains the stresses may be calculated when the elastics parameters determined from biaxial- and laboratory tests are known.

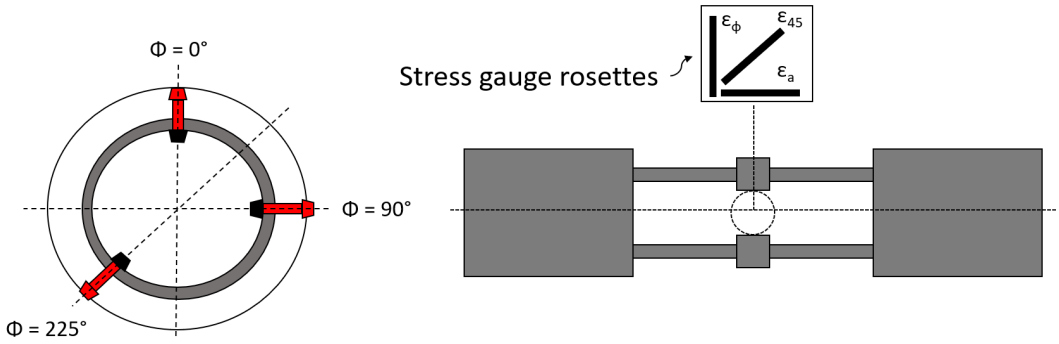

Figure 3.4: Vertical (left) and longitudinal (right) cross-section of the NTNU/SINTEF cell. Modified after SINTEF (2003).

3.3.3 Strength and weaknesses

A significant advantage of 3D overcoring is that only one borehole is necessary to obtain information on both principal stresses' direction and magnitude. Another advantage is that it is possible to monitor the stress situation over time, (Amadei and Stephansson, 1997). However, 3D overcoring provide a large amount of data. This extent of data requires more powerful computers than more straightforward and easier methods. On the other hand, the large amount of data provides higher accuracy in the results, (Amadei and Stephansson, 1997). A disadvantage with 3D overcoring is the test's sensitivity to anisotropy, grain size, and heterogeneity in the rock mass. This is expressed in some cases in scattered results, (Amadei and Stephansson, 1997).

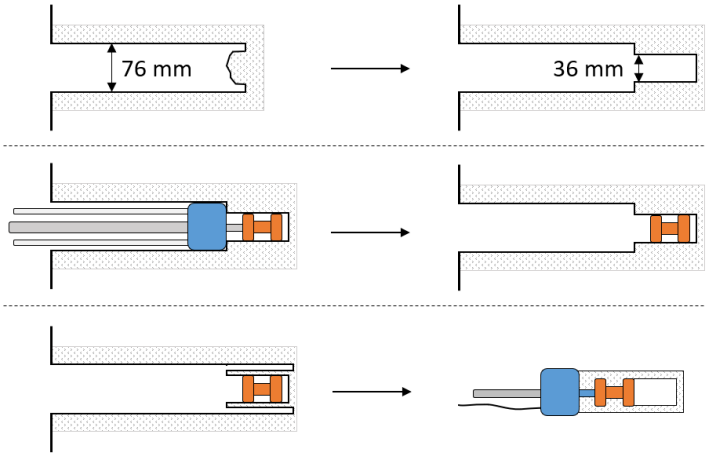

Figure 3.5: 3D Doorstopper overcoring procedure. Modified after SINTEF (2003).

Compared to 2D overcoring, 3D overcoring is more time-consuming. According to SINTEF (2003), it takes normally 1 hour to complete one single test and approximately 2 days to complete one stress tensor (7-10 single tests). Both 2D and 3D overcoring requires a rock mass with a low degree of jointing due to the overcoring lengths. Therefore, these methods are inapplicable under high rock stress conditions that can initiate core discing, (Ljunggren et al., 2003).

According to Hanssen (1997), both 2D and 3D overcoring are unsuitable for determining the location of the transition zone in hydropower projects. His PhD-thesis included a comparison of results from various measurement methods at different hydropower projects. The results from the overcoring generally showed overestimated values compared to the hydraulic methods. Although 3D overcoring provides lower magnitudes than hydraulic methods, the test still provides information on the orientation of the stresses, which according to the ISRM standard, is required when conducting hydraulic splitting tests, (Haimson and Cornet, 2003). Another disadvantage of overcoring methods is that they cover a smaller area in the rock mass than hydraulic methods, (Ljunggren et al., 2003).

3.4 Hydraulic fracturing

Hydraulic fracturing is a rock stress measurement method to determine the magnitude of the stresses in the rock mass. The test is a 2D method where the stresses perpendicular to the borehole axis are considered. American oil engineers first developed the test in the 1950s to stimulate wells in low permeability formations. Further, the method was developed to measure rock stresses, (Hudson and Harrison, 1997).

3.4.1 Methodology

The standard procedure for hydraulic fracturing is described by Haimson and Cornet (2003) and a principle sketch is presented in Figure 3.6. The test procedure involves pressurizing a sealed section of a borehole. The pressure is gradually increased until a new joint develops in the rock mass. The rising pressure is linear until it reaches the fracturing pressure, P_c, as illustrated in Figure 3.7. During this process, the pressure is monitored as a function of time. The borehole pressure drops rapidly after the pressure has reached the fracturing pressure. Simultaneous, the water flows into the rock mass while the fracture propagates furthermore. Then, the inflow is shut off, and the pressure drops until it equilibrates the minimum horizontal stress perpendicular to the joint surface. Finally, the pressure reaches the pore pressure, and the first cycle is finished. The second cycle starts when the water flow is turned on and pumped into the same section. Like the first cycle, the pressure increases linearly before the fracture is re-opened at re-opening pressure, P_r. After shut-in, the pressure drops, and the shut-in pressure, P_s, is obtained on the curve. Normally, several cycles is carried out to determine shut-in pressure. The lowest value for the shut-in pressure will theoretically be equal to σ_3 when the borehole is located parallel with σ_1 or σ_2. Therefore, the shut-in pressure should be measured for every cycle, (Li, 2018).

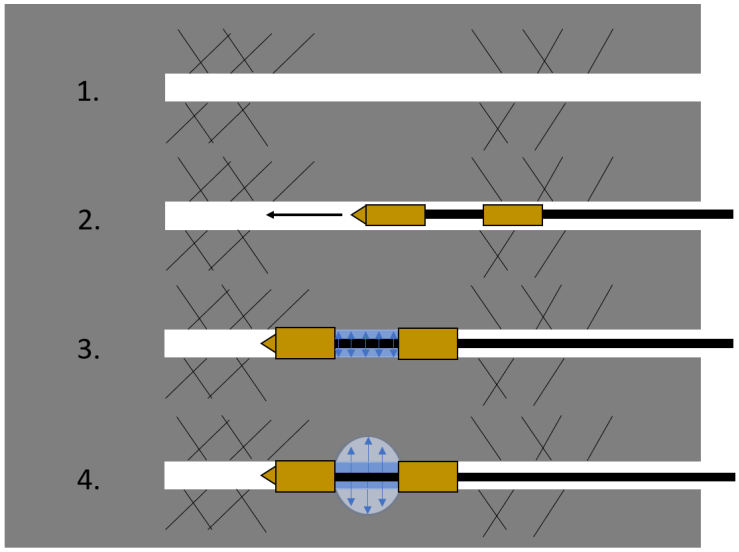

Figure 3.6: Principle sketch showing the first steps of a hydraulic fracturing test.

The graph presented in Figure 3.7 enables the determination of the major and minor principal stresses. The standard procedure for hydraulic fracturing assumes that the borehole is drilled in the direction of one of the principal stresses. Consequently, the test will provide both direction and magnitude of the minimum principal stress component. According to Haimson and Cornet (2003), the magnitude of the major principal stress can be calculated from the following equation:

$$\sigma_1 = \sigma_t + 3\sigma_3 - P_c \tag{3.2}$$

where σ_t represents the tensile strength of the rock, σ_3 the shut-in pressure and P_c the fracturing pressure.

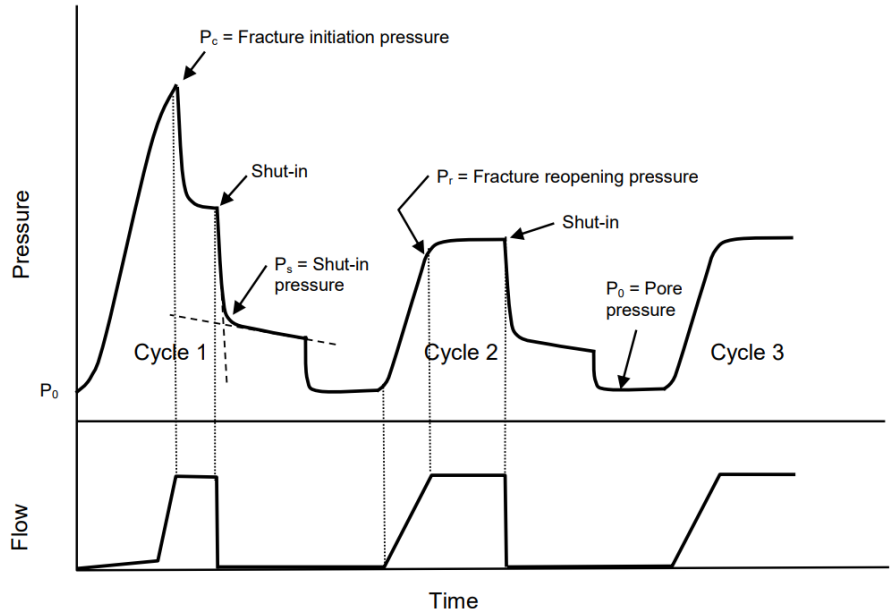

Figure 3.7: Typical recording of pressure versus time for a hydraulic fracturing measurement. P_0 is the initial pore pressure in the rock mass, (Li, 2018).

3.4.2 Practical example

SINTEF provides hydraulic fracturing tests to determine the in-situ rock stresses in Norway. The test can be carried out in both vertical holes and from underground holes in a tunnel, (SINTEF, 2003). Vertical holes can be performed down to depth of 300 m in vertical holes. According to SINTEF's test procedure, up to 24 individual tests are carried out in a minimum of four different boreholes at every test location. Typical hole depth is approximately 25-35 meters to reach a part of the rock mass that is not affected by induced stresses, (SINTEF, 2003). The orientation of the boreholes is in the same direction as one of the principal stresses. Like Haimson and Cornet (2003), SINTEF recommends 3D overcoring prior to the hydraulic fracture test to determine the holes' direction. According to the test procedure, due to borehole deviations or collapse in the hole, it is sometimes impossible to use one or more holes. It is therefore common practice to drill two extra holes as a backup.

3.4.3 Strength and weaknesses

An advantage with hydraulic test methods is that the tests, unlike the overcoring methods, measure stress directly. Therefore, knowledge about the elastic parameters is not required. According to Amadei and Stephansson (1997), this eliminates potential sources of error related to determination of the elastic properties, which improves their reliability. One advantage with hydraulic fracturing for measuring the minimum principal stress is that the International Society of Rock Mechanics (ISRM) describes a test procedure, (Haimson and Cornet, 2003). This establishes a standard procedure that allows comparison with results from around the world.

Another advantage with hydraulic fracturing is the reliability of σ_3 when the borehole is oriented in the same direction as the principal stresses. However, if the borehole's direction is random, shear stresses might occur, which will represent a significant source of error. Therefore, ISRM recommends 3D measurements to determine the rock stress direction before the hydraulic fracturing test, (Haimson and Cornet, 2003). According to SINTEF (2003), it is common to assume the stress direction based on topographical conditions if the direction is not determined based on rock stress measurement methods.

On the other hand, a disadvantage with hydraulic fracturing is that the test requires an intact part of the borehole that is not fractured. According to Tournier and Quirion (2010) it can constitute an uncertainty with the measurements if the rock mass is fractured. However, an optical televiewer can be used before the test to identify intact parts of the borehole. Another challenge with hydraulic fracturing is that it is the cost. Compared with hydraulic jacking, the cost level can be 4-5 times higher, (Ødegaard and Nilsen, 2018). The high cost is due to high-pressure special equipment and a need for experienced operators both for the implementation and interpretation of data, (Amadei and Stephansson, 1997).

3.5 Hydraulic jacking

Hydraulic jacking and hydraulic fracturing have many similarities. However, there is a fundamental difference between the two tests. Hydraulic fracturing assumes intact rock mass, and the test induces a new joint in the borehole. On the other hand, hydraulic jacking is based on the opening of existing joints in the rock mass to find the pressure at which the fracture opens, slips (if shear stresses are present) and closes, (Ødegaard and Nilsen, 2021). However, a large number of tests in boreholes with different directions are required to open a representative population of joints oriented perpendicular to the minimum principal stress, (Haimson and Cornet, 2003).

According to Ødegaard et al. (2020), there are several examples of different test procedures described in the literature, like the cyclic hydraulic jacking test (Rutqvist and Stephansson, 1996), the step rate test (described by Smith and Montgomery (2014)), the modified Lugeon test (described by Houlsby (1976)) and a jacking test described by Hartmaier et al. (1998) is the most relevant. Haimson and Cornet

(2003) describe another variant of hydraulic fracturing. This test is referred to as Hydraulic Testing on Pre-existing Fractures (HTPF), (Haimson and Cornet, 2003).

3.5.1 Methodology

Common to the various hydraulic jacking procedures is that several boreholes are drilled into the rock mass in different directions. Several holes and repeated cycles is common to improve the reliability of the results. Furthermore, a single packer is installed to isolate a section of the borehole. The packer is typically placed 5-15 meters into the rock mass to ignore the stress influence from the tunnel. Then, as can be seen in Figure 3.8, the test section is pressurized until the water pressure exceeds the in-situ normal stress acting on the existing joint. The most favorable oriented joint is opened even though the test section consists of one or several existing joints. Hydraulic jacking can be performed either as a pressure-control or a flow-control Each test cycle consist of both a step-wise pressure/flow increase and a step-wise pressure/flow decrease. During the test, the pressure is monitored.

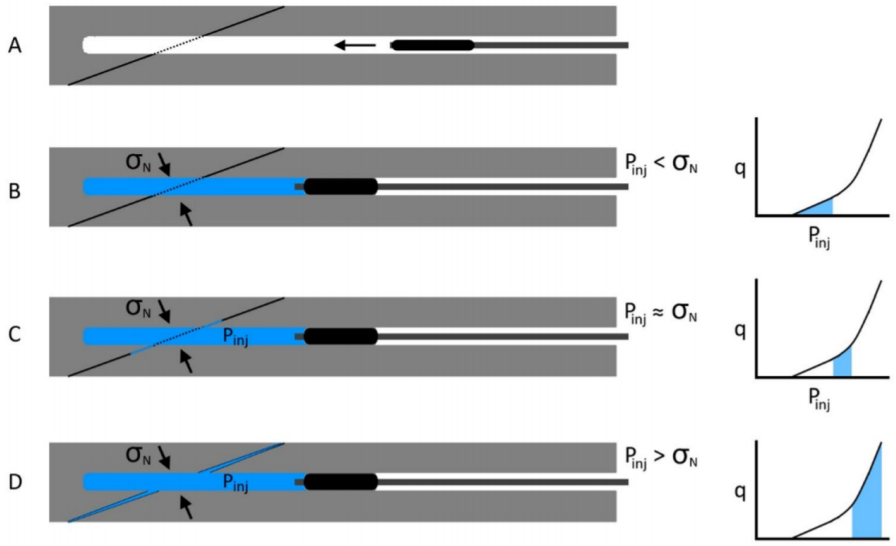

Figure 3.8: Step-wise illustration of a borehole intersected by a existing fracture. a) Installation, b) Pressurization of the test section, c) Onset of hydraulic jacking of the fracture and d) Full hydraulic jacking, (Ødegaard and Nilsen, 2021).

3.5.2 Interpretation of data from hydraulic jacking tests

There are several ways to present data from hydraulic jacking tests. The most common way is with a pressure and flow vs. time plot, which provides real-time plots from the cycles. Another common way to present the data is a flow-pressure (qP) diagram, as shown in Figure 3.8. The form of the curve provides information about the rock mass. According to Rancourt (2010), the shape pressure-time plot depends on the rock mass's permeability, elastic properties, and in-situ stress conditions. The slope of the built-up pressure curve depends on the permeability of the rock mass. In cases where the permeability is high, the slope of the qP-diagram will

be correspondingly steep. In this case, more water flows into the rock mass at a lower pressure and consequentially the pump needs to be powerful enough in order to pressurize the zone and obtain a reliable jacking curve. On the other hand, rock masses with low permeability give a flat curve. This is because the rock mass requires a higher pressure for the water to flow out into the rock mass, (Rancourt, 2010).

The aim of the hydraulic jacking test is to provide information about the normal stress acting on the existing joint. Rutqvist and Stephansson (1996) suggested that interpretation of the normal stress acting on the fracture plan should be made from the closure stages to avoid effects from non-linear fracture stiffness in the reopening phase. Referring to Figure 3.9, Hayashi and Haimson (1991) describe the fracture closure process after shut-in and divides the process into three parts. Part 1: Closure by width reduction at constant fracture depth, described as hinge-like fracture closure. Part 2: Shrinkage of length, which starts with closure at the ends. Part 3: Completely closure. After that, leakage may continue through the surface of the borehole. Raaen et al. (2001) use the same model to describe three different stiffness stages of pressure decline during flow-back tests. The first stage refers to the stiffness of the system when the joint is fully open. Stage 1 ends when the asperities of the fracture surfaces starts to touch (point A). The second stage consists of a gradually decrease in stiffness until the surface is completely closed at point B. The final stage represents the stiffness of a closed fracture. Using these models, one distinguishes between *hydraulic* and *mechanical* closure. Hydraulic closure occurs when the asperities starts to get in touch and mechanical closure is when the joint is completely closed.

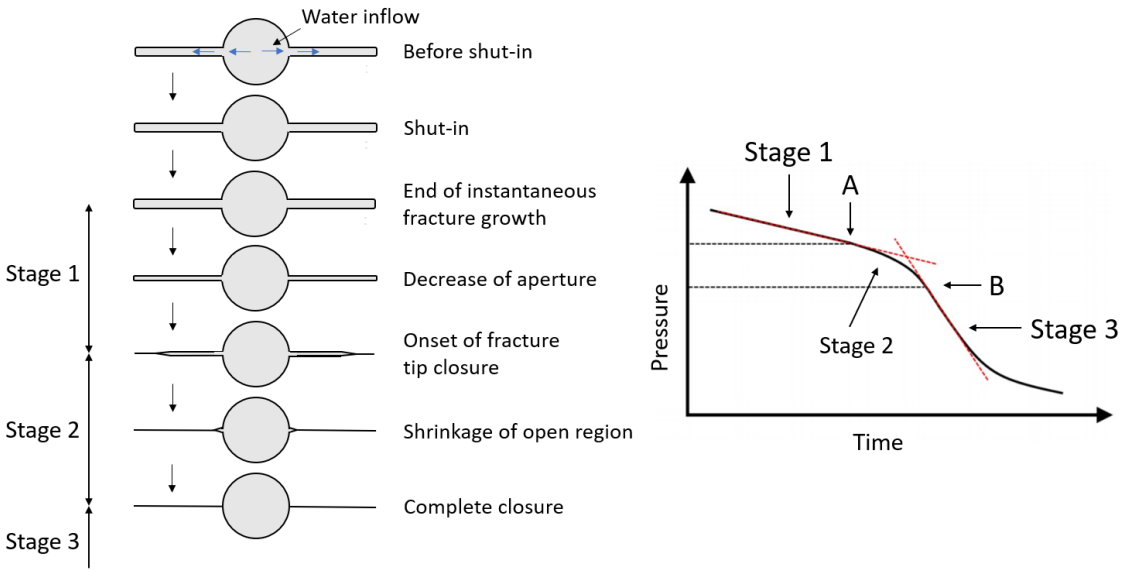

Figure 3.9: Different stages in hydraulic fracture closure process (left) with corresponding stages in an idealized pressure–time plot for the step-down stage (right). Modified after Hayashi and Haimson (1991), and Ødegaard and Nilsen (2021).

The transition between the different stages enables interpretation of the normal stress acting on the joint surface. However, Ødegaard and Nilsen (2021) state out that there are several approaches to determining fracture closure and corresponding

fracture normal stress from the pressure-time diagram. Raaen et al. (2001) state out that point of first inflection (point A) should be used, while Plahn et al. (1997) claim that the intersection point between the lines from A and B gives a better approach. On the the other hand, Savitski and Dudley (2011) suggest to use the pressure at the lower inflection point (point B). However, Ødegaard and Nilsen (2021) have shown through laboratory assessments under idealized conditions that the pressure at the lower inflection point correspond reasonably well when the magnitude of the normal stress component is known.

3.5.3 Strengths and weaknesses

One advantage of hydraulic jacking is that the test is cost-effective and rapid to perform. There is no need for special equipment beyond what is available on an average tunnel project. Besides, the test requires no skilled personal. Rapid completion of the test means that the tests interrupt the tunnel progress minimally. Ødegaard and Nilsen (2018) claim that the cost of these tests typically can be around 10–20% of what standard hydraulic fracturing tests cost. Other advantages of hydraulic jacking are that there are no test depth or orientation restrictions. However, the test needs to be performed outside the strength reduction zone, (Hudson and Harrison, 1997).

On the other hand, there is no standardized procedure for hydraulic jacking tests. As mention, the literature describes several test procedures and all the procedures make it more or less impossible to compare the results of different tests in one place. The test is generally not accepted for determining the minimum principal stress. Nevertheless, results from hydraulic jack tests have formed the final decision basis for determining the transition between unlined and lined pressure tunnel, (Ødegaard et al., 2020).

Chapter 4

Water in the rock mass

4.1 Introduction

Groundwater is a part of the hydrological cycle. Like soil, there are both groundwater flows, water pressure, and groundwater levels in rock masses. The location of the groundwater level varies depending on the type of rock and as a function of time, (Nilsen and Palmstrøm, 2000). The vast majority of underground facilities are below the groundwater level. Consequentially, it is of great importance to evaluate what type of problems the groundwater can cause. According to Nilsen (2016), this must be emphasized before, during, and after completion.

4.2 Consequences of water leakage

4.2.1 Environmental

Water leakages from or into a water tunnel with discontinuities communicating from the rock to overlying will cause a reduction of the groundwater level. Consequentially, the pore pressures in the soil reduce and increasing the effective stresses. According to Davik et al. (2002), soil consolidation due to groundwater reduction might occur. If different geological and geometric combinations are present, landslides can be triggered, as happened at Bjørnstokk in 2016, (Nordal et al., 2018). In addition, other environmental consequences of the reduction of groundwater level are environmental impact on surface water as well as plant and animal life, damage to agriculture, and reduction of groundwater reservoirs.

4.2.2 Effects of water leakage into a tunnel

Water leakage from the tunnel has consequences such as reduced groundwater levels and water loss during operation and may lead to secondary consequences such as landslides. In addition, an inflow of water in underground construction reduces the

quality of the working conditions in the tunnel. The process of drill and blasts can become significantly more challenging when water inflows and water pressures are encountered. Other consequences are damaged roads and an increasing need for pumping. Due to the unfavorable inflows, the efficiency of the drill and blast process can be reduced considerably and consequently increase the cost of the project.

In order to gain control over leakage, grouting is a practical and frequently used tool for achieving satisfactory leakage requirements. In connection with hydropower plants, one must assess leakage from the tunnel system and calculate expected lost production vs. injection cost. In an empty tunnel, inflows must be considered in connection with any environmental changes along the tunnel. This evaluation must then be considered to the adhesion associated with the maintenance of the tunnel or installations.

4.3 Theoretical background

The rock mass is composed of both intact rock and discontinuities. Most of the intact rock has, in general, very low permeability except for high porosity rocks, such as volcanic rock and some sandstones. The flow of groundwater in the rock largely depends on the properties of the discontinuities since the flows mainly take place in parts of the rock mass with greater conductivity, (Nilsen and Palmstrøm, 2000).

In a hydropower tunnel, the hydrogeological conditions will be affected in both the excavation and operation phases. After filling the water tunnels, the surrounding rock mass will become saturated, and the water gives pressure (P_w) to the rock mass equivalent to the hydrostatic water head (H). With high-pressure tunnels and shafts, there will also be possibilities for water leakage and erosion of joints. Hence, it is of great interest to study the relationship between water pressure and rock mass to assess leakage potential, (Panthi and Basnet, 2021).

4.3.1 Hydraulic conductivity of rock mass

The flow in groundwater is commonly considered to be laminar and Darcy's law is extensively used for calculations (see Equation 4.1). In the law, the hydraulic conductivity, k, is also referred to as coefficient of permeability. The parameter is commonly used to characterize hydrogeological condition and in Darcy's equation the parameter represents the coefficient of proportionality, (Nilsen and Palmstrøm, 2000).

$$k = \frac{Q}{A} \cdot i \tag{4.1}$$

where Q represents the flow rate (m^3/s), A the flow area (m^2) and i the hydraulic gradient ($i = \frac{\Delta l}{\Delta h}$). The coefficient of permeability (in m/s) largely depends on the

rock mass and the properties of the liquid. Figure 4.1 gives an illustration of flow through a cylinder and given parameters in Darcy's law.

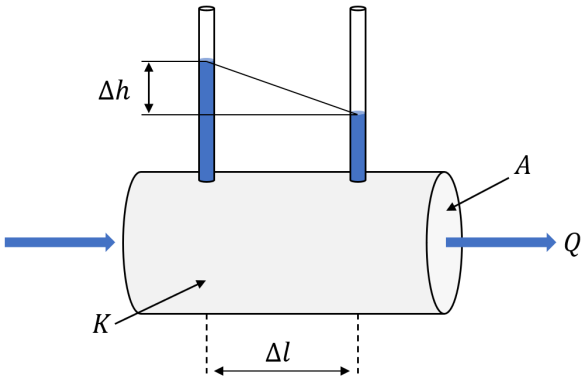

Figure 4.1: Illustration of water flowing through a cylinder showing definitions for Darcy's law as presented in Equation 4.1.

4.3.2 Factors controlling hydraulic conductivity

The conductivity depends on rock mass properties, such as porosity, pore size, grain distribution, degree of cementation, degree of jointing, joint opening, and joint alteration. Different rocks have different characteristics with respect to hydraulic conductivity. For instance, folded and sheared rocks such as shale, phyllite, and schist have low hydraulic conductivity, (Panthi, 2006). However, the conductivity is primarily governed by the degree of jointing and the character of the rock joints. According to Panthi (2006), interlinked joint sets that are open or filled with permeable materials have high conductivity. In addition, the hydraulic conductivity depends on the depth. In general, the rock mass becomes tighter with depth. As a result, the hydraulic conductivity of the rock mass generally decreases with increased depth, (Nilsen and Palmstrøm, 2000).

4.4 Approaches for assessing ground water inflow

Panthi and Basnet (2021) pinpoint that the main difficulty in leakage assessment is the quantification of possible water leakage during the operation of the pressure tunnels in hydropower plants. To date, different approaches to assessing leakage have been introduced, and one of the following two approaches are typically used:

1. Basic flow theory
2. Numerical modeling

Numerical approaches available for the estimation of water leakage will not be presented in this thesis. However, these methods can be of great use to provide estimates regarding groundwater flow in complex situations.

4.4.1 Semi-analytical methods

Panthi (2006) proposed a semi-empirical solution to estimate the specific leakage (q_t in l/min/m) from an unlined/shotcrete lined pressure tunnel based on analyzing extensive amounts of data from the Khimti headrace tunnel in Nepal (Equation 4.2). The analysis aimed to investigate the possible outflow of water and the need for grouting.

$$q_t = f_a \cdot H \cdot \frac{J_n \cdot J_r}{J_a} \tag{4.2}$$

where H is the hydrostatic water head. J_n represents the joint set number, J_r is joint roughness number and J_a describes joint alteration number in the Q-system of rock mass classification. The final parameter, f_a, is a joint permeability factor with unit l/min/m^2. The factor depends upon the physical condition of the joint sets, and values indicate less permeable joints. The factor is calculated by Equation 4.3, (Panthi and Basnet, 2021):

$$f_a = L \cdot \frac{J_p}{D \cdot J_s} \tag{4.3}$$

where L is equivalent to 1 Lugeon with a unit 1 l/min/min, J_p is joint persistence (maximum 25 m), J_s is the joint spacing of the most frequently occurring systematic joint set, and D is the shortest distance from valley side roof of the tunnel to rock slope topography to valley side. Equation 4.2 enables correlation between specific leakage and the Q-system. Figure 4.2 shows the geometrical input parameters.

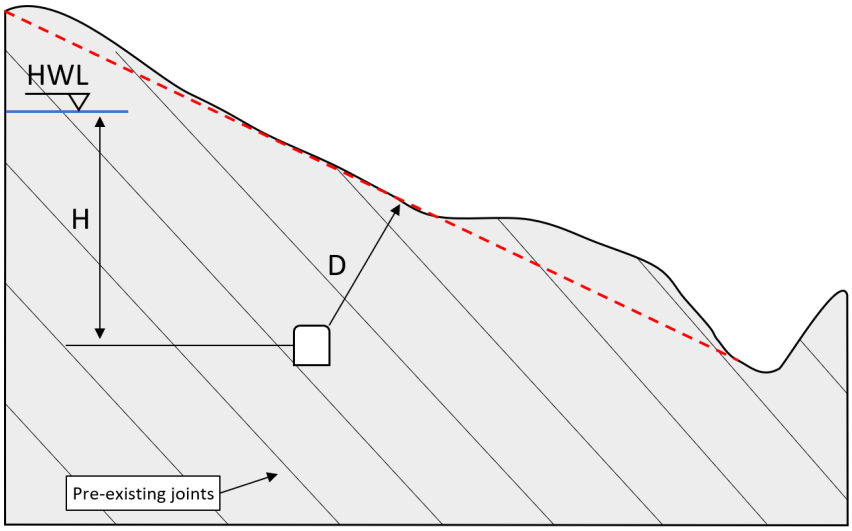

Figure 4.2: Illustration showing the input parameters in Equation 4.2. Modified after Panthi and Basnet (2021).

Chapter 5

Norwegian design principles

5.1 General

In the past 100 years, Norway has built more than 200 underground powerhouses and 4200 km-long hydropower tunnels, (Broch, 2013). At the beginning of the 20th century, the most common design principle was an almost horizontal headrace tunnel and exposed steel penstock along with the surface topography, such as at Vemork (1911) and Glomfjord hydropower plant (1920), (Panthi, 2014). Nevertheless, four power plants with unlined pressure tunnels were built at the beginning of the 20th century. At two of these (Herlandsfoss and Skar), there were leakage problems after the plants were put into operation. On the other hand, at Svelgen and Tokle hydropower plants, there were only a few or no leakages, (Broch, 1984). Although the power plants with the first unlined pressure tunnels were built in the early 1920s, the completion of Tafjord K3, which was completed in 1958, is still seen as a breakthrough for unlined pressure shafts/tunnels in Norway, (Broch, 2013). Figure 5.1 summarizes the development of Norwegian unlined tunnels.

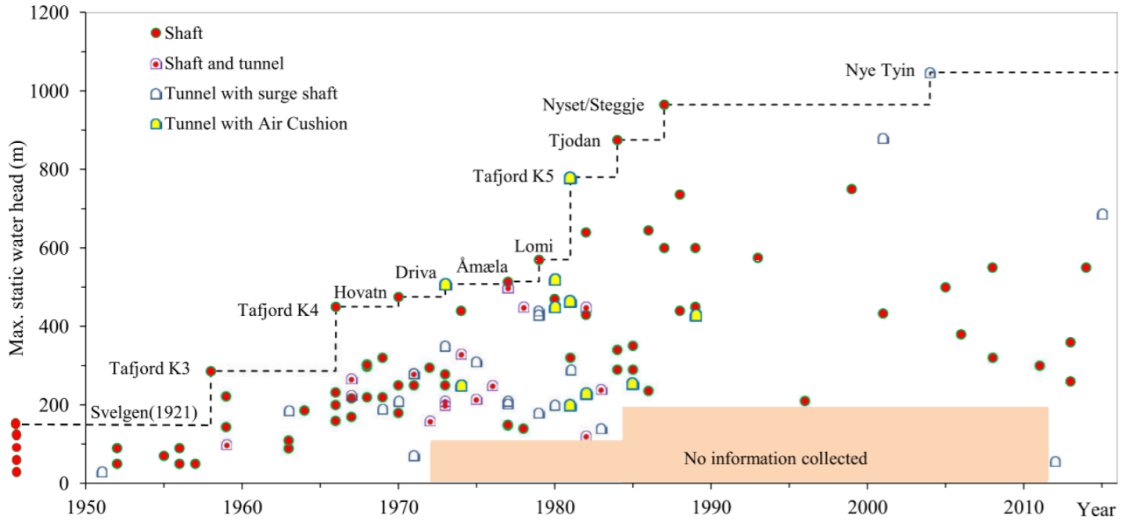

Figure 5.1: Overview of Norwegian unlined pressure shafts and tunnel with respect to max. static water head, (Panthi and Basnet, 2018). Updated from Broch (2013).

Since the 1960s, unlined pressure tunnels have been the conventional solution in the Norwegian hydropower industry. Today, over 100 unlined high-pressure shafts or tunnels have been built with water heads over 150 m. As can be seen in Figure 5.1, the record is held by the Nye Tyin hydropower plant, which was completed in 2004. The maximum water head is 1047 m.

5.2 Design features for unlined pressure tunnels

Since the first unlined tunnel was built in the first half of the 20th century, it has been agreed that the tunnel is safe if the minimum principal stress is greater than the water pressure at any point along the unlined pressure tunnel, unwanted hydraulic failure will not occur, (Broch, 1984). Today, the main principle in the construction of unlined tunnels is to ensure that the tunnel remains stable for the project's life under the various loading conditions without excessive loss of water or severe maintenance requirements. Aasen et al. (2013) suggest the following four geological characteristics to make sure that the tunnel remains operative in decades without any unfortunate situations:

1. **Sufficient confinement**
   - The entire tunnel must be set deeply enough within the rock mass to ensure that adequate in-situ compressive stress is available to prevent hydraulic jacking.

2. **Suitable rock mass**
   - The rock material must be long-term durable and preferably have reasonable and fair tunneling qualities without soluble or weak fillings.

3. **Sufficient long-term tunnel stability**
   - No slide or cave-in must occur during the power plant operation.

4. **Other essential conditions**
   - An example would be low rock mass permeability and sufficiently high groundwater level.

5.3 The Norwegian Criterion for Confinement

Today, it is estimated that over 95% of the total length of tunnels and shafts in Norway is unlined, (Panthi, 2014). Since the first unlined tunnels and shafts were built at the start of the 20th century, it has been common to use some confinement criteria for designing the hydropower scheme. Over time, this has formed the basis for different "rules of thumb" formulas and finite element methods. The purpose of these criteria has been to simplify the design of the tunnel systems.

In the 1950s and 1960s in Norway, the number of unlined pressure shafts and tunnels increased. At this time, the tunnels were designed according to the principle in Equation 5.1, (Broch, 1984):

$$h > cH \tag{5.1}$$

where h is the minimum required rock cover. H represents the hydrostatic head, while c is a constant. The parameter is set to 0.6 for valley sides up to 35° and 1.0 for valley sides above 35°. Due to constructional considerations, the slope of the shaft was between 31° and 47°, where the latter were most common, (Broch, 1984).

A significant weakness of Equation 5.1 is that it does not include either the inclination of the pressure tunnel or the density of the rock mass. Around 1970, two failures (at Byrte and Askora hydropower plants) became important for the design of Norwegian hydropower schemes. First, the rule of thumb was upgraded after the failure at Byrte in 1968, where the inclination of the pressure shaft where 60°. Second, the updated version of Equation 5.1 made the inclination of the shaft/tunnel included in the rule of thumb as presented in Equation 5.2, (Broch, 1984):

$$h > \frac{\rho_w \cdot H}{\rho_r \cdot \cos\alpha} \tag{5.2}$$

where α is the inclination of shaft or tunnel, ρ_w is the density of water, and ρ_r is the density of the rock. Then, the failure at Askora in 1970 lead to a new principle introduced by Bergh-Christensen and Dannevig (1971). The principle considers the shortest perpendicular distance (L) from the valley inclination (expressed by β) in Equation 5.3:

$$L > \frac{\rho_w \cdot H}{\rho_r \cdot \cos\beta} \tag{5.3}$$

Equation 5.2 and 5.3 have become the Norwegian rule of thumb or by some referred to as the Norwegian Criterion for Confinement. Figure 5.2 shows a graphical explanation of the various parameters in the equations. The motivation behind the further development was to correct for topographical variation and thus expand the opportunities. According to Panthi and Basnet (2018), it is worth mentioning that Equation 5.2 will be automatically satisfied in most of the unlined tunnels when Equation 5.3 is satisfied.

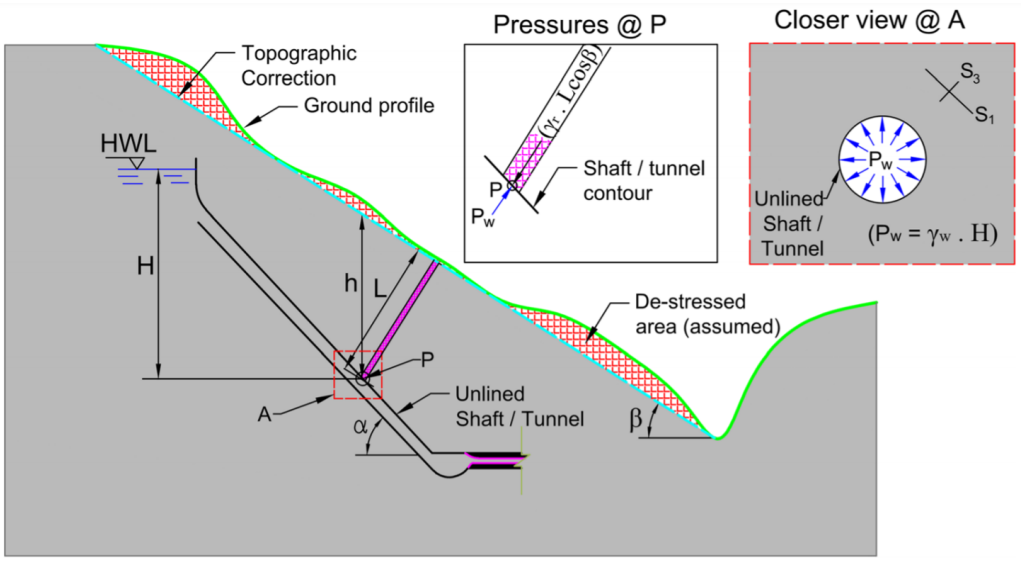

Figure 5.2: Parameters in the Norwegian Criteria for Confinement, (Basnet and Panthi, 2020).

5.4 Limitations with analytical methods for final determination of hydropower schemes

The widespread use of unlined tunnels and shafts in recent decades is due to economic reasons. This way of designing hydropower schemes provides significant time and cost-saving by replacing steel liners and penstocks with unlined tunnels, (Ødegaard et al., 2020). Another advantage is that overburden criteria are based on simple mathematics, and the method is a fast and cheap way to design hydropower schemes, as there is no need for expensive and complicated software.

On the other hand, the rule of thumb indicates the only minimum required rock mass coverage. However, as presented in Section 2.3, several factors like inhomogeneities, geological structures, or tectonic activities may affect the relationship between vertical coverage and the principal stresses' magnitude. To address this uncertainty, it is common practice to include a factor of safety in the calculation. However, the actual value will never be known. Benson (1989) claims that a safety factor of 1.3 is sufficient for good rock masses, but in cases where the properties of the rock mass are well investigated, it is possible to reduce this factor to 1.1. In Norway, it is common to use a safety factor between 1.2 and 1.5, (Aasen et al., 2013).

Although the rules of thumb have contributed to several successful projects, there are examples of projects where hydraulic failure has occurred. According to Ødegaard et al. (2020), failures have occurred at nine hydropower plants in Norway since 1919. Common to these projects is that different overburden criteria have been used in the design. Several authors have pointed out that these criteria must be used carefully and not for the final design of unlined pressure tunnels, (Benson, 1989; Rancourt, 2010; Ødegaard and Nilsen, 2018). Nevertheless, the criteria are used for the final design of unlined pressure tunnels, at least until recently, (Ødegaard et al., 2020).

The principle is based on a two-dimensional consideration. Since the geometry is simplified, the calculations only provide an idealized estimation of the rock stresses. Rancourt (2010) points out that a shortcoming with the overburden criteria is that they are so simple that there is no need for geological expertise to use them, as the equations do not consider neither hydrogeological or geological variations that can affect the stress situation. Thus, this might lead to an overestimation of the rock stresses. Ødegaard et al. (2020) completed a study of calculated and measured values for the minimum principal stresses at 15 hydropower plants built after 1990. In seven cases, the minimum principal stress was overestimated. However, there was only a correlation in two of the cases, (Ødegaard et al., 2020).

The findings in Ødegaard et al. (2020) show that it is impossible to rely on overburden criteria. The article highlights the importance of rock stress measurements before the final design. If not, the consequences can be significant. As a result of the operation's delayed start, hydraulic jacking of the rock mass has financial consequences for the owner. Besides, there is a possibility that hydraulic jacking can lead to consequences for third parties. In 2016, leakage from the tunnel triggered a landslide that destroyed approximately 100 meters of FV76 (county road), (Nordal et al., 2018). The minor principal stress was not verified, and the final location of the transition zone was located based on rules of thumb. However, the stresses turned out to be lower than expected, and hydraulic jacking occurred.

An independent expert group lead by Professor Steinar Nordal from NTNU recommended in its report that The Norwegian Water Resources and Energy Directorate (NVE) sets requirements for measuring rock stresses as standard when designing unlined pressure tunnels, (Nordal et al., 2018). Today, there are no explicit requirements for rock stress measurements in the Dam Safety Regulations other than "... it must be documented that the concrete plug and the rock can withstand the applied forces. Necessary testing and securing of the rock must be done before the concrete plug is built," (Damsikkerhetsforskriften, 2009).

Basnet and Panthi (2018) investigated ten selected projects in Norway where the overburden criteria were used for the final design. The review included both successful projects like Nye Tyin and unsuccessful projects like Herlandsfoss. The projects were compared both numerically and analytically. Favorable and unfavorable conditions were evaluated against five main categories and are presented in Table 5.1. Common to successful projects is that the entire pressure shaft or tunnel is built in solid rock masses such as gneiss and granite. Furthermore, the pressure shaft or tunnel is located at a significant distance from the valley sides, and there are no nearby major faults or zones of weakness. On the other hand, the failure projects all have challenging geology and terrain. These projects are built in weak rocks with unfavorable combinations of nearby faults or weakness zones and de-stressed areas, (Basnet and Panthi, 2018).

Table 5.1: Favorable and unfavorable ground conditions for the applicability of Norwegian confinement criteria, (Basnet and Panthi, 2018)

Category	Favorable conditions	Unfavorable conditions
Topography	Relatively gentle valley slope topography	Deep, steep and complex valley slope topography
Rock mass and jointing	Homogeneous and strong rock mass formations with no or single joint set having tight joint wall, wide spacing and anti-dip against valley slope	Highly porous rock mass of volcanic and sedimentary origin; Jointed rock mass having more than two systematic and long persisting joint sets with one or more joint sets dipping steeply towards valley slope
Faults and weak/crushed zones	No nearby major faults and zones of weakness	Nearby fault and zones of weakness that are parallel or cross-cutting to the valley slope
In-situ stress state	The minimum principal stress always higher than the static water head	De-stressed area and location not far away from the steep valley slope topography; Not sufficiently far away from the locally overstressed areas
Hydrogeology	Hydrostatic water line below natural groundwater table or tunnel aligned deep into the rock mass and far away from the steep valley slope restricted flow paths to reach valley slope topography	Hydro-static line above the groundwater table and relatively near from the valley side slope; Highly permeable and communication joint sets

5.5 Further development of design principle

Historical design criteria have been widely based on rock cover assumptions, and there is no doubt that the rules of thumb have been important in developing Norwegian and international hydropower. In addition to the Norwegian criterion, several different criteria have been used all over the world. Rancourt (2010) presents an overview of the evolution of the design criteria. However, several authors have claimed that such overburden criteria must be treated with caution, (Benson, 1989; Rancourt, 2010; Ødegaard and Nilsen, 2018). Recent studies have suggested improvements to the criteria or pointed out that current practice needs changes to reduce the risk of hydraulic failures, (Rancourt, 2010; Ødegaard and Nilsen, 2018). Three opportunities for improvement have been identified in the literature:

1. Procedure for determining the required factor of safety, (Rancourt, 2010)
2. State-of-art criteria, (Panthi and Basnet, 2018)
3. Development of a standardized, simplified hydraulic jacking test, (Ødegaard et al., 2020)

5.5.1 Use of safety factor

Research conducted by Rancourt (2010) suggests from a comprehensive numerical analysis that a factor of safety between 1.1 and 1.9 is sufficient to avoid hydraulic jacking. Through the research, Rancourt proposed a methodology for determining the necessary factor of safety (FS) in the preliminary assessment, as shown in Equation 5.4. The factor is intended to be used in the Norwegian Criterion for Confinement.

$$FS = F_a \cdot F_b \cdot F_c \tag{5.4}$$

where F_a represents the rock mass geological characteristics, F_b the rock overburden and F_c characterizes the structural geology situation. Tabulated values for Equation 5.4 are presented in Appendix A

5.5.2 State-of-art criteria

An important prerequisite for the confinement criterion is that it must reflect the actual value for minimum principal stress. In other areas of the world, where the geotectonic conditions are different than in Scandinavia, the rules of thumb must be used with caution, (Panthi and Basnet, 2017). Through a study of minimum principal stress in three typical topographies that can be found around the world, Panthi and Basnet (2018) suggested a state-of-art modification of the Norwegian confinement. Two of the models (1 and 2) describe typically Norwegian topographies. These topographies consist of a steep and deep side, while the other side is a flat higher-lying area. On the other hand, two models (2 and 3) represent an almost symmetrical and steep mountainside like in the Himalayas. The updated criterion is presented in Equation 5.5, and the factors are the same as those described in Figure 5.2.

$$L > f_g \cdot \frac{\gamma_w \cdot H}{\gamma_r \cdot \cos\beta} \tag{5.5}$$

where f_g represents a factor of safety. The study suggests two different multiplication factors (f' and f'') based on the ratio between the valley depth and the left and right sides. The purpose of this ratio is to be able to describe different topographies. The multiplication factors are presented in Figure 5.3. The first factor includes stress changes due to variation in topography. On the other hand, the second factor includes both stress changes and the presence of a weakness zone on the valley's left side. Panthi and Basnet (2018) claim that the proposed updated equation can be used in the preliminary design of unlined pressure tunnels/shafts in similar geological and geotectonic areas as in the Himalayas.

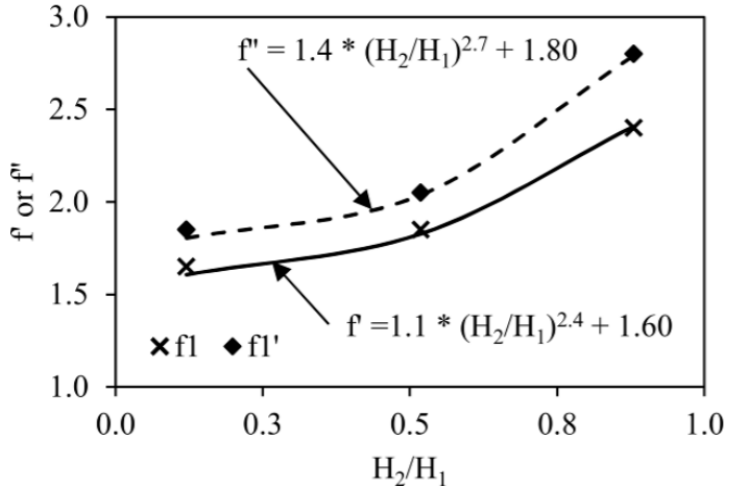

Figure 5.3: Multiplication factors for use in preliminary design of an unlined pressure tunnel/shaft, (Panthi and Basnet, 2018).

5.5.3 Development of a standardized, simplified hydraulic jacking test

Ødegaard and Nilsen (2018) claim that only one or two rounds of measurements normally are performed on Norwegian hydropower projects due to budget limitations. Thus, the minimum of test locations is the opposite of a continuous stress log along the tunnel. To get closer to this ideal situation, Ødegaard and Nilsen (2018) propose a new strategy for determining the final location of transition zones. The authors suggest that standardized hydraulic fracturing tests should still be performed at critical locations and supplemented by simplified jacking tests along the entire length of the pressure tunnel. In preliminary assessments, like preparing tender documents, overburden criteria may still serve as a valuable and simple tool, (Ødegaard et al., 2020). However, they should be treated with caution.

To increase the number of test site, Ødegaard and Nilsen (2021) suggested a Rapid Step-Rate Test (RSRT). The test is based on existing hydraulic methods, and laboratory experiments have confirmed the ability of this test. The results from the laboratory experiments demonstrate good agreement between measured and anticipated values of normal stress. In contrast to existing step-rate tests, RSRT enables rapid and semi-automated testing due to smaller increments and, short and fixed steps. As described in Section 3.5, current hydraulic stress measurements require skilled operators. RSRT is semi-automatic since the fixed steps can be pre-programmed in a computer-controlled pump.

Ødegaard and Nilsen (2021) point out that field verification is needed to assess the field applicability. The author of this master's thesis has been privileged to participate in the field measurements. The results and experiences will be presented and discussed later in the thesis.

Chapter 6

Løkjelsvatn hydropower project

6.1 General

The Løkjelsvatn hydropower project is located about 70 km northeast of Haugesund in Norway. As seen in Figure 6.1, the project is located in Litledalen in Etne municipality and Vestland county. The existing hydropower plants in the valley consist of the Litledalen (from 1920) and Hardeland hydropower plants (from 1950/1958). Løkjelsvatn hydropower plant is a new plant that contributes to an expansion of the power production in the valley, (SKL, 2018).

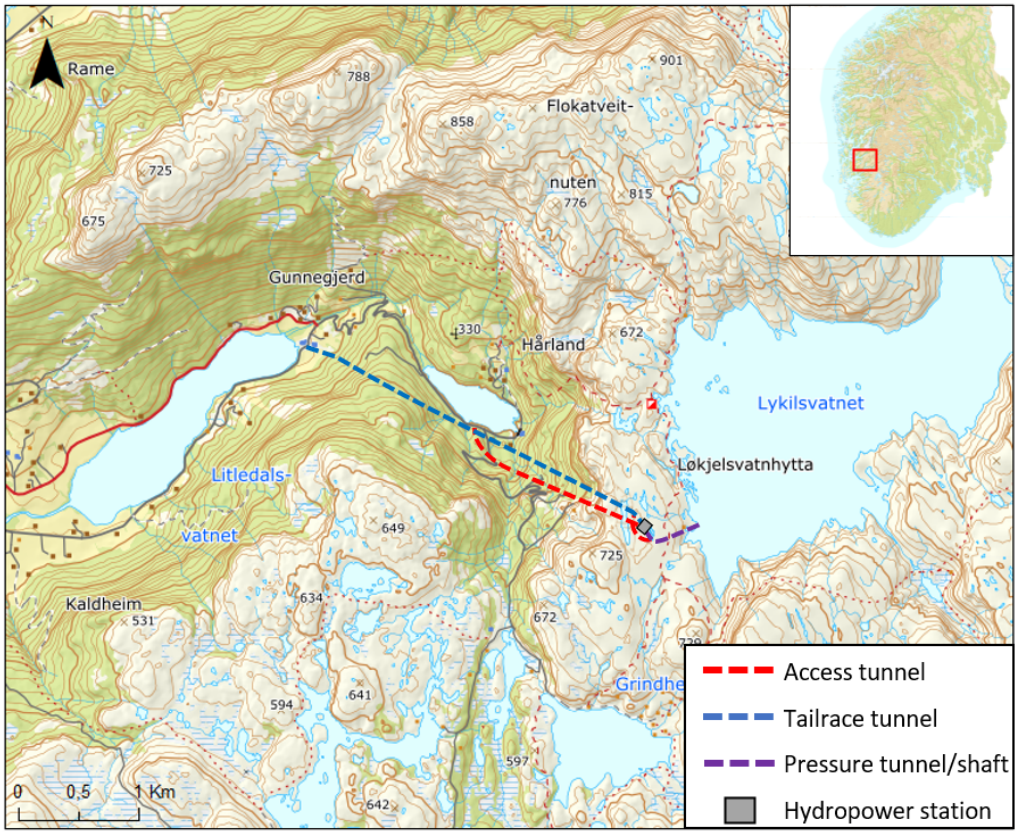

Figure 6.1: Map of Løkjelsvatn hydropower plant. Source: www.norgeskart.no

The project has an installed capacity of 60 MW and utilizes a head of 550 meters between the reservoirs at Løkjelsvatn (also called Lykilsvatnet) and Litledalsvatnet. The head is currently being utilized in the Hardeland and Litledalen hydropower plants. A pressurized tunnel system from the reservoir leads the water to the hydropower station built underground. Then, the tailwater comes out from the tailrace tunnel close to Litledalsvatnet. As can be seen in Figure 6.2, the project consists of a headrace tunnel, a vertical shaft, a pressure tunnel, an underground powerhouse and an access tunnel. In addition, the waterways consist of a tailrace tunnel which is not illustrated in the profile.

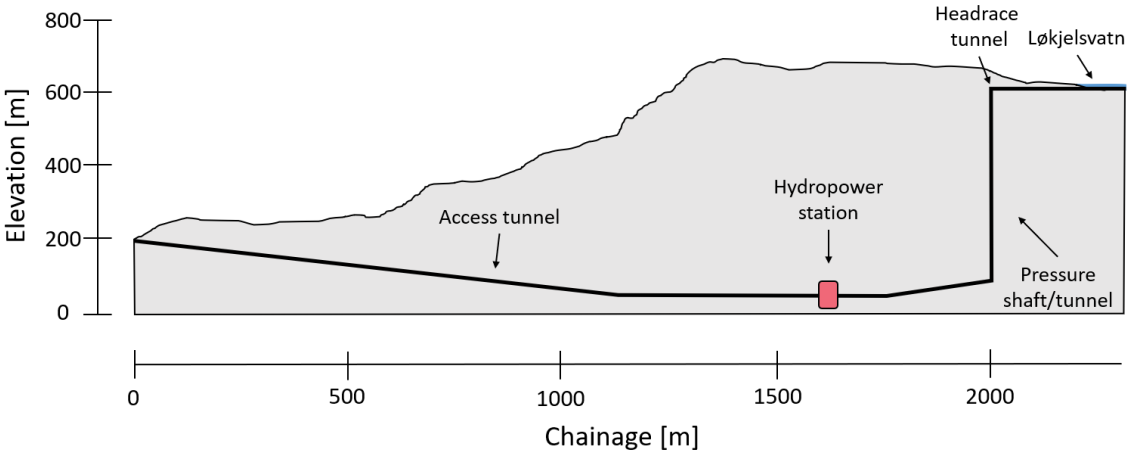

Figure 6.2: The longitudinal profile along with the waterway system.

6.2 Geology

6.2.1 Regional geology

No reports have been found that indicate detailed geological mapping in Etne. Still, studies of reports from nearby areas such as Sauda and Vindafjord provide information about the geology in the region, (NGU, 1975; NGU, 2013).

The project is located in the transition between the Precambrian basement and Caledonian nappes as shown in Figure 6.3. In general, regional geology is strongly affected by previous geological events. Thrust faults, metamorphic and jointed rock masses frequently occur in the region, (Ramberg et al., 2013). The origin of the rock masses in the region varies from the Precambrian to the Cambrian-Silurian age. The bedrock, which consists of Precambrian rocks, has its origin in the Sveconorwegian orogeny and plate collisions 1130 to 970 million years ago. According to Ramberg et al. (2013), a high-grade metamorphosis took place in southwestern parts of Norway at the end of this period. Today, different varieties of amphibolite and gneiss are common rock types in the region.

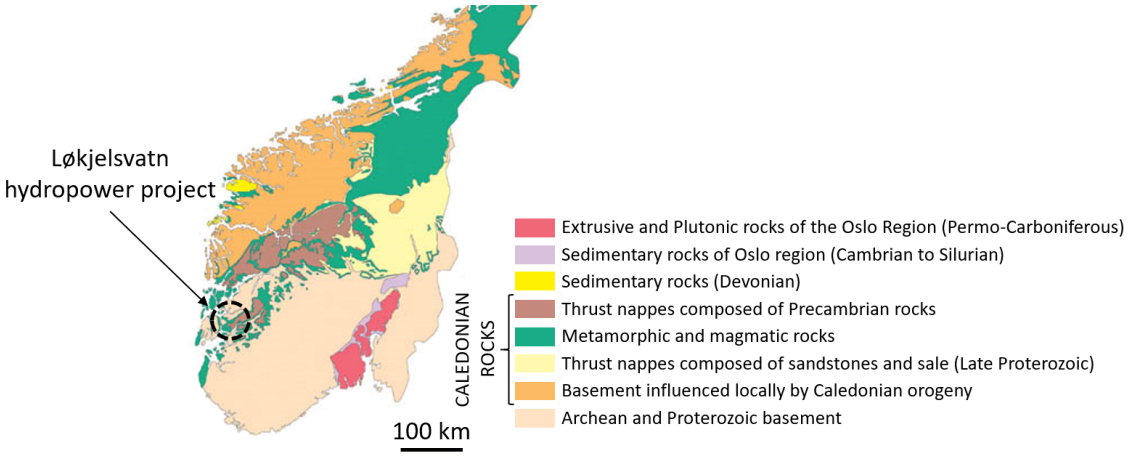

Figure 6.3: Simplified Geological Map of southern parts of Norway. Modified after NGU (2015).

The region consists of thrust nappes composed of Precambrian origin, (Ramberg et al., 2013). The nappes were pushed in over the mainland during the Caledonian mountain-building event. Etne dominates by rocks classified as *lower* allochthon. This layer includes nappes, which during the Caledonian orogenesis were transported shorter than the overlying nappes (*middle* and *upper*), (Ramberg et al., 2013). The lower nappes are mostly sedimentary deposits, and the metamorphism is characterized by low pressure and temperature. Examples of typical rocks in the region are phyllites, mica shale, or quartz-rich shale.

According to NGU (2014), the nappes in southern part of Vestland is a part of the Buadals Nappe (Viste Thrust sheet has also been used). These rocks are characterized by more or less quartz-rich and/or graphite-rich schist/phyllite, especially in the Ryfylke region. The boundary with the underlying autochthonous phyllite is often challenging to locate due to similar characteristics. In northern areas, the extend of the Buadals Nappe is several hundred meters in some areas, (NGU, 2014).

The structural geology in the area is characterized by displacement. According to NGU (1975), the thrust nappes have two main directions, NW-SE and Ø-W to ØNØ-VSV. In the Precambrian rocks, the displacement is in the NW to N/NW direction.

6.2.2 Project geology

According to geology maps from NGU (The Geological Survey of Norway) and findings in SWECO (2017), the rock types in the project area consist of two main types (see Figure 6.4). One part consists of phyllite or mica-schist/shale, and the other part consists of bedrock, such as amphibolite/gneiss. The bedrock is characterized as amphibolite, hornblende, and mica-rich gneiss (in some areas with migmatite textures), (SWECO, 2017).

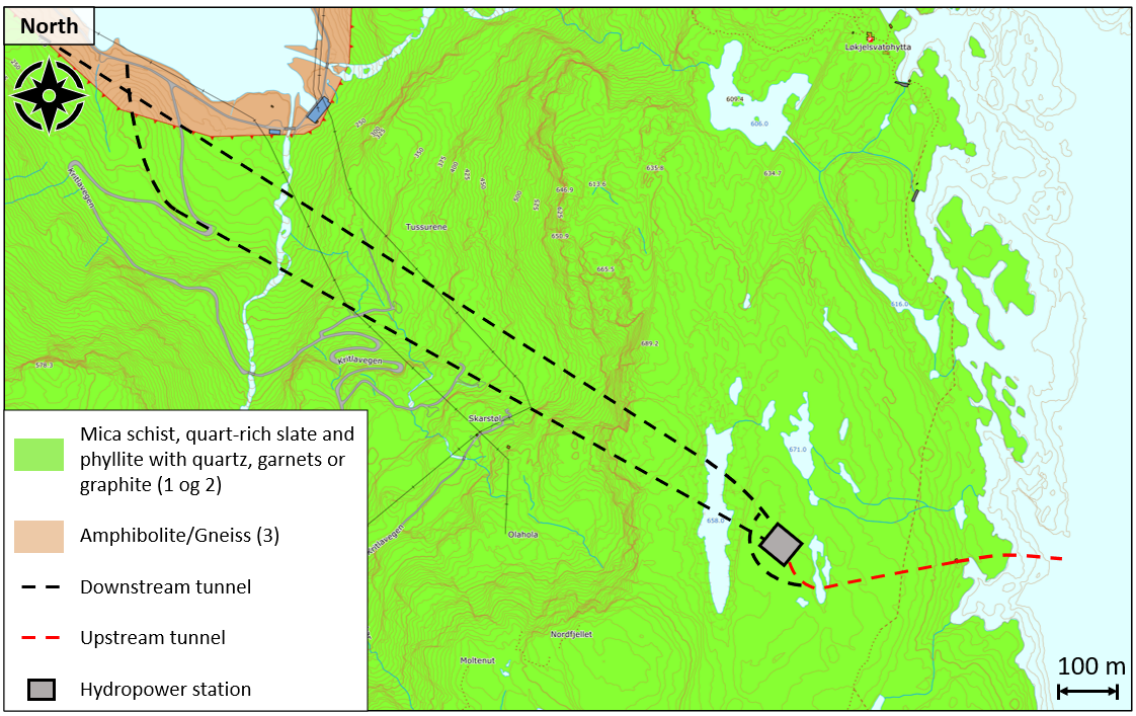

Figure 6.4: General geological map of the project area. Source: www.NGU.no

The geological report highlights three rock types that are important for the project. Picture of the most common rock types are presented in Figure 6.5, (SWECO, 2017):

1. **Phyllite:**
   - This rock type is strongly affected by metamorphism and has a noticeable content of quartz. Quartz occurs in highly concentrated veins and bodies, which usually are folded. The degree of jointing is massive to blocky, and the surface is characterized as rough and undulating (see Figure 6.5a).

2. **Phyllite/Slate:**
   - The rock type is characterized as heavily jointed with schistosity. According to the geological report, is not possible to identify the transition between this and the rock mass above (see Figure 6.5b).

3. **Gneiss (Fine-grained):**
   - The rock was characterized as granitic gneiss with some elements of amphibolite.

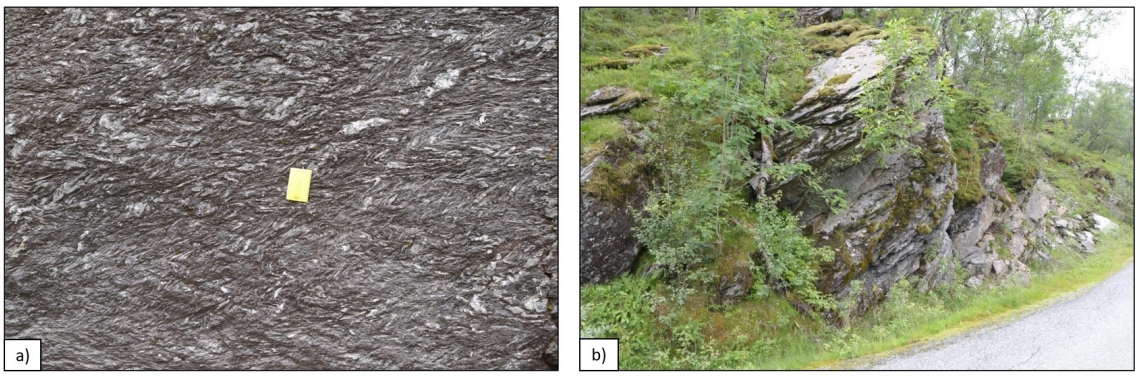

Figure 6.5: Pictures of two different rock types in the project area. The pictures show phyllite with quartz lenses (a) and phyllite with distinct foliation plane (b), (SWECO, 2017).

6.2.3 Topography and weakness zones

Slopes of naked rocks and scattered vegetation dominate the area between Løkjelsvatn and Litledalen. Close to the valley side, the rock mass consists of open and continuous joints. Geological mapping has identified one main joint set (1a) in addition to the foliation (1b) plus a random joint set (1c), as presented in Figure 6.6, (SWECO, 2017).

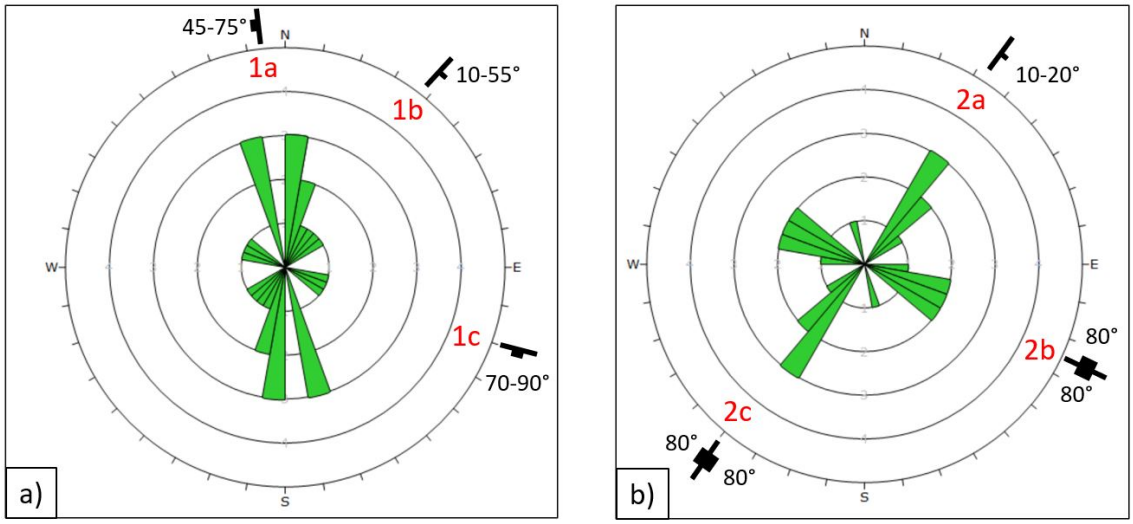

Figure 6.6: Joint rosettes from the surface between Løkjelsvatn and the hydropower station (a), and the valley side (b) identify two joint sets and the foliation. Modified after SWECO (2017).

Figure 6.7 indicates two distinct weakness zones, denoted by 1 and 2. These zones cut the terrain above the access tunnel, and the width is significantly more than 10 meters in some places. The dip is relatively steep, almost vertical. In the area close to the lake at 658 MASL, open joints are predominant. The rock mass is intensely fractured, especially between the elongated lake area at 658 MASL and the slope against the valley. Figure 6.7 illustrates this area, which consists of a 300-400 meters wide lineament. Intensely fractured with random directions within the lineament describes this area within the lineament. In some places, the thicknesses are in some up to 10 meters with unknown depth, (SWECO, 2017).

On the valley side, the terrain consists of a blocky rock mass with few and pervasive joints. The terrain is steep, with up to 100 meters of steep mountainsides. Field mapping has identified the foliation (2a) and two approximate vertical joint sets (2b and 2c), as shown in Figure 6.6. Within the same area, two prior landslides have been observed during field mapping, (SWECO, 2017). Throughout the area, the surface dominates by discontinuities oriented in a northeast-southwest and northwest-southeast direction with a relatively steep dip, (SWECO, 2017).

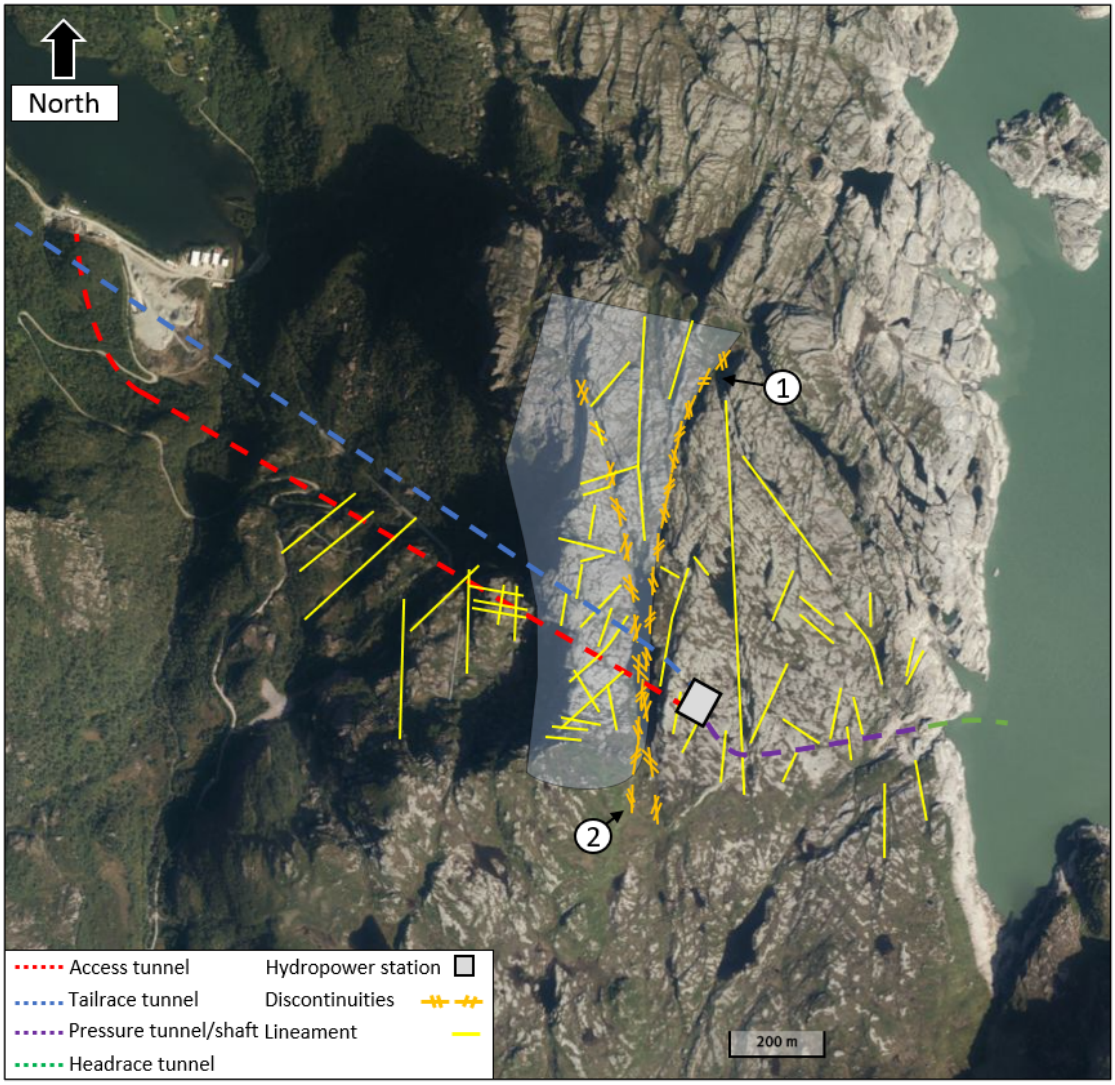

Figure 6.7: Overview of tunnel alignment with indicated discontinuities (orange) and lineaments (yellow) close to the hydropower station. Source: www.norgeskart.no

6.3 Rock stress measurements during construction by SINTEF

During the construction of the access tunnel, rock stress measurements were carried out at four different locations. These tests have been carried out as hydraulic fracturing (HF) based on the procedure described in Section 3.4. The test locations are refered to as HF-1 to HF-3 in Figure 6.8. The rock stress measurements at HF-4 will be presented in Chapter 8. The test procedure and principle of hydraulic fracturing is described in Section 3.4. The results of the tests are shown in Table 6.1. A test is considered successful if the test achieves the fracturing of the rock mass.

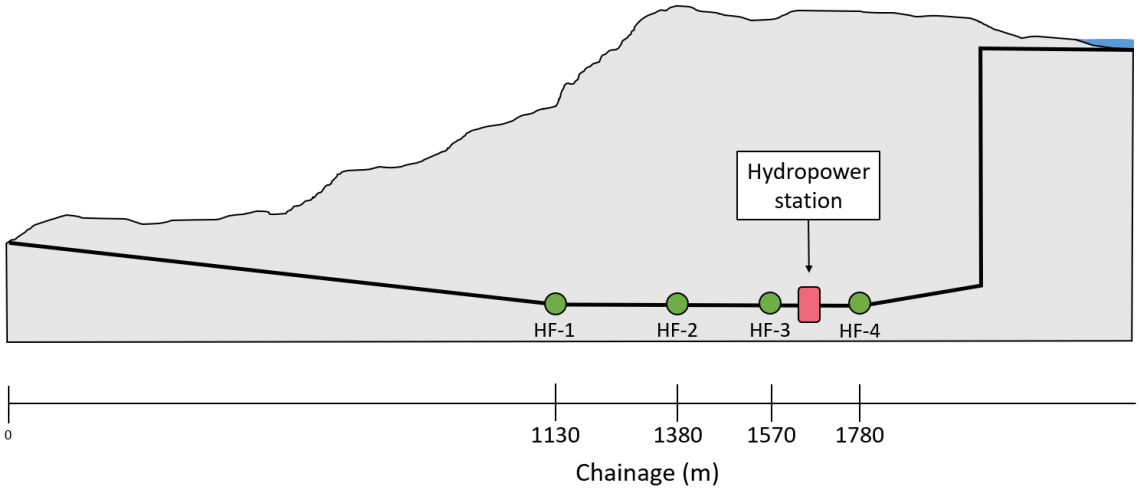

Figure 6.8: Overview of rock stress measurements during construction, e.g. HF-1 refers to the first test at chainage 1130 m. The final location of the hydropower station is marked.

Table 6.1: Overview of rock stress measurements along the access tunnel during construction, (SINTEF, 2020).

Chainage	Number of tests	Successful tests	Succesful rate [%]	Min [MPa]	Mean [MPa]	Max [MPa]	St.dev. [MPa]
1130	24	17	70.8	3.5	5.2	7.4	1.1
1380	18	13	72.2	3.3	4.8	6.8	0.7
1570	8	3	37.5	4.2	5.6	6.5	1.0

6.4 Leakage during construction

Periodically, the excavation has met challenges in the access tunnel due to high inflow. Especially between chainage 1100 m and 1600 m, the progress has been laborious. Consequently, this has led to a strong need for grouting to prevent the water from filling the tunnel. A study of the drilling reports for the holes drilled for rock stress measurements at chainage 1380 m and 1570 m shows high leakage values. Especially at chainage 1380 m, the report from the contractor shows up to 3500 l/min from specific boreholes. In Table 6.2 some of the data are summarized, (YIT, 2020). The reports indicate that the water contact is located 14 to 17 meters from the tunnel wall. At chainage 1570 m, the leakage occurs at 4.5 to 20 meters into the rock mass.

Table 6.2: Overview of key values from drilling reports on chainage 1380 m and 1570 m, (YIT, 2020).

Chainage	Length of borehole [m]	Drill rate [m/min]	q_{min} [l/min]	q_{mean} [l/min]	q_{max} [l/min]
1380	31.5	1.5-2.0	1750	1982	>3000
1570	31.5	1.5-2.0	10	1355	3500

6.5 Description of test area

Final rock stress measurements were carried out at the Løkjelsvatn hydropower project in January 2021. Figure 6.9 shows a sketch of the planned transition zone, which is the intersection between the access tunnel and the pressure tunnel. In this area, hydraulic fracturing, 3D overcoring, and Rapid Step-Rate Test (RSRT) were carried out. The figure shows details of the test location and the boreholes. Borehole L1 to L4 were only used for RSRT. On the other hand, boreholes L18 to L23 were drilled for hydraulic fracturing. Two rock samples (Sample 1 and Sample 2) were collected from the test area.

6.5.1 Geology

At the upstream side of the hydropower station, the rock mass alternates between two layers of phyllite. In general, two layers are most prominent: One compact (represented by Sample 1) and one layer that appears more foliated and schistose (represented by Sample 2). The two main variants are shown in Figure 6.10 with a registered boundary between the two layers. The mineral composition varies. Hence, Sample 1 and Sample 2 were brought back to the laboratory in Trondheim to determine the mineral compositions (XRD). The sampling position is indicated in Figure 6.9.

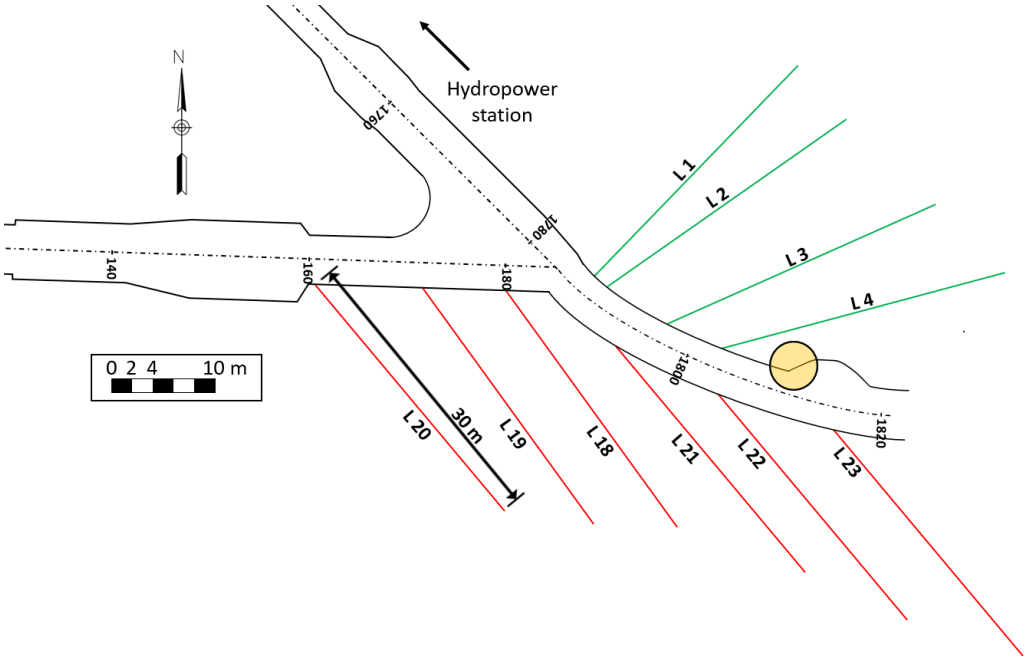

Figure 6.9: Illustration of test area shows location and direction of test holes. L1 to L4 were subjected to RSRT only, while both tests are tested in L18 to L23. Sampling position for Sample 1 and 2 is marked with a yellow circle.

The compact layer dominates the rock mass along the tunnel. The surface is gray to light gray with light-colored grains, probably quartz. Quartz-filled veins and quartz lenses are observed, together with small-scale folding patterns. The joint surfaces tend to have a rough to smooth surface, and the degree of jointing consists of one joint set and the foliation, plus random joints. The foliation plane forms the most prominent joint set with a spacing of 40-60 cm. The almost vertical joint set has rough and flat surfaces with a joint spacing of 1-2 m.

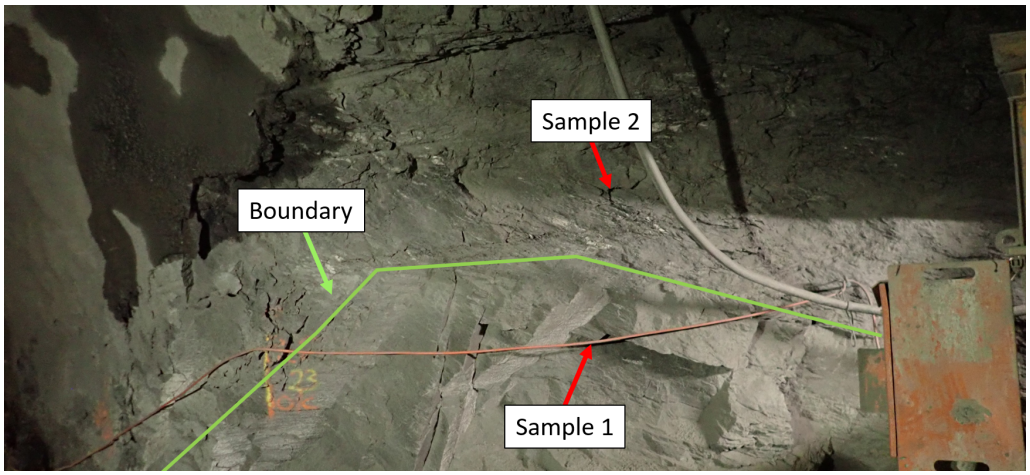

Figure 6.10: Picture showing sampling position for Sample 1 and Sample 2 at chainage 1815 m. The boundary between the two layers is indicated.

The second variant of phyllite is dark gray to black and has a shiny cleavage with a smooth and rough surface. The surface is smooth and planar, possibly due to graphite or chlorite minerals. One joint set and random jointing are registered in the phyllite, where the most pronounced joints follow the foliation plane. The joint spacing is generally 0.5-1 m.

Both units of the rock mass have a distinct foliation. As shown in Figure 6.11, one main joint set (J1) is identified beside the foliation. Table 6.3 summarizes the strike and dip values collected at the test location. The dip angle of J1 and J2 is relatively steep, and varying between 52-85°.

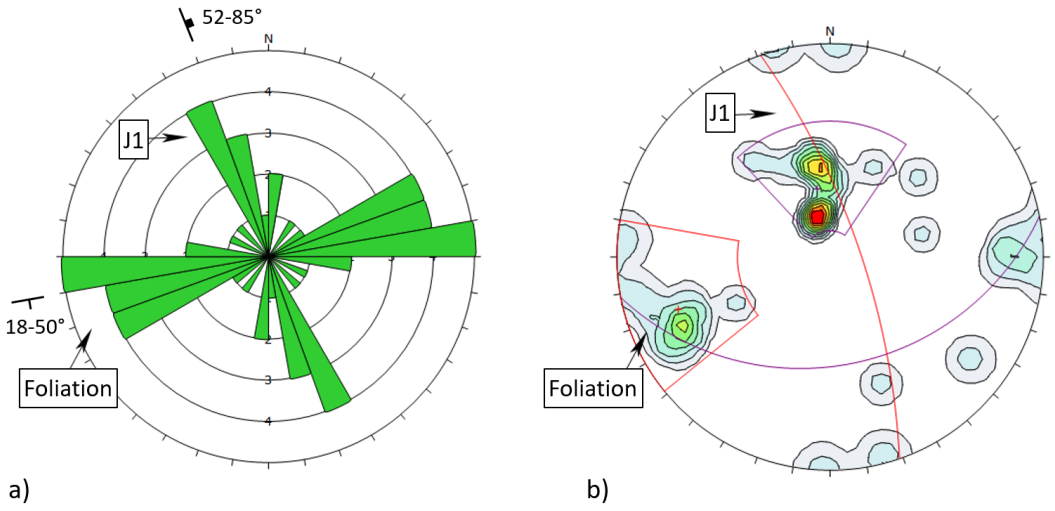

Figure 6.11: Orientation of the joints identified during field mapping presented in a rosette (a) and a contour plot (b).

Table 6.3: Strike and dip mean values

Catory	Unit	Strike	Dip	Quantity
Foliation	Phyllite	N062-089°Ø	18-50°S	11
J1	Phyllite	N012-030°V	52-85°NE	7
Random	Phyllite			11
Total				29

6.5.2 Rock mass classification based on the Q-system

The rock mass quality at the test area was mapped during fieldwork, and registration was mainly carried out according to the Q-system as defined by Barton et al. (1974). The Q-values were mapped at 10 locations close to the different boreholes (L1 to L4 and L18 to L23). The mapped values are listed in Table 6.4, which give a mean value of 6.5. Based on the chart, as presented in Appendix A, the rock mass quality can be classified as *poor* to *good*. In general, the rock mass appears to be compact except for the areas with the foliated and schistose variant of phyllite, which are more fractured and consequently have lower RQD-value.

Table 6.4: Rock mass quality at test location.

ID	RQD	J_n	J_r	J_a	J_w	SRF	Q-value
L1	75 - 80	3 - 6	1 - 4	4 - 8	1	1	1.6 - 27
L2	70 - 75	3 - 6	1 - 4	4 - 8	1	1	1.5 - 25
L3	45 - 50	3 - 6	1 - 4	4 - 8	1	1	0.9 - 17
L4	75 - 80	3 - 6	1 - 4	4 - 8	1	1	1.6 - 27
L18	55 - 60	3 - 6	1 - 4	4 - 8	1	1	1.1 - 9
L19	55 - 60	3 - 6	1 - 4	4 - 8	1	1	1.1 - 20
L20	55 - 60	3 - 6	1 - 4	4 - 8	1	1	1.1 - 20
L21	70 - 75	3 - 6	1 - 4	4 - 8	1	1	1.5 - 25
L22	70 - 75	3 - 6	3 - 4	4 - 8	1	1	4.4 - 25
L23	75 - 80	3 - 6	3 - 4	4 - 8	1	1	4.7 - 27

6.5.3 Rock mass classification based on GSI

The geological strength index (GSI) is a system of rock mass classification developed to link the failure criterion to engineering geology observations in the field, (Hoek and Brown, 2019). In order to determine the GSI parameter from the Q-system for further evaluations such as numerical modeling, several empirical formulas have been suggested, such as Hoek et al. (1995):

$$GSI = 9log_e(\frac{RQD}{J_n} \cdot \frac{J_r}{J_a}) + 44 \tag{6.1}$$

Later Hoek et al. (2013) further developed the Equation 6.1, and suggested the following solution applying the parameters of the Q-system:

$$GSI = \frac{52(J_r/J_a)}{(1 + J_r/J_a)} + \frac{RQD}{2} \tag{6.2}$$

Based on Q-values presented in Section 6.5.2, this approach gives a range between 43-73 with Equation 6.1. On the other hand, Equation 6.2 estimates the GSI to 28-66. The results from these empirical approaches are presented in Figure 6.12 with lower and upper bound based on the field mapping at Løkjelsvatn.

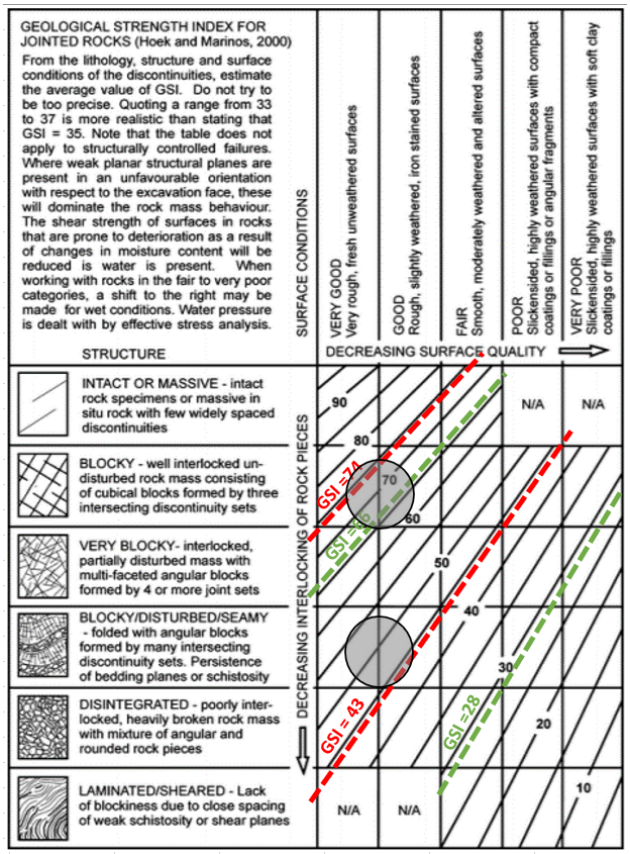

Figure 6.12: Range of GSI-values based on Equation 6.1 (red) and Equation 6.2 (green) indicated in GSI chart presented in Hoek and Brown (2019). Grey circles represents GSI-values based on observations in the field.

Hoek (2007) claims that these empirical have proved to be reliable, particularly for poor quality rock masses and for rocks with lithological peculiarities. Therefore, it is recommended that GSI-values should be evaluated directly from the chart presented in Figure 6.12 and not from empirical classifications, (Hoek, 2007). The surface conditions consist of good to very good conditions with fresh unweathered and rough surfaces in the field area. The rock mass varies between relatively compact with few intersecting joint set to the persistence of schistosity. Even if the upper part of the range is most typically for the rock mass, the schistosity needs to be considered calculations.

Chapter 7

Laboratory examination

During fieldwork in January 2021, rock samples from the transition zone were obtained. The primary purpose of the laboratory work is to achieve information about the mechanical properties. In addition, it is advantageous to understand the material's mechanical behavior and compare the results with similar rocks from other locations. The author tested the samples with assistance from senior engineers Gunnar Vistnes and Jon Runar Drotninghaug at the Rock Mechanics Laboratory at NTNU. The procedures and results from the laboratory investigations will be presented in this chapter.

7.1 X-ray Powder Diffraction (XRD)

An important part of the rock mass characterization is to determine the mineralogical composition and texture. The most common methods of these types of analyses are thin section and X-Ray diffraction techniques, (ISRM, 1978a). During the fieldwork, two layers of phyllite with different mechanical properties were observed. Figure 7.1 shows the two samples. Sample 1 represents the compact layer, and Sample 2 represents the schistose layer. Based on observations, there are indications that the mineral composition varies between the layers. Therefore, in order to be able to assess the mineral content and distinguish between the different ones, X-Ray powder diffraction (XRD) has been carried out. Only XRD was completed during the laboratory examination since only an approximate mineralogical composition is necessary.

XRD is based on the diffraction of X-Ray waves from the crystal lattice in the minerals. The incident rays will be reflected from different planes when X-Rays hit a crystal. Bragg's law is used to express the conditions. No mineral has the same space between the atomic planes, and therefore, the angle calculated enable mineral identification, (Mitchell and Soga, 2005).

7.1.1 Procedure

Figure 7.1 shows the two samples collected at the test location (see Figure 6.9). The procedure of XRD starts with grinding a representative rock piece into a fine powder and packed into a sample holder. Then, the upper surface is flattened and placed into the x-ray machine. During the test, the diffracted x-rays are continuously recorded as the sample and deflector go through a range of angles. The intensity of the diffracted waves is recorded, and an XRD plot gives the result. By comparing peak positions in the XRD plots with reference patterns, the mineral compositions were found.

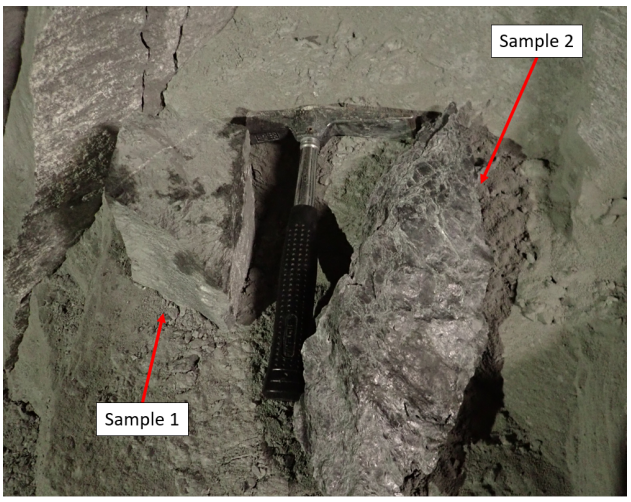

Figure 7.1: Picture showing Sample 1 and Sample 2 before grinding.

7.1.2 Results

The results are summarized in Table 7.1, and the plot of the X-Ray patterns from the analysis is given in Appendix B. The plot shows the mineralogical content in the sample. It can be seen from the table that the samples mainly are composed of quartz and muscovite. Minor components are chlorite, albite, pyrrhotite, calcite, and magnesite. Chlorite minerals likely contribute to the smooth surface that has been observed in the rock mass. As can be seen in the table, the minerals representing the two samples do not vary considerably.

Table 7.1: Results from XRD analysis of phyllite

Mineral	Sample 1 [%]	Sample 2 [%]
Quartz	39	42
Muscovite	36	41
Chlorite	15	9
Albite	11	7
Pyrrhotite	0	1
Calcite	< 1	< 1
Magnesite	< 1	< 1

7.2 Sonic velocity

Before the Uniaxial compressive strength test (UCS), the sonic velocity was tested in the specimen. Sonic wave velocities are related to density, and density is related to rock composition. By definition, the propagation of seismic waves' velocities is determined by the appropriate elastic modulus and densities. Hence, these velocities provide important information about the rock mass, (Condie, 2015).

In this test, only compressional body waves (P-waves) were performed. In the case of micro-cracked, fractured, or jointed rock masses, the P-wave velocity will reduce. Similar, strongly anisotropic rocks such as slate and phyllites show significant velocity differences when testing parallel or perpendicular to the foliation plane, (Barton, 2006). Tsidzi (1997) shows through extensive laboratory assessment a distinct effect of the measurement direction to the foliation plane.

7.2.1 Procedure

The equipment consists of a generator that permits continuous sound wave generation with high power over a wide frequency. The wave generated from the generator was sent through the specimen and received by the receiver. At the coupling points, where the transmitter and the receiver were in contact with the specimen, an ultrasonic gel with high viscosity provides contact between the elements. Figure 7.2 illustrates the setup with the test directions to the foliation plane.

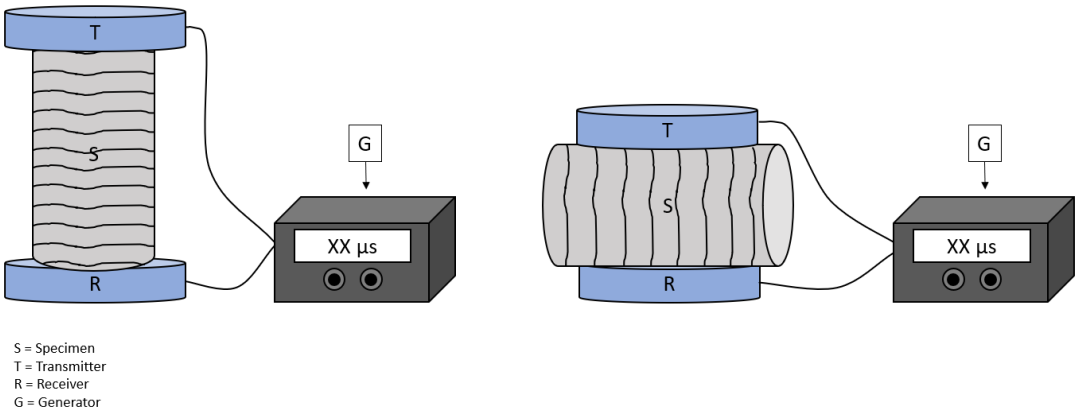

Figure 7.2: Setup for the velocity tests indicating axial (left) and diametral (right) direction.

Figure 7.3 shows UCS 1 to UCS-4 before the testing. As can be seen in the figure, the samples have small-scale folding patterns. However, the length direction of the samples tends to be perpendicular to the foliation. The sonic velocities were tested in both longitudinal and diametric directions of the specimen to assess the degree of anisotropy.

Figure 7.3: Photo of UCS-1, UCS-2, UCS-3 and UCS-4 (from left to right) before testing.

7.2.2 Results

Table 7.2 summarizes the results from the tests. In the longitudinal direction, the mean wave velocity is 4934 m/s. On the other hand, the mean wave velocity in the diametric direction is 5738 m/s. These results give a ratio of 1.16 between the diametric and longitudinal directions. The ratio is in good agreement with previous studies of wave velocities in anisotropic rocks, (Tsidzi, 1997). Typically, the coefficient of anisotropy varies between 1.0 and 1.40 since the velocity parallel to the foliation is greater than the velocity perpendicular to the foliation, (Barton, 2006)

Table 7.2: Results from sonic velocity test on UCS samples.

Sample	Length [mm]	Diameter [mm]	Longitudinal direction		Diametric direction		V_d/V_l
			Sampling time [μs]	Wave velocity [m/s]	Sampling time [μs]	Wave velocity [m/s]	
UCS-1	108.89	39.66	21.4	5088	6.9	5748	1.13
UCS-2	108.84	39.69	21.4	5086	7.3	5436	1.07
UCS-3	95.03	39.66	19.0	5002	6.5	6102	1.23
UCS-4	93.00	39.65	20.4	4559	7.0	5664	1.24
Mean	-	-	-	4934	-	5738	1.16
St.dev.	-	-	-	219	-	239	0.09

7.3 Uniaxial compressive strength test

The primary purpose of UCS tests is to determine the strength and the elastic parameters of the samples. These parameters provide information about the behavior of the rock mass. In addition, the parameters are important for the reliability of numerical analysis. According to Golod et al. (1975) parameters like mineral composition, structure, texture, bedding, jointing, and water content are some of the factors affecting the strength of rock samples. Bieniawski and Bernede (1979) describes the standard procedure for determining the uniaxial compressive strength and deformability of rock material. The procedure has been followed by the author.

7.3.1 Procedure

The samples were obtained during fieldwork in January 2021. Furthermore, the samples were prepared for testing. According to the standard, a height to diameter ratio of 2.5 to 3.0 is required. When preparing the samples, the foliation plane to the block made it challenging to obtain satisfactory lengths with intact cores. The height to diameter ratio for UCS-3 and UCS-4 does not meet the requirements in Bieniawski and Bernede (1979). However, the results are threatened with caution due to the limited number of alternative samples.

The test was performed at Rock Mechanics Laboratory at NTNU in Trondheim in 26.02.2021-01.03.2021. The equipment was a GCTS RTR-4000 rock press. Before installation, the samples were applied to a plastic cap for the protection of test equipment. Further, the specimens were loaded axially during gradually increasing loading until fracture occurred. The time frame was monitored with three extensometers, two axial and one radial. Photo of the sample setup without the axial extensometer and acoustic emission sensors is shown in Figure 7.4.

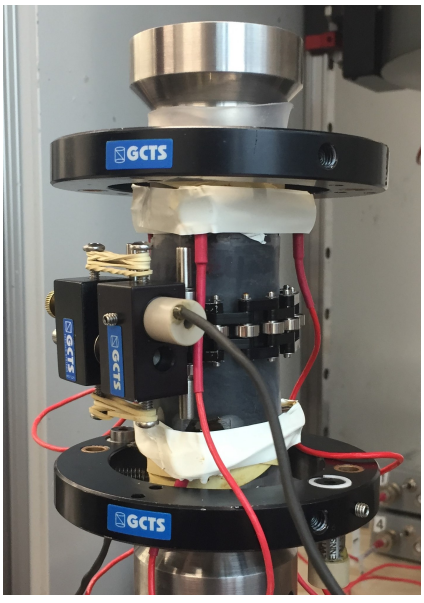

Figure 7.4: Photo of test setup with acoustic emission sensor for UCS testing.

7.3.2 Results

The results from the UCS test are presented in Table 7.3. Young's modulus and Poisson's ratio are determined in the linear elastics range. Still, some adaptions have been done to fit the tangent to the graph. The curves of UCS-1 to UCS-4 are presented in Appendix B. The graph shows axial stress vs. axial and radial strain. The post-peak behavior after yielding is removed in these curves.

Table 7.3: Results from UCS analysis of phyllite

Sample	Diameter [mm]	Length [mm]	Weight (dry) [g]	Density [g/cm^3]	UCS [MPa]	UCS_{50} [MPa]	E-modulus [GPa]	Poisson's ratio
UCS-1	39.66	108.89	379.15	2.819	71.9	69.0	38.19	0.34
UCS-2	39.69	108.84	380.04	2.822	74.3	71.3	32.42	0.35
UCS-3	39.66	95.03	331.01	2.820	67.7	64.9	32.24	0.36
UCS-4	39.65	93.00	323.92	2.821	55.8	53.5	27.92	0.34
Mean	-	-	-	2.821	67.4	64.7	32.69	0.35
St.dev	-	-	-	0.001	7.1	6.8	3.60	0.01

The results indicate that the uniaxial compressive strength 67.4 MPa, while E-modulus is 32.7 GPa and Poisson's ratio is 0.35. However, the test was performed on cores with a diameter of 40 mm. Therefore, an equation suggested by Hoek and Brown (1980) is used to find the corresponding strength for cores of 50 mm, which is the recommended size of test samples. Thus, the UCS used in further calculations is 64.7 MPa.

Two different modes of failure were observed. As can be seen in Figure 7.5, shear failure occurred in UCS-1, UCS-2, and UCS-4. The failure plane was covered with some crushed material with lower friction. On the other hand, the mode of failure for the fourth specimen (UCS-3) might be described as multiple fracturing. The failure plane tends to be more fractured with means of fine-grained material with low friction.

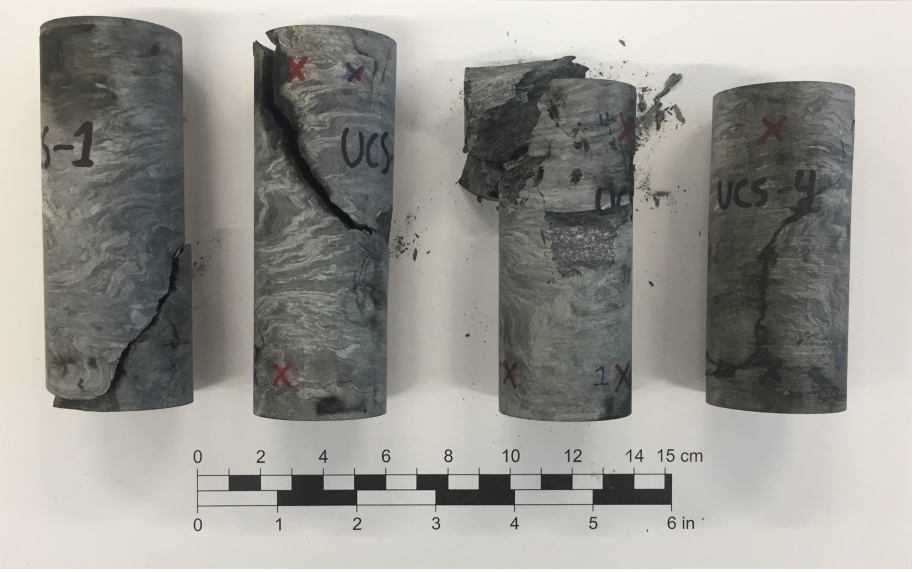

Figure 7.5: Failure modes observed in specimens after tests. From left: UCS-1, UCS-2, UCS-3 and UCS-4.

7.4 Acoustic emission

ISRM (2017) defines acoustic emission (AE) as "... high-frequency elastic waves emitted from defects such as small cracks (microcracks) within a material when stressed, typically in the laboratory. During propagation of cracks, strain energy is released as elastic waves." Therefore, AE enables the study of the loading rate dependence of acoustic emissions for observing failure in rock samples due to highly sensitive sensors, (ISRM, 2017).

7.4.1 Procedure

The equipment consists of six sensors in two groups with a 60-degree angle between the sensors. Three sensors are placed at the upper part, while the rest are located at the lower part. Each of these sensors is connected to an amplifier and a band-pass filter to reduce noise. The system is then connected to a PC for continuous digital monitoring during the UCS test. Finally, the measured values from AE are interpolated to fit data from UCS.

7.4.2 Results

Results from UCS testing with AE sensor for UCS-4 are shown in Figure 7.6. As can be seen in the graph, the stress-strain curve includes four stages: compaction (O-A), elastic (A-B) and plastic deformation (B-C), and the residual strength stage (D). Generally, in the first stage, the primary microcracks in the sample close with the increase of axial stress. There are almost no generated microcracks inside the

rock in the second stage, which correspond to the stress-strain curve's linear part. The irreversible plastic deformation occurs in the plastic deformation stage as the stress keeps increasing. At the same time, a large number of new micro cracks and joints form and expand rapidly in the rock specimens, resulting in brittle failures.

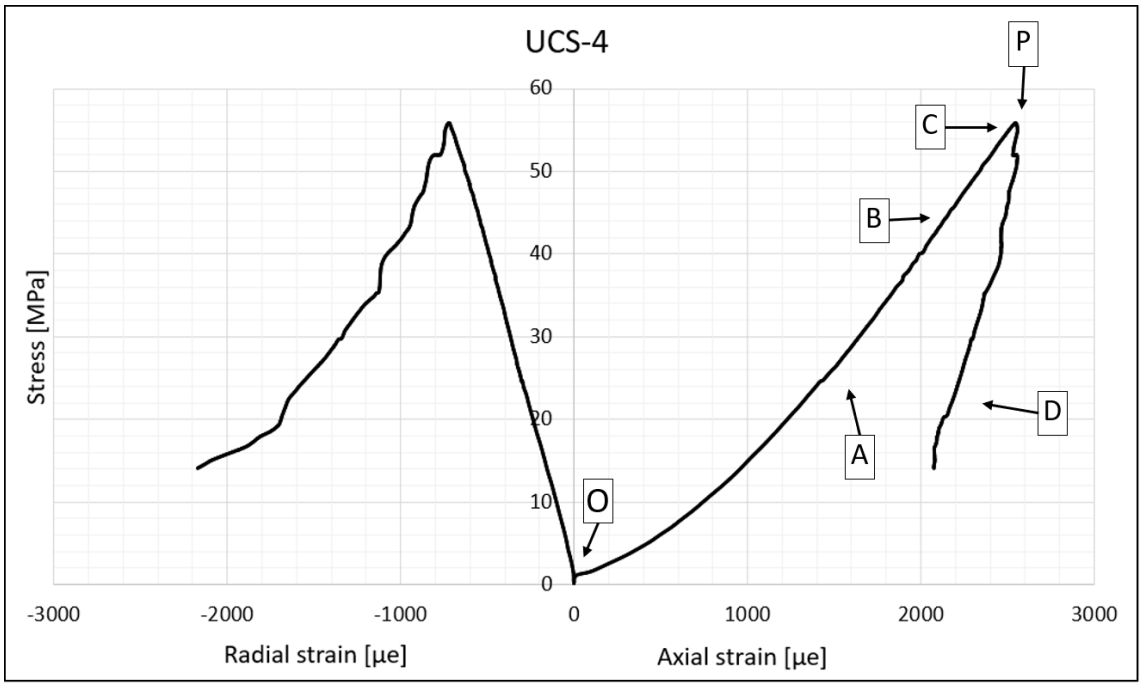

Figure 7.6: Stress-strain curve from testing of UCS with points indicating different stages during the test.

Figure 7.7 shows a corresponding graph of the AE hits during the tests. In the first stage, the compaction stage, an increase in AE hits due to the closure of primary cracks. As can be seen in the figure, the number of AE hits is significant in this stage. In the second stage, the number of AE hits is low, and the cumulative AE curves are relatively stable during the elastic stages. The transition between elastic and plastic deformation is indicated at point (C), and this point is prominent in the stress vs. volumetric strain curve. Then, at the plastic stage, the number of AE hits fluctuates at a large amplitude. A continuous nonlinear increase and a peak occur. Finally, suddenly brittle failure takes place whereafter the maximum AE count. Complete stress-strain curves of all tests with associated AE data during uniaxial compression are presented in Appendix B. Corresponding volumetric strain curves are shown in the same appendix.

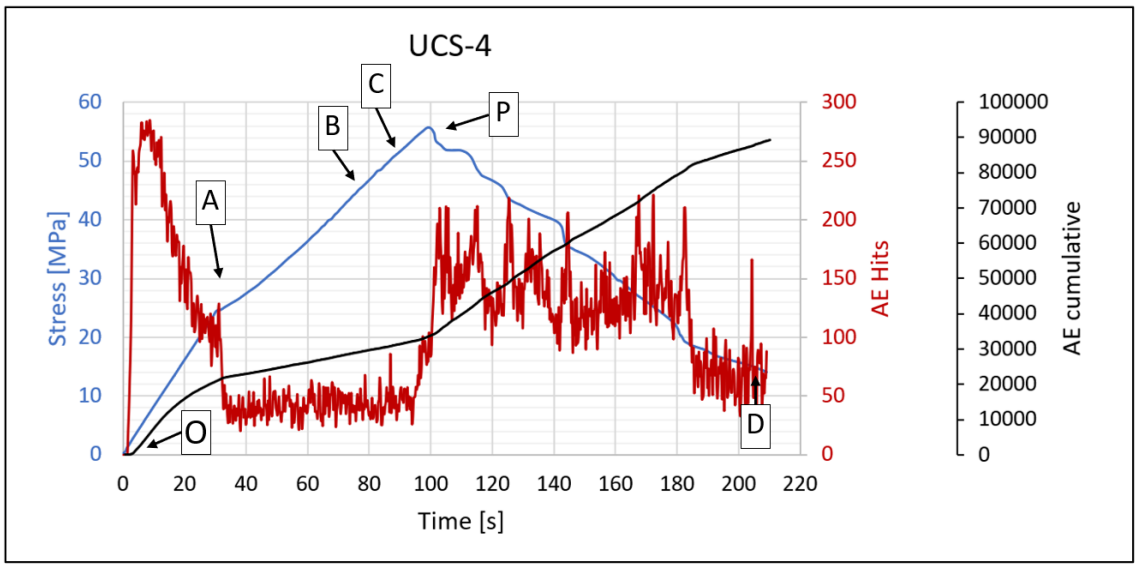

Figure 7.7: Stress curve (black) for UCS-4 as a function of time with registered AE hits (red). The black line represents the total number of AE hits.

7.5 Brazilian test

The purpose of the Brazilian test is to measure the tensile strength of a rock specimen indirectly. The test is mainly intended for the classification and characterization of intact rock, (ISRM, 1978b). The Brazilian test is commonly and widely used to determine the tensile strength of rock thanks to its easy sample preparation and simplicity of testing, (Tang and Hudson, 2010).

7.5.1 Procedure

In short, disc-formed test samples with a diameter of approximately 50 mm and thickness half of the diameter were prepared. Then, the circular disc is placed between two claws and loaded diametrically until a tensile fracture is provoked. The tests were conducted in a GCTS Point Load Tester (Enerpac PLT-1000). In total, nine tests were carried out. Finally, the tensile strength (σ_t) is calculated with Equation 7.1, (ISRM, 1978b):

$$\sigma_t = \frac{2}{\pi} \cdot \frac{P}{Dt} \tag{7.1}$$

where P represents measured load at failure, D is the diameter of the sample and t is the thickness.

7.5.2 Results

As can be seen in Figure 7.8, two tests were invalid due to incorrect fracture development. A test is considered valid if the initiated fracture pass upper and lower loading points. All test results are presented in Appendix B. However, during the test, a leak occurred in the pump, and it had to be repaired. The jack was then calibrated with a test cell to reduce deviations. After the repair, the results showed a large deviation between the results before and after changing the cylinder. Therefore, the tensile strength is calculated based on values from the last five tests. Table 7.4 summarizes the results from the valid tests. The results give a tensile strength of 7.85 MPa with a standard deviation of 1.13 MPa.

Figure 7.8: Photo of samples B-1 to B-9 after tensile failure. B-1 and B-6 have invalid failure.

Table 7.4: Results from Brazilian test.

Test	Diameter [mm]	Thickness [mm]	Pressure [kN]	σ_t [MPa]
B-5	50.94	25.37	17.26	8.50
B-7	50.95	25.16	18.89	9.38
B-8	50.99	24.91	13.36	6.70
B-9	51.01	25.10	13.74	6.83
Mean	-	-	-	7.85
St.dev.	-	-	-	1.13

7.6 Point load test

The purpose of the point load test is as an index for rock classification and characterization. The test may also be used to predict other strength parameters, for example, uniaxial tensile and compressive strength, (ISRM, 1985). The principle is that a piece of rock is loaded between two steel points and loaded until fracture occurs. According to Nilsen and Palmstrøm (2000), the advantage of the test is that the point load strength index (I_s) on specimens can be determined in the field without preparations. In addition, the equipment is simple. The point load strength index is defined by Equation 7.2, (ISRM, 1985).

$$I_s = \frac{P}{{D_e}^2} \tag{7.2}$$

where P represents measured load at failure and D_e is equivalent sample diameter.

7.6.1 Procedure

The samples were collected during fieldwork in January 2021, and the position for obtained sample (Test 1-35) is between boreholes L18 and L19 (see Figure 6.9). The remaining samples are taken from the same block used for UCS and Brazilian test. The samples were cut out from the block with a 40 mm thick and circular cutter. Furthermore, the length of the specimen is adapted to satisfy requirements in the standard. Common for Test 1-35 is that the length direction is parallel or perpendicular to the foliation plane. An example of the specimen (Test 1-35) is presented in Figure 7.9. ISRM (1985) emphasizes that care should be taken to ensure that the load is applied perpendicularly to the weakness planes in similar situations.

7.6.2 Results

Sixteen tests were carried out with loading parallel with the foliation plane, and 30 tests were done perpendicular to the foliation. A total of 22 tests were considered invalid due to requirements in ISRM (1985). The test results are given in Appendix B. In addition, the obtained mean values and anisotropy index from the testing are calculated according to ISRM (1985) and presented in Table 7.5.

The point load index results indicate that the samples proved to be very strong in the direction perpendicular to the foliation plane. On the other hand, the strength in the direction parallel to the foliation was governed by the strength of the weakness planes. The anisotropy index indicates that the rock type is more than three times stronger perpendicular than parallel to the foliation. According to Table 2.1 the results indicates that the rock types is *highly anisotropic*.

Figure 7.9: Picture of the specimen illustrating the direction of the foliation plane.

The foliation plane's unfavorable direction relative to most of the specimen's length direction has affected the high number of invalid tests. During the testing in the diametrical direction, it was challenging in several of the tests to obtain valid fractures of complex folding in the sample. Even with precautions, only a few of the tests were approved. In the axial direction, most of the invalid tests are due to crushing of the samples.

The samples were submerged in water at room temperature seven days before testing to simulate the conditions in a pressurized tunnel or shaft. However, during the test, the rock pieces seemed dry, and the water had migrated only a few millimeters into the blocks. This may indicate that the rock is impermeable and will need a longer time to be fully saturated than seven days.

Table 7.5: Results from point load index test

	Mean [MPa]	St.dev. [MPa]
Mean $I_{s(50)}$ (perpendicular)	2.28	0.16
Mean $I_{s(50)}$ (parallel)	6.25	0.91
Anisotropy index, I_a	2.73	-

Chapter 8

Field measurements at Løkjelsvatn

8.1 3D Overcoring

Hydraulic fracturing assumes that the borehole orientation is in one of the principal stress directions if hydraulic fracturing is carried out according to standard procedure. At HF-4 (see Figure 6.8), 3D rock stress measurements were performed by SINTEF before the hydraulic fracturing tests to determine the orientation of in-situ principal stresses with greater certainty. The direction of the hydraulic fracturing holes is determined based on results from 3D overcoring.

8.1.1 Setup and procedure

The cell used in the test is a CSIR cell developed by NTNU and SINTEF. The setup and test procedure are described in detail in Section 3.3.

8.1.2 Results

The results from 3D overcoring are summarized in Table 8.1, (SINTEF, 2021). The computer program called DISO developed by SINTEF was used to calculate the magnitude and orientation of principal stresses from the measured elastic parameters and strain readings. The software calculates in-situ stresses from 3D drilling statically by randomly selecting strain values at different hole depths. These calculations give a statistical prediction and presentation of mean stress values with statistical deviations.

Further, the results are converted into the horizontal plane. As can be seen in Table 8.1, the maximum principal stress is oriented almost in the vertical direction. Thus, the intermediate and minor principal are oriented in the horizontal plane, (SINTEF, 2021).

Table 8.1: Results from 3D measurements, (SINTEF, 2021).

	Trend/Plunge	Value	Unit
σ_1	N264°Ø/90°	17.99 ± 0.41	MPa
σ_2	N163°Ø/0°	16.10 ± 1.80	”
σ_3	N72°Ø/0°	9.40 ± 1.00	”
$^*\sigma_v$	N0°Ø	17.20	”
$^*\sigma_H$	N162°Ø	16.10	”
$^*\sigma_h$	N72°Ø	10.20	”

*Converted from measured strain

8.2 Hydraulic fracturing

Hydraulic fracturing is carried out by SINTEF at the planned transition zone to measure the minimum principal stress to assess the possibility of leakage. The test was carried out in the period 11-16.01.2021, (SINTEF, 2021). A total of 21 individual experiments were carried out in five different boreholes with directions based on the results from 3D rock stress measurement presented in Section 8.1.2.

8.2.1 Setup and procedure

This measurement procedure of the hydraulic fracturing tests and the determination of the results follow the procedure described in Section 3.4. The measurements were carried out in 1 m long test sections defined by a straddle packer. The first test section is placed at the bottom of the hole. Then, the remaining tests are placed with 3 m intervals. All holes had a dimension of 64 mm.

8.2.2 Results

A total of 21 hydraulic fracturing tests have been performed, where 11 of these were considered successful. Table 8.2 shows the results of the successful tests. A test is considered successful when the test achieves fracturing in the test section. The average of all measured shut-in pressures from the successful fracturing tests in hole L21 is 9.1 MPa. In the same hole, the results vary between 7.3 MPa and 13.2 MPa. The lowest registered shut-in pressure is 7.3 MPa in hole L21 (Test 17 in Table 8.2).

Table 8.2: Successfull results from hydraulic fracturing, (SINTEF, 2021).

Hole	Orientation [Trend/Plunge]	Test ID	Packer depth [m]	P_b [MPa]	P_r [MPa]	P_{si} 1st [MPa]	P_{si} 2nd [MPa]	P_{si} 3rd [MPa]
H1 (L20)	N150°E/(+)5°	1	25.2	23.2	18.0	11.1	10.6	10.6
		2	22.2	19.5	15.0	10.9	10.6	9.9
		3	19.2	23.0	18.5	13.1	14.9	13.4
		4	16.2	20.6	18.0	13.3	12.1	11.9
		5	13.2	21.1	14.6	11.4	11.4	11.4
H3 (L18)	N150°E/(+)5°	13	28.2	26.7	22.0	11.4	14.1	17.3
H4 (L21)	N150°E/(+)5°	16	28.2	18.9	15.3	8.4	8.1	8.3
		17	25.2	21.5	10.0	8.1	7.6	**7.3**
		18	22.2	17.2	12.0	8.1	8.0	8.1
		19	19.2	21.8	21.8	7.7	8.8	9.7
		21	13.2	25.8	18.0	13.2	12.8	11.7

8.3 Hydraulic jacking

A hydraulic jacking test was carried out close to the planned transition zone. The test was done in cooperation with PhD candidate Henki Ødegaard at the Department of Geosciences and Petroleum at NTNU in order to assess further the field applicability of the proposed Rapid Step-Rate Test (RSRT) as briefly described in Section 5.5.3. The test aims to measure the stress acting perpendicular to joints in the rock mass by reopening existing joints. As shown in Figure 6.9, eleven holes have been drilled for various rock stress measurements. L18 to L23 was drilled based on results from 3D overcoring. However, L18 could not be used for hydraulic jacking because of a fixed injection rod. On the other hand, L1 to L4 was drilled for RSRT in cooperation with the contractor.

8.3.1 Setup and test procedure

The equipment is calibrated and operated by Injeksjonsteknikk, a specialized company in various rock and ground support techniques. As can be seen in Figure 8.1, a single inflatable packer is fixed to rigid rods with a pressure transducer to isolate the test section. At the other end of the setup, a pump with a maximum flow capacity of 22 L/min ensures water inflow to the test section. A flow meter and a pressure gauge are connected to the setup, which provides digital data directly.

Some of the equipment used in the test are shown in Figure 8.2. The left picture shows the setup of the pump with measuring devices and valves in the correct order. The right picture describes the split that leads the water to either the test section or isolation of the packer.

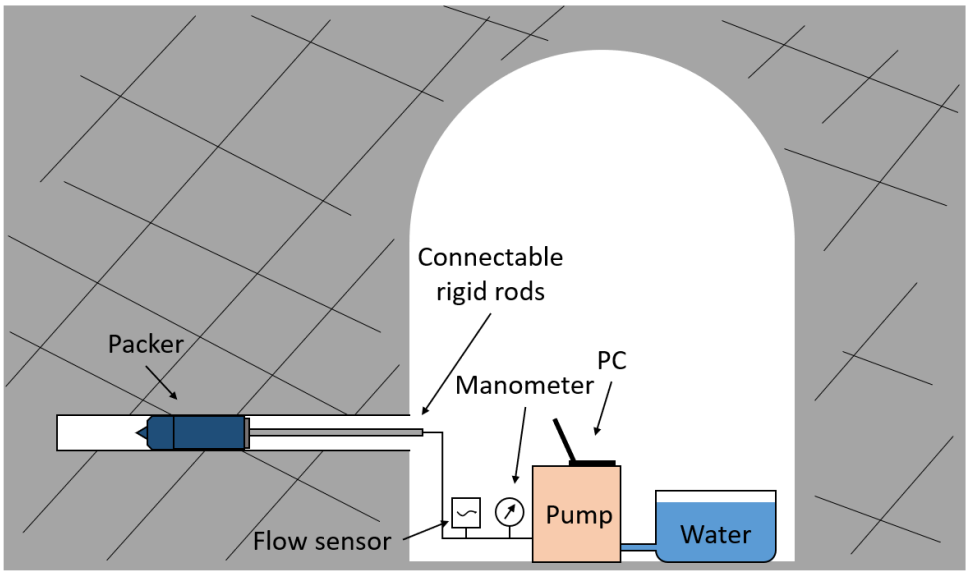

Figure 8.1: Illustration of the various components used to carry out hydraulic jacking tests.

The test procedure is developed by PhD candidate Henki Ødegaard and is based on experiences from Ødegaard and Nilsen (2021). The tests are planned as cyclic tests with step-wise flow increments. In contrast to Rutqvist and Stephansson (1996) as presented in Section 3.5, this procedure has a faster increase in flow. The tests were conducted in cycles with a step-wise increase and decrease of inflow. The test procedure consisted of a change in flow rate of 0.2 L/min every other second. A total of 31 hydraulic jack tests were performed.

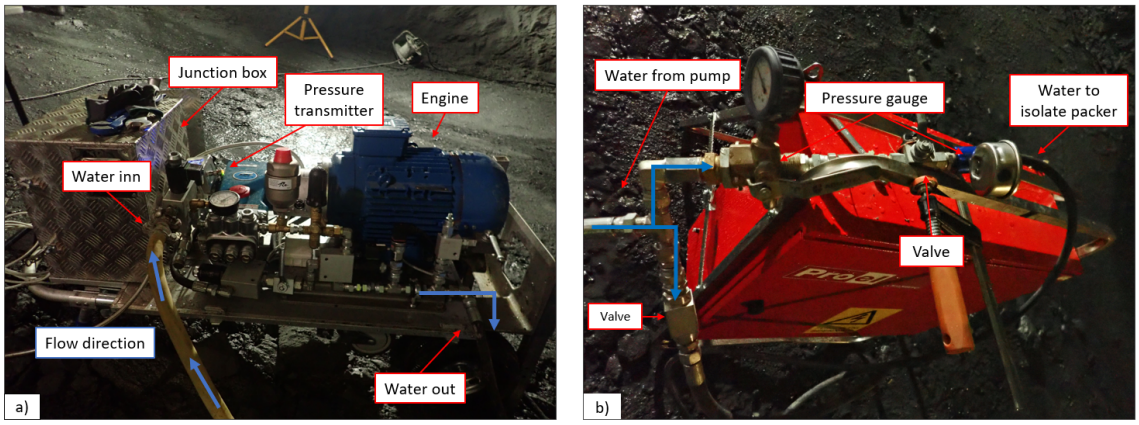

Figure 8.2: The pump system consists of a pump (Cat 550), pressure transmitter, flow meter that enables digital monitoring of the test.

8.3.2 Results

Table 8.3 summarizes the results from the tests. As can be seen from the table, L22-1 and L23-1 failed. During these tests, it was not possible to build up sufficient pressure to open existing joints. This may be due to contact with high-permeable joints contributing to higher drainage in the rock mass than the pump's capacity.

Of nine test holes, test results from four were considered successful. The pressure-time curve of L1, L3, L20, and L21 shows a typical development for opening and closing. An example is presented in Figure 8.3. According to the theory presented in Section 3.5, there is expected a distinct breakpoint in the closing phase. This breakpoint enables graphical reading of the closure pressure, P_{close}, acting on the joint surfaces. Results from all tests are presented in Appendix C.

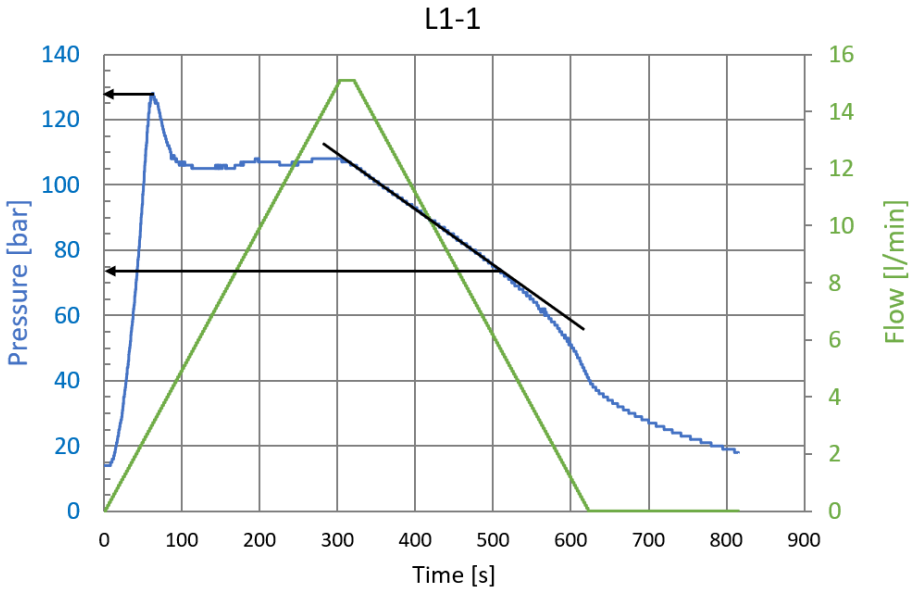

Figure 8.3: Results from L1-1 with pressure (blue) and flow (green)

8.3.3 Interpretation of results from RSRT

In some cases, where the graph does not show a distinct breakpoint, a derivation plot can make it easier to determine the closing pressure, (Raaen et al., 2001). Mathematically, a derivative plot will clarify the transition from linear to non-linear development. As can be seen in Figure 8.4, the derivative plot gives a more accurate determination of the closure pressure.

On the other hand, L2, L4, and L19 show deviating results from the theory. The results from borehole L2 do not indicate a clear breakpoint in the closing phase. This discrepancy may be because the joint is not fully jacked as a result of limited pumping capacity. Based on the theory proposed by Hayashi and Haimson (1991) and described in Section 3.5.2, it can be assumed that the rock mass is not fully hydraulically opened, but possibly located somewhere in Stage 2.

Furthermore, L4 shows low closing pressures. There are several possible reasons for this. One reason may be that a bypass leakage was detected during the test on both the borehole's upstream and downstream sides. Another possible explanation may be an unfavorable orientation to the tunnel. The stress state may have been affected by excavation due to too short distance between the borehole and the tunnel.

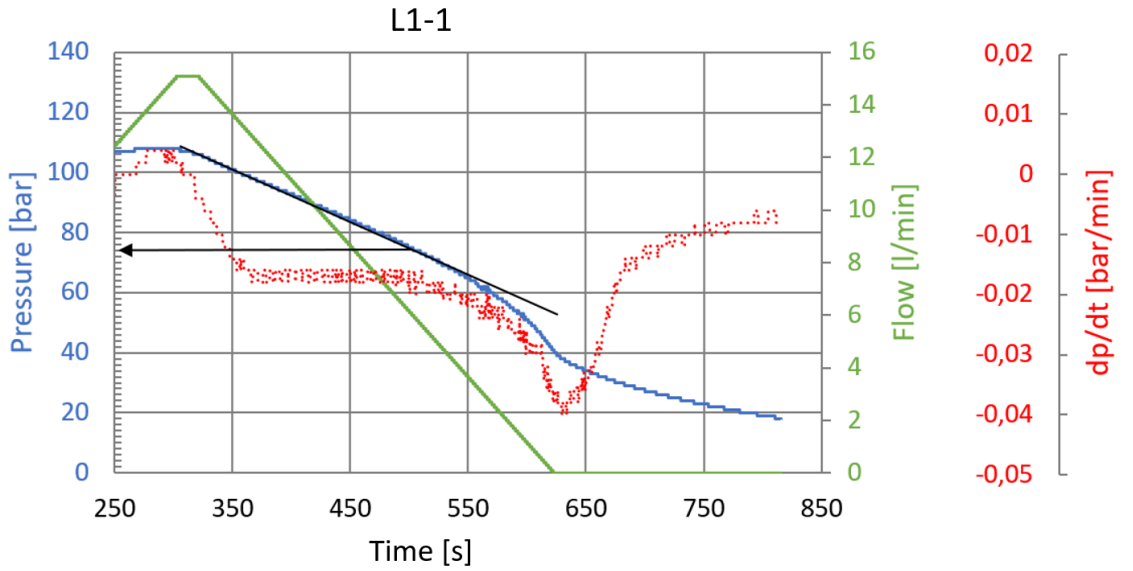

Figure 8.4: Interpretation of results from L1-1 with pressure (blue), flow (green) and dp/dt (red). P_{close} is marked in the graph.

In addition, L19 has no breaking point in the pressure-time diagram. As an example, Figure 8.5 presents data from L19-1 with no linear phases. Besides, results from L19 are not included in further assessment due to leakage bypass to L18 during the tests.

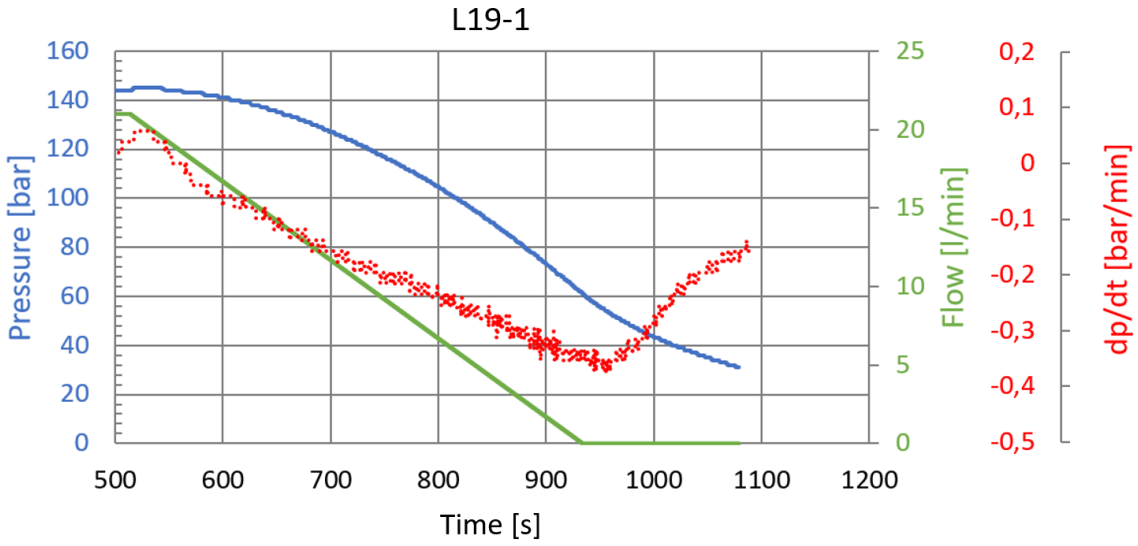

Figure 8.5: Interpretation of results from L19-1 with pressure (blue), flow (green) and dp/dt (red). The test is considered as unsuccessful due to bypass leakage during the test.

Another method for determining the closure pressure presented in Rutqvist and Stephansson (1996) (among others) was also used. Instead of studying pressure as a function of time, the flow was plotted against pressure. Figure 8.6 presents an example of this method on the data from L1-1 and L19-1. Complete interpretation of pressure-flow diagram is available in Appendix C.

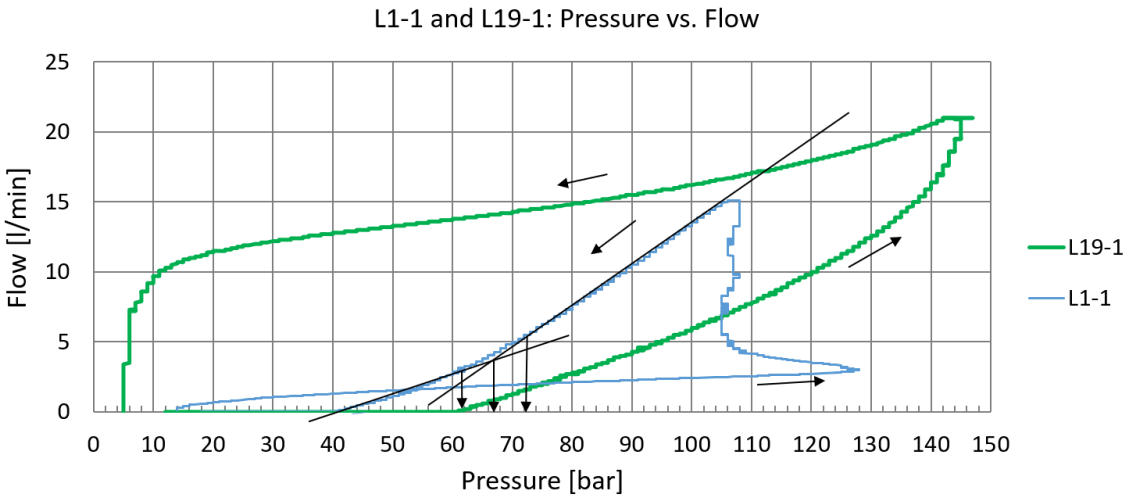

Figure 8.6: Data from L1-1 and L19-4 presented in a flow-pressure diagram with interpreted results.

As can be seen in Figure 8.6, the graph indicates the transitions from different stages in the closure phases, such as intersection, and upper and lower inflection point in L1-1. In L19-1, no straight lines are identified in the closure phase. These results coincide with the results from pressure-time diagrams.

The results from the tests are presented as both pressure-time and pressure-flow in Appendix C. The results from the approved tests (both pressure-time and pressure-flow) are compiled and presented in Figure 8.7. The box diagrams indicate that pressure-time give a slightly more conservative result than pressure-flow in the majority of the cases. Hartmaier et al. (1998) states that the lower bound values obtained from these tests in a given volume of rock is considered representative of the minimum principal stress. If this is taken into account, the rock mass will be able to resist a water pressure of 6.0 MPa. Thus, the safety factor at Løkjelsvatn is equal to 1.1 as the maximum water pressure corresponds to 5.5 MPa.

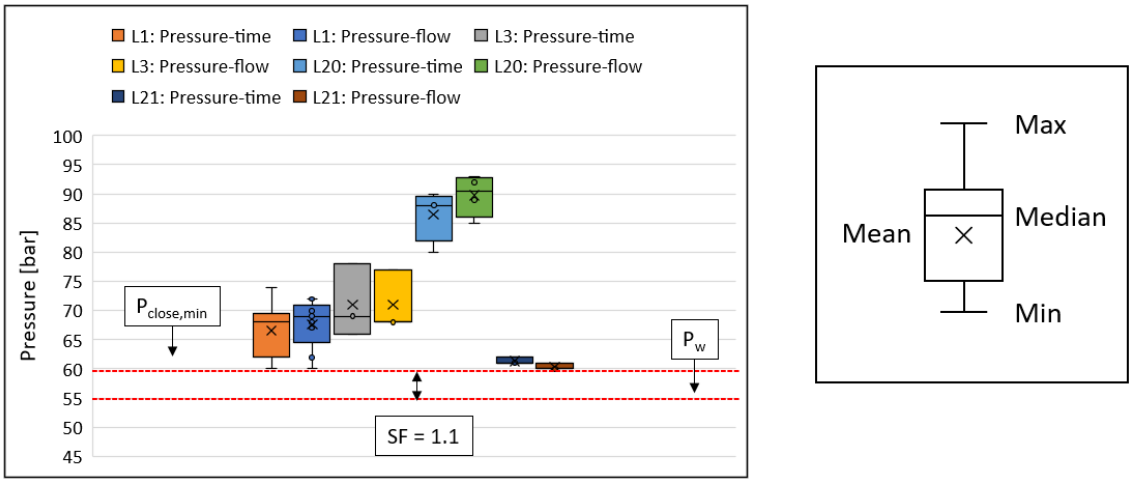

Figure 8.7: Review of the successful results from RSRT (left) with definition of box diagram (right).

Table 8.3: Results from hydraulic jacking at Løkjelsvatn hydropower project. P_{close} represents the upper inflection point unless otherwise stated.

Hole	Trend/Plunge	Test ID	Packer depth [m]	ΔQ [L/min]	Δt [s]	P_b [MPa]	P_r [MPa]	P_{close} [MPa]
L1	N40°E/(-)5°	L1-1	8.5	0.1	2	12.8	-	7.4
		L1-2	8.5	0.1	2	-	6.7	6.9
		L1-3	8.5	0.1	2	-	6.1	6.8
		L1-4	8.5	0.1	3	-	5.8	7.0
		L1-5	8.5	0.1	3	-	5.6	6.6
		L1-6	8.5	0.1	3	-	5.8	6.4
		L1-7	10.5	0.1	2	-	5.8	6.0
		L1-8	10.5	0.1	2	-	5.6	6.0
		L1-9	10.5	0.1	2	-	5.4	6.8
L2*	N55°E/(+)5°	L2-1	8.5	0.1	2	9.6	-	-
		L2-2	8.5	0.1	2	-	5.3	-
		L2-3	8.5	0.1	2	-	5.0	-
L3	N66°E/(-)5°	L3-1	10.5	0.1	2	16.8	-	6.9
		L3-2	10.5	0.1	2	-	4.3	7.8
		L3-3	10.5	0.1	2	-	4.6	6.6
L4*	N75°E/(+)5°	L4-1	8.5	0.1	2	8.4	-	-
		L4-2	8.5	0.1	2	-	44	-
		L4-3	8.5	0.1	2	-	42	-
L19*	N144°E/(+)3°	L19-1	10.5	0.1	2	-	8.4	-
		L19-2	10.5	0.1	2	-	9.0	-
		L19-3	10.5	0.1	2	-	12.0	-
		L19-4	10.5	0.05	2	-	11.0	-
L20	N140°E/(+)3°	L20-1	10.5	0.1	2	11.8	-	8.0
		L20-2	10.5	0.1	2	-	8.0	8.8
		L20-3	10.5	0.1	2	-	7.8	8.8
		L20-3	10.5	0.1	2	-	7.6	9.0
L21	N140°E/(+)3°	L21-1	8.5	0.1	2	-	6.4	6.1
		L21-2	8.5	0.1	2	-	5.3	6.1
		L21-3	8.5	0.1	2	-	5.3	6.2
L22**	N140°E/3°(+)	L22-1	8.5	0.1	2	-	-	-
L23**	N144°E/3°(+)	L23-1	8.5	0.1	2	-	-	-

*Not possible to distinguish between different inflection points

**Failed

Chapter 9

Numerical modeling

The software applied for the numerical modeling is a product of RocScience Inc and is a 2D finite element program called RS2, which can be used for both soil and rock applications, (RocScience, 2021). The author has used the 11th edition of the program to solve the problems with a license from NTNU. In 2D, modeling is carried out as plane strain analysis in RS2. For more information about the program, the reader is referred to the help page of RS2 provided by RocScience Inc.

The problem is divided into two steps (Step 1 and Step 2) to assess stresses and the leakage potential at Løkjelsvatn with numerical modeling. The first step back-calculates the in-situ stresses along the tunnel alignment based on results from three different stress measurement methods conducted at chainage 1780 m. Results from these models give an estimate of magnitudes and orientations of the principal stresses. Then, the second step evaluates four different cross-sections of the pressurized tunnel/shaft based on results from Step 1. Figure 9.1 illustrates the process of how the numerical modeling was carried out.

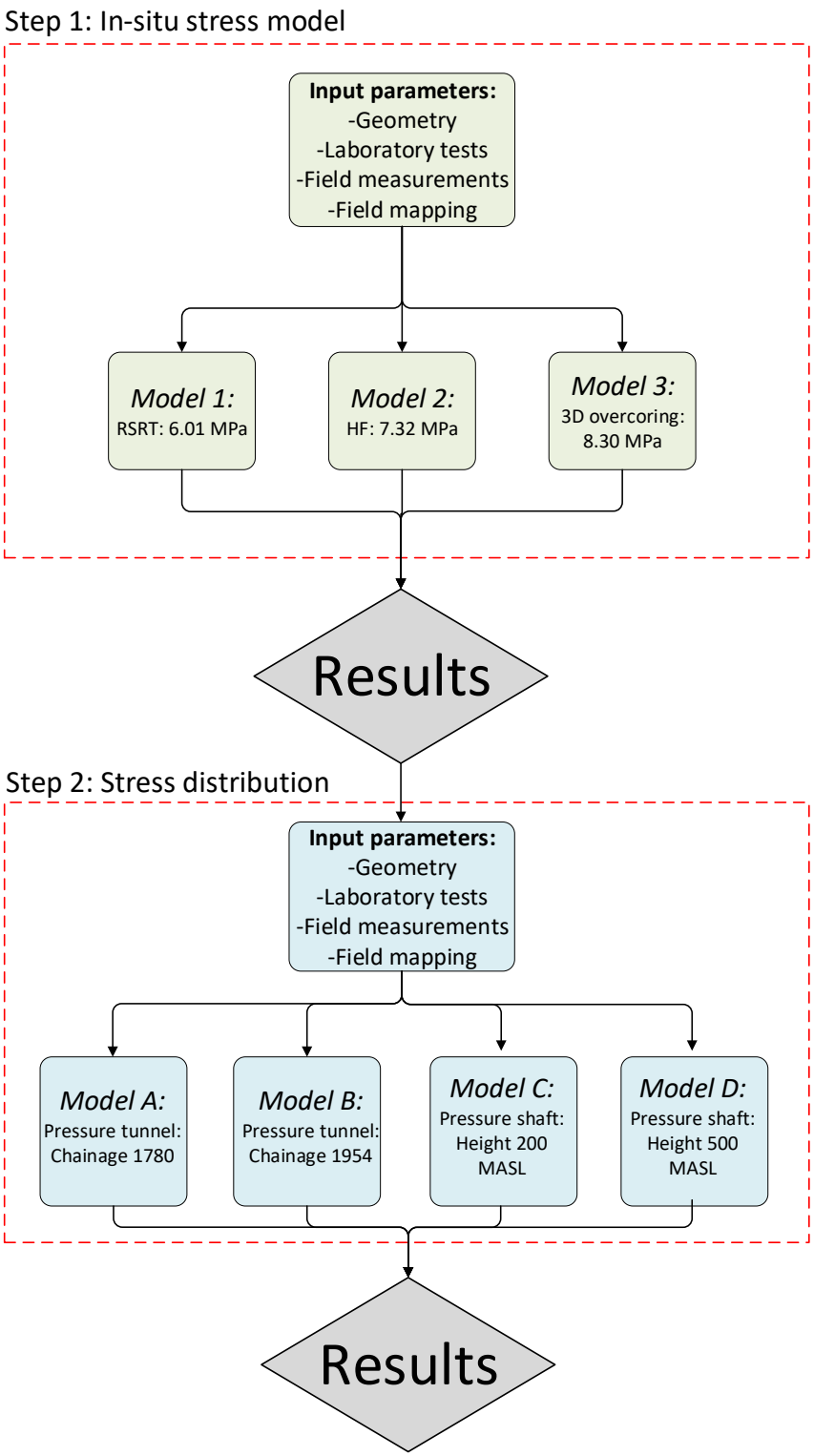

Figure 9.1: Flow chart of the numerical modeling process.

9.1 Establishing input parameters for numerical modeling

Numerical modeling requires accurate input parameters to achieve reliable results. In this case, input parameters are selected based on the results from the laboratory, field measurements, and engineering geological mapping at the field. In addition, some adaptions have been made, and RocData was used to evaluate and determine strength envelopes and other parameters for different failure criteria, (RocScience, 2021). In the calculations it is decided to apply formulas of Hoek and Diederichs (2006) and Hoek et al. (2002), and formulas presented by Panthi (2006). The formulas suggested by Panthi (2006) are well suited for anisotropic rock masses, such as phyllites. This section defines the input parameters in the models. Table 9.1 summarizes the input parameters used in the elastic analysis of the cases from Løkjelsvatn.

Table 9.1: Input parameters for rock mass.

Parameter	Description	Value	Unit	Source
γ	Specific weight	28.21	kN/m^3	Section 7.3
σ_{ci}	Intact rock mass strength	67.4	MPa	”
E_{ci}	Intact def. modulus	32.69	GPa	”
ν	Poisson's ratio	0.35	-	”
σ_t	Tensile strength	7.85	MPa	”
I_a	Strength anisotropy index	2.73	-	Section 7.6
GSI	Geological strength index	50/70	-	Figure 6.12
m_i	Material constant	7	-	Section 9.1.2
D	Disturbance factor	0	-	”
σ_{cm}	Rock mass strength	8.67/12.165	MPa	Section 9.1.3
E_{rm}	Rock mass modulus	4.47/23.96	GPa	Section 9.1.4

9.1.1 Stress conditions

Results from the rock stress measurements are implemented in the models to evaluate in-situ rock stresses condition along tunnel/shaft alignment. As stated by Hartmaier et al. (1998), the lower bound values obtained from rock stress measurements in a given volume of rock are considered representative of the minimum principal stress. Chapter 8 gives the measured values from different rock stress measurement methods, which form the input stress parameters in the analysis.

The in-situ stress models from the first step give the orientations of the principal stresses. In 2D, the model cross-section is made normal to the tunnel axis. The assumption makes it necessary to reorient the directions and magnitudes of the horizontal stresses into an in-plane and an out-plane component, since the maximum horizontal stress makes an angle (θ) to the tunnel axis, (Basnet and Panthi, 2018). This can be solved either by using Equation 9.1 and 9.2 or the stress transformation tool in RS2. For simplicity, it is assumed that σ_h=σ_H, except for Model 3 (with

results from 3D overcoring). In this case, both the magnitude and the orientation of the principal stresses are known.

$$\sigma_{in-plane} = \sigma_H \cos^2\theta + \sigma_h \sin^2\theta \tag{9.1}$$

$$\sigma_{out-plane} = \sigma_H \sin^2\theta + \sigma_h \cos^2\theta \tag{9.2}$$

9.1.2 Hoek-Brown parameters

The Generalized Hoek-Brown Criterion consists of three material parameters, m_i, D and GSI. m_i represents a material constant for intact rock. D is a disturbance factor which depends upon the degree of disturbance to which the rock mass has been affected by blast damage and/or stress relaxation. The GSI parameter relates the failure criterion to geological observations (like surface conditions and structures). The parameters are determined on the basis of field mapping and discretionary assessments, (Hoek and Brown, 2019).

In this case, the material constant (m_i) is set to 7. Ideally, this parameter is determined through a triaxial test, (Hoek, 2007). However, no triaxial tests have been carried out, and RocData gives a table from where an appropriate value can be selected. According to RocData, 7±3 is typically for phyllites. The second parameter, the disturbance factor (D), represents the contour quality. During the field mapping, it was observed that the tunnel contour appeared to be little affected by drilling and blasting. Thus, the factor is set to 0. Hoek and Brown (2019) point out that the factor must be determined carefully. Wrong determination can lead to a conservative and inappropriate design. The last parameter, GSI, enables emphasis on geological observations and structures.

9.1.3 Compressive strength

Results from UCS tests determine the strength of intact specimens in the laboratory. However, the parameter does not represent the entire rock mass strength. Several empirical formulas have been proposed to estimate the rock mass strength based on the strength of intact rock (σ_{ci}), such as Equation 9.3 suggested by Hoek et al. (2002) and implemented in RS2.

$$\sigma_{cm} = \sigma_{ci} \cdot \left[exp(\frac{GSI - 100}{9 - 3D}) \right]^a \tag{9.3}$$

Panthi (2006) suggested an equation (Equation 9.4) to estimate the rock mass strength (σ_{cm}) for rock masses influenced by schistosity.

$$\sigma_{cm} = \frac{\sigma_{ci}^{1.5}}{60} \tag{9.4}$$

9.1.4 Elastic parameters

Elastic parameters are determined in laboratory tests. The Poisson's ratio, ν, is 0.35 and is a measure of the Poissons's effect, the deformation of a material in directions perpendicular to the specific loading direction. On the other hand, the intact deformation modulus, E_{ci}, describes the ratio between applied stress and corresponding strain within the elasticity limit. However, a jointed rock mass does not behave elastically. Therefore, the term modulus of deformation describes the modulus better than Young's modulus, (Panthi, 2006). According to Nilsen and Palmstrøm (2000), direct measurements of this parameter are expensive and time-consuming. Therefore, several empirical equations have been proposed. Panthi (2006) summarizes different empirical formulas.

Common for the differential equations is that they are based on different classification systems, like RMR or the Q-system. Therefore, Panthi (2006) suggested an equation which provides determination of the rock mass deformation based on intact rock strength (σ_{ci}) and elasticity modulus (E_{ci}). The equation is well suited for schistose, foliated, and bedded rocks with low compressive strength:

$$E_{rm} = \frac{\sigma_{ci}^{0.5}}{60} \cdot E_{ci} \tag{9.5}$$

As presented in Section 6.5.3, GSI=50 and GSI=70 represent the rocks mass in best and worst case. 4.47 GPa represents the rock mass deformation modulus in the worst case (GSI = 50) where the rock mass are more affected by schistosity. On the other hand, in the best case (GSI = 70), the rock mass deformation modulus is calculated using RocData. In this case, E_{rm}= 23.96 GPa represents the rock mass deformation modulus.

9.2 Step 1: In-situ stress model

The geometry and the setup of the Step 1 models are presented in Figure 9.2. The topography is based on data from Kartverket (2021) and plotted in RS2. The profile follows the access tunnel to the hydropower station and further along the pressurized part of the hydropower scheme connecting the intake.

In Figure 9.2, the zone of interest is highlighted. In the zone, the mesh density is increased to improve the accuracy of the calculations, since the area outside this zone is not that significantly important regarding hydraulic fracturing. In order to avoid edge affections in the calculations and isolate the zone of interest, the model height and width are extruded. As shown in the figure, the sides are restrained in the X-direction only, while the top surface is free. The lower boundary is restrained in Y-direction, and all four corners are restrained in both X- and Y-directions. The gravity field stress is chosen to calculate the stress level. With this approach, the surface forms a free surface with no restrained nodes. A homogeneous and elastic material is assumed, and the specific weight is set to 28.21 kN/m^3 based on laboratory testing results (see Table 7.3 in Section 7.3).

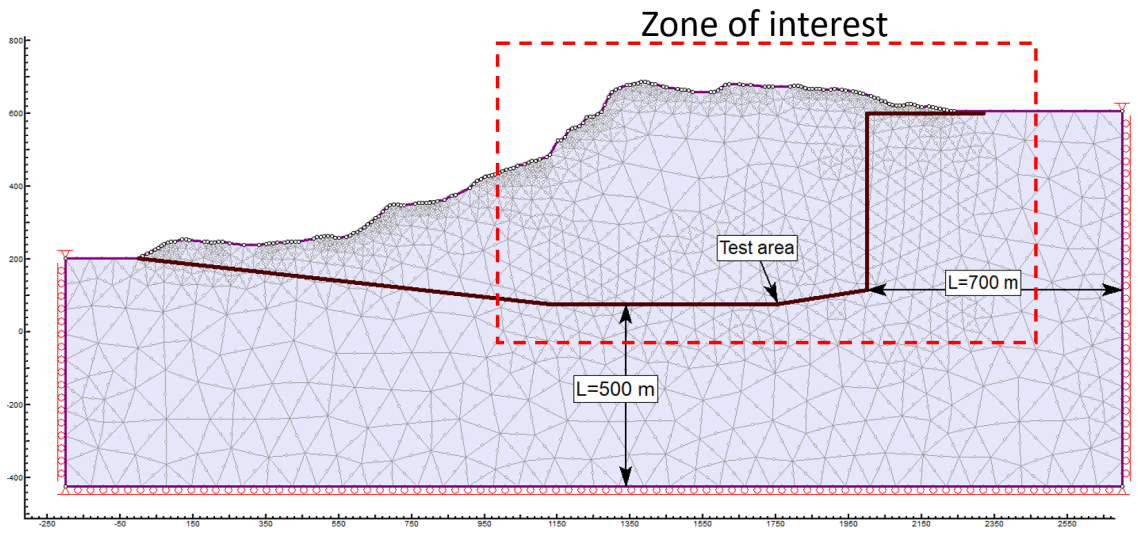

Figure 9.2: Geometry of in-situ stress model. The red dotted line indicates the pressurized part of the hydropower scheme and parts of the access tunnel where rock stress measurements have been carried out.

9.2.1 Results

As presented in Section 8.3.2, the lower bound values obtained from rock stress measurements are considered to represent the minimum principal stress at the test area. To calculate the in-situ stress state and the stress tensors magnitudes, different K-ratios are tested through trial and error to calculate the measured values for the minor principal stresses. Table 9.2 summarizes the achieved results.

Table 9.2: Results from trial and error to determine K-value.

Model	Measurement method	σ_3 [MPa]	σ_z [MPa]	σ_1 [MPa]	K
1	RSRT	**6.06**	15.49	16.16	0.55
2	HF	**7.32**	15.45	16.14	0.63
3	3D overcoring	**8.40**	15.41	16.12	0.70

Figure 9.3 presents a contour plot of the results from the numerical analysis in Model 1 with highlighted points of interest. The plot displays the results in the model geometry based on a range of values divided into a number of subranges. As can be seen in the figure, the contour lines close to the surfaces largely follows the topography. This phenomenon is described further in Section 2.3.5. However, the topography has less impact on the results with increasing depth. Appendix D presents contour plots showing the results in the other two cases.

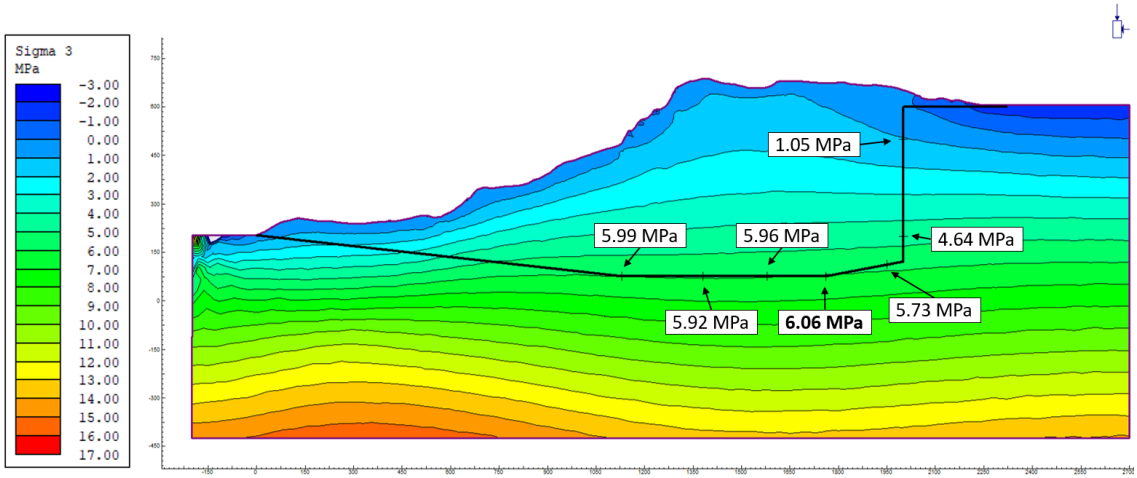

Figure 9.3: Simulation of stress conditions (σ_3) along the tunnel profile. Applied K-ratio is 0.55.

Figure 9.4 shows a close-up of the transition zone from the results presented in Figure 9.3 and the contour options are adjusted to distinguish different stress levels. As can be seen from the figure, the stress trajectories that indicate the orientations of σ_1 and σ_3 are approximately vertical and horizontal. These results will, in addition to the calculated K-value, be used to determine the stress conditions in Step 2, which assess the stresses and potential for hydraulic jacking and leakage from the pressurized part of the tunnel/shaft.

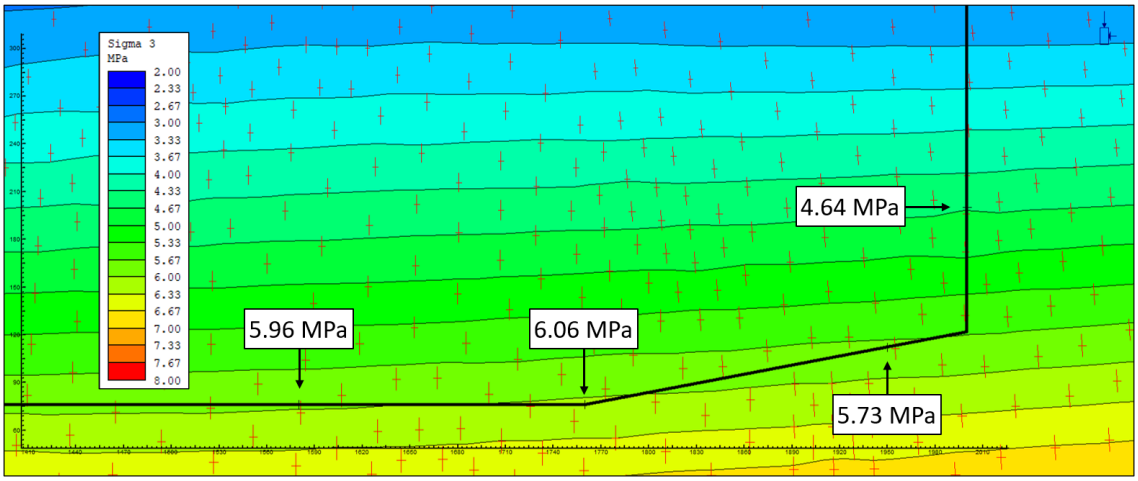

Figure 9.4: Close-up of the transition zone with stress trajectories in Model 1.

9.3 Step 2: Stress analysis on the pressurized tunnel/shaft

The results from Step 1 are based on back-calculates of the in-situ stress state in the rock mass. Results from the elastic calculations give magnitudes of the principal stresses for the Step 2 analysis. The main aim of the Step 2 analysis is to evaluate the stress distribution around the pressurized tunnel and shaft. Four cross-sections (A to D) are selected (see Figure 9.5) to evaluate the stress state along the pressurized tunnel and shaft. Cross-section A represents the transition zone, B the upper part of the pressurized tunnel, and C and D represent the shaft.

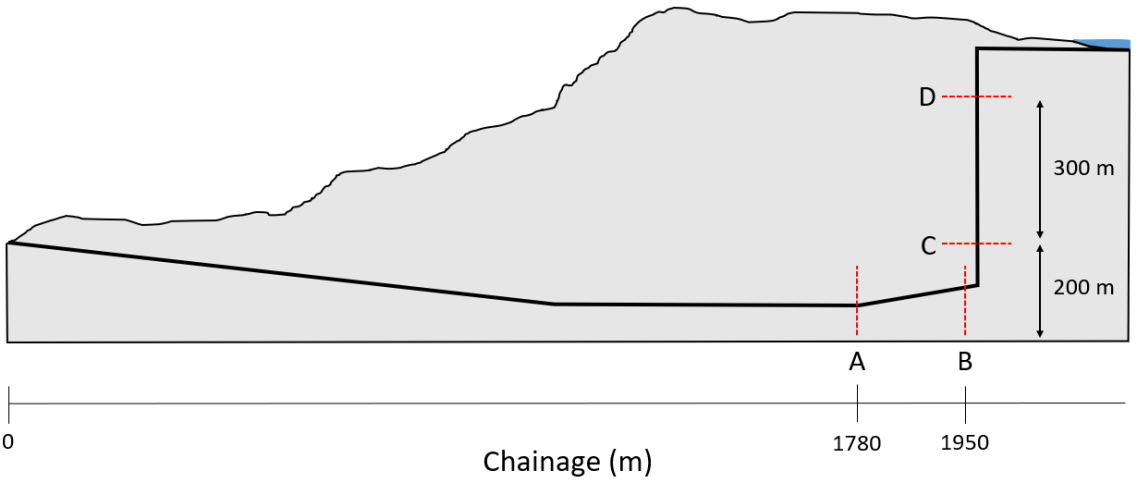

Figure 9.5: Location of cross section A to D used in further calculations.

9.3.1 Model geometry

Figure 9.6 shows the orientation of cross-section A-A'. Similar to the other models, the in-plane direction represents the downstream direction. The orientation of the cross-section is perpendicular to the tunnel orientation. The figure shows the strike and dip of the foliation and the most distinct joint set (J1) in the rock mass. Field mapping forms the basis of the values (see Section 6.5.1), and the indicated values in the figure represent mean values based on the joint rosettes.

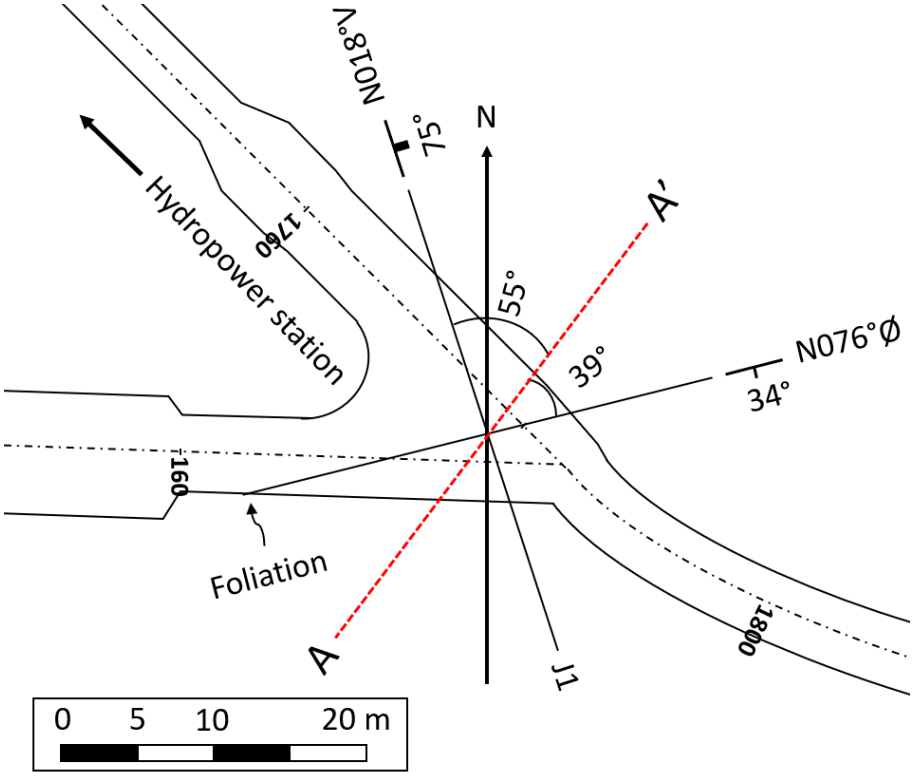

Figure 9.6: Red dotted line indicates cross section perpendicular to the tunnel.

In this case, the orientations of the cross-section are not perpendicular to the planes representing the foliation or the joint set. Thus, the planes have an apparent dip compared to the cross-section. For any inclined plane (except a vertical one), the true dips are always greater than any apparent dip, (Rowland et al., 2007). The apparent dips are calculated with a nomogram, also called an alignment diagram. The diagram involves three variables that have a mathematical relationship with one another. A straight line connects the variables in the diagram, (Rowland et al., 2007). Table 9.3 summarizes the corrected values for the dip angles in Model A and Model B, which are implemented in the geometry of the models.

Table 9.3: Apparent dips calculated with a nomogram presented in Rowland et al. (2007).

Model	Foliation/Joint set	True dip	Angle between strike and apparent dip	Apparent dip
A	Foliation	34°	39°	**20°**
	J1	75°	55°	**71°**
B	Foliation	34°	85°	**≈ 34°**
	J1	55°	0°	**0°**

Figure 9.7 shows the geometry of Model 1. As indicated with line A-A', the direction into the plane represents the downstream direction. The illustration is a discontinuous model and introduces the foliation and the most prominent joint set. Corresponding apparent dips are presented in Table 9.3. The foliation joints are inserted into the model with the mean dip of 20° and a joint spacing of 0.5 m. The J1 joints have joint space of 1.5 m and a mean dip of 71°. Joints have been introduced to provide an overview of the joint geometry around the tunnel for further assessments. Appendix D presents a similar illustration of Model B, Model C, and Model D.

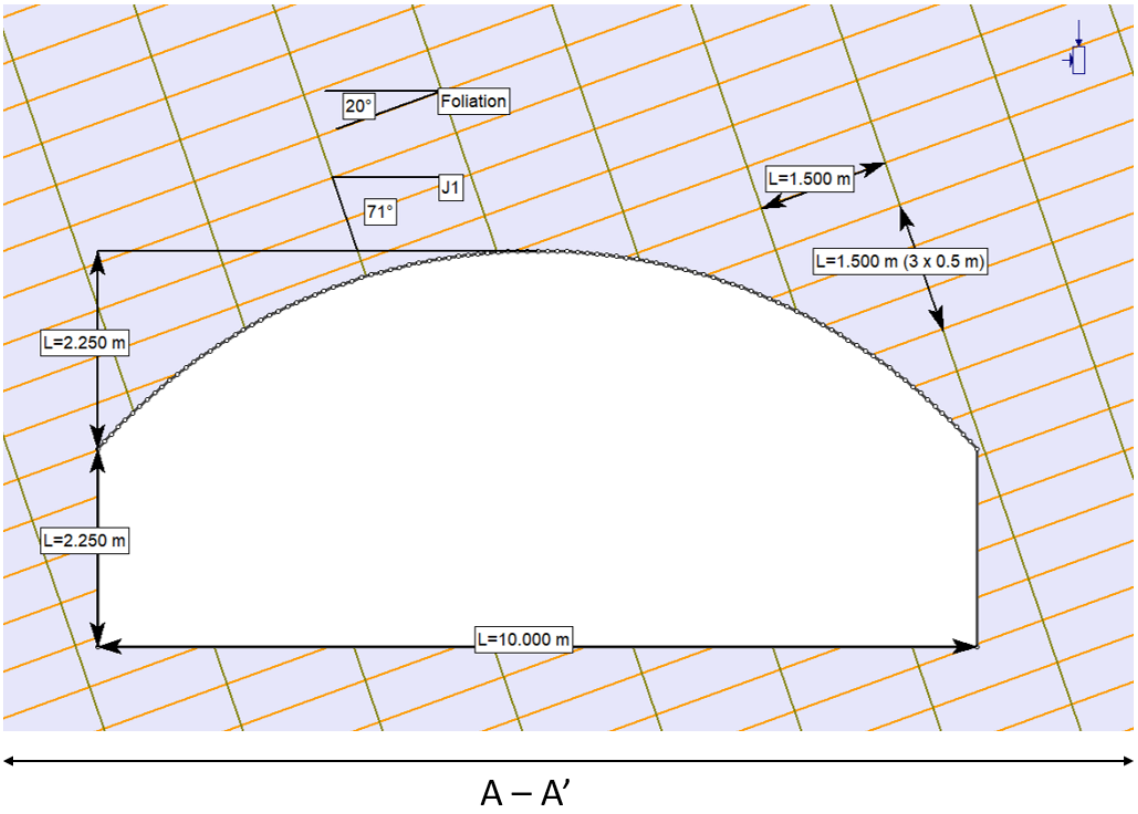

Figure 9.7: Tunnel geometry in Model A.

The illustration in Figure 9.8 shows the distance from the excavation to the external boundaries. The externals are restrained in both X- and Y-directions, and the four corners are restrained in both directions. The mesh type is *graded* with *six noded triangles* as element mode.

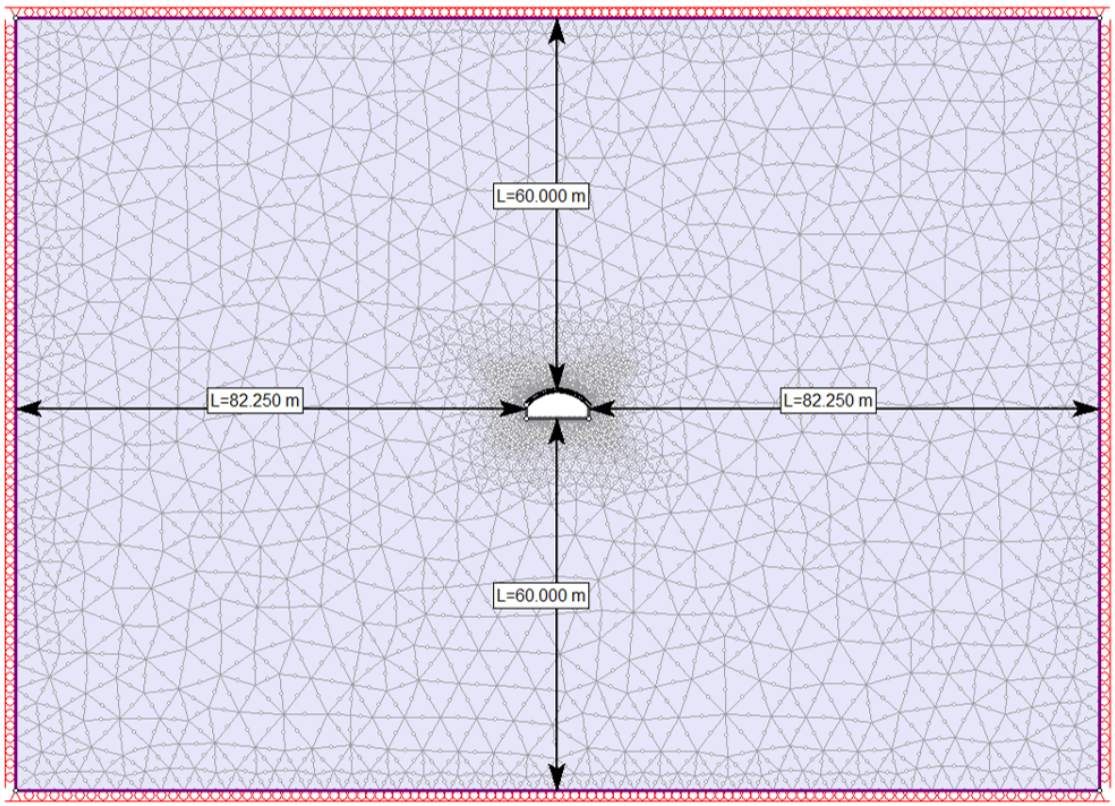

Figure 9.8: Complete model with boundaries used in Model A.

9.3.2 Results

To assess the hydraulic failure of the unlined pressure tunnel and shaft at Løkjelsvatn, back-calculation of the results from rock stress measurements estimates the stress redistribution zone around the tunnel. A stress profile was established to illustrate the stress development as a function of distance along a straight line from the tunnel contour and into the rock mass in the vertical and horizontal direction. The results from Model A1 are presented in Figure 9.9.

A stress redistributed zone occurs outside the tunnel where the minor principal stress is less than the in-situ stress state due to excavation. On the other hand, the peak stress concentration is moved out from the periphery of the tunnel, as seen in the Figure 9.9. Then the stress level decreases with increasing distance from the tunnel. As reflected in the figure, the minor principal stress reaches in-situ stress level at a distance corresponding to about two times the diameter of the tunnel. Appendix D presents similar figures from the other models.

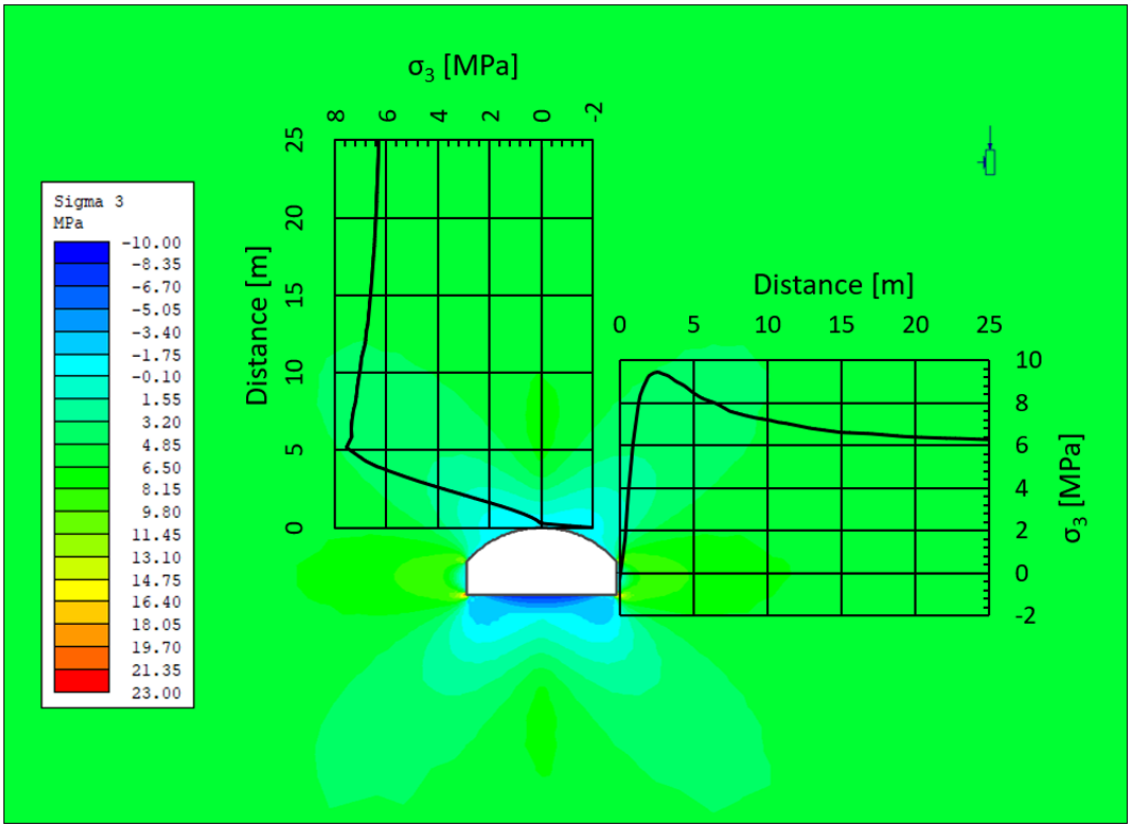

Figure 9.9: Development of the magnitude of σ_3 as function of distance from the tunnel contour.

Figure 9.10 illustrates the depth from the tunnel contour to a stress level which corresponds to the hydrostatic water pressure. As can be seen in the figure, the maximum depth, in this case, is 20.5 meters. Appendix D presents similar figures from the other models. Table 9.4 summarizes the depths in the different models with an overview of the input stress magnitudes. Model A1 represents the most critical case where the depth of the affected zone is most significant.

The results indicate the depth of the area around the tunnel/shaft where hydraulic jacking can occur when the tunnel is in operation and exposed to water pressure. In addition, the results from the calculations show that the extent of the stress re-distribution zone becomes smaller if the ratio between major and minor principal stresses decreases.

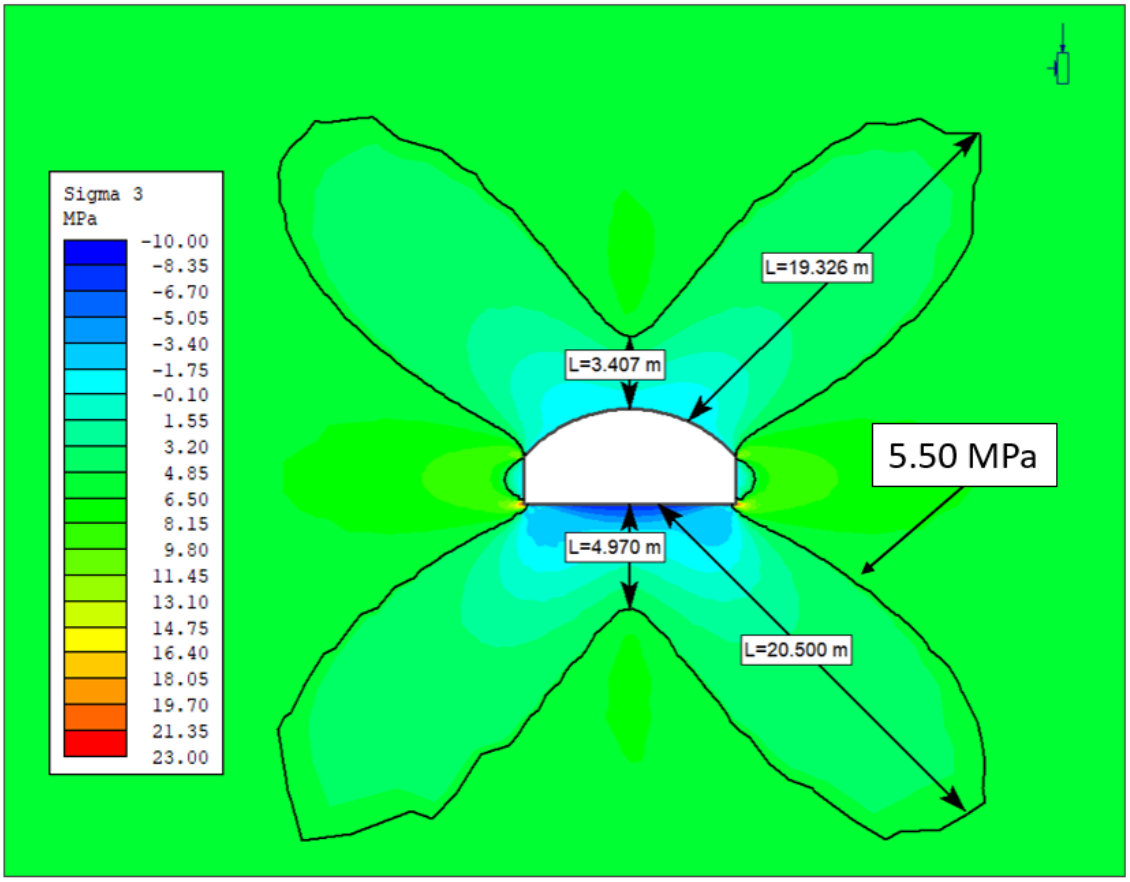

Figure 9.10: The result from elastic modeling of Model A1 showing the stress reduction zone around the excavation. 5.5 MPa represents the hydrostatic water pressure at chainage 1780 m.

Table 9.4: Results showing the maximum size of the zone with a lower stress level than the water pressure.

Model ID	σ_3 [MPa]	σ_1 [MPa]	$\sigma_h = \sigma_H$ [MPa]	P_w [MPa]	Max depth [m]
A1	6.06	16.16	-	5.50	20.5
A2	7.31	16.14	-	”	9.3
A3	8.40	16.12	-	”	6.7
B1	8.40	15.18	-	5.18	7.6
B2	5.73	15.16	-	”	3.5
B3	6.89	15.15	-	”	2.5
C1	-	-	4.64	4.25	3.8
C2	-	-	5.59	”	1.6
C3	-	-	6.42	”	1.1
D1	-	-	1.05	1.25	*
D2	-	-	1.31	”	5.8
D3	-	-	1.54	”	2.1

*σ_h<P_w

Chapter 10

Assessment of hydraulic failure and leakage potential at Løkjelsvatn hydropower plant

In order to evaluate the potential for hydraulic failure and quantify the leakage potential at Løkjelsvatn, geometrical and semi-empirical assessments have been carried out. Such tools enable comparison with experiences from Norwegian and international projects. In this way, understanding the rock mass at Løkjelsvatn's applicability as a host for unlined tunnels/shafts can be assessed in more detail, especially in combination with results from laboratory examination and numerical modeling.

10.1 Comparison with Norwegian criterion for confinement

In order to evaluate the appropriateness of the Norwegian criterion for confinement at Løkjelsvatn, a theoretical factor of safety (FoS) represents the ratio between the geometric parameters in the criterion and the water pressure. The ratio describes how much stronger a system is than it needs to be for an intended pressure. Mathematically, the Norwegian confinement criteria presented in Section 5.3 can be rewritten as:

$$FoS_1 = h \cdot (\frac{\gamma_r \cdot \cos\alpha}{P_w}) \tag{10.1}$$

$$FoS_2 = L\cos\beta \cdot (\frac{\gamma_r}{P_w}) \tag{10.2}$$

where P_w represents the hydrostatic pressure. The equations above are based on rock mass overburden and are used in mathematical equations to estimate the rock mass's expected resistance theoretically. The ratio between the minimum stress and the water pressure determines the factor of safety. If the water pressure exceeds the

water pressure, hydraulic failure occurs. Thus, the most realistic safety factor can be expressed as:

$$FoS_3 = \frac{\sigma_3}{P_w} \tag{10.3}$$

The corresponding factors of safety are calculated based on geometrical input parameters as illustrated in Figure 10.1. The various test sites (HF-1 to HF-4) along the tunnel profile represent the initially planned positions for the hydropower station. A line with a slope of 23° seems to be a reasonable estimate of the slope to the valley side. The maximum water head is 550 m, and it is assumed that the density of the rock mass is 0.028 MN/m^3 based on results from laboratory examination (see Chapter 8).

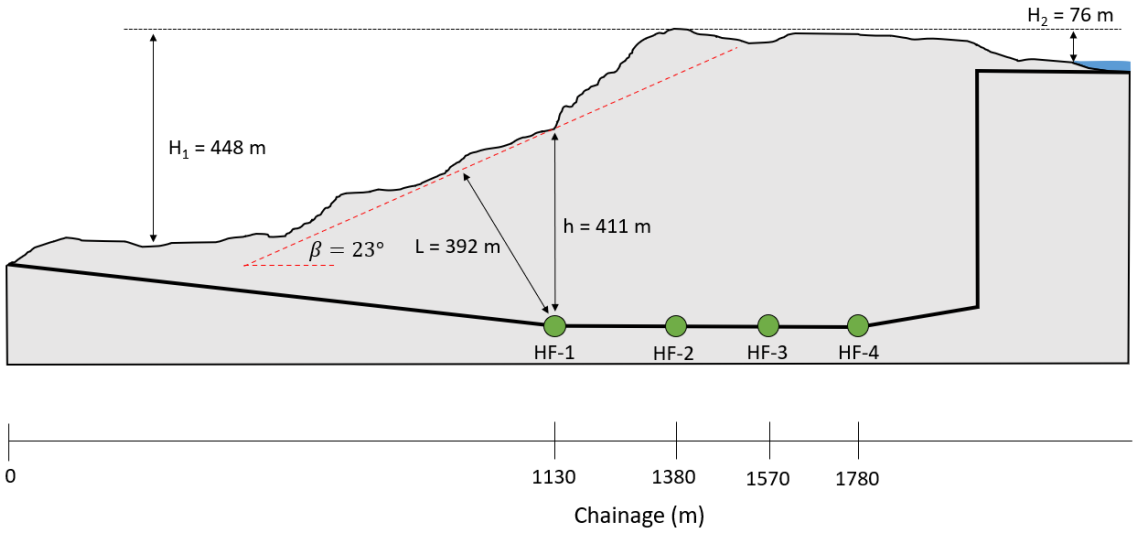

Figure 10.1: Overview of locations with geometrical parameters for calculating factor of safety (FoS) along the access tunnel.

Table 10.1 summarizes the input parameters and results from the calculations. As shown in the table, the factor of safety (FoS_1 and FoS_2) based on the overburden criteria is significantly greater than 1. Thus, the results indicate a sufficient stress level from a theoretical perspective. On the other hand, comparison with measured values (FoS_3) shows a ratio lower than 1. As a result, the tunnel is moved deeper into the rock mass to avoid de-stressed areas near the valley and achieve a higher minimum principal stress level.

Table 10.1: Analysis of factors of safety at four location (HF-1 to HF-4) along the access tunnel.

Location	H [m]	P_w [MPa]	γ_r [MN/m^3]	h [m]	α [°]	β [°]	L [m]	L$\cos\beta$ [m]	σ_3 [MPa]	FoS_1	FoS_2	FoS_3
HF-1	550	5.5	0.028	411	0	23	392	360.8	3.5	2.11	1.85	0.64
HF-2	550	5.5	0.028	510	0	23	483	444.6	3.3	2.62	2.28	0.60
HF-3	550	5.5	0.028	582	0	23	563	518.2	4.2	2.99	2.66	0.76
HF-4	550	5.5	0.028	597	0	23	619	569.8	7.3	3.06	2.92	**1.33**

10.2 Comparison with suggested developments of the Norwegian confinement criteria

As presented in Section 5.5, different authors suggest further development of the Norwegian confinement. In the section, two alternative methods from Rancourt (2010), and Basnet and Panthi (2018) are highlighted. It is of interest to compare these with measured values to assess the suitability of the approaches at Løkjelsvatn to assess the various proposed developments of the criterion.

If the approach of Rancourt (2010) forms the basis, the necessary factor of safety is 1.43. As presented in Section 5.5, the factor is a product of three parameters: *Rock mass characteristics*, *Cover to tunnel diameter ratio* and *Presence of Structures*. The rock mass is described as anisotropic with low E-modulus based on the proposed factor of safety. Thus, the first parameter, F_a, is set to 1.3. Since the cover to tunnel diameter ratio is greater than 20, the second parameter, F_b is set to 1.1. Then, the last parameter, F_c is set to 1.0 due to no presence of structures.

Panthi and Basnet (2018) suggested that results from the Norwegian confinement criteria should multiply with a factor (f' or f"), which varies between 1.6 to 3.0. f' is the multiplication factor that includes the stress change due to only changes in topography. On the other hand, f" is the factor that includes stress change due to both changes in topography and the presence of weakness zones. At Løkjelsvatn, the terrain is similar to topography 1 in the article. Topography 1 is described in contrast to topography 2 and 3 as relatively flat terrain beyond the top of the hill and is described as typical for Norwegian topographies.

The input parameters in the proposed approach by Panthi and Basnet (2018) are based on the ratio between the valley depth to the left and the right. The various input parameters are illustrated in Figure 10.1 and the results presented in Table 10.1 are used in the calculations. In this case, the Norwegian confinement criteria should be multiplied by a factor 1.616 and 1.812, representing f' and f" respectively.

Table 10.2 compares the factor of safety suggested by Rancourt (2010) and state-of-art factor from Basnet and Panthi (2018) with the FoS_3 from Equation 10.2. The results show that even if terrain corrections that include another valley or geological parameters are considered, the overburden criteria still give underestimated values for the case at Løkjelsvatn.

Table 10.2: Comparison of measured σ_3 with suggested developments of the Norwegian confinement criteria.

Location	L [m]	h [m]	H_1 [m]	H_2 [m]	*f'*	*f"*	FoS_3/f'	$FoS_3/f"$	FoS_3/FS^*
HF-1	392	411	448	76	1.616	1.812	0.394	0.351	0.445
HF-2	483	510	"	"	"	"	0.371	0.331	0.420
HF-3	563	582	"	"	"	"	0.473	0.421	0.534
HF-4	619	597	"	"	"	"	0.821	0.732	0.928

*FS, suggested by Rancourt (2010)

10.3 Semi-analytical solution to estimate leakage potential

As presented in Section 4.4.1, Panthi (2006) proposed a semi-analytical solution to estimate the specific leakage (q_t in l/min/m) from an unlined or shotcrete-lined pressure tunnel. The criterion consists of J_n, J_r and J_a of the Q-system of rock mass classification, hydrostatic height, H, and a correction factor, f_a. The mapped Q-values form the basis of the calculations (see Section 6.5.2). It is assumed in the calculations that the mapped Q-values remain constant along the unline pressure tunnel for simplification. The correction factor consists of J_p, J_s and D. D is measured using Civil 3D based on the terrain model, while observations in the field form the basis of J_s (see Section 6.5.1). The last parameter, J_p, is selected based on values used for the corresponding rock quality classes (Q-system), (Panthi and Basnet, 2021). Table 10.3 gives the input parameters and most significant results from the calculations.

Table 10.3: Input parameters and results of leakage assessment along the pressurized part of the waterways based on a semi-empirical solution suggested by Panthi (2006). The input Q-parameters represents mean values based on field mapping presented in Section 6.5.2.

Statistical values	J_p	J_s	D	f_a	H	Rock mass parameters			q_t
	[m]	[m]	[m]	[l/min/m^2]	[m]	J_n	J_r	J_a	[l/min/m]
Min	2	0.5	398	0.0015	25	3	1	0.75	0.03
Mean	-	-	563	0.0100	378	4.5	2.7	6	**7.68**
Max	5	2	679	0.0251	549	6	4	8	28.89

The results above summarize the calculations presented in Appendix C and the results indicate that 7.68 l/min/m gives an average estimate of leakage along the pressure tunnel from the top of the shaft and to the hydropower station based on mean values. The same results are presented graphically in Figure 10.2 and show the leakage development along the unlined pressure tunnel. In total, the length of the studied area is 843 m, which provides a theoretical leakage of 107.9 l/s (or 6474 l/min) along the pressurized tunnel. The statistical range of the calculations is presented in Table 10.4. The minimum values represent the best-case scenario. On the other hand, maximum values represent the worst-case scenario.

Table 10.4: Statistical range of the calculations presented in Appendix C.

	Unit	Min	Mean	Max	St.dev.
$q_{t,min}$	[l/min/m]	0.03	0.48	0.72	0.19
$q_{t,mean}$	”	0.70	**7.68**	10.73	2.79
$q_{t,max}$	”	1.88	19.18	28.89	7.48

The results presented in Appendix C is displayed in Figure 10.2. The illustration shows the mean results from the calculations along the tunnel. As can be seen in the illustration, the results indicating minimum and maximum leakage are calculated close to the hydropower station. As seen in Figure 10.2, the risk of leakage potential increases as the hydrostatic pressure increases and reaches its maximum at close to the hydropower station. In the figure, theoretical values for minimum principal stress are plotted based on Equation 2.3 presented in Chapter 2 . As can be seen from the graph, the theoretical stress level is higher than the water pressure along the entire pressurized part.

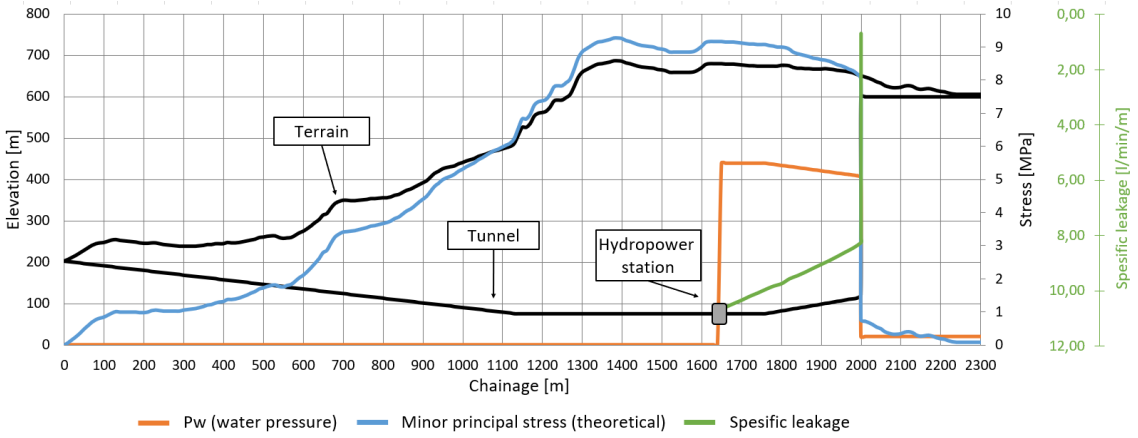

Figure 10.2: Vertically section of the tunnel alignment showing hydrostatic pressure and specific leakage along the tunnel. Theoretical minimum horizontal based on Equation 2.3 shows higher pressure than the hydrostatic head.

Chapter 11

Discussions

11.1 Assessment of common and future practice for the final design of hydropower plants

There is a broad agreement that if the minor principal stress is greater than the maximum water pressure at any point along the unlined pressure tunnel or shaft, hydraulic fracturing and loss of water will not occur. In Norway, most of the total length of water tunnels consists of tunnels with minimal rock support. Even though large-scale hydropower development has been completed, construction of unlined waterways will continue in Norway in the years to come. Robust tools are required to minimize the probability of unwanted hydraulic failures. This section will discuss current and future practices in the design of hydropower plants with unlined waterways.

11.1.1 Evaluation of past and present practice for design of Norwegian hydropower power plants

The uncertainties related to the use of the overburden criteria are well known in the industry. Still, the equations have been used in a large number of projects over several decades. Today, numerous hydropower plants have been built with an installed capacity of over 10 MW with unlined waterways. Although the majority of these have avoided failures, hydraulic jacking has occurred at nine reported plants. Until recently, hydraulic failure has occurred as a results of no or limited verification of the rock stresses, which has led to stress anomalies not being detected.

An example is Løkjelsvatn, which shows how rock stresses can differ from one place to another and deviate from the theory. The experiences emphasizes the importance of rock stress measurements and flexibility in the construction phase. Numerical modeling is a helpful tool that can increase the understanding of the rock mass, especially in challenging geological areas to provide a significantly more accurate overview on the in-situ stress conditions. Not only is it essential to avoid hydraulic failure, but it can provide a more accurate determination while considering the

permanent rock support. In addition, stress measurements are necessary to be able to perform reliable numerical, analytical and empirical calculations. From a long-term perspective, it is not inconceivable that it may be of interest to the project owner to have the necessary overview of the conditions in the rock mass.

It is claimed that the Norwegian Water Resources and Energy Directorate (NVE) should set requirements for rock stress measurements. Today, there are no explicit requirements for verifying the rock stresses when building unlined pressure tunnels or shafts in the Dam Safety Regulations. What corresponds to sufficient documentation is questionable. Due to economic and practical reasons, it is too easy to minimize the number of rock stress measurements or avoid the measurements and consequently increase the risk of hydraulic failure.

11.1.2 Evaluation of Norwegian confinement criteria from Løkjelsvatn

As summarized in Table 10.1 and presented in Figure 11.1, there is a large discrepancy between measured and theoretical values for minor principal stress. FoS_3 is lower than 1.0 for all measurements except HF-4, although FoS_1 and FoS_2 are significantly higher than 1.0. The results are consistent with predicted stress levels for 15 Norwegian hydropower plants presented in Ødegaard et al. (2020). In combination with the results in Ødegaard et al. (2020), the results from Løkjelsvatn illustrate the weaknesses by using the overburden criteria as a tool for final determination of the magnitudes of minimum principal stresses.

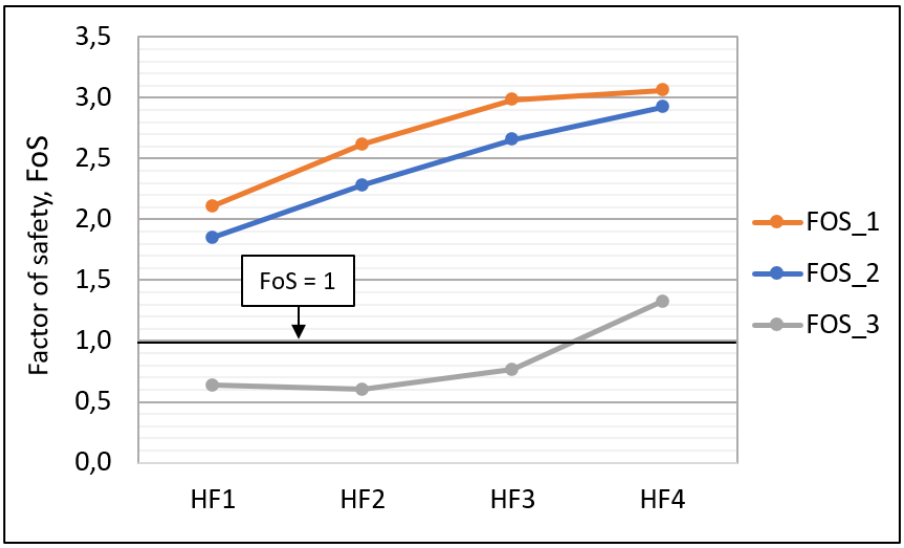

Figure 11.1: A graphic representation of various factors of safety at Løkjelsvatn based on geometric input parameters in the the Norwegian criteria for confinement and measured stress levels.

The overburden criteria are a valuable tool for preliminary assessments. However, the limitations must be considered, and the equations must be treaten with caution. The limitations of the overburden criteria, such as two-dimensional consideration and the lack of consideration of geological parameters, are well known. Consequentially, various improvements to the well-known Norwegian Criteria for Confinement

have been proposed. Therefore, this thesis looks at two different methods for determining the necessary safety factor that can be implemented in the Norwegian inclusion criterion. Table 10.2 summarizes the results. Compared to measured values for minimum principal stresses, neither Rancourt (2010) nor Panthi and Basnet (2018) provide a satisfying factor of safety. Still, these newer approaches provide a more conservative approach compared to the original criterion.

Compared with a selection of successful and unsuccessful projects reviewed by Basnet and Panthi (2018), there is little indication that FoS_2 and FoS_3 in this order of magnitude should give hydraulic failure during operation. However, as pointed out in Section 2.3, many factors might affect the stress level in the rock mass, even within a relatively small, delimited area. Therefore, it should be asked whether a single measurement at a random location in the rock mass gives the correct picture of the stress level in the rock mass. For example, if the rock stress measurements are performed in an area with a satisfactory stress level and the rest of the tunnel is located in a de-stressed area, the measurements will overestimate stress values. In these cases, this will constitute a significant element of uncertainty.

In an ideal situation, stress measurement methods measure the stress levels for every drill and blast cycle, enabling a continuous stress log and establishing a full-fledged stress model. In this way, stress anomalies in the rock mass can be identified. An essential prerequisite for increasing the number of test sites is that the measurements do not cause undesirable hindrances to other tunneling activities. As the hydraulic fracturing test is time-consuming and costly due to special equipment and expertise requirements, conducting hydraulic fracturing tests regularly along tunnels will be unlikely. Rapid Step-Rate Test (RSRT) is a test procedure that can help increase the number of test sites along the tunnel due to low costs. Compared to experiences from related simplified tests, the cost level is around 10-20% of standard hydraulic fracturing tests.

11.1.3 Evaluation of results and experiences from RSRT as a tool for measuring rock stresses

The experiences from the field measurements at Løkjelsvatn are promising and show that it is possible to carry out RSRT quickly and efficiently. For example, compared to other rock stress measurement methods, the experiences from Løkjelsvatn show that it is possible to obtain an estimate of the closing pressure within typically 10-20 min per test, compared to 1-2 hours for hydraulic fracturing tests. Another advantage is that the equipment is simple, and parts of the test can be pre-programmed. Therefore, a semi-skilled person can also perform the test. Furthermore, the test is valid in all directions, regardless of the orientation of the principal stresses. Besides, the test is valid for all hole depths, if the test section locates outside the stress re-distribution zone (SRZ).

On the other hand, the disadvantages of RSRT are that, at present, there are few reference projects. Although the experiences from Løkjelsvatn are reasonable, it would be an advantage for the robustness of the test to study correlations in more

detail. Uncertainty of the test is related to the interpretation of the results. In this case, the results were interpreted graphically and analytically. According to the theory and as studied in more detail in Section 3.5.2, there is a distinct change in stiffness when decreasing the flow. This is seen as three separate phases. The transition between these phases makes it possible to determine the closing pressure. However, there is a disagreement between which point describes the closure pressure most correctly. The current situation with uncertainty about whether the closure pressure should be determined by the intersection point, the upper inflection point or the lower inflection point is not satisfactory. At Løkjelsvatn, the upper inflection point fit best with the results from hydraulic fracturing.

Graphic determination is a straightforward process. However, this method opens up for subjectivity. Derivative plots reduce this uncertainty. In such a plot, deviations from linear development express the change in stiffness. In this case, the use of derivative plots simplified determining the inflection points, even when it was initially challenging to determine the points graphically. Similarly, qP-plot can be used to determine the closing pressure. The results from the review of data indicate that the results from qP-plots are slightly higher. Still, a combination of the different methods of interpretation can be an advantage.

In total, RSRT was conducted in nine different holes with 31 tests, of which the results from 19 of these tests from four different holes are considered successful, resulting in a success rate of 61.3% for the total number of tests. Compared to the achieved success rate for hydraulic fracturing as presented in Table 6.1, this is somewhat below the achieved success rate for HF-1 and HF-2, which is 70.8% and 72.2%, respectively, and significantly higher than HF-3 (37.5%). Similar, the success rate for RSRT is slightly above HF-4, which is 52.4%.

If the number of test holes with successful results are compared with the number of boreholes in which tests have been carried out, the result will be different. RSRT achieves a rate of 44%. Similarly, HF-1, HF-2, and HF-3 achieve 75%, while HF-3 achieves a success rate of 25%. On average, this gives a success rate of 62.5% for the hydraulic fracturing. Thus, based on the results, HF may achieve a higher success rate than the number of successful tests versus the number of tested holes. Still, the duration time of RSRT is significantly faster, which can increase the total number of tests.

Six successful RSRTs were completed in the same hole as the hydraulic fracturing tests. Figure 11.2 presents a graphical comparison of the results from L20 and L21. As can be seen from the box diagram, the results from RSRT are logically lower than the results from HF, and there is a lower range in the results from RSRT. One possible reason may be the difference in the length of the test section. If the lowest measured values obtained from the hydraulic fracturing test estimate the minimum principal stresses and that a similar approach is used to evaluate the results from RSRT, the ratio between the tests are 1.24 and 1.20 for L20 and L21, respectively. Thus, 1.22 becomes an average correction factor between the tests. However, the calculation basis is uncertain. Both tests have only been carried out in two of the same holes, and compared to other projects, the correlation between hydraulic fracturing and jacking tests is unknown.

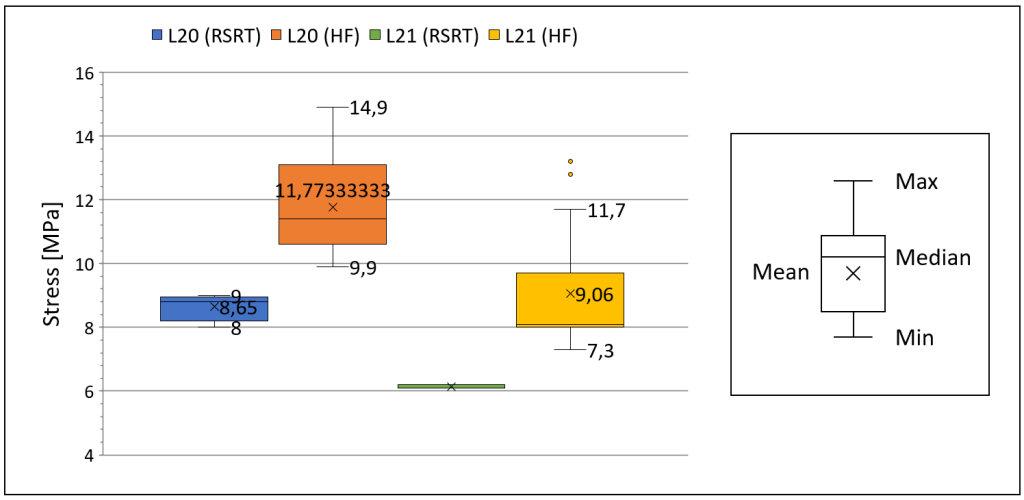

Figure 11.2: Comparison of results from HF and RSRT conducted in L20 and L21 (left) with definition of box diagram (right).

11.2 Assessment on hydraulic failure and leakage potential at Løkjelsvatn hydropower plant

The consequences of hydraulic failure are significant. For example, if a large amount of water disappear into the rock mass, there could be significant consequences for the surroundings, third parties, and loss of income for the owner. Therefore, the potential for leakage and hydraulic failure must be well assessed before, during, and after construction.

11.2.1 Evaluation of results from rock stress measurements

Three independent stress measurement methods measured the stress conditions by the planned transition zone to assess whether the confining pressure is sufficient to avoid hydraulic failure. The results from 3D overcoring and hydraulic fracturing measure the minimum principal stress in the rock mass directly, while RSRT measures the stress perpendicular to the reopened joint. For geometric reasons, this latter value will be lower than the minimum principal stress.

The calculated theoretical stress in the horizontal plane ($\sigma_{h,\text{ theoretical}} = 8.85$ MPa) is somewhat lower than the measured stresses from 3D overcoring ($\sigma_H = 16.1$ MPa and $\sigma_h = 10.20$ MPa), which indicates that the tectonic or geological conditions are affecting the stress levels in the area. According to Equation 2.4 the tectonic contribution must be 1.35 MPa. Calculated vertical stress ($\sigma_{v\text{ theoretical}} = 16.43$ MPa) is marginally lower than measured vertical stress ($\sigma_v = 17.2$ MPa).

The magnitude of the vertical stress component correlates with theoretical values, which fits with findings in Myrvang (2002). The same applies to the magnitude of the major horizontal stress component. The direction is oriented in the NW to SE direction, which corresponds with the regional stress directions in the area studied

in more detail in Section 2.5. The ratio between the maximum horizontal stress component and the vertical stress component (σ_H/σ_v) is 0.92, which is less than the findings in Simonsen (2018), who concluded with an average of 1.2.

Based on results from hydraulic fracturing, the achieved factor of safety at Løkjelsvatn is 1.33. Compared to previous Norwegian projects, this is sufficient to avoid hydraulic failures. Benson (1989) claims that a safety factor of 1.3 is sufficient for good rock masses. Nevertheless, in cases where the rock mass properties are well investigated, this factor can be reduced to 1.1. In Norway, it is common with a safety factor of 1.3 to 1.5, (Aasen et al., 2013).

11.2.2 Evaluation of calculated in-situ stresses from numerical modeling

In-situ stress conditions in the rock mass were studied in more detail with RS2. Three models were established based on the rock stress measurements. Figure 11.3 shows factors of safety with results from numerical modeling along the pressurized tunnel and shaft. As shown in the figure, sufficient confinement pressures are obtained for the entire pressure shaft when the minimum principal stress represents the values for the measured minimum principal stresses (7.32 MPa and 8.40 MPa). On the other hand, the results from the numerical modeling indicate that sufficient confinement pressure is not obtained if the input parameter is 6.0 MPa. Based on the numerical modeling results, it is reasonable to assume that hydraulic failure does not occur along the pressure shaft.

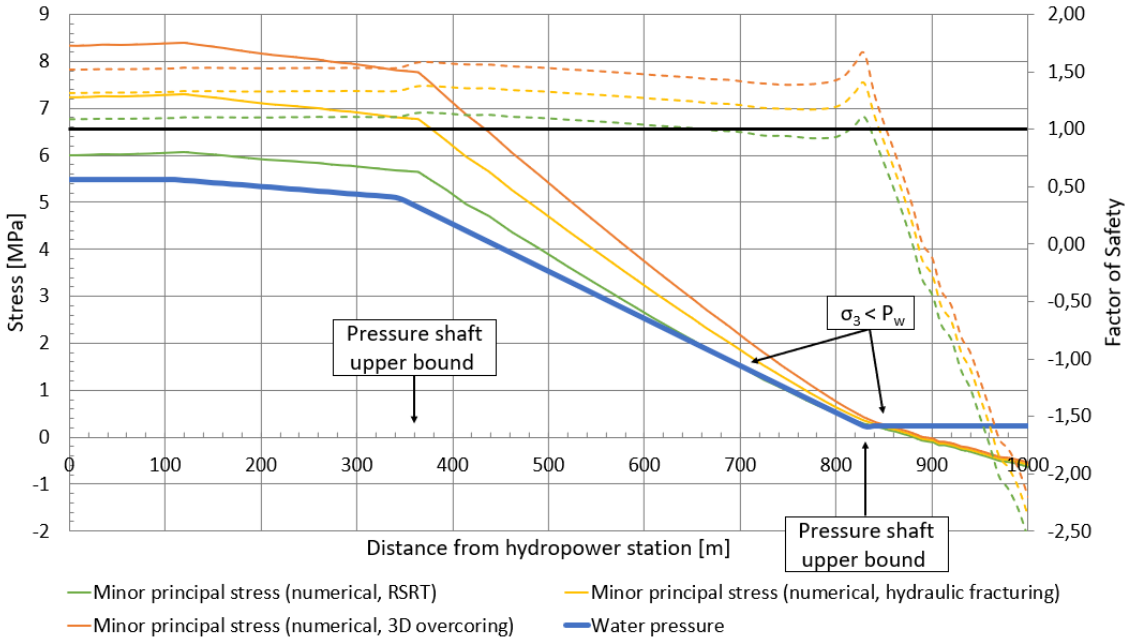

Figure 11.3: Results from numerical modeling (Step 1) and respectively factors of safety. Dotted lines represent the corresponding factor of safety.

11.2.3 Evaluation of leakage potential

In addition to geological and geometric parameters, the leakage potential depends on the stresses around the tunnel. Pressure at failure will be different depending on whether the fracture occurs inside or outside the SRZ. Due to the excavation of the tunnel, a stress-reduced zone occurs around the tunnel. As presented in Section 2.4, the depth of this zone depends upon the ratio between the maximum and minimum principal stresses and the geometry of the tunnel. In weak and anisotropic rocks such as the phyllites, the size of this zone increases compared with hard and strong rocks. Thus, the depth of SRZ and the number of joints within this zone significantly impact the leakage potential.

Results from numerical modeling of four different parts of the pressurized tunnel and shaft with different input values for minor principal stress show the calculated depth of SRZ. The results indicate that the SRZ is most profound when the minor principal stress at the test site is least. These results accord with the theory presented in Section 2.4. Table 9.4 indicates depths up to 20 meters in Model A1. Within this area, the minimum principal stress is lower than the water pressure at the relevant point along the tunnel. For example, the similar depth in Model A2 is a maximum of around the diameter of tunnel. The leakage within this area is therefore largely dependent on the joint conditions. For example, if there are open joints within this zone, significant leakage might occur.

However, based on field mapping, there is little to indicate that there are joints with considerable conductivity within the immediate vicinity of the tunnel. Although there are examples with more schistosity areas in the rock mass, the joints in their entirety appear compact.

11.2.4 Evaluation of the leak potential from semi-analytical estimation

The average specific leakage from the vertical shaft and the pressurized tunnel was estimated to 7.68 l/min/m. It is believed that the estimate is somewhat conservative. The calculations assume that the pressure tunnel from the hydropower station until the shaft is completely without shotcrete. In reality, shotcrete covers the roof and the majority of the walls. Since the leakage from the lower part of the shaft is most significant, the total leakage is likely lower. Assuming that all leakage occurs in the pressure shaft, the average specific leakage can be adjusted down to 5.20 l/min/m as shown in Figure 11.4.

Compared with leakage measurements made at chainage 1380 m during the access tunnel excavation which indicated leakage from a single hole to 1500-3000 L/min, the calculations gave an average estimate of 6474 L/min along the pressurized tunnel and shaft. At chainage 1380 m, the location of the tunnel face is below a strongly de-stressed area. As highlighted in the geological engineering report, the surface consists of deep, open, and penetrating joints. However, aerial photographs indicate that the rock mass is more compact, with potentially lower conductivity in the area

of the pressurized part of the tunnel system. In addition, during the inspection in January 2021, the tunnel was described as dry with a few drips. Therefore, compared to previous parts of the access tunnel, such as 1380 and 1570, there is no need for injection in this area.

On the other hand, leakage from the tunnel is not desirable. However, it is a time-consuming, expansive, and demanding job to minimize leakage. Nevertheless, it is desirable to minimize the leakage to an acceptable level. Panthi (2006) claims that specific leakage should not exceed 1-1.5 l/min/m. The average leakage from 7.68 l/min/m is far above the recommended level, which indicates that the tunnel should be sealed compared to the suggested maximum allowable limits. The author recommends considering a cost-benefit analysis of the effect of sealing parts or the entire pressurized part of the tunnel system.

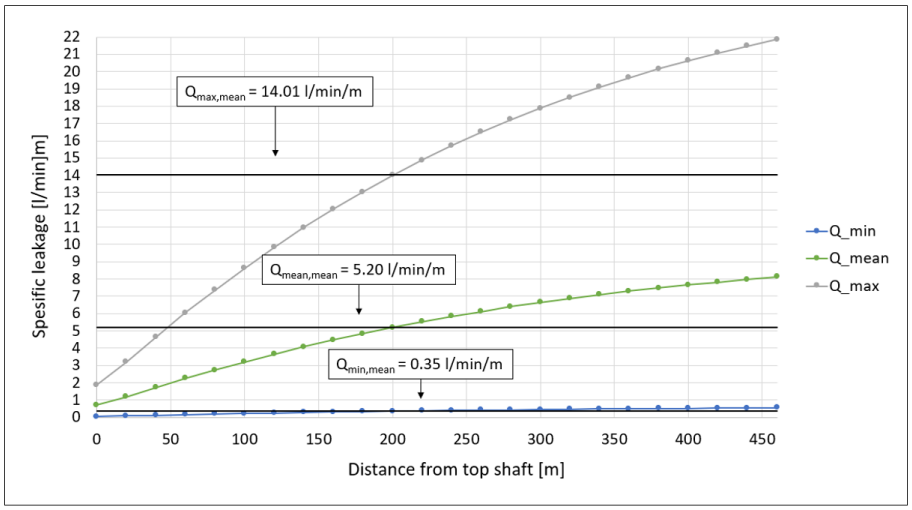

Figure 11.4: Leakage potential from top to bottom of the pressure shaft.

11.2.5 Uncertainties in leakage assessments

Several factors may have affected the result in the determination of the specific leakage. A combination of field mapping and geometric assessment with a CAD tool, such as Civil 3D, gives a quantification of the input parameters in the formula proposed by Panthi (2006). The leakage formula consists of three Q-parameters and three specific parameters. The last three factors are relatively straightforward, while the Q-parameters are based only on mapping at one location during fieldwork in January 2021. At the time, the face of the tunnel was at the test site. Thus, it is assumed that the values remain constant throughout the pressurized parts of the tunnel system for the sake of simplicity. Still, the mapped values give the best estimation of the parameters.

NGI (2015) closely describes the quantification of the Q-parameters. The joint set number (J_n) and joint roughness number (J_r) are relatively straightforward to determine. On the other hand, quantifying representative values for the joint alteration number (J_a) is challenging. The filling material impacts the amount of theoretical

leakage into the rock mass, and therefore the parameter should be given extra attention in the mapping. Compared with the other Q-parameters included in the formula, greater uncertainty is associated with this parameter. In addition, most of the tunnel contour was covered with shotcrete during fieldwork, which made the mapping difficult and has contributed to a certain amount of uncertainty.

11.2.6 Evaluation of topography and geological parameters

Assessing the stress conditions in Litledalen includes a study of the topography. For example, the topography close to the valley side consists of deep, steep, and complex slope topography. Furthermore, studies of aerial photographs (see Figure 6.7 in Section 6.2.3) show that HF-1 to HF-3 are located underneath a strongly jointed area. Different directions on the lineaments indicate that the area is exposed to tectonic activity in several rounds at different times and is a strong indicator that the area may be de-stressed. Thus, the in-situ stress state might be significantly lower than expected, and consequentially, the tunnel needs to be steel or concrete-lined. Alternatively, relocation of the hydropower station is possible to avoid the de-stressed area, which has been the solution at Løkjelsvatn.

Compared with both favorable and unfavorable conditions suggested by Basnet and Panthi (2018) (see Table 5.1 in Section 5.4), the geological surroundings at HF-1 to HF-3 indicate that the confinement criterion is less suitable for unlined pressurized waterways. However, the geological conditions are improving inwards in the rock mass, as seen from the FoS_3 at HF-4.

11.3 Comparison with Norwegian failure and successful cases

Basnet and Panthi (2018) analyzed both failure and successful Norwegian projects. As presented in Table 5.1 in chapter 5, the authors proposed a list of favorable and unfavorable conditions for the applicability of Norwegian confinement criteria.

The project at Løkjelsvatn is like the old headrace tunnel at Tamakoshi project in Nepal compared to four similar projects in Norway, as gathered in Basnet and Panthi (2020). Three of these projects represent projects where leakage has occurred, while one project (Nye Tyin) is considered a success, and no problems have been reported. Different elements such as topography, rock mass, and jointing, faults and weakness zones, and in-situ stress state are compared in Table 11.1.

When comparing important aspects of four selected projects, there is little indication that the project at Løkjelsvatn will be unsuccessful. Based on the table, several of the conditions at Løkjelsvatn are similar to the project at Nye Tyin. It is the geology of the area and the fracture conditions that are different. Still, the foliation at Løkjelsvatn is dipping against the valley slope, which is advantageous according to the summary in Table 5.1.

Table 11.1: Comparison of Løkjelsvatn with other Norwegian projects based on Basnet and Panthi (2018).

Category	Byrte	Askara	Fossmark	Nye Tyin	Løkjelsvatn
Topography	Steep valley slope (β=41°), unlined shaft located close to valley slope	Two steep slopes in two different directions, unlined tunnels is about 150 m above valley bottom	Relatively steep slope, deep fjord valley, tunnel is about 350 m above fjord bottom	Gentle slope topography tunnel is located far away and well below valley bottom	Complex topography, high pressure tunnel is located far away and below valley bottom to avoid the valley slope
Rock mass and jointing	Precamabrian Granitic gneiss rock, two main joint sets with random joints. Joints are filled with silt and clay	Devonian sand stone, two distinct joint set; i.e foliation and steeply dipping cross joints filled with silt and clay	Precambrian granitic gneiss, two distinct joint sets, steeply dipping towards and away from valley slope, joints are open to filled with silt and clay	Precambrian dark gneiss in the high pressure part of the tunnel, joints are tight due to high confinement	Phyllite (lower allochton) with Precambrian origin. Two main joint set with random joints, joints are filled with silt and clay
Faults and weakness zones	Two weakness zones and one big fault called 'Byrte fault'	A crushed zone separates fractured rock mass with massive one	Stress attenuation due to deep fjord valley, destressing due to the weakness zone, σ_3 is less than water pressure in most locations of unlined shaft and tunnel	No nearby fault or weakness zones	No nearby faults or zone of weaknesses in the high pressure part.
In-situ stress state	More than two third of the section of the shaft is located in the de-stressed area. σ_3 is not always more than water pressure	Stress attenuated towards both steep slopes, destressing in the fractured sandstone above crushed zone, σ_3 is less than water pressure at outer reach of the tunnel	Steep attenuation due to deep fjord valley, destressing due to weakness zone, σ_3	High confinement below the valley bottom due to high horizontal stress, σ_3 is always greater than water pressure	σ_3 is always greater water pressure in the upstream side of the hydropower station

Chapter 12

Conclusions and recommendations

12.1 Conclusion

The purpose of the thesis has been to examine the use of unlined waterways in Norwegian hydropower plants, how stresses can create challenges when determining the final hydropower scheme, and finally, how the Rapid Step-Rate Test can help to attain a better understanding of the rock stresses. The assessments have been made based on a combined literature and case study. The literature section looks more closely at which conditions affect the stresses in the rock mass and how to measure them. On the other hand, data from Løkjelsvatn, which is under construction in the southwestern part of Norway, has been collected and studied in more detail. The complex topography and challenging geological conditions have caused a de-stressed area, which give measured stresses far below expected values. Consequentially, this has led to delays and increased costs. Finally, the field applicability of the RSRT have been verified and compared to established test procedures.

Based on the assessment and experiences in this thesis, it can be concluded that:

- Design criteria are a helpful tool in the project conception and preliminary phase, such as preliminary positioning of the transition zone. Still, the criteria are not sufficient for the final determination of the transition zone. Overburden criteria consider a 2D situation and do not take tectonic, geological, or hydrogeological conditions into account. The analysis of the geometric input parameters in The Norwegian Criteria for Confinement at Løkjelsvatn indicates notable discrepancies between measured and theoretical stress levels. Therefore, avoiding rock stress measurements is unacceptable when determining the transition zone's location in unlined waterways.
- Today, the number of rock stress measurements are limited due to economic reasons. Within a relatively small area, the stresses can vary considerably from place to place. In these cases, there is significant uncertainty as to whether these individual measurements provide a realistic picture of the rock stresses in the rock mass. To conclude, this practice is unsatisfactory and arrangements from all involved parts must be done to increase the number of test sites.

- The experience with carrying out the Rapid Step-Rate Test (RSRT) at Løkjelsvatn is convincing and shows that it is possible to fast and efficiently carry out measurements of the stress level (typically 10-20 min pr. test compared to 1-2 hours for traditional tests). However, based on the number of successful test holes at chainage 1780 m, the success rate of RSRT was 44.0% versus 75.0% for hydraulic fracturing. Besides, data from hydraulic fracturing conducted in the same hole (L-20 and L-21) indicate a ratio between the lowest obtained stress levels to HF/RSRT = 1.22. Still, as the RSRT test is faster to execute, one can achieve an increased number of test locations and consequently achieve measurements of a larger area of the rock mass. Hence, the RSRT shows affirmative abilities as a supplementary test method.

- Hydraulic fracturing at chainage 1780 m gives a factor of safety to 1.33 (σ_3=7.32 MPa). Similarly, the results from RSRT give a factor of safety to 1.1. In this thesis, numerical modeling of the tunnel system with results from rock stress measurement gives no points along the pressure tunnel or shaft where the water pressure exceeds the minimum stress level. The lowest factor of safety is achieved along the tailrace tunnel close to the top of the shaft. It is planned to use the existing access tunnel, which was excavated several decades ago, and previous instabilities are unknown to the author. To conclude, based on the results and similar projects in Norway, there is little indication that hydraulic failure will occur.

- Application of a semi-analytical approach proposed by Panthi (2006) was used to estimate specific leakage from the unlined tunnel. The result indicated an average specific leakage of 7.68 l/min/m from the pressure tunnel and shaft.

12.2 Recommandations

In future work with Norwegian and international hydropower plants, it is recommended to look more closely at the following elements based on results, experiences, and assessments in this thesis:

- Until recently, there are examples of rock stresses not being verified before final location. This practice are not satisfactory. Therefore, it is recommended that rock stress measurements be required in the Dam Safety Regulations and that project owners understand the importance of conducting not just one but several rounds of rock stress measurements to increase the understanding of the stresses in the rock mass.

- Compared to the proposed maximum allowable leakage limits, the semi-empirical leakage level from the pressurized part of the tunnel system at Løkjelsvatn is too high. Therefore, it should be considered whether the tunnel should be sealed to reduce leakage.

- The results and experiences from the implementation of RSRT at Løkjelsvatn are good. There are currently few reference projects. It is recommended to strengthen the validity of RSRT by studying any correlations with established methods for rock stress measurements further beyond what has been done in this thesis. This comparison should be made by arranging for double testing in conjunction with rock stress measurements in the years ahead.

Bibliography

Aasen, O., Ødegaard, H., and Palmstrøm, A. (2013). Planning of Pressurized Headrace Tunnel in Albania, in Broch, Grasbakken og Stefanussen (ed.) *Hydropower tunnelling II, Publication No. 22.* 1st edition. Oslo: NFF, pp.21-27.

Amadei, B., Savage, W., and Swolfs, H. (1987). Gravitational stresses in anisotropic rock masses, *International Journal of Rock Mechanics and Mining Sciences and geomechanics abstracts*, 24(4), pp.5-14.

Amadei, B. and Stephansson, O. (1997). *Rock Stress and Its Measurement.* 1st edition. Dordrecht: Springer.

Barton, N. (2006). *Rock Quality, Seismic Velocity, Attenuation and Anisotropy.* Boca Raton: CRC Press.

Barton, N., Lien, R., and Lunde, J. (1974). Engineering Classification of Rock Masses for the Design of Tunnel Support, *Rock Mechanics*, 6(4), pp.189-236.

Basnet, C. B. and Panthi, K. K. (2018). Analysis of unlined pressure shafts and tunnels of selected Norwegian hydropower projects, *Journal of Rock Mechanics and Geotechnical Engineering*, 10(3), pp.486-512.

Basnet, C. B. and Panthi, K. K. (2019). Evaluation on the Minimum Principal Stress State and Potential Hydraulic Jacking from the Shotcrete-Lined Pressure Tunnel: A Case from Nepal, *Rock Mechanics and Rock Engineering*, 52(7), pp.2377-2399.

Basnet, C. B. and Panthi, K. K. (2020). Detailed engineering geological assessment of a shotcrete lined pressure tunnel in the Himalayan rock mass conditions: A case study from Nepal, *Bulletin of Engineering Geology and the Environment*, 79(1), pp.153–189.

Benson, R. (1989). Design of unlined and lined pressure tunnels, *Tunnelling and Underground Space Technology*, 4(2), pp.155-170.

Bergh-Christensen, J. and Dannevig, N. (1971). Engineering geological evaluations of the unlined pressure shaft at the Mauranger hydropower plant. Technical report. Oslo, Norway: GEOTEAM A/S.

Bieniawski, Z. and Bernede, M. (1979). Suggested methods for determining the uniaxial compressive strength and deformability of rock material, *International Journal of Rock Mechanics and Mining Sciences*, 16(2), pp.135-140.

Broch, E. (1984). Development of Unlined Pressure Shafts And Tunnels in Norway, in *Hydropower tunnelling I, Publication No. 3.* 1st edition. Oslo: NFF, pp.11-21.

Broch, E. (2013). Underground hydropower projects - lessons learned in home country and from projects abroad, in Broch, Grasbakken og Stefanussen (ed.) *Hydropower tunnelling II, Publication No. 22.* 1st edition. Oslo: NFF, pp.21-27.

Brown, E. and Hoek, E. (1978). Trends in relationships between measured in-situ stresses and depth, *International Journal of Rock Mechanics and Mining Sciences and geomechanics abstracts*, 15(4), pp.211-215.

Condie, K. C. (2015). *Earth as an evolving planetary system*. 3rd edition. Cambridge: Academic Press.

Damsikkerhetsforskriften (2009). *Forskrift 21. desember 2009 nr. 1600 om sikkerhet ved vassdragsanlegg*. Available at: https://lovdata.no/dokument/SF/forskrift/2009-12-18-1600 (Accessed: 25.02.2021).

Davik, K., Kveen, A., Aasen, O., Åndal, T., Kjølberg, R., and Heimli, P. (2002). *Berginjeksjon, Håndbok nr. 1*. Oslo: NFF.

Fejerskov, M. (1996). *Determination of in-situ rock stresses related to petroleum activities on the Norwegian Continental Shelf*. PhD. Trondheim: NTNU.

Fejerskov, M. and Myrvang, A. (1995). In-situ rock stress pattern on the Norwegian continental shelf and mainland, *8th ISRM Congress*. Tokyo, 25-29.09.1995.

Golod, G., Krasilova, N., Ladygin, V., and Shaumian, L. (1975). Factors controlling solid rock strength, *Bulletin of engineering geology and the environment*, 11(1), pp.65-69.

Haimson, B. and Cornet, F. (2003). Suggested Methods for rock stress estimation — Part 3: Hydraulic fracturing (HF) and/or hydraulic testing of pre-existing fractures (HTPF), *International Journal of Rock Mechanics and Mining Sciences*, 40(7), pp.1011-1020.

Hanssen, T. (1997). *Investigations of some rock stress measuring techniques and stress field in Norway*. PhD. Trondheim: NTNU.

Hartmaier, H., Doe, T., and Dixon, G. (1998). Evaluation of hydrojacking tests for an unlined pressure tunnel, *Tunnelling and Underground Space Technology*, 13(4), pp.393-401.

Hayashi, K. and Haimson, B. (1991). Characteristics of shut-in curves in hydraulic fracturing stress measurements and determination of in situ minimum compressive stress, *Journal of Geophysical Research*, 96(B11), pp.311-321.

Heidbach, O., Barth, A., Müller, B., Reinecker, J., Stephansson, O., Tingay, M., and Zang, A. (2016). *WSM quality ranking scheme, database description and analysis guidelines for stress indicator*. (World Stress Map Technical Report 16-01), GFZ German Research Centre for Geosciences. Available at: https://gfzpublic.gfz-potsdam.de/rest/items/item_4732890_3/component/file_4732894/content (Accessed 11.02.2021).

Hoek, E. (2007). *Practical Rock Engineering*. RocScience. Available at: https://www.rocscience.com/documents/hoek/corner/Practical-Rock-Engineering-Full-Text.pdf (Accessed 08.02.2021).

Hoek, E. and Brown, E. (1980). *Underground excavations in rock*. London: Institution of Mining and Metallurgy.

Hoek, E. and Brown, E. (2019). The Hoek–Brown failure criterion and GSI – 2018 edition, *Journal of Rock Mechanics and Geotechnical Engineering*. 11(3), pp.445-463.

Hoek, E., Carranza-Torres, C., and Corkum, B. (2002). Hoek–Brown failure criterion – 2002 edition. *Mining and Tunnelling Innovation and Opportunity - Proceedings of the 5th North American Rock Mechanics Symposium and 17th Tunnelling Association of Canada Conference*. Ed. by Hammah et al. Toronto: University of Toronto, pp.267-273.

Hoek, E., Carter, T., and Diederichs, M. (2013). Quantification of the Geological Strength Index Chart, *47th US Rock Mechanics/Geomechanics Symposium*. San Francisco, 23-26.06.2013.

Hoek, E. and Diederichs, M. (2006). Empirical estimation of rock mass modulus, *International Journal of Rock Mechanics and Mining Sciences*, 43, pp.203-215.

Hoek, E., Kaiser, P., and Bawden, W. (1995). *Support of underground excavations in hard rock*. 1st edition. Rotterdam: Balkema.

Hoek, E. and Marinos, P. (2000). Predicting tunnel squeezing problems in weak heterogeneous rock masses, *Tunnels and tunneling international*, 32(11), pp.45-51.

Hooker, V. and Duvall, W. (1971). *In situ rock temperature: Stress investigations in rock quarries*. (7589). Washington: U.S. Bureau of Mines Report of Investigations.

Houlsby, A. C. (1976). Routine Interpretation of the Lugeon Water-test, *Quarterly Journal of Engineering Geology and Hydrogeology*, 9(4), pp.303-313.

Hudson, J., Cornet, F., and Christiansson, R. (2003). ISRM Suggested Methods for rock stress estimation — Part 1: Strategy for rock stress estimation, *International Journal of Rock Mechanics and Mining Sciences*, 40(7), pp.991-998.

Hudson, J. and Harrison, J. (1997). *Engineering Rock Mechanics: An Introduction to the Principles*. 1st edition. Amsterdam: Elsevier Science and Technology.

ISRM (1978a). Suggested Method for Petrographic Description of Rocks, *International Journal of Rock Mechanics and Mining Sciences & Geomechanics Abstracts*. 15(2), pp.43-45.

ISRM (1978b). Suggested Methods for Determining Tensile Strength of Rock Materials, *International Journal of Rock Mechanics and Mining Sciences*, 15, pp.99-103.

ISRM (1985). Suggested method for determining point load strength, *International Journal of Rock Mechanics and Mining Sciences*, 22(2), pp.51-60.

ISRM (2017). Suggested Method for Laboratory Acoustic Emission Monitoring, *Rock Mechanics and Rock Engineering*. 50, pp.665-674.

Jaeger, J. C., Cook, N. G. W., and Zimmerman, R. W. (2009). *Fundamentals of rock mechanics*. 4th edition. Hoboken: Wiley-Blackwell.

Kartverket (2021). *Høydedata*. Available at: https://hoydedata.no/LaserInnsyn/ (Accessed: 23.04.2021).

Leeman, E. R. (1969). The 'Doorstopper' and triaxial rock stress measuring instruments developed by the C.S.I.R., *Journal of the South African Institute of Mining and Metallurgy*, 69(7), pp.305-339.

Li, C. (2018). *Rock Mechanics*. Trondheim: NTNU.

Lia, L., Aas, M. N., and Killingtveit, Å. (2017). Increased generation from upgrading and extension projects, *International Journal on Hydropower and Dams*, 24(4), pp.75-78.

Ljunggren, C., Chang, Y., Janson, T., and Christiansson, R. (2003). An overview of rock stress measurement methods, *International Journal of Rock Mechanics and Mining Sciences*, 40(7), pp.975-989.

Martin, C. and Chandler, N. (1993). Stress heterogeneity and geological structures, *International Journal of Rock Mechanics and Mining Sciences & Geomechanics Abstracts*, 30(7), pp.993-999.

Ministry of Petroleum and Energy (2021). *Electricity production*. Available at: https://energifaktanorge.no/en/norsk-energiforsyning/kraftproduksjon/hydropower (Accessed 09.03.2021).

Mitchell, J. and Soga, K. (2005). *Fundamentals of Soil Behaviour*. 3rd edition. New Jersey: Wiley.

Myrvang, A. (1996). *Kompendium i bergmekanikk*. Trondheim: NTNU.

Myrvang, A. (2002). Hvordan står det til med bergspenningene i Norge? *Fjellsprengningskonferansen 2002*. Oslo, 21-22.11.2002.

NGI (2015). *Using the Q-system*. Available at: https://www.ngi.no/eng/Services/Technical-expertise/Engineering-geology-and-rock-mechanics/Q-system (Accessed 08.04.2021).

NGU (1975). *Berggrunnskart Sauda*. (B250, 1:250 000). Trondheim: Geological Survey of Norway (NGU).

NGU (2013). *Berggrunnskart Vindafjord*. (1213-1, 1:50 000). Trondheim: Geological Survey of Norway (NGU).

NGU (2014). *Geological and geophysical investigations for the Rogfast project*. (341500). Trondheim: Geological Survey of Norway (NGU).

NGU (2015). *Bedrock geology, Norway*. Available at: https://www.ngu.no/en/topic/bedrock-geology-0 (Accessed 08.05.2021).

Nilsen, B. (1979). *Stabilitet av høye fjellskjæringer*. PhD. Trondheim: NTH.

Nilsen, B. and Palmstrøm, A. (2000). *Engineering geology and Rock engineering*. 1st edition. Oslo: Norwegian Group for Rock Mechanics.

Nilsen, B. (2016). *Ingeniørgeologi berg - grunnkurskompendium*. Trondheim: NTNU.

Nordal, S., Grøv, E., Emdal, A., and L'Heureux, J. (2018). *Skredene i Tosbotn, Nordland 1. og 2. april 2016. Report from research group set up by Nordland County Municipality*. Available at: https://www.nfk.no/_f/p34/i7e686f6b-c4ef-4f78-832b-5aea0ce744c8/tosbotn-rapport_15-mai-2018.pdf (Accessed 20.10.2020).

NVE (2021). *Facts of Energy*. Available at: https://www.nve.no/energiforsyning/kraftproduksjon/vannkraft/vannkraftdatabase/ (Accessed 10.03.2021).

Ødegaard, H., Barkved, H., and Nilsen, B. (2020). Design of unlined pressure tunnels in Norway - limitations of empirical overburden criteria and significance of in-situ rock stress measurements, *ISRM International Symposium Eurock 2020 - Hard Rock Engineering*. Trondheim, 14-19.06.2020.

Ødegaard, H. and Nilsen, B. (2018). Engineering Geological Investigation and Design of Transition Zones in Unlined Pressure Tunnels, *10^{th} Asian Rock Mechanics Symposium, The ISRM International Symposium for 2018*. Singapore, 29.10-03.11.2018.

Ødegaard, H. and Nilsen, B. (2021). Rock Stress Measurements for Unlined Pressure Tunnels: A True Triaxial Laboratory Experiment to Investigate the Ability of a Simplified Hydraulic Jacking Test to Assess Fracture Normal Stress, *Rock Mechanics and Rock Engineering*, Published online 27.03.2021, DOI: https://doi.org/10.1007/s00603-021-02452-9.

Palmström, A. and Broch, E. (2017). The design of unlined hydropower tunnels and shafts: 100 years of Norwegian experience, *The International Journal of Hydropower & Dams*, 24(3).

Panthi, K. K. (2006). *Analysis of engineering geological uncertainties related to tunnelling in Himalayan rock mass conditions*. PhD. Trondheim: NTNU.

Panthi, K. K. (2012a). A probabilistic approach in assessing tunnel squeezing – a discussion based on tunnel projects from Nepal Himalaya , *46th US Rock Mechanics/Geomechanics Symposium*. Chicago, 24-27.06.2012.

Panthi, K. K. and Basnet, C. B. (2021). Fluid Flow and Leakage Assessment Through an Unlined/Shotcrete Lined Pressure Tunnel: A Case from Nepal Himalaya, *Rock Mechanics and Rock Engineering*, 54(5), pp.1-19.

Panthi, K. and Basnet, C. (2017). Design review of the headrace system for the Upper Tamakoshi project, Nepal, *International Journal on Hydropower and Dams*, 24(1), pp.60-67.

Panthi, K. K. (2012b). Evaluation of rock bursting phenomena in a tunnel in the Himalayas, *Bulletin of Engineering Geology and the Environment*, 71(4), pp.761-769.

Panthi, K. K. (2014). Norwegian Design Principle for High Pressure Tunnels and Shafts: Its Applicability in the Himalaya, *Hydro Nepal: Journal of Water, Energy and Environment*, (14), pp.36-40.

Panthi, K. K. and Basnet, C. B. (2018). State-of-art design guidelines in the use of unlined pressure tunnels/shafts for hydropower scheme, *10th Asian Rock Mechanics Symposium, The ISRM International Symposium for 2018*. Singapore, 29.10-03.11.2018.

Plahn, S., Nolte, K., and Miska, S. (1997). A Quantitative Investigation of the Fracture Pump-In/FIowback Test, *SPE Production & Facilities*. 12(1), pp.20-27.

Raaen, A., Skomedal, E., Kjørholt, H., Markestad, P., and Økland, D. (2001). Stress determination from hydraulic fracturing tests: the system stiffness approach, *Rock Mechanics and Mining Sciences*. 38, pp.529-541.

Ramberg, I. B., Bryhni, I., Nøttvedt, A., and Rangnes, K. (2013). *Landet blir til: Norges geologi*. 2nd edition. Trondheim: Norwegian Geological Society.

Rancourt, A. (2010). *Guidelines for preliminary design of unlined pressure tunnels*. PhD. Montreal: McGill University.

Roberts, D. and Myrvang, A. (2004). Contemporary stress orientation features in bedrock, Trøndelag, central Norway, and some regional implications, *NGU Bulletin*, 442, pp.53-63.

RocScience (2021). *Getting Started with RS2*. Available at: https://www.rocscience.com/help/rs2/getting_started/getting_started.htm (Accessed: 08.05.2021).

Rowland, S., Duebendorfer, E., and Schiefelbein, I. (2007). *Structural Analysis and Syntesis*. 3rd edition. Malden: Blackwell.

Rutqvist, J. and Stephansson, O. (1996). A cyclic hydraulic jacking test to determine the in situ stress normal to a fracture, *International Journal of Rock Mechanics and Mining Sciences*, 33(7), pp.695-711.

Savage, W. (1978). The development of residual stress in cooling rock bodies, *Geophysical Research Letters*, 5(8), pp.633-636.

Savitski, A. and Dudley, J. (2011). Revisiting Microfrac In-situ Stress Measurement via Flow Back - A New Protocol, *SPE Annual Technical Conference and Exhibition*. Denver, 30.10-02.11.2011.

Simonsen, A. L. L. (2018). *Updated Norwegian In Situ Rock Stress Database*. Master's thesis. Trondheim: NTNU.

SINTEF (2003). *In situ rock stress measurements - Brief description of methods applied by Sintef*. Available at: https://www.sintef.no/globalassets/upload/

teknologi_og_samfunn/berg-og-geoteknikk/lister/brosjyre-bergmekanikklab-05.pdf (Accessed: 03.02.2021).

SINTEF (2020). Hydraulic fracturing at Løkjelsvatn hydropower plant. SINTEF Community.

SINTEF (2021). Rock stress measurements at Løkjelsvatn hydropower plant. SINTEF Community.

Sjöberg, J., Christiansson, R., and Hudson, J. (2003). Suggested Methods for rock stress estimation — Part 2: Overcoring methods, *International Journal of Rock Mechanics and Mining Sciences*, 40(7), pp.999-1010.

SKL (2018). *SKL får konsesjon til å bygge Løkjelsvatn Kraftverk*. Available at: https://skl.as/2018/08/21/skl-far-konsesjon-til-a-bygge-lokjelsvatn-kraftverk/ (Accessed 11.03.2021).

Smith, M. and Montgomery, C. (2014). *Hydraulic fracturing. Emerging trends and technologies in petroleum engineering*. Hoboken: CRC Press.

SSB (2018). *Vi bruker mindre strøm hjemme*. Available at: https://www.ssb.no/energi-og-industri/artikler-og-publikasjoner/vi-bruker-mindre-strom-hjemme (Accessed: 18.05.2021).

Stephansson, O., Ljunggren, C., and Jing, L. (1991). Stress measurements and tectonic implications for Fennoscandia, *Tectonophysics*, 189(1), pp.317-322.

SWECO (2017). Løkjelsvatn Kraftverk, Ingeniørgeologisk anbudsrapport.

Tang, C. and Hudson, J. (2010). *Rock Failure Mechanisms: Explained and Illustrated*. Boca Raton: CRC Press.

Tournier, J. and Quirion, M. (2010). Hydraulic jacking tests in crystalline rocks for hydroelectric projects in Quebec, Canada. *Rock Stress and Earthquakes - Proceedings of the 5th International Symposium on In-Situ Rock Stress*. Beijing, 25-27.08.2010.

Tsidzi, K. (1997). Propagation characteristic of ultrasonic waves in foliated rocks, *Bull. Int. Association of Eng. Geology*, 56, pp.103-113.

UN (2021). *7: Affordable and clean energy*. Available at: https://www.un.org/sustainabledevelopment/energy/ (Accessed: 16.05.2021).

YIT (2020). Rapport for sondér- og injeksjonsboring.

Ziegler, M., Loew, S., and Amann, F. (2016). Near-surface rock stress orientations in alpine topography derived from exfoliation fracture surface markings and 3D numerical modelling, *International Journal of Rock Mechanics and Mining Sciences*, 85, pp.129-151.

Zoback, M. L., Zoback, M. D., Adams, J., Assumpção, M., Bell, S., Bergman, E. A., Blümling, P., Brereton, N. R., Denham, D., Ding, J., Fuchs, K., Gay, N., Gregersen, S., Gupta, H. K., Gvishiani, A., Jacob, K., Klein, R., Knoll, P., Magee, M., Mercier, J. L., Müller, B. C., Paquin, C., Rajendran, K., Stephansson, O., Suarez, G., Suter, M., Udias, A., Xu, Z. H., and Zhizhin, M. (1989). Global patterns of tectonic stress, *Nature*, 341, pp.291-298.

Appendix A: Standard chart and figures

Appendix A consists of the following appendices:

1. Rock support chart based on the Q-system, (NGI, 2015).
2. Procedure for determining necessary factor of safety (FoS) for preliminary design, (Rancourt, 2010).

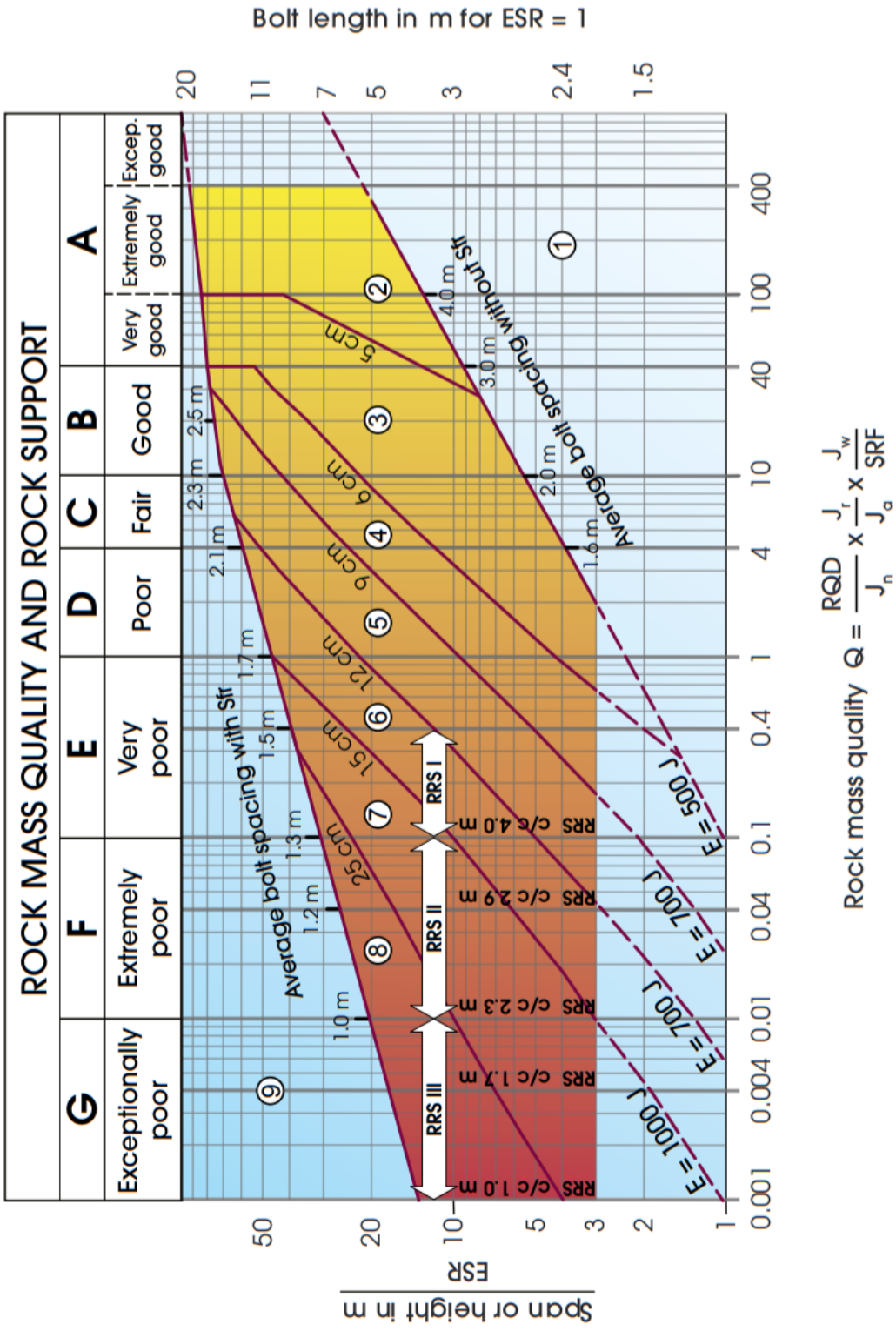
Bolt length in m for ESR = 1
ROCK MASS QUALITY AND ROCK SUPPORT
G
F
E
D
C
B
A
Exceptionally poor
Extremely poor
Very poor
Poor
Fair
Good
Very good
Extremely good
Excep. good
Span or height in m
ESR
Average bolt spacing without Str
Average bolt spacing with Str
5 cm
9 cm
12 cm
15 cm
25 cm
RRS I
RRS II
RRS III
RRS c/c 4.0 m
RRS c/c 2.9 m
RRS c/c 2.3 m
RRS c/c 1.7 m
RRS c/c 1.0 m
E = 1000 J
E = 700 J
E = 500 J
Rock mass quality Q = RQD/J_n x J_r/J_a x J_w/SRF

Procedure for determining necessary factor of safety (FoS) for preliminary design, Rancourt (2010).

Parameter	Description	Factor of Safety
A. Rock Mass Characteristics		**Fa**
Soft, low modulus (E_{rm}<5 GPa) Highly anisotropic	Sedimentary Metamorphic Horizontal lying	1.3
Medium modulus (5-20 GPa) Anisotropic	Sedimentary Metamorphics Volcanic	1.2
Hard, high modulus (>20 GPa) Isotropic, with slight foliation	Gneiss	1.1
	Massive	1.0
B. Cover to tunnel diameter ratio	**C/DT**	**Fb**
	< 5	Not recommended
	5-10	1.2
	10-20	1.15
	> 20	1.1
C. Presence of Structures		**Fc**
Within 2 D_T of distance Consider semi-lined section	Yes	1.1
	Perpendicular to surface	1.2
	No	1.0

Appendix B: Results from laboratory examination

Results from laboratory tests of phyllite from Løkjelsvatn. The samples were collected from the transition zone.

1. XRD: 210034 Løkjelsvatn 1
2. XRD: 210035 Løkjelsvatn 2
3. UCS: Stress-strain curves of Sample 1 1 to Sample 4
4. UCS: Stress-strain curve with AE-sensors
5. Results from The Brazilian test
6. Results from Point load test

XRD: 210034 Løkjelsvatn 1

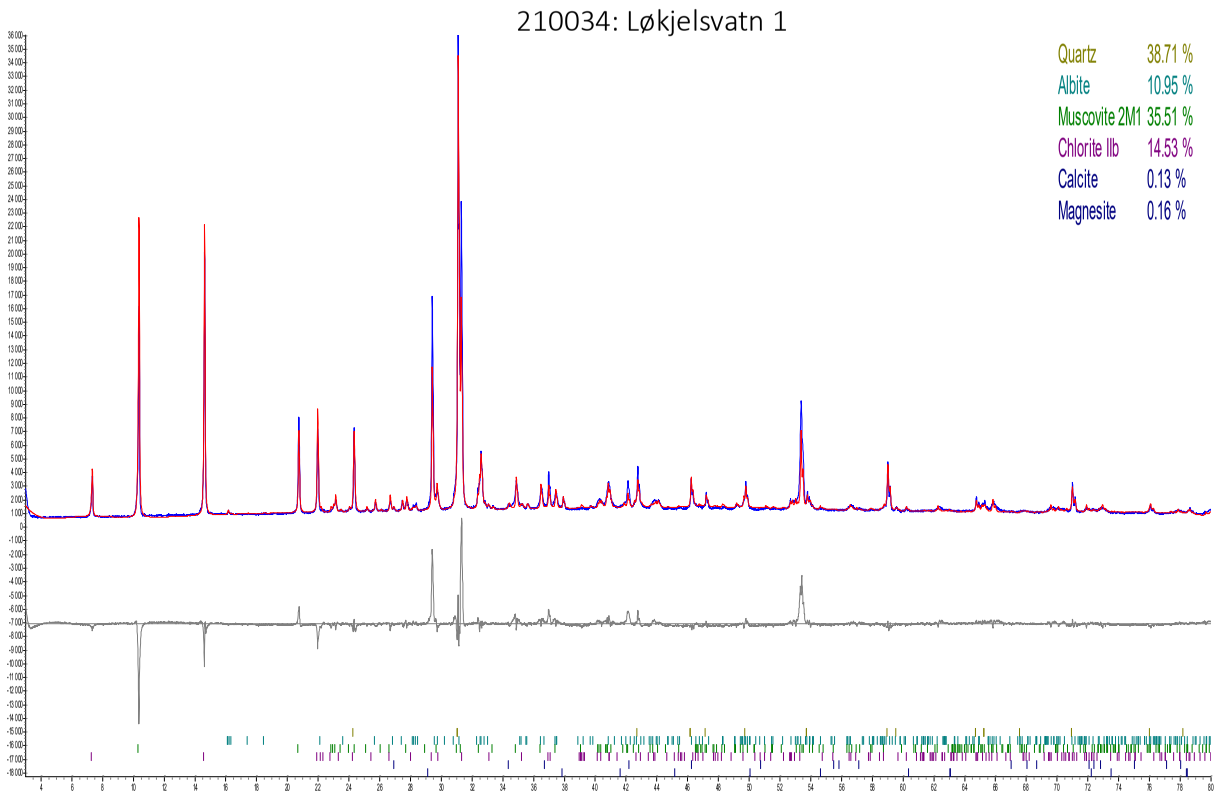

XRD: 210035 Løkjelsvatn 2

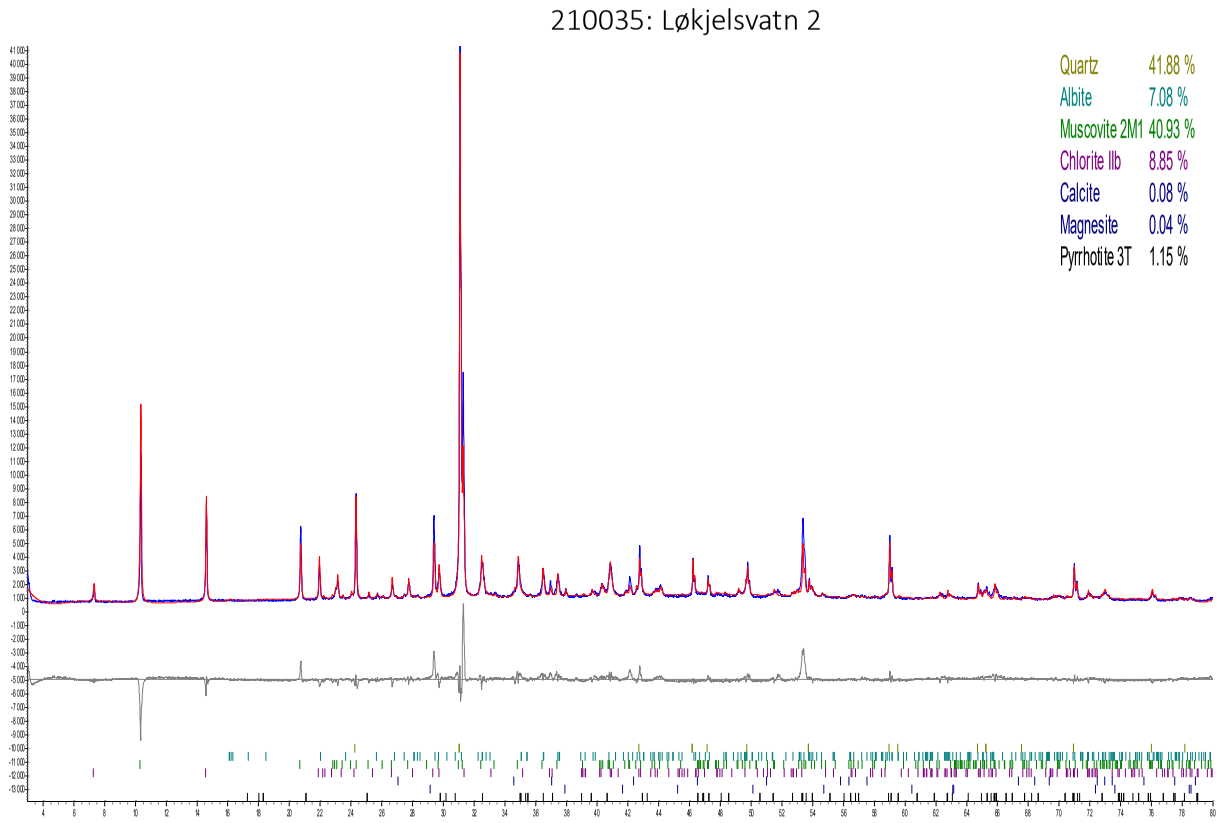

UCS: Stress-strain curves of samples 1-4

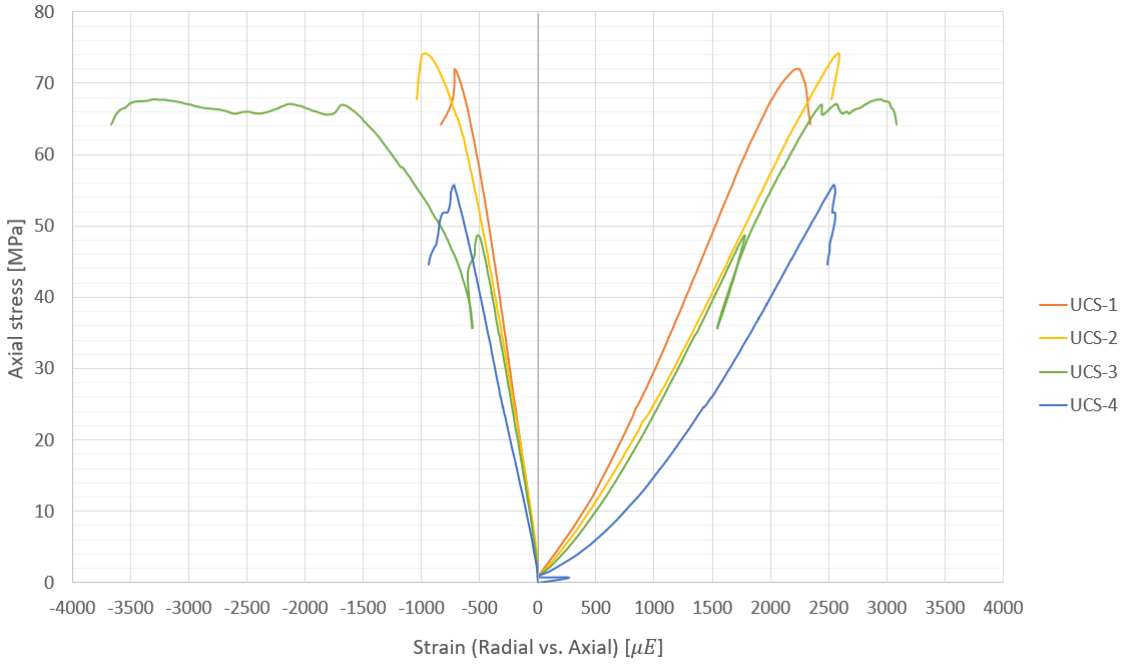

UCS: Stress-strain curve with AE sensors

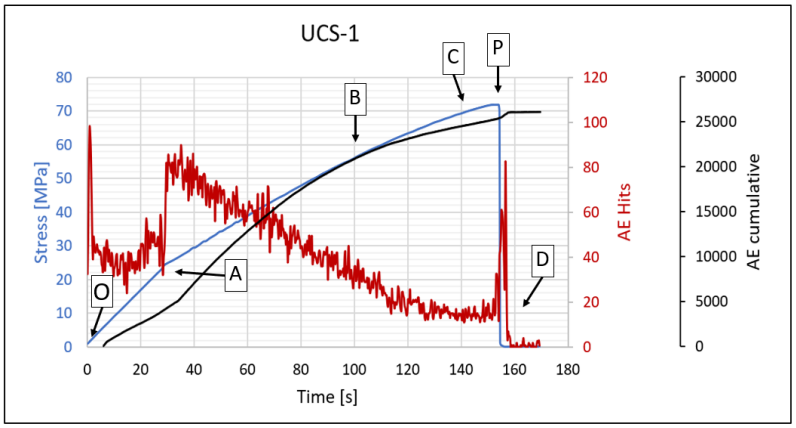

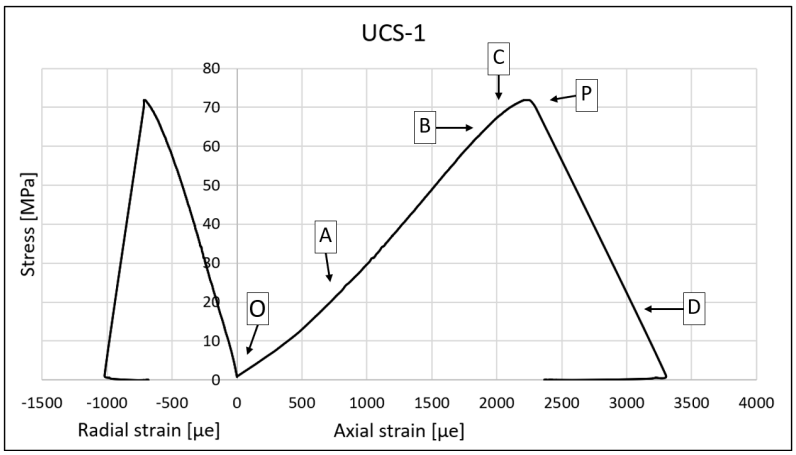

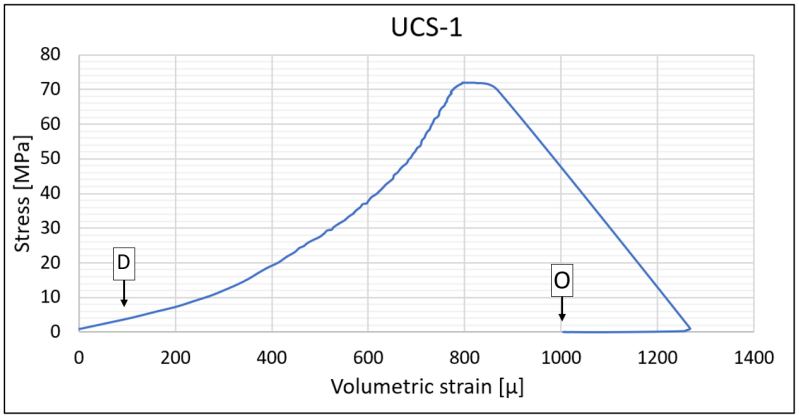

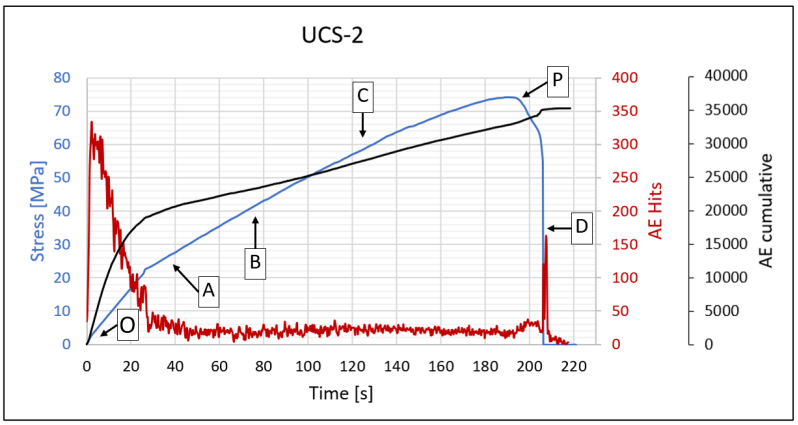
UCS-2
Stress [MPa]
AE Hits
AE cumulative
Time [s]
O
A
B
C
D
P

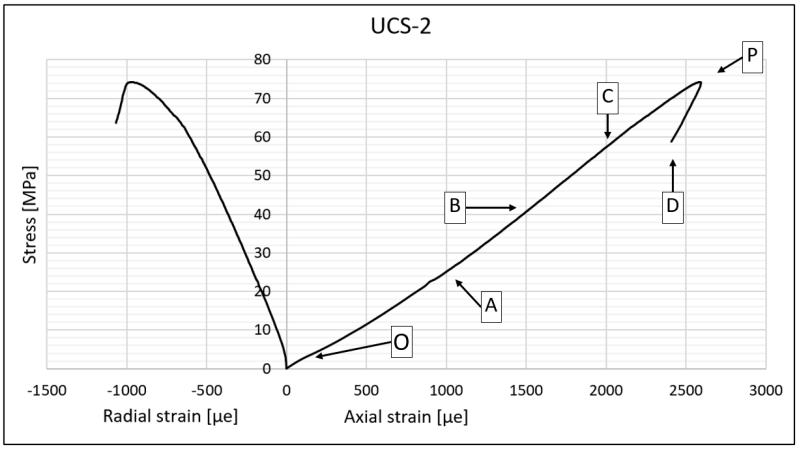
UCS-2
Stress [MPa]
Radial strain [με]
Axial strain [με]
O
A
B
C
D
P

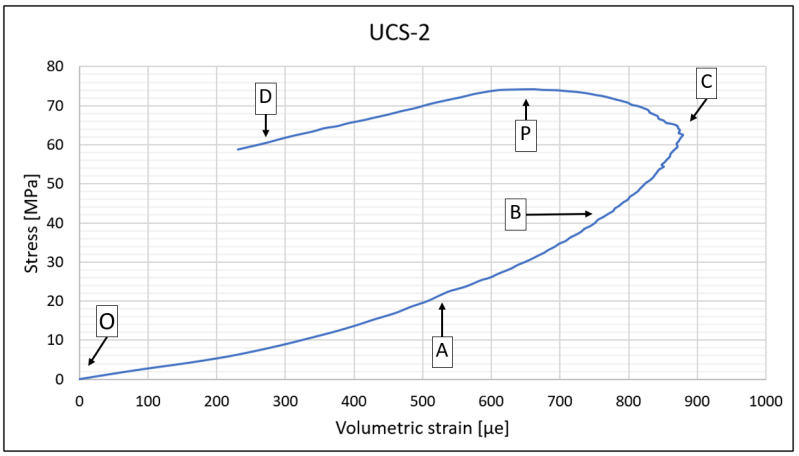
UCS-2
Stress [MPa]
Volumetric strain [με]
O
A
B
C
D
P

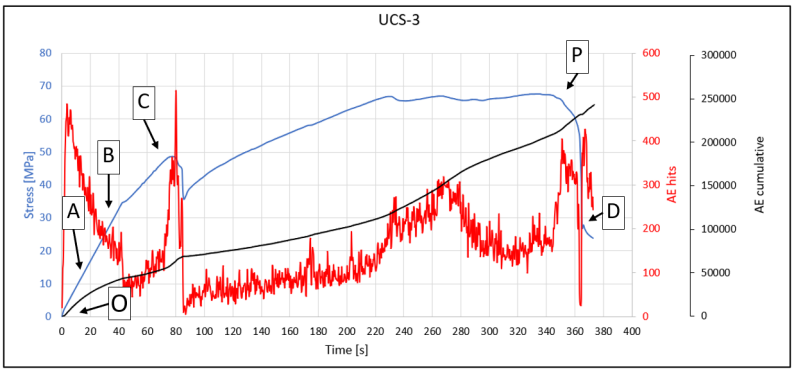
UCS-3
Stress [MPa]
AE hits
AE cumulative
Time [s]
A
B
C
D
O
P

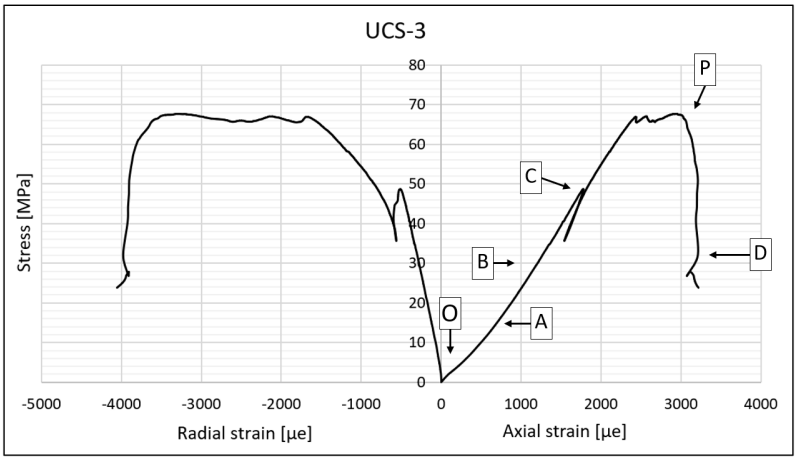
UCS-3
Stress [MPa]
Radial strain [με]
Axial strain [με]
A
B
C
D
O
P

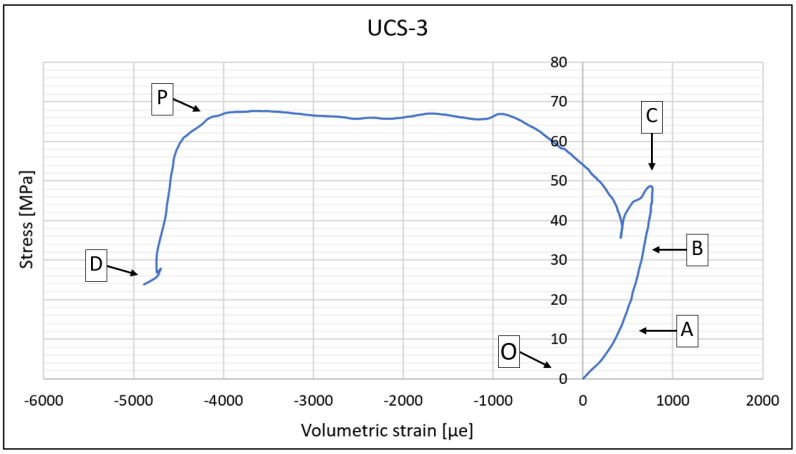
UCS-3
Stress [MPa]
Volumetric strain [με]
A
B
C
D
O
P

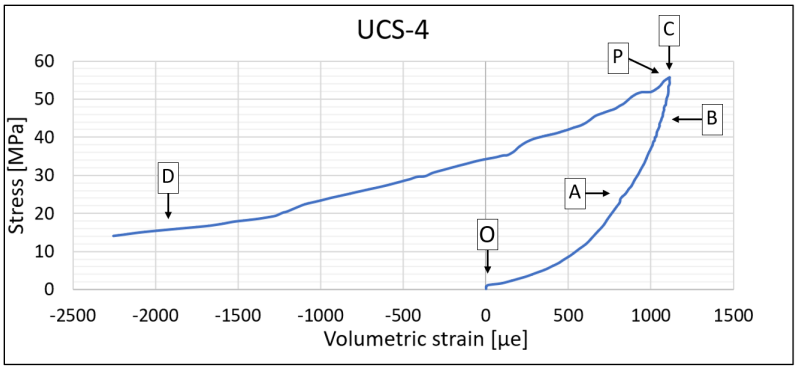
UCS-4
C
P
B
A
D
O
60
50
40
30
20
10
0
Stress [MPa]
-2500
-2000
-1500
-1000
-500
0
500
1000
1500
Volumetric strain [με]

Results from The Brazilian test

	Test #	Diameter [mm]	Thickness [mm]	Weight, dry [g]	Density, dry [cm^3]	Pressure [kN]	σ_t (MPa)	Comment
Brazil	1	50,97	25,17	142,79	2,780	23,14	11,48	Not valid
	2	50,90	25,37	145,17	2,812	28,48	14,04	
	3	50,88	25,32	144,28	2,803	21,5	10,62	
	4	50,92	25,35	144,81	2,805	22,54	11,12	
	5	50,94	25,37	144,18	2,788	17,26	8,50	
	6	50,94	25,04	143,35	2,809	10,95	5,47	Not valid
	7	50,95	25,16	143,55	2,798	18,89	9,38	
	8	50,99	24,91	140,03	2,753	13,36	6,70	
	9	51,01	25,1	141,66	2,762	13,74	6,83	

Results from Point load test

Test #	Direction to foliation (Perpendicular/Parallel)	Diametral/Axial	W [mm]	D [mm]	Load [kN]	Pressure [MPa]	D_e^2 [mm^2]	D_e [mm]	I_s	F	$I_{s(50)}$	Comment
1	Parallel	Diametral	-	61,48	8,34	8,05	3779,79	61,48	2,13	1,10	**2,34**	
2	Parallel	Diametral	-	61,48	3,06	2,95	3779,79	61,48	0,78	1,10	0,86	Not valid
3	Parallel	Diametral	-	61,47	10,06	9,71	3778,56	61,47	2,57	1,10	2,82	Not valid
4	Parallel	Diametral	-	61,50	4,50	4,34	3782,25	61,50	1,15	1,10	1,26	Not valid
5	Parallel	Diametral	-	61,48	8,62	8,32	3779,79	61,48	2,20	1,10	2,42	Not valid
6	Parallel	Diametral	-	61,58	7,74	7,47	3792,10	61,58	1,97	1,10	**2,16**	
7	Parallel	Diametral	-	61,51	6,66	6,43	3783,48	61,51	1,70	1,10	**1,86**	
8	Parallel	Diametral	-	61,48	2,52	2,43	3779,79	61,48	0,64	1,10	0,71	Not valid
9	Parallel	Diametral	-	61,50	2,96	2,86	3782,25	61,50	0,76	1,10	0,83	Not valid
10	Parallel	Diametral	-	60,49	7,10	6,85	3659,04	60,49	1,87	1,09	**2,04**	
11	Parallel	Diametral	-	61,48	9,10	8,78	3779,79	61,48	2,32	1,10	**2,55**	
12	Parallel	Diametral	-	61,50	4,96	4,79	3782,25	61,50	1,27	1,10	1,39	Not valid
13	Parallel	Diametral	-	61,51	7,04	6,79	3783,48	61,51	1,80	1,10	1,97	Not valid
14	Normal	Axial	61,52	22,92	13,36	12,89	1795,32	42,37	7,18	0,93	**6,67**	
15	Normal	Axial	61,51	23,80	11,86	11,44	1863,94	43,17	6,14	0,94	**5,75**	
16	Normal	Axial	61,46	47,37	16,36	15,79	3706,86	60,88	4,26	1,09	4,65	Not valid
17	Normal	Axial	61,48	29,81	12,28	11,85	2333,49	48,31	5,08	0,98	**5,00**	
18	Normal	Axial	61,46	29,02	15,78	15,23	2270,91	47,65	6,71	0,98	6,56	Not valid
19	Normal	Axial	61,46	40,11	24,28	23,43	3138,74	56,02	7,46	1,05	**7,86**	
20	Normal	Axial	61,51	24,96	14,66	14,15	1954,79	44,21	7,24	0,95	**6,85**	
21	Normal	Axial	61,48	24,11	9,02	8,70	1887,30	43,44	4,61	0,94	4,33	Not valid
22	Normal	Axial	61,53	20,78	10,92	10,54	1627,96	40,35	6,47	0,91	5,88	
23	Normal	Axial	61,54	35,65	11,16	10,77	2793,36	52,85	3,86	1,03	3,95	Not valid
24	Normal	Axial	61,52	24,64	11,28	10,89	1930,04	43,93	5,64	0,94	**5,32**	
25	Normal	Axial	61,51	30,64	17,04	16,44	2399,63	48,99	6,85	0,99	6,79	Not valid
26	Normal	Axial	61,53	45,06	7,88	7,60	3530,11	59,41	2,15	1,08	2,33	Not valid
27	Normal	Axial	61,46	20,22	14,22	13,72	1582,28	39,78	8,67	0,90	**7,82**	
28	Normal	Axial	61,49	32,00	12,26	11,83	2505,33	50,05	4,72	1,00	**4,72**	
29	Normal	Axial	61,54	24,62	6,00	5,79	1929,10	43,92	3,00	0,94	2,83	Not valid
30	Normal	Axial	61,48	23,27	14,80	14,28	1821,55	42,68	7,84	0,93	**7,30**	
31	Normal	Axial	61,54	31,60	19,26	18,59	2476,02	49,76	7,51	1,00	**7,49**	
32	Normal	Axial	61,47	22,43	17,60	16,98	1755,51	41,90	9,67	0,92	**8,93**	
33	Normal	Axial	61,52	17,39	14,46	13,95	1362,15	36,91	10,24	0,87	8,94	Not valid
34	Normal	Axial	61,48	26,93	11,14	10,75	2108,05	45,91	5,10	0,96	4,91	Not valid
35	Normal	Axial	61,49	18,84	10,26	9,90	1475,01	38,41	6,71	0,89	**5,96**	
36	Parallel	Diametral	-	39,60	4,14	4,00	1568,16	39,60	2,55	0,90	**2,29**	
37	Parallel	Diametral	-	39,45	5,46	5,27	1556,30	39,45	3,39	0,90	**3,04**	
38	Parallel	Diametral	-	39,62	4,20	4,05	1569,74	39,62	2,58	0,90	**2,33**	
39	Normal	Axial	39,59	21,16	7,62	7,35	1066,62	32,66	6,89	0,83	**5,69**	
40	Normal	Axial	39,60	22,31	3,64	3,51	1124,88	33,54	3,12	0,84	**2,61**	
41	Normal	Axial	39,58	22,69	8,60	8,30	1143,46	33,82	7,26	0,84	6,09	Not valid
42	Normal	Axial	39,62	26,11	5,88	5,67	1317,14	36,29	4,31	0,87	3,73	Not valid
43	Normal	Axial	39,60	19,52	6,60	6,37	984,20	31,37	6,47	0,81	**5,25**	
44	Normal	Axial	39,60	33,08	3,98	3,84	1667,90	40,84	2,30	0,91	2,10	Not valid
45	Normal	Axial	39,61	23,20	6,04	5,83	1170,05	34,21	4,98	0,84	4,20	Not valid
46	Normal	Axial	39,62	26,62	7,10	6,85	1342,87	36,65	5,10	0,87	4,44	Not valid

Appendix C: Results from calculations and field measurements

Results from calculations and field measurement. This section consist of results from semi-empircal equation proposed by Panthi (2006) and results from Rapid Step-Rate Test, which were conducted at Løkjelsvatn 22-24. January 2021.

1. Leakage calculations: Semi-empirical equation to evaluate leakage.
2. RSRT: Complete pressure/flow vs. time for all tests
3. RSRT: Succesfull tests with derivative plot
4. RSRT: Pressure vs. Flow for all tests

Leakage calculations: Semi-empirical equation to evaluate leakage

Input terrain parameters			Geometrical parameters		f_a			q_t [l/min/m]		
X [m]	Z [m]	Chainage [m]	D [m]	H [m]	Min	Mean	Max	Min	Mean	Max
1640	76	1640	570	549	0,0018	0,0096	0,0175	0,72	10,73	28,89
1660	76	1660	578	549	0,0017	0,0095	0,0173	0,71	10,58	28,49
1680	76	1680	585	549	0,0017	0,0094	0,0171	0,70	10,45	28,15
1700	76	1700	592	549	0,0017	0,0093	0,0169	0,70	10,33	27,82
1720	76	1720	600	549	0,0017	0,0092	0,0167	0,69	10,19	27,45
1740	76	1740	607	549	0,0016	0,0091	0,0165	0,68	10,07	27,13
1760	76	1760	615	549	0,0016	0,0089	0,0163	0,67	9,94	26,78
1780	79	1780	619	546	0,0016	0,0089	0,0162	0,66	9,82	26,46
1800	83	1801	620	542	0,0016	0,0089	0,0161	0,66	9,74	26,23
1820	86	1821	628	539	0,0016	0,0088	0,0159	0,64	9,56	25,75
1840	88	1841	633	537	0,0016	0,0087	0,0158	0,64	9,45	25,45
1860	92	1861	637	533	0,0016	0,0086	0,0157	0,63	9,32	25,10
1880	96	1882	642	529	0,0016	0,0086	0,0156	0,62	9,18	24,72
1900	99	1902	648	526	0,0015	0,0085	0,0154	0,61	9,04	24,35
1920	102	1922	654	523	0,0015	0,0084	0,0153	0,60	8,91	23,99
1940	106	1943	660	519	0,0015	0,0083	0,0152	0,59	8,76	23,59
1960	109	1963	668	516	0,0015	0,0082	0,0150	0,58	8,60	23,17
1980	112	1983	676	513	0,0015	0,0081	0,0148	0,57	8,45	22,77
2000	122	2005	679	503	0,0015	0,0081	0,0147	0,56	8,25	22,22
2000	142	2025	663	483	0,0015	0,0083	0,0151	0,55	8,11	21,86
2000	162	2045	647	463	0,0015	0,0085	0,0155	0,54	7,97	21,47
2000	182	2065	631	443	0,0016	0,0087	0,0158	0,53	7,82	21,06
2000	202	2085	615	423	0,0016	0,0089	0,0163	0,52	7,66	20,63
2000	222	2105	600	403	0,0017	0,0092	0,0167	0,50	7,48	20,15
2000	242	2125	585	383	0,0017	0,0094	0,0171	0,49	7,29	19,64
2000	262	2145	570	363	0,0018	0,0096	0,0175	0,48	7,09	19,11
2000	282	2165	556	343	0,0018	0,0099	0,0180	0,46	6,87	18,51
2000	302	2185	542	323	0,0018	0,0101	0,0185	0,45	6,64	17,88
2000	322	2205	528	303	0,0019	0,0104	0,0189	0,43	6,39	17,22
2000	342	2225	615	283	0,0016	0,0089	0,0163	0,41	6,10	16,50
2000	362	2245	502	263	0,0020	0,0110	0,0199	0,39	5,83	15,72
2000	382	2265	490	243	0,0020	0,0112	0,0204	0,37	5,52	14,88
2000	402	2285	478	223	0,0021	0,0115	0,0209	0,35	5,20	14,00
2000	422	2305	467	203	0,0021	0,0118	0,0214	0,33	4,84	13,04
2000	442	2325	456	183	0,0022	0,0121	0,0219	0,30	4,47	12,04
2000	462	2345	446	163	0,0022	0,0123	0,0224	0,27	4,07	10,96
2000	482	2365	436	143	0,0023	0,0126	0,0229	0,25	3,65	9,84
2000	502	2385	428	123	0,0023	0,0129	0,0234	0,22	3,20	8,62
2000	522	2405	420	103	0,0024	0,0131	0,0238	0,18	2,73	7,36
2000	542	2425	412	83	0,0024	0,0133	0,0243	0,15	2,24	6,04
2000	562	2445	407	63	0,0025	0,0135	0,0246	0,12	1,72	4,64
2000	582	2465	402	43	0,0025	0,0137	0,0249	0,08	1,19	3,21
2000	600	2483	398	25	0,0025	0,0138	0,0251	0,05	0,70	1,88

RSRT: Complete pressure/flow vs. time for all tests

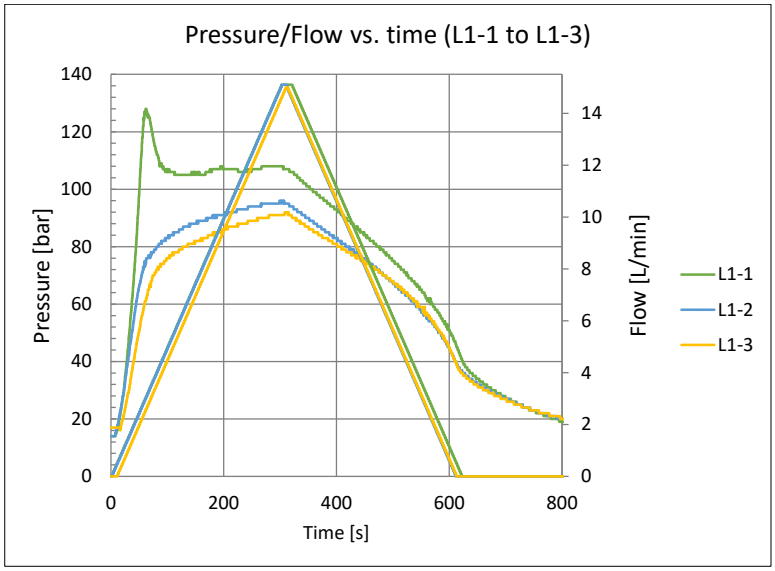

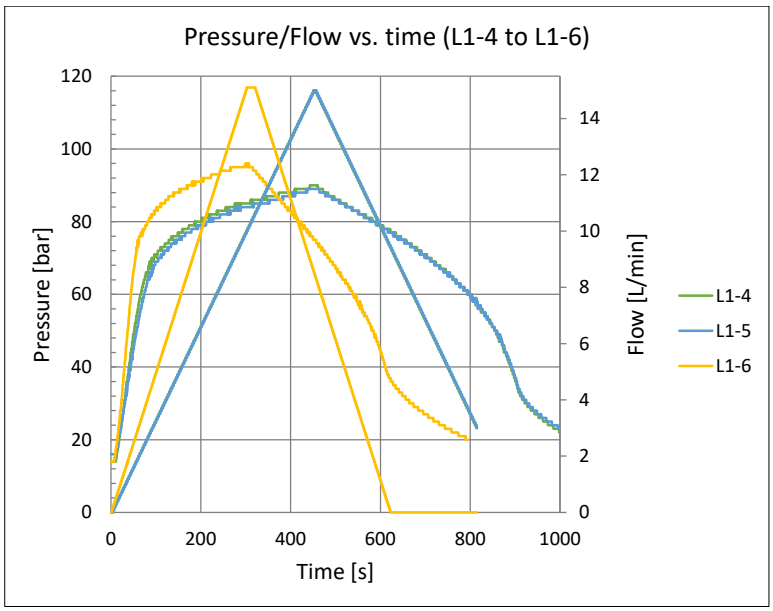

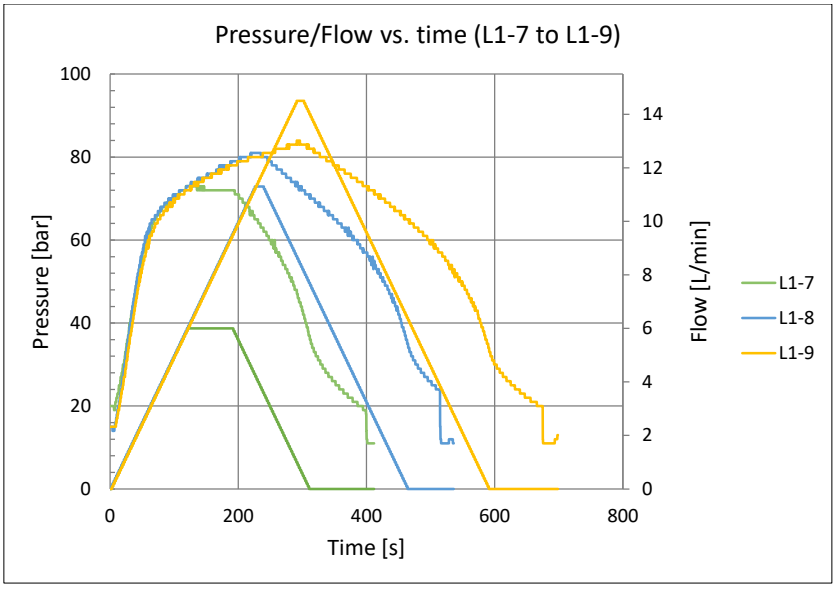
Pressure/Flow vs. time (L1-7 to L1-9)
Pressure [bar]
Flow [L/min]
Time [s]
0
20
40
60
80
100
0
2
4
6
8
10
12
14
0
200
400
600
800
L1-7
L1-8
L1-9

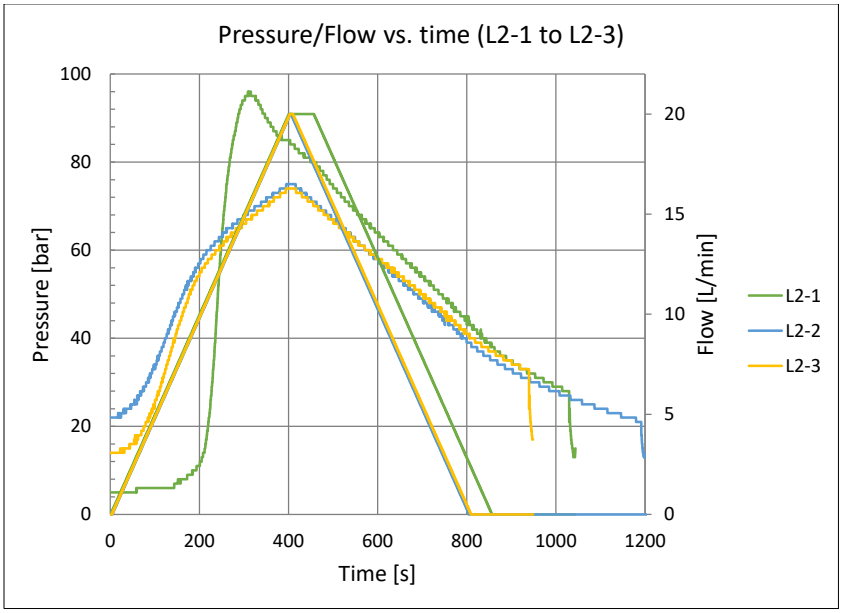
Pressure/Flow vs. time (L2-1 to L2-3)
Pressure [bar]
Flow [L/min]
Time [s]
0
20
40
60
80
100
0
5
10
15
20
0
200
400
600
800
1000
1200
L2-1
L2-2
L2-3

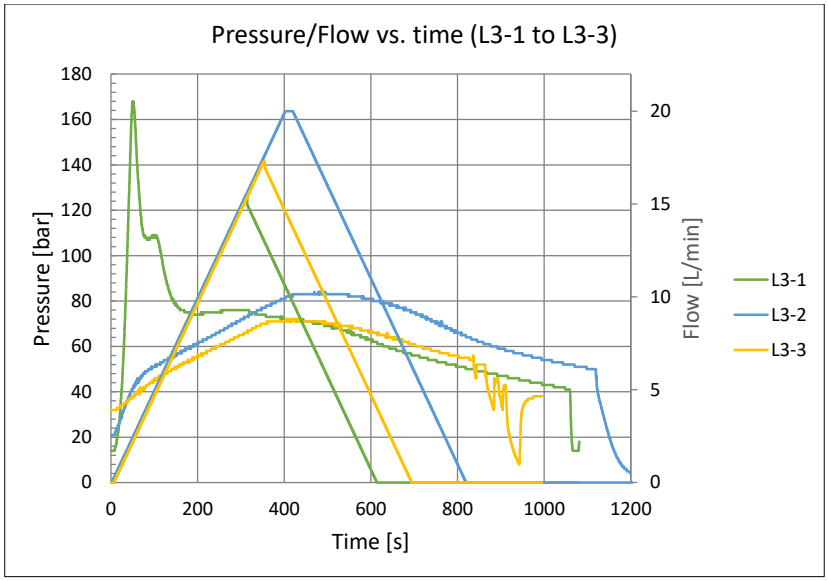
Pressure/Flow vs. time (L3-1 to L3-3)
Pressure [bar]
Flow [L/min]
Time [s]
0
20
40
60
80
100
120
140
160
180
0
5
10
15
20
0
200
400
600
800
1000
1200
L3-1
L3-2
L3-3

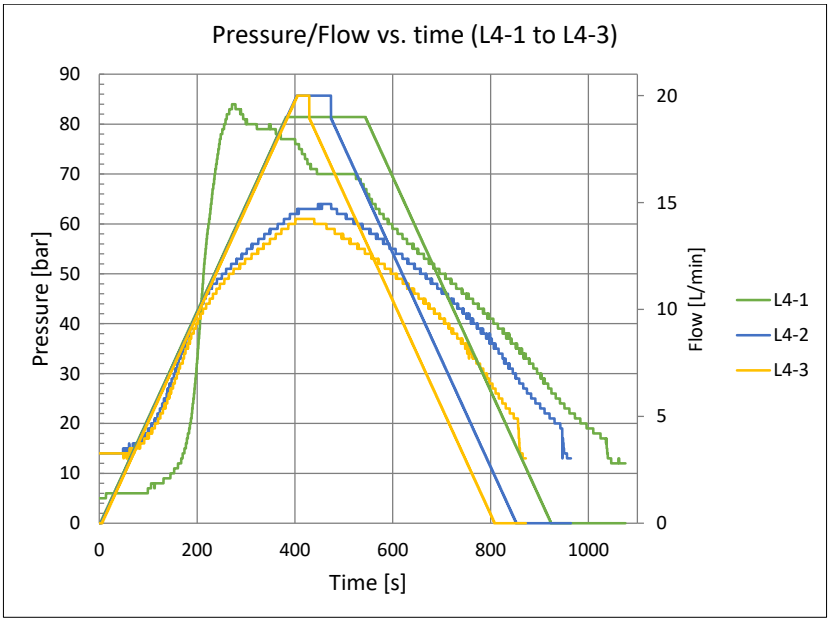
Pressure/Flow vs. time (L4-1 to L4-3)
Pressure [bar]
Flow [L/min]
Time [s]
0
10
20
30
40
50
60
70
80
90
0
5
10
15
20
0
200
400
600
800
1000
L4-1
L4-2
L4-3

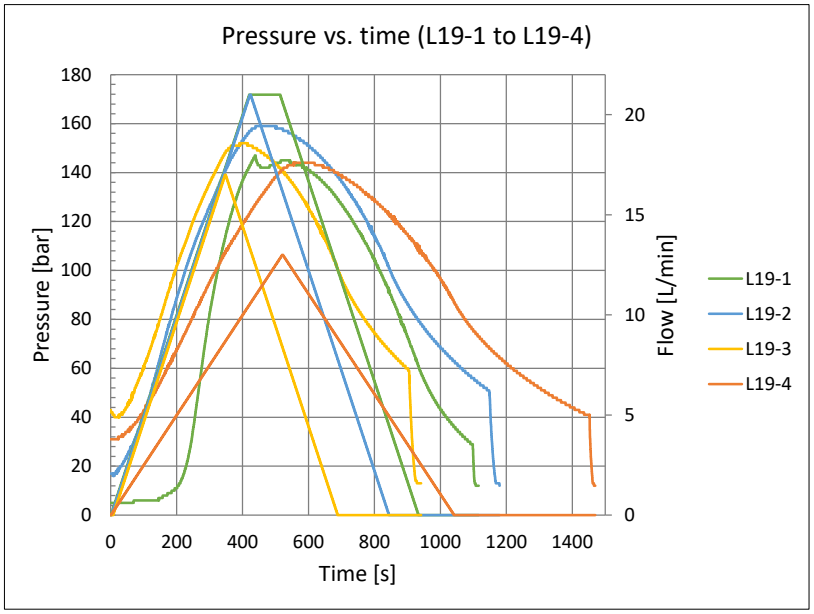
Pressure vs. time (L19-1 to L19-4)
Pressure [bar]
Flow [L/min]
Time [s]
0
20
40
60
80
100
120
140
160
180
0
5
10
15
20
0
200
400
600
800
1000
1200
1400
L19-1
L19-2
L19-3
L19-4

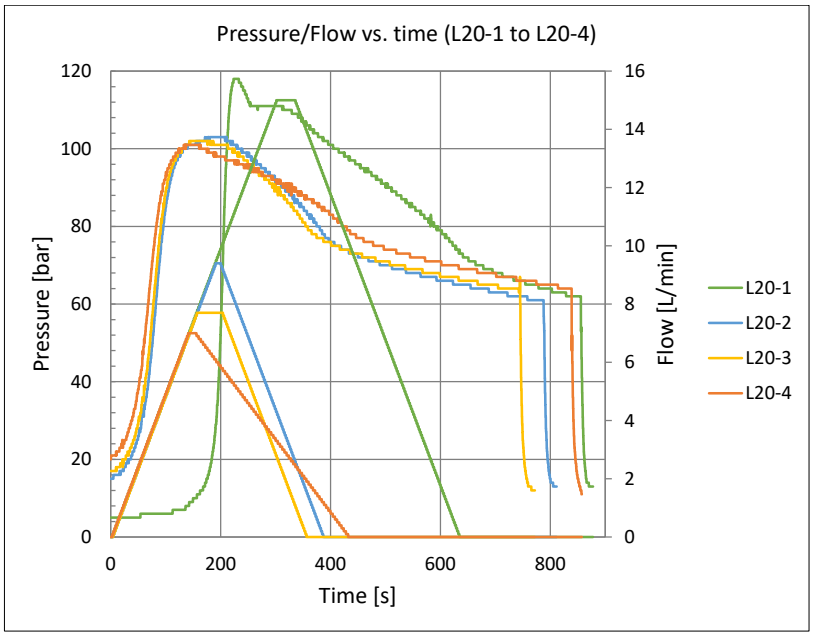
Pressure/Flow vs. time (L20-1 to L20-4)
Pressure [bar]
Flow [L/min]
Time [s]
0
20
40
60
80
100
120
0
2
4
6
8
10
12
14
16
0
200
400
600
800
L20-1
L20-2
L20-3
L20-4

RSRT: Succesfull tests with derivative plot

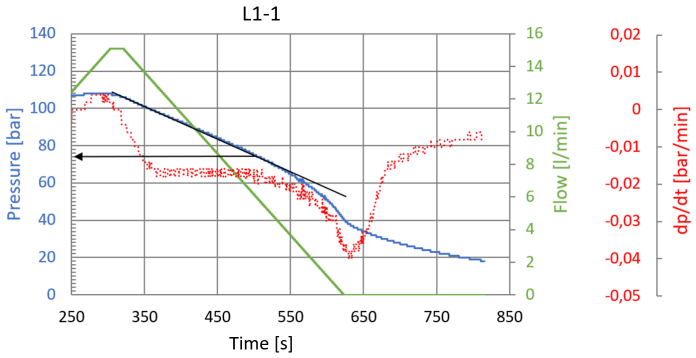

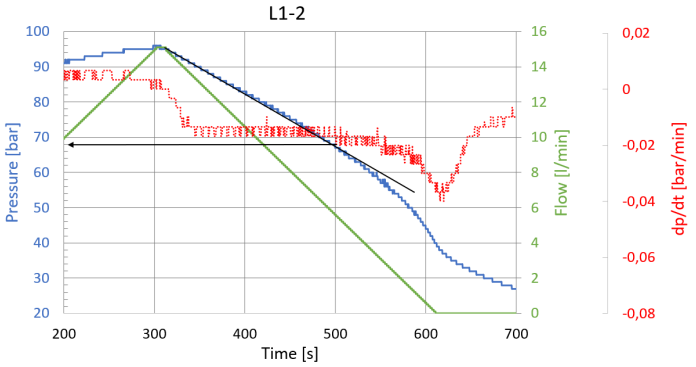

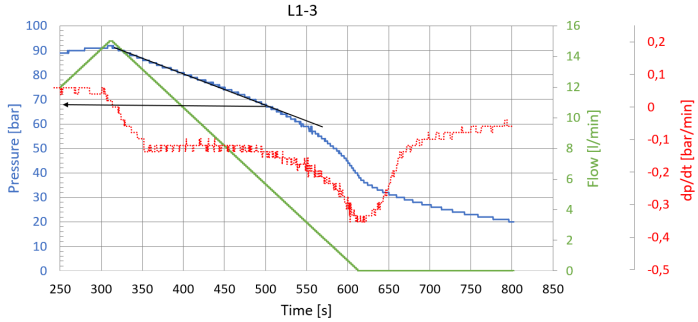

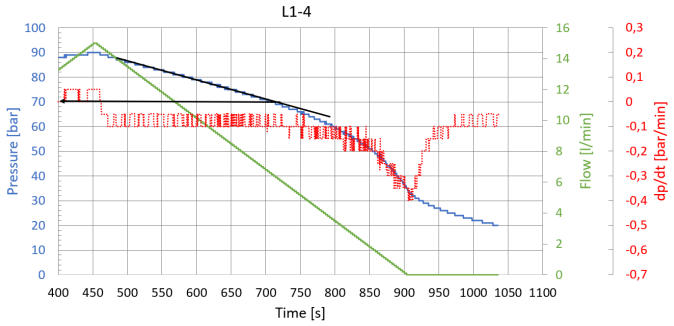

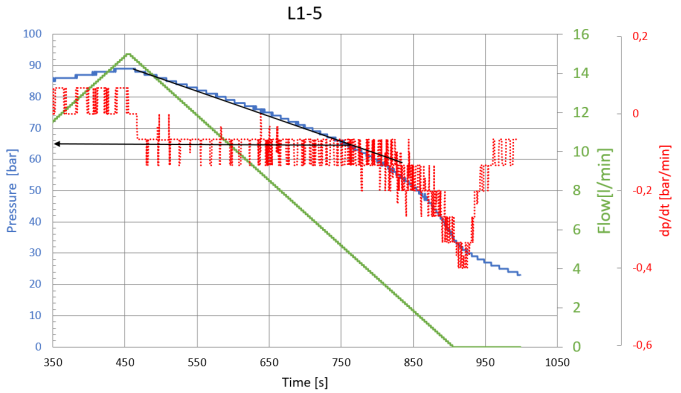
L1-5
Pressure [bar]
Flow[l/min]
dp/dt [bar/min]
Time [s]

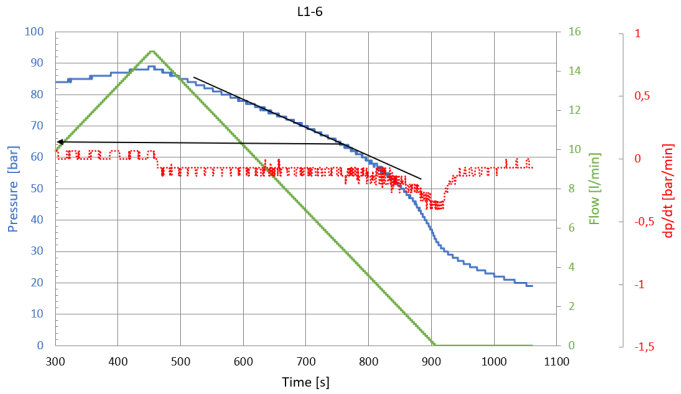
L1-6
Pressure [bar]
Flow [l/min]
dp/dt [bar/min]
Time [s]

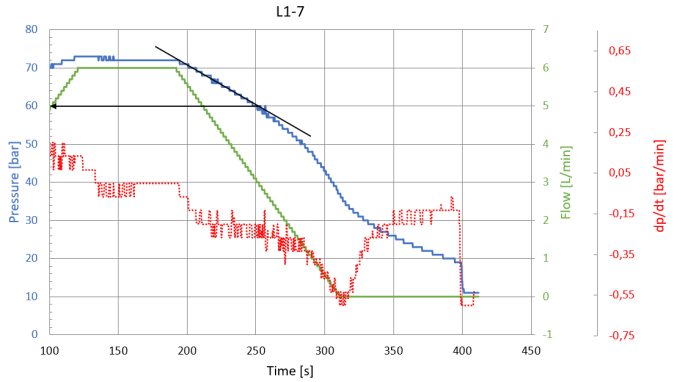
L1-7
Pressure [bar]
Flow [L/min]
dp/dt [bar/min]
Time [s]

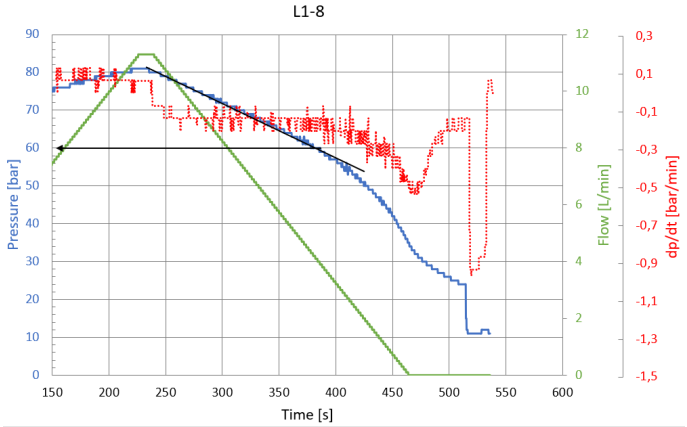
L1-8
Pressure [bar]
Flow [L/min]
dp/dt [bar/min]
Time [s]

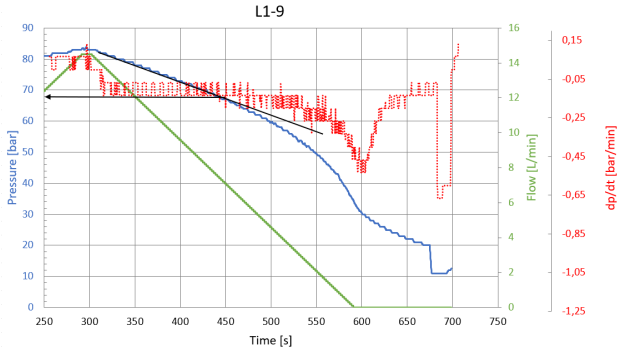
L1-9
Pressure [bar]
Flow [L/min]
dp/dt [bar/min]
Time [s]

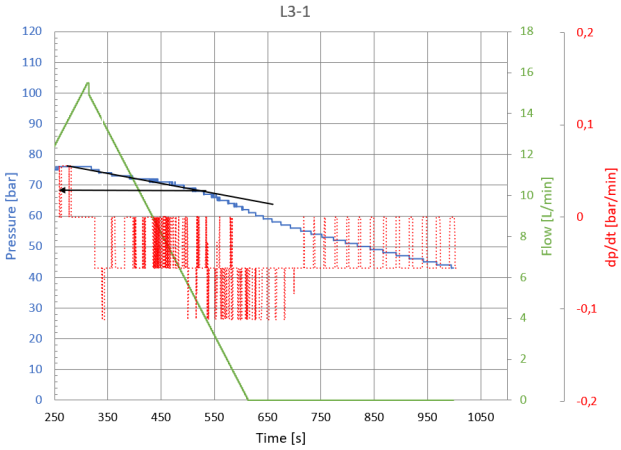
L3-1
Pressure [bar]
Flow [L/min]
dp/dt [bar/min]
Time [s]

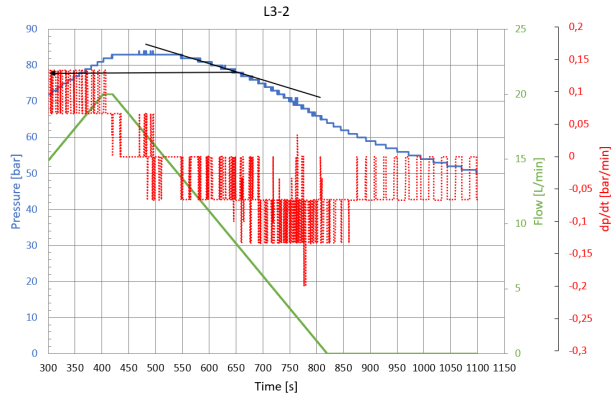
L3-2
Pressure [bar]
Flow [L/min]
dp/dt [bar/min]
Time [s]

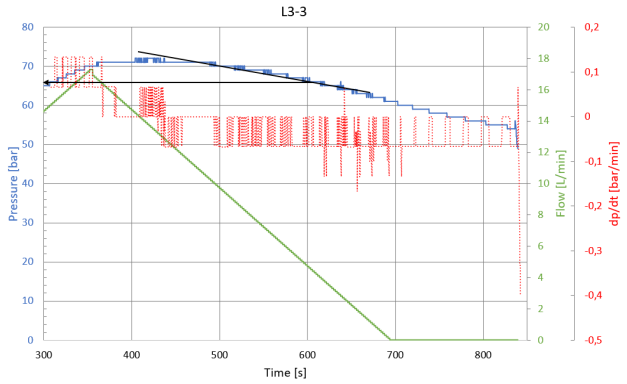
L3-3
Pressure [bar]
Flow [L/min]
dp/dt [bar/min]
Time [s]

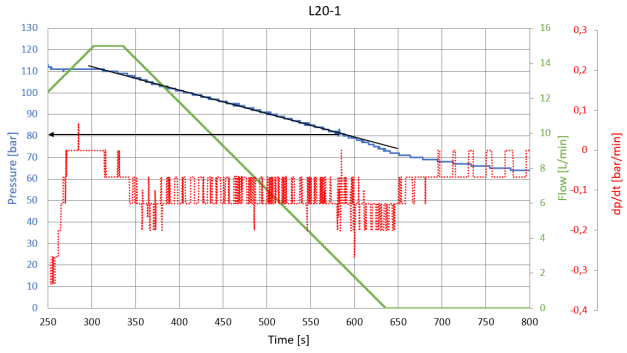
L20-1
Pressure [bar]
Flow [L/min]
dp/dt [bar/min]
Time [s]

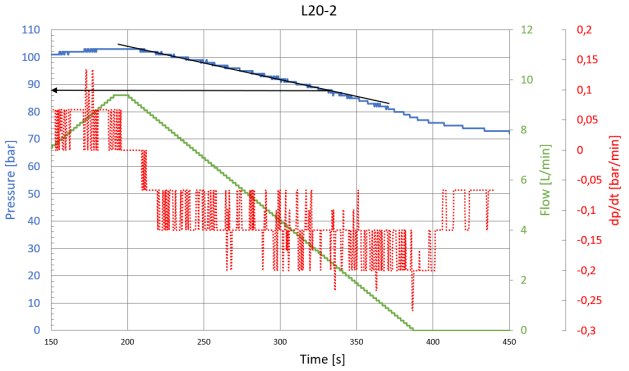
L20-2
Pressure [bar]
Flow [L/min]
dp/dt [bar/min]
Time [s]

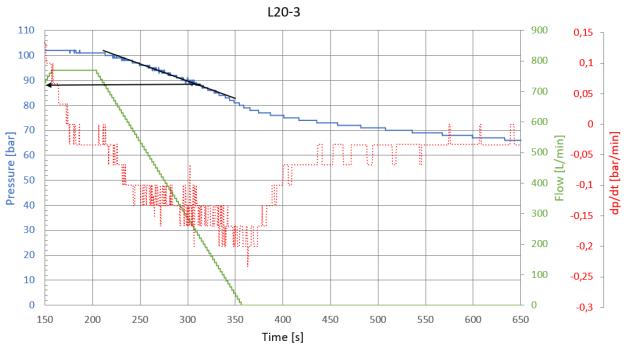
L20-3
Pressure [bar]
Flow [L/min]
dp/dt [bar/min]
Time [s]

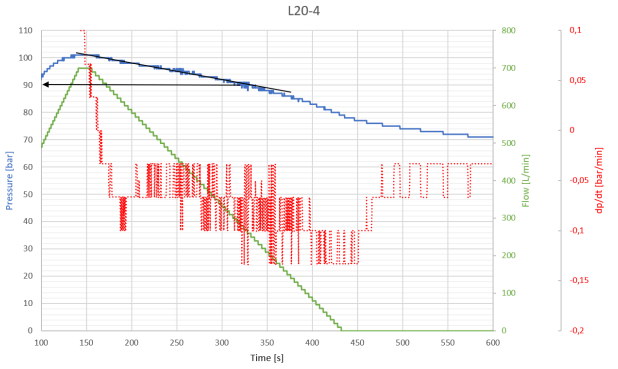
L20-4
Pressure [bar]
Flow [L/min]
dp/dt [bar/min]
Time [s]

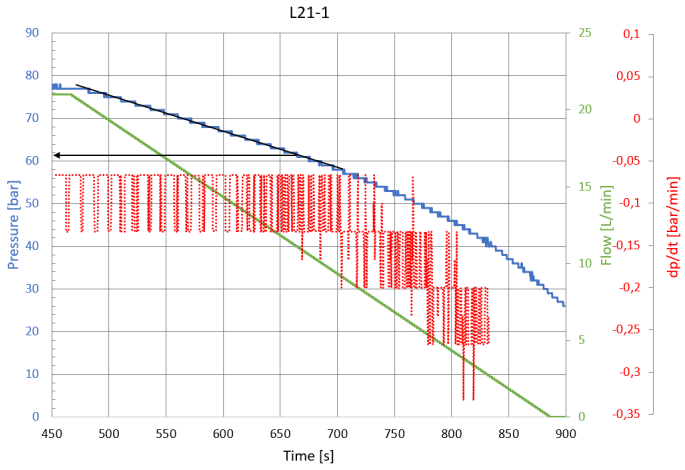
L21-1
Pressure [bar]
Flow [L/min]
dp/dt [bar/min]
Time [s]

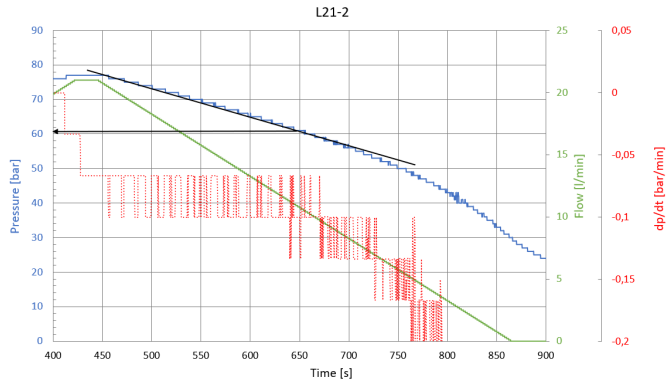
L21-2
Pressure [bar]
Flow [l/min]
dp/dt [bar/min]
Time [s]

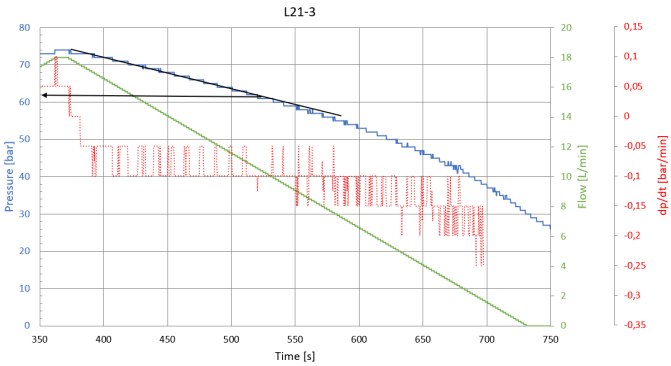
L21-3
Pressure [bar]
Flow [L/min]
dp/dt [bar/min]
Time [s]

RSRT: Pressure vs. Flow, all tests

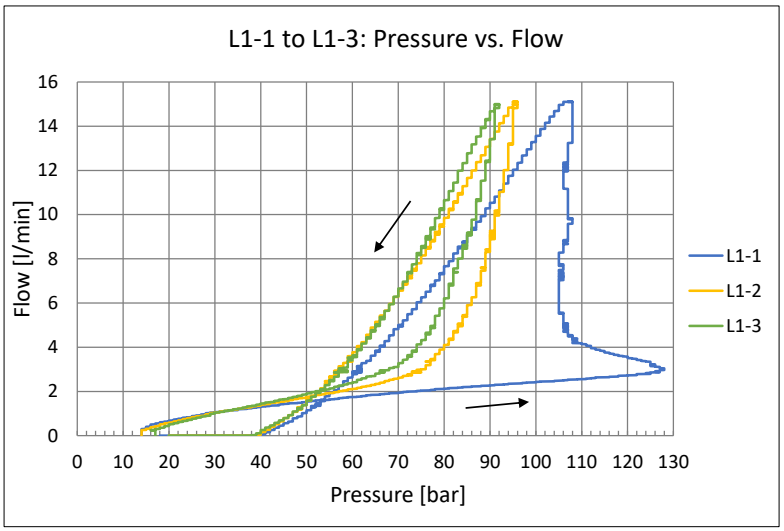

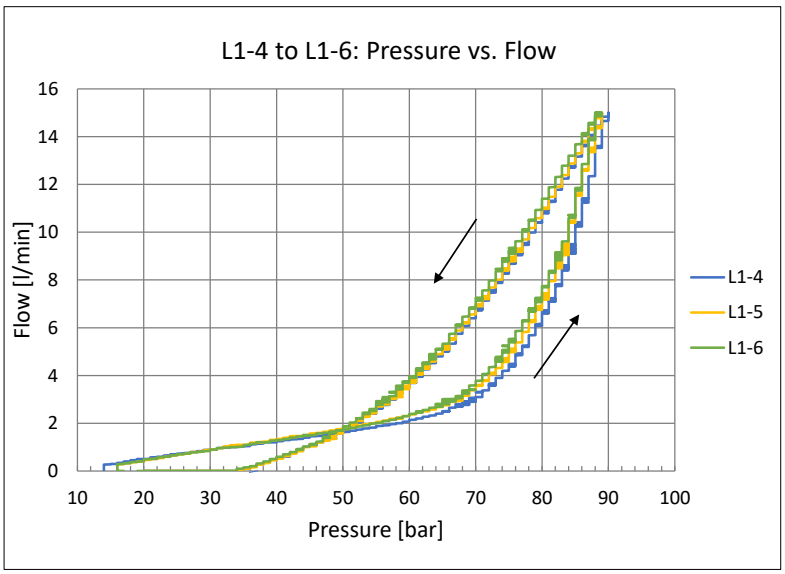

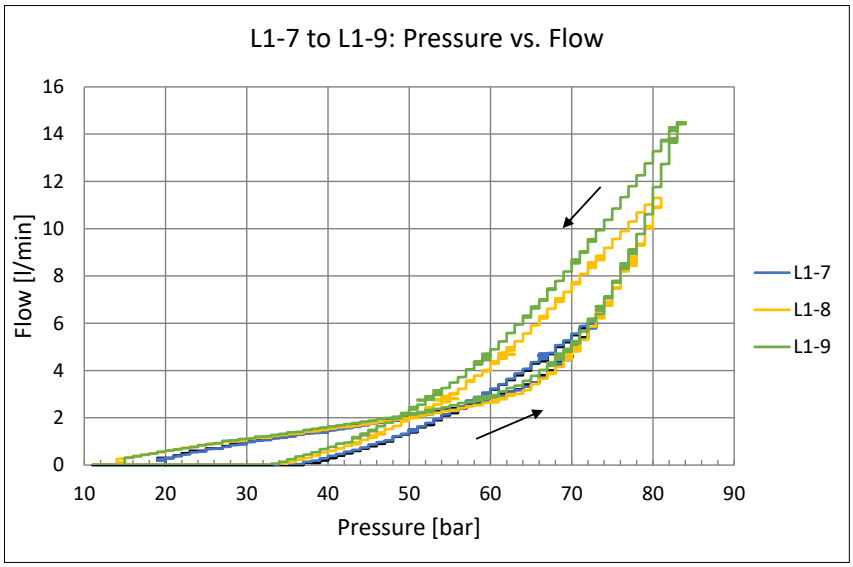
L1-7 to L1-9: Pressure vs. Flow
Flow [l/min]
Pressure [bar]
L1-7
L1-8
L1-9

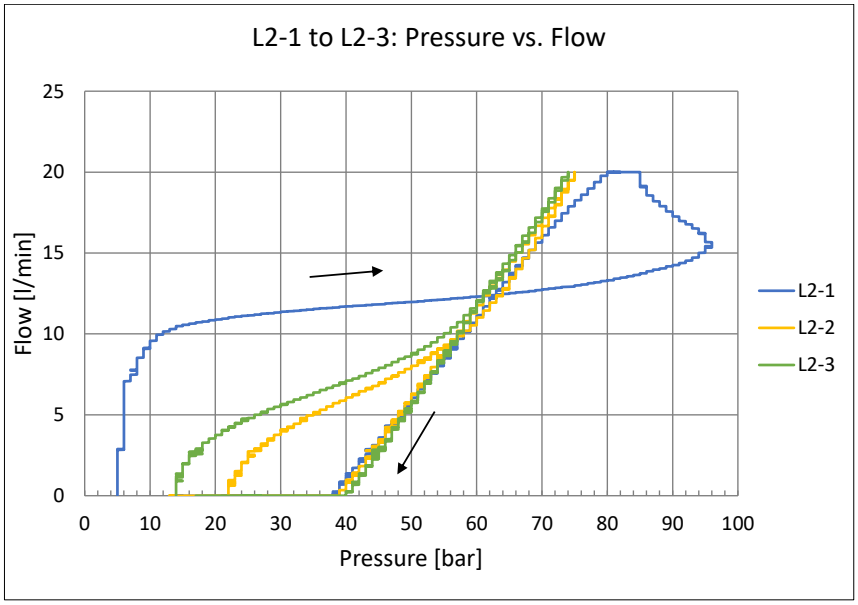
L2-1 to L2-3: Pressure vs. Flow
Flow [l/min]
Pressure [bar]
L2-1
L2-2
L2-3

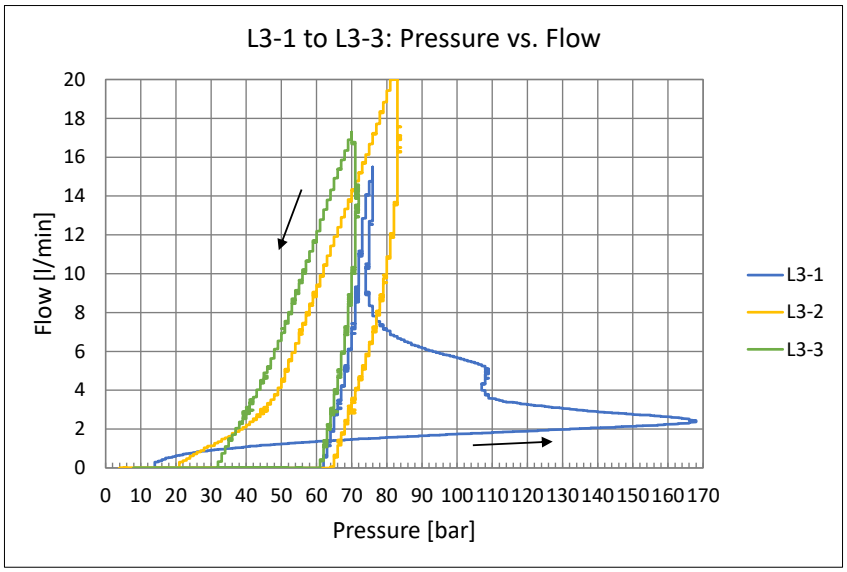
L3-1 to L3-3: Pressure vs. Flow
Flow [l/min]
Pressure [bar]
L3-1
L3-2
L3-3

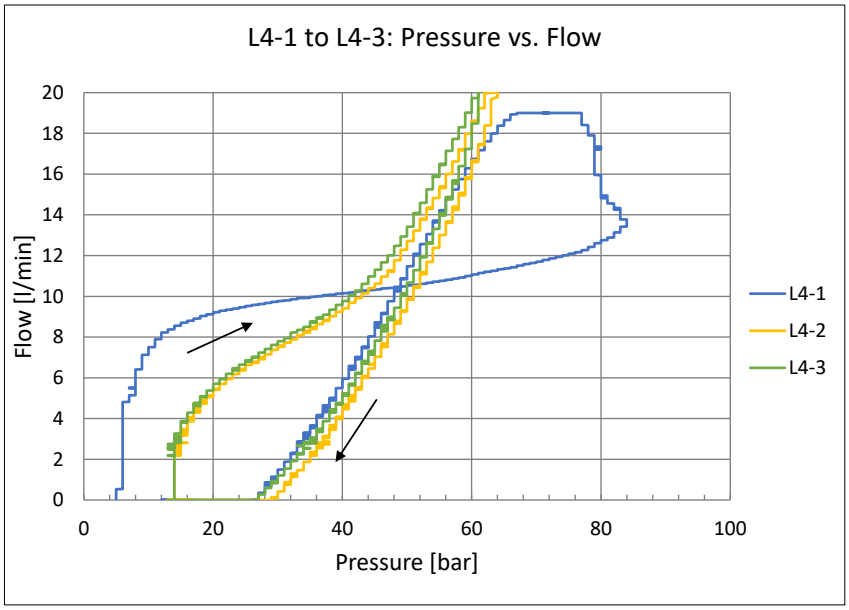
L4-1 to L4-3: Pressure vs. Flow
Flow [l/min]
Pressure [bar]
L4-1
L4-2
L4-3

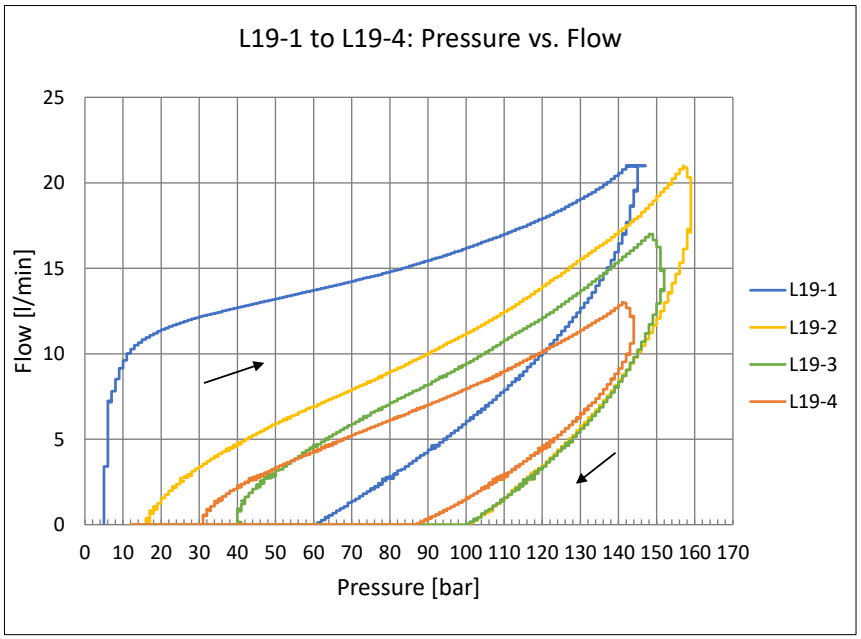
L19-1 to L19-4: Pressure vs. Flow
Flow [l/min]
25
20
15
10
5
0
0 10 20 30 40 50 60 70 80 90 100 110 120 130 140 150 160 170
Pressure [bar]
L19-1
L19-2
L19-3
L19-4

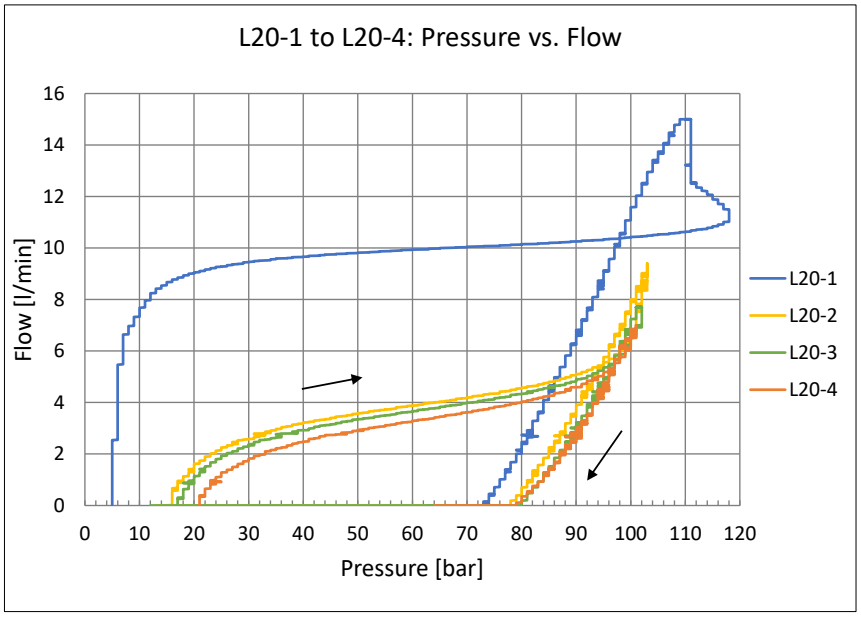
L20-1 to L20-4: Pressure vs. Flow
Flow [l/min]
16
14
12
10
8
6
4
2
0
0 10 20 30 40 50 60 70 80 90 100 110 120
Pressure [bar]
L20-1
L20-2
L20-3
L20-4

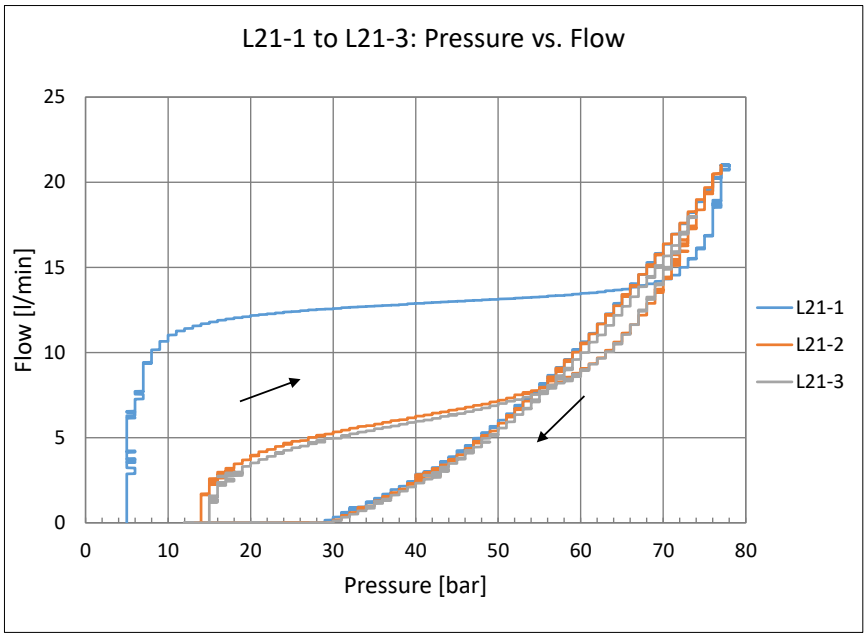
L21-1 to L21-3: Pressure vs. Flow
Flow [l/min]
25
20
15
10
5
0
0
10
20
30
40
50
60
70
80
Pressure [bar]
L21-1
L21-2
L21-3

Appendix D: Numerical modeling

Results from numerical modeling based on measured stress levels.

1. Step 1: In-situ stress models based on results from hydraulic fracturing and 3D overcoring at chainage 1780.
2. Step 2: Geometry and setup for Model B, C and D
3. Step 2: Depth of redistribution zone around the tunnel
4. Step 2: Development of minor principal stress as a function of distance from tunnel contour

Step 1: In-situ stress models based on results from hydraulic fracturing at 1780

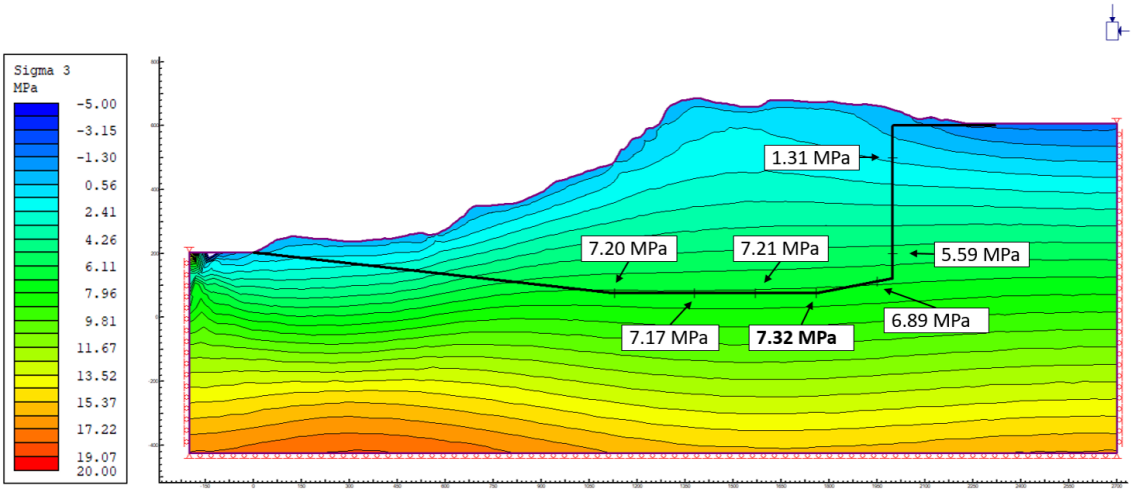

Step 1: In-situ stress models based on results from 3d overcoring at 1780

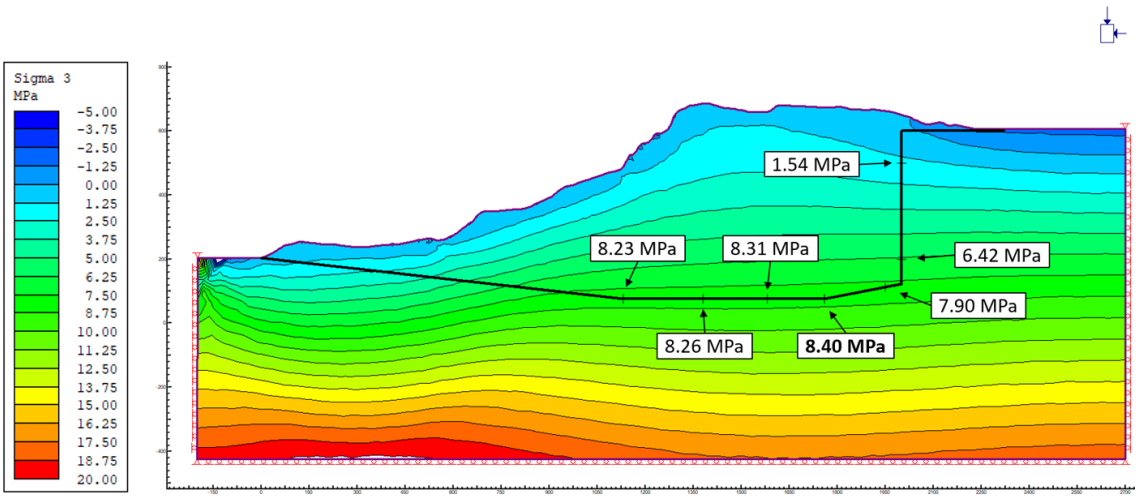

Step 2: Geometry and setup for Model B

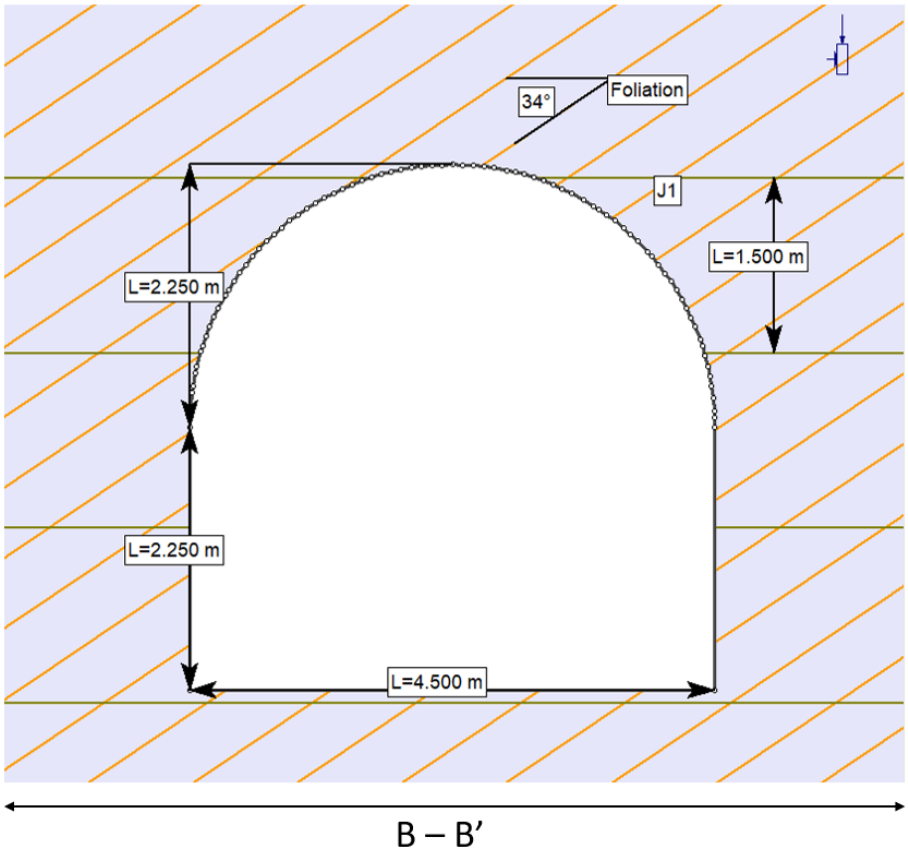

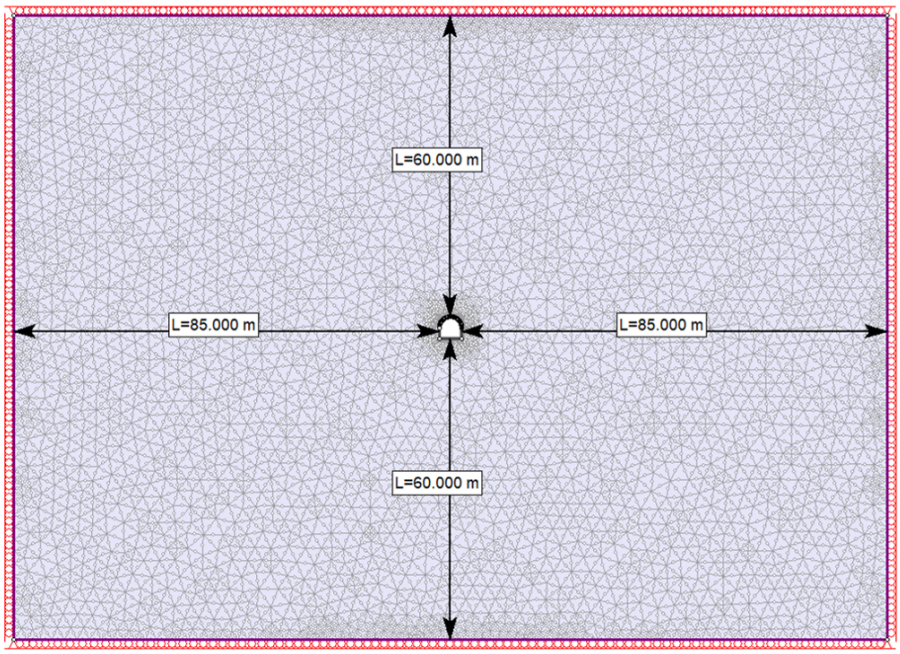

Step 2: Geometry and setup for Model C and D

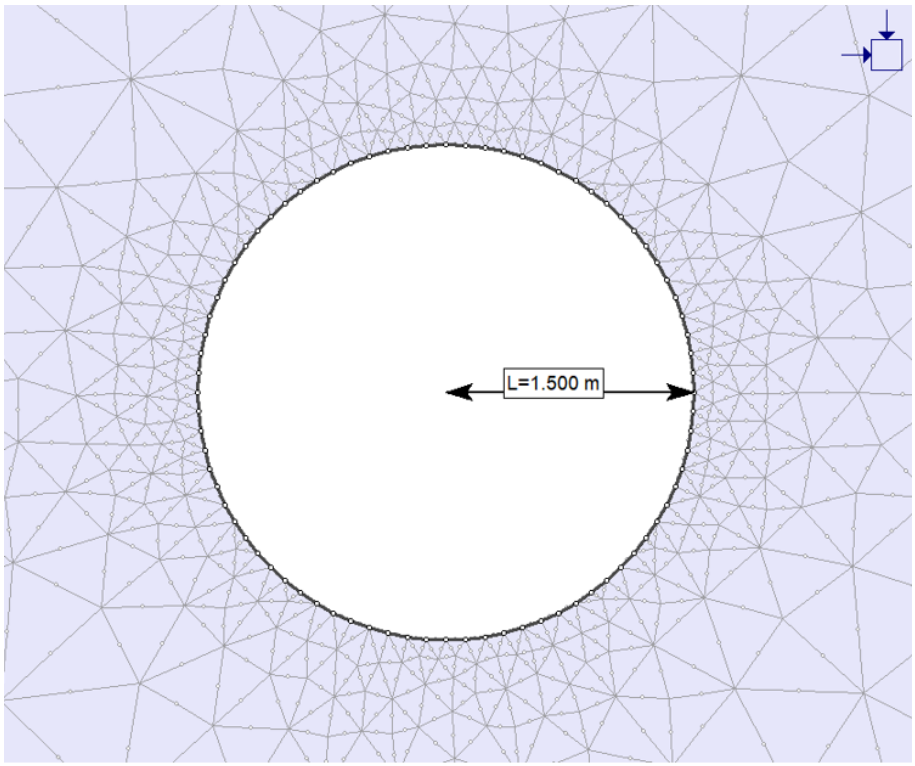

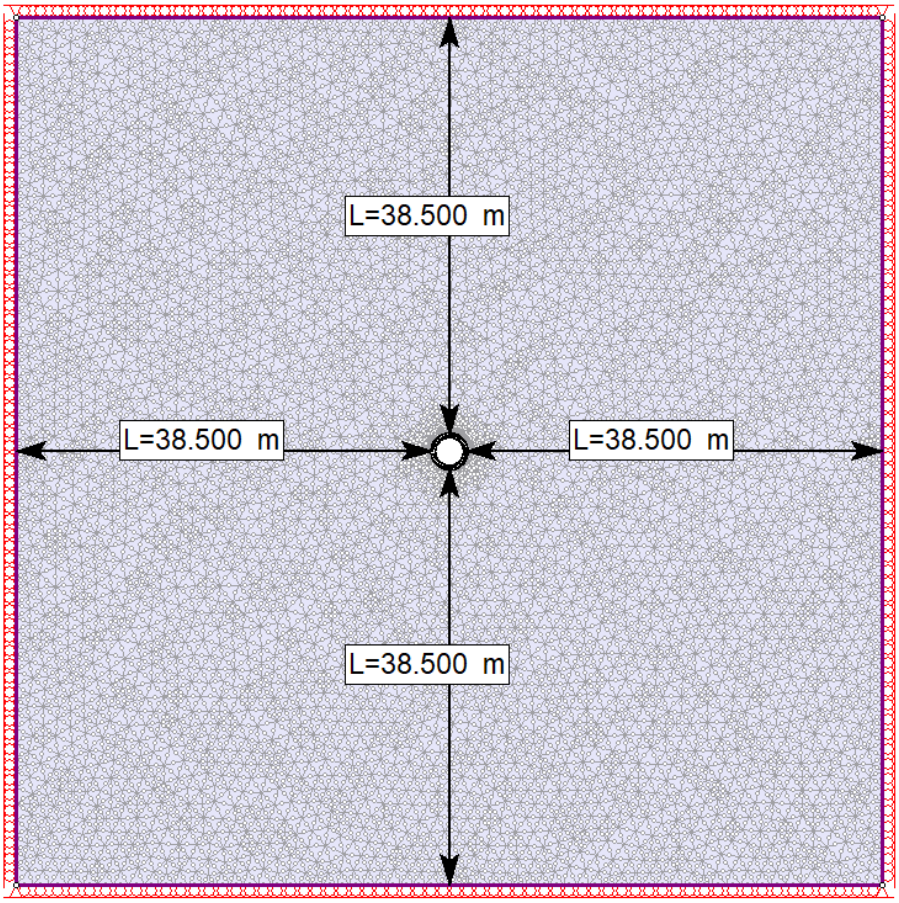

Step 2: Depth of impact zone

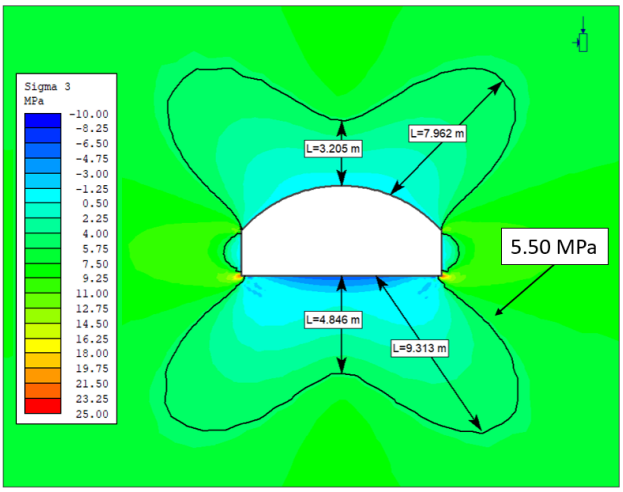

Model A2

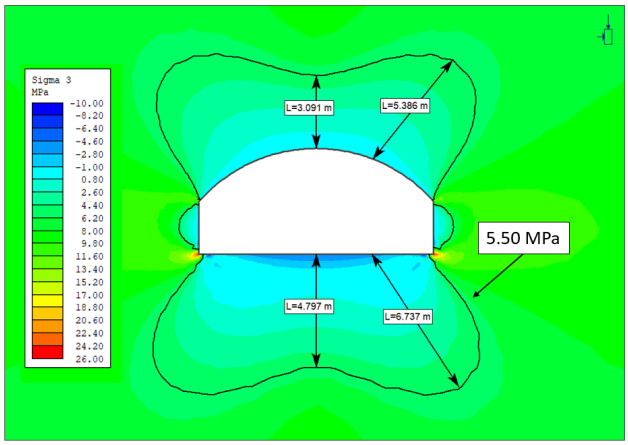

Model A3

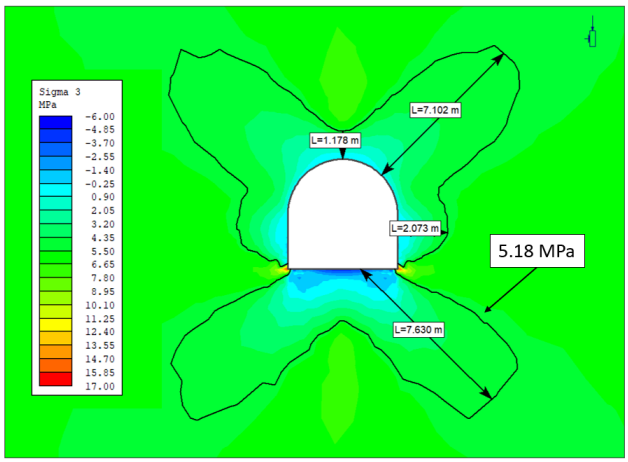

Model B1

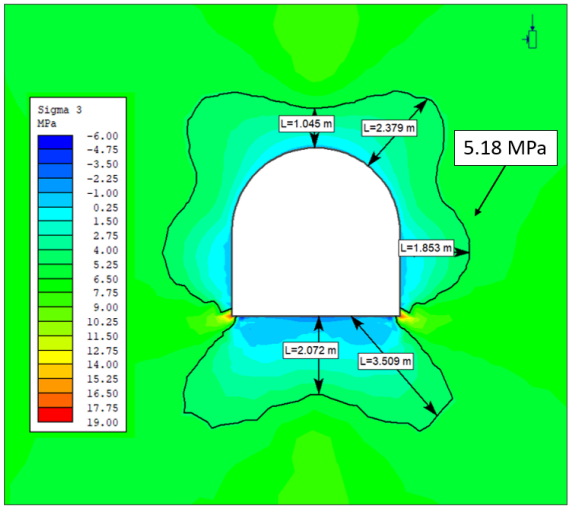

Model B2

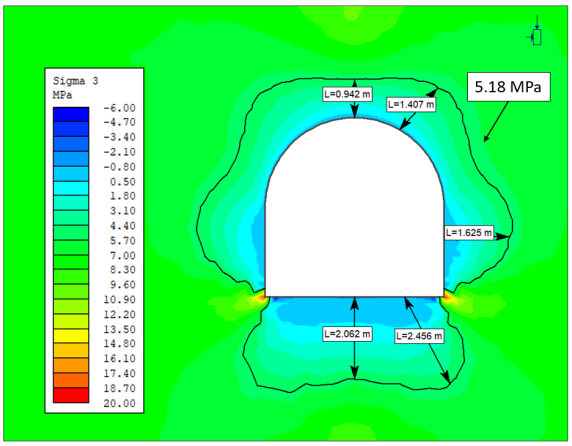

Model B3

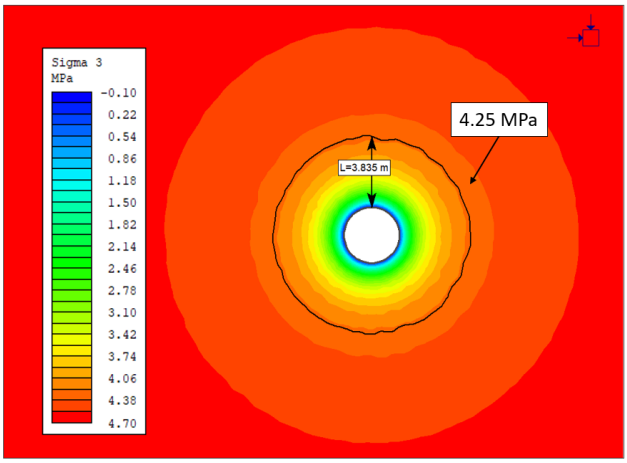

Model C1

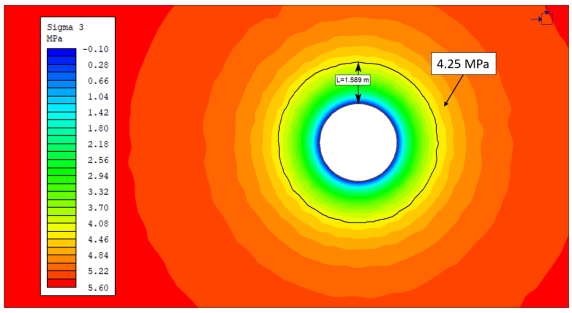

Model C2

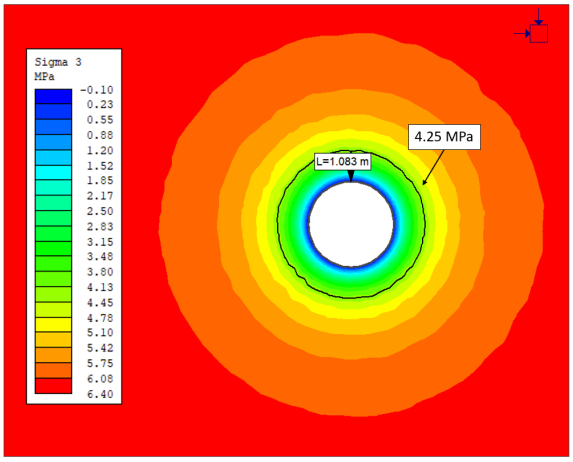

Model C3

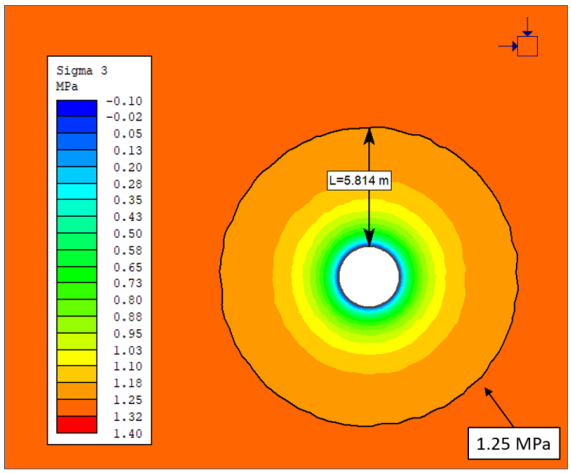

Model D2

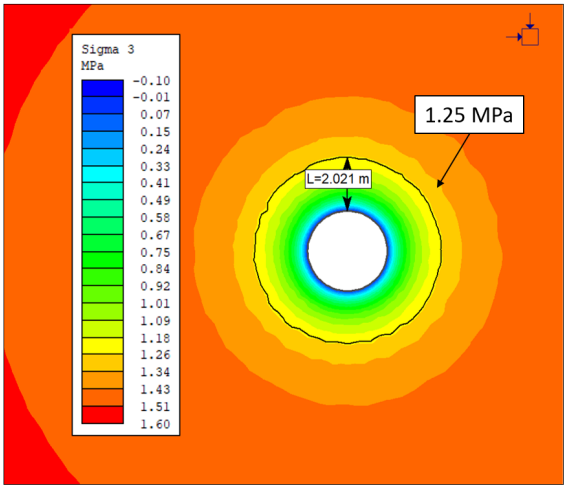
Sigma 3
MPa
-0.10
-0.01
0.07
0.15
0.24
0.33
0.41
0.49
0.58
0.67
0.75
0.84
0.92
1.01
1.09
1.18
1.26
1.34
1.43
1.51
1.60
1.25 MPa
L=2.021 m

Model D3

Step 2: Development of minor principal stress as a function of distance fromtunnel contour

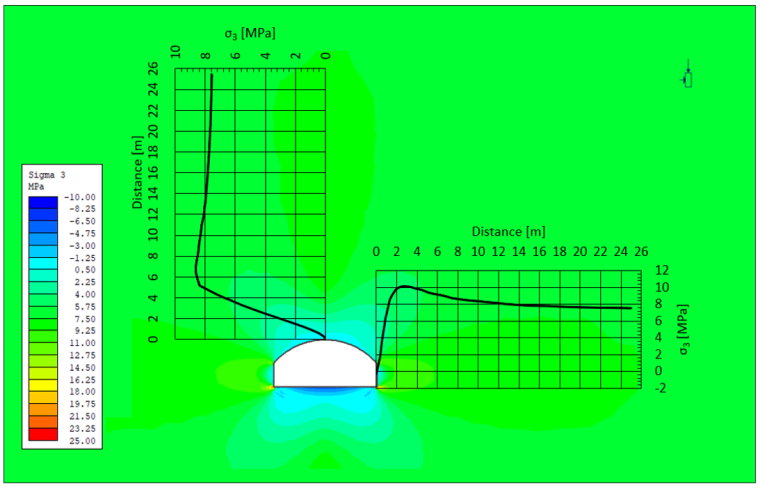

Model A2

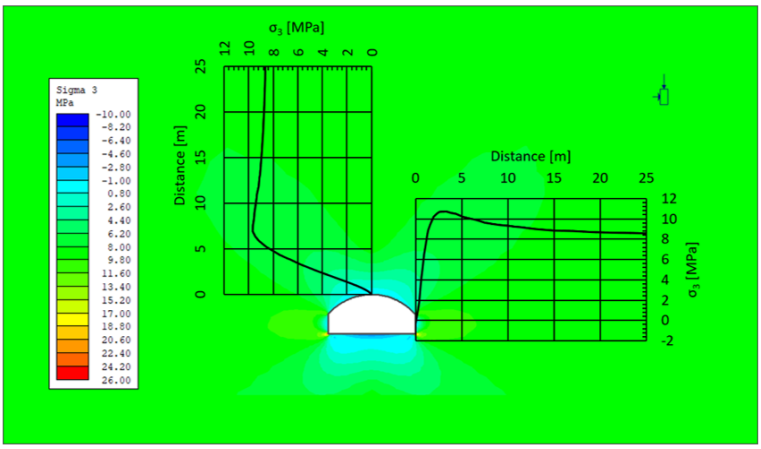

Model A3

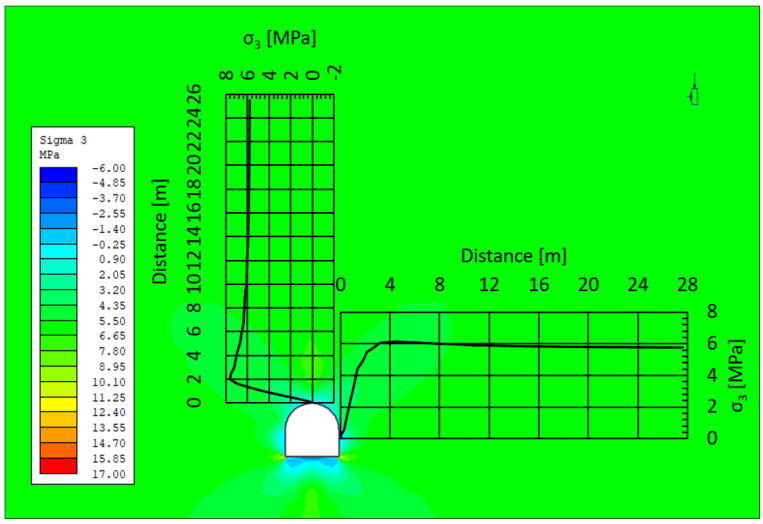

Model B1

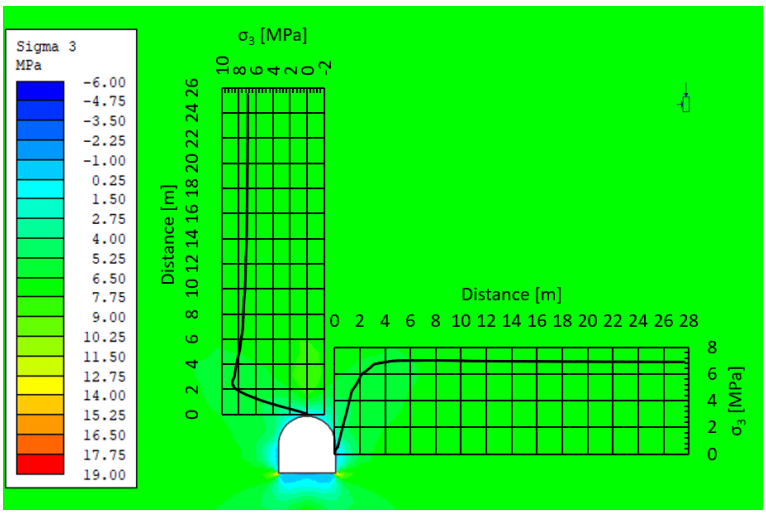

Model B2

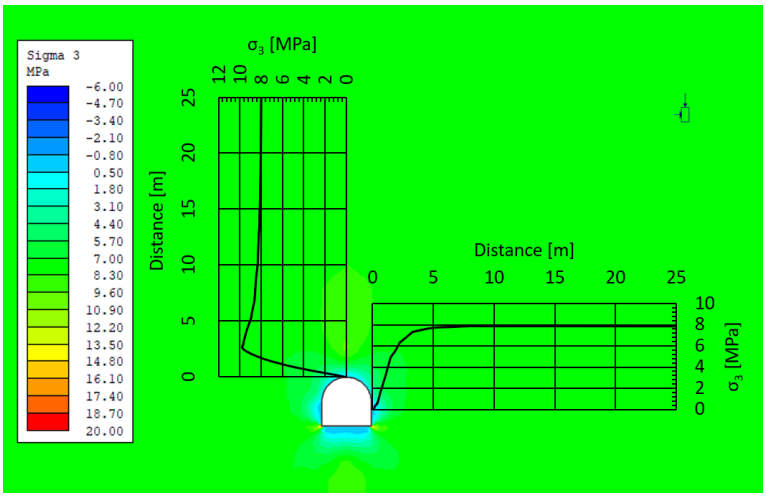

Model B3

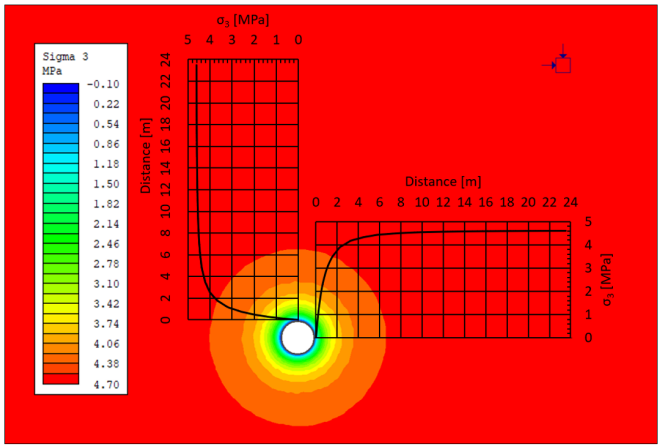

Model C1

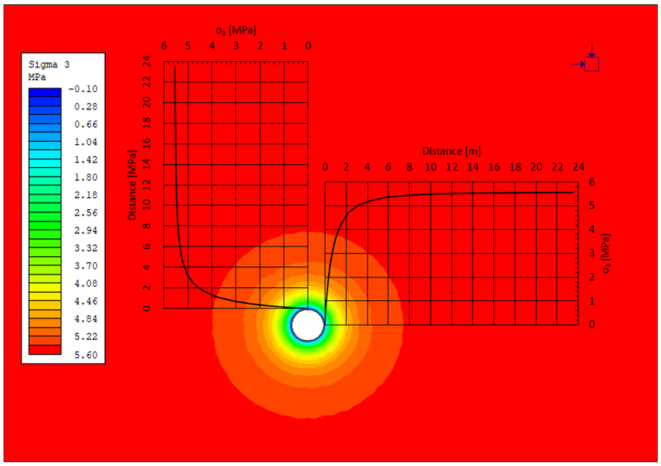

Model C2

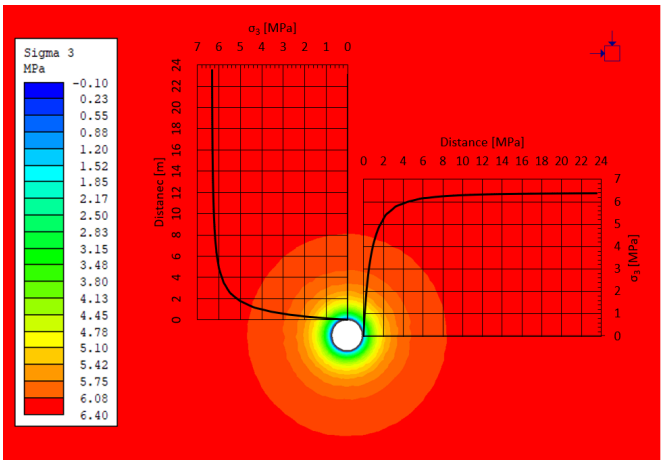

Model C3

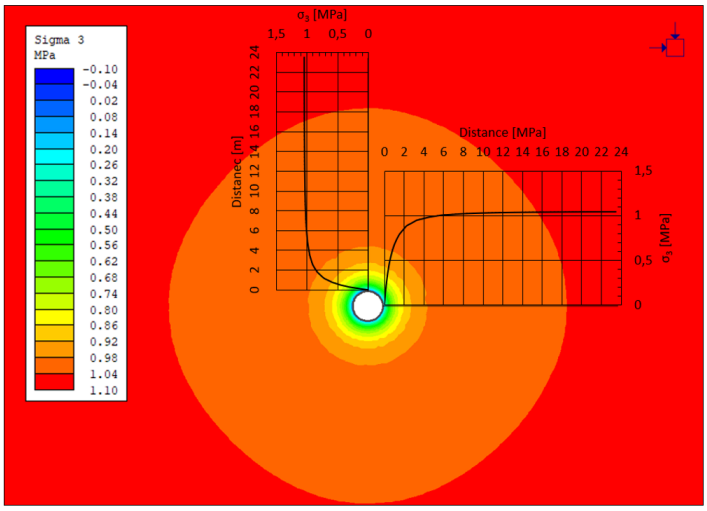

Model D1

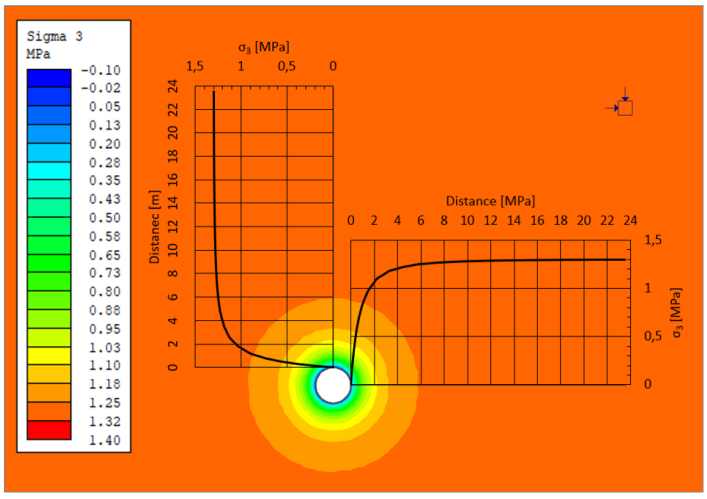

Model D2

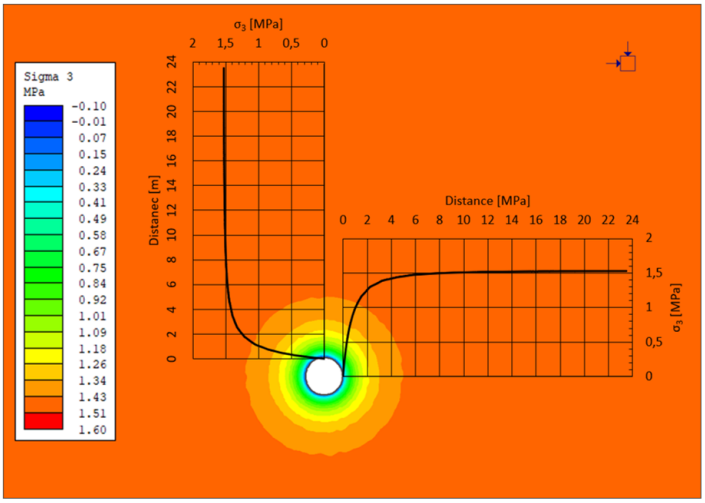
Sigma 3
MPa
-0.10
-0.01
0.07
0.15
0.24
0.33
0.41
0.49
0.58
0.67
0.75
0.84
0.92
1.01
1.09
1.18
1.26
1.34
1.43
1.51
1.60
σ3 [MPa]
2 1,5 1 0,5 0
Distanec [m]
0 2 4 6 8 10 12 14 16 18 20 22 24
Distance [MPa]
0 2 4 6 8 10 12 14 16 18 20 22 24
σ3 [MPa]
2 1,5 1 0,5 0

Model D3

Erlend Andreassen

Assessment of minimum principal stress and potential hydraulic jacking at Løkjelsvatn Hydropower Project

NTNU
Norwegian University of
Science and Technology